UNIVERSITAT DE BARCELONA

Improved Preparative Chemical Methodologies to Address Challenging Targets: Synthetic, Semi-synthetic and Multicomponent Approaches

Marina Pedrola Teixell

Universitat de Barcelona

Facultat de Farmàcia i Ciències de l'Alimentació

Improved Preparative Chemical Methodologies to Address Challenging Targets: Synthetic, Semi-synthetic and Multicomponent Approaches

Marina Pedrola Teixell

2022

Universitat de Barcelona

Facultat de Farmàcia i Ciències de l'Alimentació

Programa de Doctorat de Química Orgànica

Improved Preparative Chemical Methodologies to Address Challenging Targets: Synthetic, Semi-synthetic and Multicomponent Approaches

Memòria presentada per Marina Pedrola Teixell per optar al títol de doctor per la Universitat de Barcelona

Memòria dirigida i revisada per:

Prof. Rodolfo Lavilla Grifols

Unitat de Química Farmacèutica, Facultat de Farmàcia i Ciències de l'Alimentació, Universitat de Barcelona i IBUB

Presentada per:

Marina Pedrola Teixell

Marina Pedrola Teixell
Barcelona, 2022

The present thesis has been mainly developed at the Laboratory of Medicinal Chemistry, in the Faculty of Pharmacy (Department of Pharmacology, Toxicology and Therapeutic Chemistry, Unit of Medicinal Chemistry), from September 2018 to September 2021.

Some part of the experimental work has been performed at the Supramolecular Chemistry Laboratory in the Institute of Advanced Chemistry of Catalonia (IQAC) and at the Laboratories in the Barcelona Science Park.

This work has been supported by the Marató TV3 Foundation.

Per l'Òscar i la tieta M. dels Àngels,

que tot l'esforç invertit als laboratoris d'arreu permeti avançar en el tractament de les malalties que encara no tenen cura, així com seguir millorant la qualitat dels tractaments existents.

Acknowledgements

Aquesta tesi no hagués estat possible sense el suport, guia i contribució de diverses persones.

Entre elles i, en primer lloc, hi incloc el meu director, el Dr. Rodolfo Lavilla. Gracias por contar conmigo, Rodolfo, y permitir adentrarme en el complejo mundo de las reacciones multicomponente. Un mundo inesperado que te reta constantemente y que, sin lugar a duda, voy a echar de menos des del primer día de mi nueva etapa.

Poniendo orden en el laboratorio y ayudando a solventar obstáculos del día a día, entre las sombras de estos cuatro años he contado con el apoyo de la Dr. Ghashghaei. Gracias Ulduz, por ser la mano que me coge siempre y la cabeza que piensa cuando de la mía ya sale humo.

A més, tots els resultats biològics recollits en aquesta tesi són fruit de col·laboracions amb diversos grups. Estic especialment agraïda d'haver tingut l'oportunitat de col·laborar i obtenir resultats fructuosos amb el Dr. Miquel Viñas, el Dr. Raúl Estévez, el Dr. Thomas Haarmann-Stemmann, i els respectius integrants de cada grup. Els resultats exposats, tanmateix, no haguessin estat possible sense el suport tècnic dels serveis de ressonància de la Universitat de Barcelona i del CSIC, així com dels serveis d'espectroscòpia de masses. En especial, vull mencionar el record d'Eva Dalmau.

Per altra banda, ha estat un plaer compartir espai amb tots els professors de la unitat: Dr. Carmen Escolano, Dr. Diego Muñoz-Torrero, Dr. M. Dolors Pujol, i Dr. Santiago Vázquez; així com amb el personal administratiu i tècnic: Maite, Laura i Javier. Agraeixo també l'ajuda que ens van oferir la Dr. Gemma Fabriàs, Dr. Nacho Alfonso, Dr. Juan B. Blanco, Dr. Gemma Triola i Dr. Antonio Delgado en la nostra estada al CSIC, sense deixar de recordar molt especialment l'Antonio.

Finalment, però sense restar importància, volia agrair el suport de tots els companys que he tingut al llarg d'aquests quatre anys. Companys del CSIC, de farmàcia, Erasmus i màsters. Companys de vitrina, de despatx, de laboratori i de planta. Companys de mudances, de bikinis, de focaccias, de dinars amb taper i de dinars sense taper, de cervesetes a la gespa en època covid i de cervesetes al bar en èpoques covid free. Tot i no haver compartit projectes amb la majoria, heu sigut el millor acompanyament del meu doctorat, i l'heu amenitzat com ho fa un bon formatge al vi. Per acabar, amics, amigues, family, i totes aquelles persones que, sense saber de què va aquesta tesi, s'han interessat pel seu progrés casi més que jo mateixa: més que agraïda!

Marina Pedrola

Barcelona, Juny 2022

Index

Abbreviations

δ	Chemical shift
μW	Microwave
3-CR	3-component reaction
4-CR	4-component reaction
Aa	Aminoacid
ADME	Absorption, distribution, metabolism, and excretion
AHR	Aryl hydrocarbon receptor
Aq.	Aqueous
BBB	Blood–brain barrier
BIOS	Biology-oriented synthesis
CBD	Condition-based divergence
BFE	High bond-forming efficiency
CBX	Carbenoxolone
CNS	Central nervous system
COSY	Correlation spectroscopy
Cryo-EM	Cryogenic electron microscopy
CSIC	Spanish National Research Council
DBU	1,8-diazabicyclo[5.4.0]undec-7-ene
DCPIB	4-[(2-butyl-6,7-dichloro-2-cyclopentyl-2,3-dihydro-1-oxo-1H-inden-5-yl)oxy]butanoic acid
DHFR	Dihydrofolate reductase
DIDS	4,4'-diisothiocyano-2,2'-stilbenedisulfonic acid
DIEA	N,N-diisopropylethylamine
DMAP	4-dimethylaminopyridine
DMF	N,N-dimethylformamide
DMSO	Dimethyl sulfoxide
DOS	Diversity-oriented synthesis
EAA	Excitatory amino acids
HMBC	Heteronuclear multiple bond correlation spectroscopy
Eq.	Equivalents
HSQC	Heteronuclear single quantum coherence spectroscopy
EtOAc	Ethyl acetate
EU	European Union
FICZ	6-formylindolo[3,2-b]carbazole
FOS	Function-oriented synthesis
GBB	Groebke-Blackburn-Bienaymé
GFP	Green fluorescent protein
HPLC	High-performance liquid chromatography
IDIBELL	Institute of Biomedical Research of Bellvitge
IMCRs	Isocyanide-based multicomponent reactions
IUF	Leibniz Research Institute for Environmental Medicine
LC-MS	Liquid chromatography–mass spectrometry
LDA	Lithium diisopropylamide
LRRC8	Leucine-rich repeat-containing family 8
MCA	Middle cerebral artery
MCAO	Mouse model of transient occlusion of the middle cerebral artery
MCRs	Multicomponent reactions
MCR^2	Combining two (or more) different types of MCRs
MRS	Modulating reaction sequences
MRSA	Methicillin-resistant *Staphylococcus aureus*
NMDA	N-methyl-D-aspartate receptor

NMM	N-methylmorpholine
NMR	Nuclear magnetic resonance
NPPB	5-nitro-2-(3-phenylpropylamino)benzoic acid
PAL	Photoaffinity Labelling
PAPs	Photoaffinity probes
PDB	Protein Data Bank
PyBOP	Benzotriazol-1-yl oxytripyrrolidinophosphonium hexafluorophosphate
Rt	Room temperature
RVD	Regulatory volume decrease
RVI	Regulatory volume increase
SAR	Structure-activity-relationship
SMX	Sulfamethoxazole
SRR	Single reactant replacing
T2D	Type 2 diabetes
THF	Tetrahydrofolic acid
THF	Tetrahydrofuran
TLC	Thin-layer chromatography
TMP	Trimethoprim
TMS	Trimethylsilyl
TOS	Target-oriented synthesis
TPD	2,3,5-triphenyltetrazolium chloride
TTC	2,3,5-Triphenyltetrazolium chloride
UV	Ultraviolet radiation
VRAC	Volume-regulated anion channel
v/v	Volume/volume
WT	Wild type

Chapter I

General Introduction and Objectives

1.1. Introduction

1.1.1. Within the Boundaries of the Biological Activity Space

When considering the possible virtual molecules and the compounds that chemists would and could ever expect to make, the resulting number is so vast that it reminds to the immensity of the universe. Chemists worldwide suggested the metaphoric concept of "chemical space" to describe such idea, pointing out that the exploration of chemical space up to this point has been extremely limited.

Pushing the analogy further, molecules that can modulate biological processes are hardly ever identified among all the possible existing molecules. This happens because much of the chemical space contains nothing of biological interest, and "stars" (compounds with biological activity) are just found from time to time. However, luckily for researchers, those stars are not outspread throughout chemical space, but rather concentrated in a limited part named "biological activity space".[1,2] In such space, the most notably region is the "ADME space", which contains drug-like small molecules setting optimal properties in regard to the well-known Lipinski rules (Figure 1.1).[3]

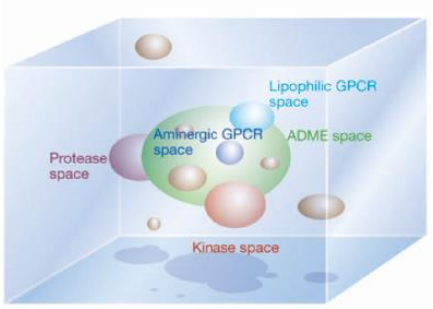

Figure 1.1. Representation of the metaphoric relation between the entire chemical space (light blue) and the areas occupied by compounds with specific affinity for biological targets. Examples of such biological molecules are those from major gene families (colored in brown), and other specific gene families (colored in purple, blue and orange). The green space refers to the intersection of compounds with drug-like properties (that is, the ADME space) (taken from Lipinski).[1]

Natural products coming from fungi, plants, bacteria, and marine organisms have historically been the models within the biological activity space.[4,5] Although they have served as inspiration for the development of many hits, leads and successful drugs, the actual problem is that most of the natural products target the same range

of “classical” proteins. Therefore, addressing undruggable and/or unprecedented biological targets must be based on innovative chemical structures, notably differing from the connectivity found in natural products.[6]

To a large extent, it is expected to find unexplored molecular diversity leading to innovation in drug discovery if chemistry is driven into the unknown biological activity space.[6] That is, to enhance the chances of inquiring as many diversified stars as possible, development of novel chemical reactivity, methodologies, and strategies that facilitate the quest are essential. Otherwise, using classical chemical methods would result a fruitless task considering the huge possibilities within the biological activity space yet to explore.

1.1.2. Main Synthetic Strategies in Organic Chemistry

Taking a retrospective look, Organic Chemistry has tackled the exploration of new biological activity space through two main strategies. On one hand, through the development of new reactions and synthetic approaches (like developing new reagents or new catalysts) that allow shortening chemical routes, thus facilitating the formation of novel complex structural types in a rapid manner (Figure 1.2, orange arrow). Secondly, through the development of chemical tools that simplify the structure of bioactive target compounds and allow rapid access to a large array of similar structural types. Examples of the latter methodologies are combinatorial chemistry, semi-synthetic strategies, and target, function, and diversity-oriented synthesis – referred to as TOS, FOS, and DOS, respectively (Figure 1.2, green arrow).

However, as the study of the chemical space is still underexplored, the development of approaches relying on both kinds of synthetic innovations are yet essential for keeping the progress.

Several meaningful reviews and research articles have summarized the impact of the strategies mentioned beforehand in providing molecular diversity and drug-like compounds of biological relevance.[7–14]

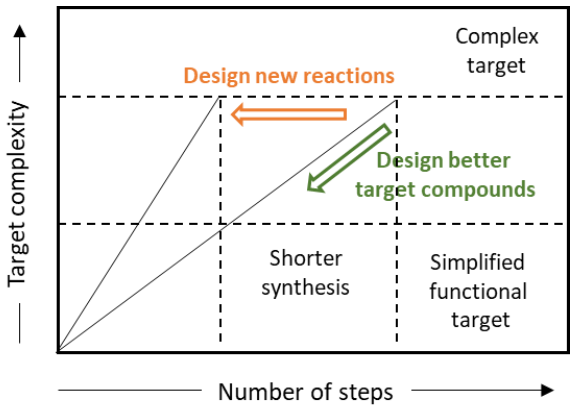

Figure 1.2. Improving the exploration of chemical space with new reactions or with simplified structural targets (adapted from Wender et. al.).[11]

1.1.3. Heterocyclic Compounds as Privileged Scaffolds in Medicinal Chemistry and Drug Discovery

Although marketed drugs usually cover an extended range of chemical structural types, the most common scaffolds among drug-like small molecules are aromatic heterocyclic moieties.

The central role of heterocycles in medicinal chemistry comes not only from the special physicochemical properties that they might confer to the whole molecule (such as suitable lipophilicity, solubility, or polarity, leading to improved ADME profiles), but also from the interactions with targets that both heteroatoms and cycloaromatic structures offer.[15,16] Besides, ring systems are known to take part in electronic distribution, dimensionality, and scaffold rigidity.[17] Hence, ring systems and heterocycles are extremely usual building blocks in drug discovery and are considered as “privileged structures”.

Back in 1988, Evans and coworkers conceived the concept of “privileged structures” for referring to those simple functionalization frameworks which provided products that selectively bind to different target proteins.[18] After that first description, the concept has been greatly introduced in medicinal chemistry in a way that, nowadays, privileged scaffolds are considered a requisite for the design of chemical screening libraries. Ideally, such collections of small molecules offer a great molecular diversity and are suitable for the rapid screening of ligands in front of a variety of targets. This

great structural variability has allowed the discovery of novel biologically active compounds in a wide range of therapeutic areas.

Some interesting reviews have organized heterocyclic commercialized drugs and bioactive compounds in advanced clinical trial stages on behalf of their activity, and also regarding the type of heterocyclic moieties that they contain.[15,16,19] Although the most commonly used heterocycles within those marketed drugs include nitrogen, sulfur, or oxygen heteroatoms in five or six-membered rings,[17] *N*-heterocyclic systems are the most abundant scaffolds. Thus, remarkable examples of classical drugs with *N*-heterocycle moieties are listed below (Figure 1.3).

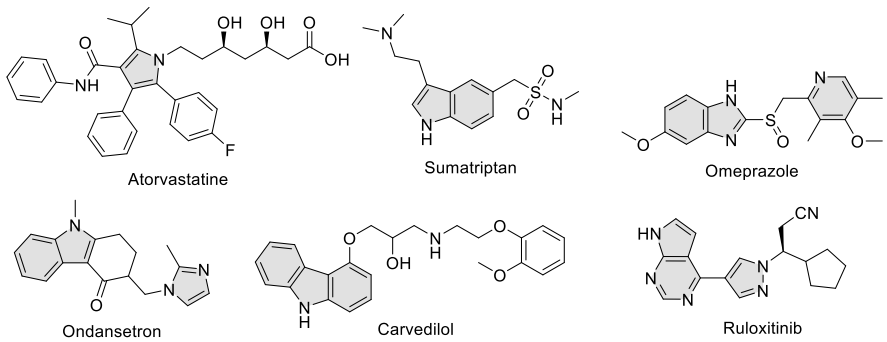

Figure 1.3. Meaningful drugs with *N*-heterocyclic scaffolds.

The great importance that heterocycles have in medicinal chemistry and drug discovery entail a growing interest in pushing chemistry to the discovery of novel methodologies that promote efficient and fast access to heterocyclic scaffolds. So, in this context, we highlight the significance of investigating new approaches, not only for the synthesis of heterocyclic structures from non-heterocyclic reactants, but also for examining the intrinsic reactivity of common heterocycles.[20]

1.1.4. VRAC, DHFR and AhR as Challenging Targets

The volume-regulated anion channel (VRAC), dihydrofolate reductase (DHFR) and aryl hydrocarbon receptor (AhR) are proteins with very different locations, properties, and activities. What they have in common, though, is the fact that the three of them present drawbacks and shortcomings when are considered as biological targets.

First, VRAC is a chloride channel ubiquitously expressed in the membrane of all over the cells. As most of the anion channels, selective and specific modulators have been hardly reported, and cryo-EM structures of VRAC together with some ligands only add more questions to the intriguing nature of its binding site. Many studies have related astrocytic VRAC with the neuronal damage observed after ischemic episodes in the brain, so VRAC has been considered as a potential target in stroke incidents (Figure 1.4).

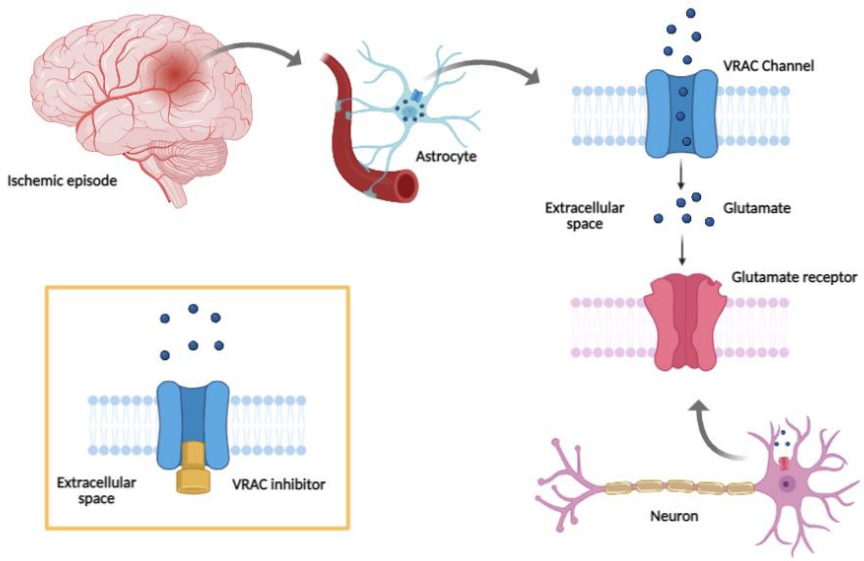

Figure 1.4. Hypothetic role of VRAC in ischemic episodes (created with BioRender.com).

DHFR is an enzyme involved in the folate metabolic pathway, essential for maintaining bacterial growth. Some drugs have been commercialized as effective DHFR inhibitors for treating bacterial infections. Even though, bacterial drug-resistances closely related to structural modifications on the DHFR binding site are emerging, and the known agents for treating bacterial infections become inactive. The occurrence of such drug-resistant bacteria, as the methicillin-resistant *Staphylococcus aureus* (MRSA) strain and multidrug resistant *Pseudomonas aeruginosa*, leads to a significant stress for health systems all over the world. As current available clinical treatments do not meet the urgent demand, finding new inhibitors to overcome the issue of antibiotic resistance is considered one of the world's most urgent public health challenges (Scheme 1.1).

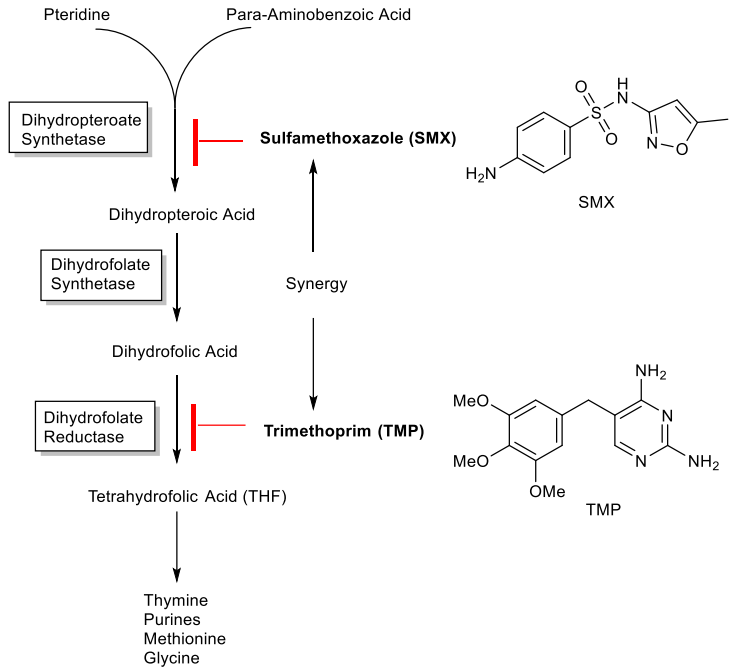

Scheme 1.1. DHFR in the pathway of the folic acid biosynthesis (adapted from Pedrola et. al).[21]

Finally, AhR is a transcription factor that works as a sensor detecting changes in the cellular environment. As cells are susceptible to molecular changes, some proteins integrate environmental, microbial, and endogenous signals into specific cellular responses by controlling gene expression. AhR not only regulates gene expression involved in a broad variety of physiological and pathological processes (like in immune response, xenobiotic metabolism, and carcinogenesis), but also works as an E3 ubiquitin ligase promoting proteasomal degradation of target proteins.[22–25] Thereby, targeting AhR might be regarded as a therapeutic strategy in autoimmune, neoplasm, and degenerative diseases. Due to its two-faced nature, either its activation or inhibition might be beneficial. 6-formylindolo[3,2-b]carbazole (FICZ) is among the most potent activators of AhR known so far. Although it was first identified over 20 years ago, nowadays there is a huge shortage in structure-activity-relationship (SAR) studies, probably due to the lack of efficient synthesis of FICZ and derivatives, together with poor information regarding the AhR binding pocket. Therefore, screening of

novel and assorted ligands is considered the main strategy for the development of future therapies targeting AhR (Figure 1.5).

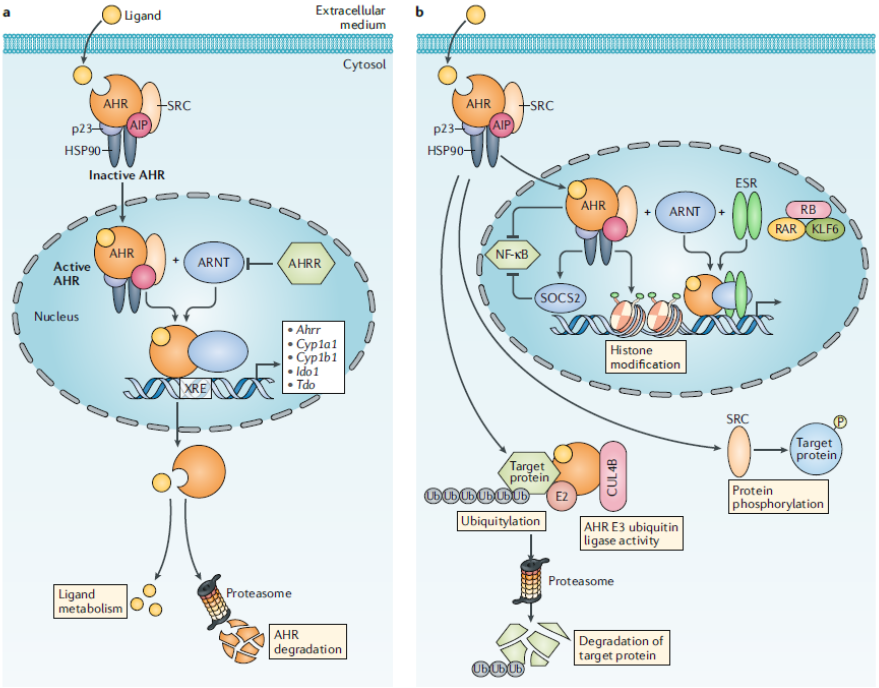

Figure 1.5. AHR signaling pathways (taken from Rothhammer et. al.).[22]

1.2. Objectives

In the present thesis, we focus on the investigation of innovative chemical strategies for the formation of novel and meaningful scaffolds. Such privileged structures might address challenging targets that face great drawbacks as lack of ligands and/or selective modulators. As a main requisite, novel processes must offer robustness, experimental facility, and wide structural diversity.

Besides focusing our research on the quest of bioactive molecules, we give close attention to total and semi-synthesis, and multicomponent reactions (MCRs), because of the great impact that these methodologies display in hit finding, drug and reaction discovery (Scheme 1.2).

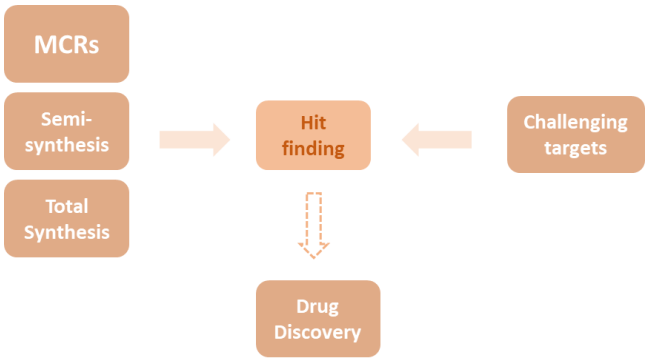

Scheme 1.2. Development of tools leading to advanced hits for underexplored targets.

The detailed goals of each chapter are described as followed:

Chapter II. Development of Novel Blockers of the Chloride Channel LRRC8/VRAC

- Prepare the original hits, based on a semi-synthetic strategy for the carbenoxolone (CBX) and a multistep synthetic route for the 4-[(2-butyl-6,7-dichloro-2-cyclopentyl-2,3-dihydro-1-oxo-1H-inden-5-yl)oxy]butanoic acid (DCPIB).

- Prepare structurally modified derivatives to get conclusions about the SAR. We design a hit process optimization to obtain less-complex target

compounds with comparable or superior biological function in a practical and even synthetically novel manner.

- Pharmacomodulate the original hits or the most potent derivatives to improve CNS penetration trough prodrug approaches or introduction of bioisosteres.

- Design a photo-probe based on the structure of a VRAC blocker to investigate the binding mode of our compounds with the residues along the binding site of the channel.

- Select the two most suitable hits, regarding the potency inhibiting the channel and the capacity of crossing the BBB, to scale-up them in suitable amounts for testing them in a rat model of stroke.

Electrophysiological experiments are performed in collaboration with Raúl Estévez and coworkers (from the Institute of Biomedical Research of Bellvitge, IDIBELL), while the in vivo test is performed by Carles Justicia and Anna Planas (from the Spanish National Research Council, CSIC)**.**

Chapter III. Multicomponent Reactions towards the Synthesis of Bioactive Compounds

Considering multicomponent reactions (MCRs) as a tool that facilitates chemical exploration and rapid synthesis of potential bioactive compounds, we have divided the chapter into the following blocks:

From Drugs to Drugs: towards Improved Antibiotics

- Incorporate marketed drugs in MCR approaches to obtain drug-derivatives with a different scaffold. Such task may require an optimization of reaction conditions.

- Prepare a library of Trimethoprim (TMP) derivatives by using the Groebke-Blackburn-Bienaymé (GBB) MCR. We may want to carefully select the components of the MCR, which should cover a wide structural range.

- Study the microbial growth inhibition of our set of compounds in Grampositive and Gramnegative bacterial strains.
- Select the two most potent TMP-derivatives and study their antimicrobial profile in detail.

Microbial experiments are performed in collaboration with Miquel Viñas and coworkers (from IDIBELL).

Extended MCRs with Indole Aldehydes

- Explore chemical synthetic procedures beyond MCRs. We aim to develop a novel methodology that allow us to access complex polyheterocyclic frameworks in a facile manner (in one-pot or two steps at most), using indole carbaldehyde as a key component.
- Prepare a library of novel AhR ligands with a wide variety of structural scaffolds up to several functionalization points.
- Study the role of the novel polyheterocyclic systems as AhR-activating agents.

Biological experiments are performed in collaboration with Thomas Haarmann-Stemmann and coworkers (from the Leibniz Research Institute for Environmental Medicine, IUF).

Bibliographic Revision

- Review recent publications about multicomponent reactions that incorporate heterocycles as inputs.
- Select and summarize the most impactful works to present the current state of the topic.

1.3. Bibliography

[1] C. Lipinski, A. Hopkins, *Nature* **2004**, *432*, 855–861.

[2] C. M. Dobson, *Nature* **2004**, *432*, 824–828.

[3] C. Lipinski, F. Lombardo, B. W. Dominy, P. J. Feeney, *Adv. Drug Deliv. Rev.* **1997**, *23*, 3–25.

[4] D. A. Dias, S. Urban, U. Roessner, *Metabolites* **2012**, *2*, 303–336.

[5] A. G. Atanasov, S. B. Zotchev, V. M. Dirsch, C. T. Supuran, *Nat. Rev. Drug Discov.* **2021**, *20*, 200–216.

[6] J. L. Reymond, R. Van Deursen, L. C. Blum, L. Ruddigkeit, *Medchemcomm* **2010**, *1*, 30–38.

[7] S. L. Schreiber, *Science.* **2000**, *287*, 1964–1969.

[8] M. Feher, J. M. Schmidt, *J. Chem. Inf. Comput. Sci.* **2003**, *43*, 218–227.

[9] M. D. Burke, S. L. Schreiber, *Angew. Chem. Int. Ed.* **2004**, *43*, 46–58.

[10] B. R. Stockwell, *Nature* **2004**, *432*, 846–854.

[11] P. A. Wender, V. A. Verma, T. J. Paxton, T. H. Pillow, *Acc. Chem. Res.* **2008**, *41*, 40–49.

[12] D. E. Bergbreiter, S. Kobayashi, *Chem. Rev.* **2009**, *109*, 257–258.

[13] W. R. J. D. Galloway, A. Isidro-Llobet, D. R. Spring, *Nat. Commun.* **2010**, *1*, DOI 10.1038/ncomms1081.

[14] E. Ruijter, R. Scheffelaar, R. V. A. Orru, *Angew. Chemie Int. Ed.* **2011**, *50*, 6234–6246.

[15] A. Gomtsyan, *Chem. Heterocycl. Compd.* **2012**, *48*, 7–10.

[16] J. Jampilek, *Molecules* **2019**, *24*, 10–13.

[17] R. D. Taylor, M. Maccoss, A. D. G. Lawson, *J. Med. Chem.* **2014**, *57*, 5845–5859.

[18] J. Kim, H. Kim, S. B. Park, *J. Am. Chem. Soc.* **2014**, *136*, 14629–14638.

[19] M. M. Heravi, V. Zadsirjan, *RSC Adv.* **2020**, *10*, 44247–44311.

[20] O. Ghashghaei, M. Pedrola, C. Escolano, R. Lavilla, in *Multicomponent React. Towar. Heterocycles* (Eds.: E.V. Van der Eycken, U.K. Sharma), WILEY-VCH GmbH, **2022**, pp. 1–43.

[21] M. Pedrola, M. Jorba, E. Jardas, F. Jardi, O. Ghashghaei, M. Viñas, R. Lavilla, *Front. Chem.* **2019**, *7*, DOI 10.3389/fchem.2019.00475.

[22] V. Rothhammer, F. J. Quintana, *Nat. Rev. Immunol.* **2019**, *19*, 184–197.

[23] A. Mejía-García, E. González-Barbosa, C. Martínez-Guzmán, M. A. Torres-Ramos, M. S. Rodríguez, S. Guzmán-León, G. Elizondo, *Toxicology* **2015**, *337*, 47–57.

[24] F. Ohtake, Y. Fujii-Kuriyama, S. Kato, *Biochem. Pharmacol.* **2009**, *77*, 474–484.

[25] F. Ohtake, A. Baba, I. Takada, M. Okada, K. Iwasaki, H. Miki, S. Takahashi, A. Kouzmenko, K. Nohara, T. Chiba, Y. Fujii-Kuriyama, S. Kato, *Nature* **2007**, *446*, 562–566.

Chapter II

Development of Novel Blockers of the Chloride Channel LRRC8/VRAC

2.1. Introduction and Background

2.1.1. Epidemiology of Stroke

Stroke is the second leading cause of death after heart disease in Europe, and a common cause of adult disability. It affects around 1.1 million inhabitants of Europe each year and, according to the most recent report, in 2017 stroke accounted for 405.000 deaths (9%) in men and 583.000 (13%) deaths in women.[1,2]

As Europe is currently facing an increase in the ageing of population, both the incidence and the prevalence of stroke will inevitably continue to rise over the next years (Graphic 2.1a,b). Similarly, the corresponding costs directly linked to stroke events, including the long-term sequels, health care overall costs, and productivity losses are expected to follow the same trend. On the contrary, most European Union (EU) countries have reported significant declines in stroke mortality rates (Graphic 2.1c). Those improvements are linked to advances in therapeutic options and acute management of the disease over the recent years.[3] Overall, these data suggest an urgent need to keep investigating and developing new treatments and post-stroke therapeutic strategies to handle the situation.

Nowadays, emergency treatments of ischemic strokes mainly consist in restoring the blood flow in the patient's brain through invasive procedures or delivering systemic drugs that quickly remove the cause of the stroke. However, the speed in managing the incident is critical, as not treating a stroke rapidly enough would not only reduce changes of survival, but also increase complications and sequels.

(a)

(b)

(c)

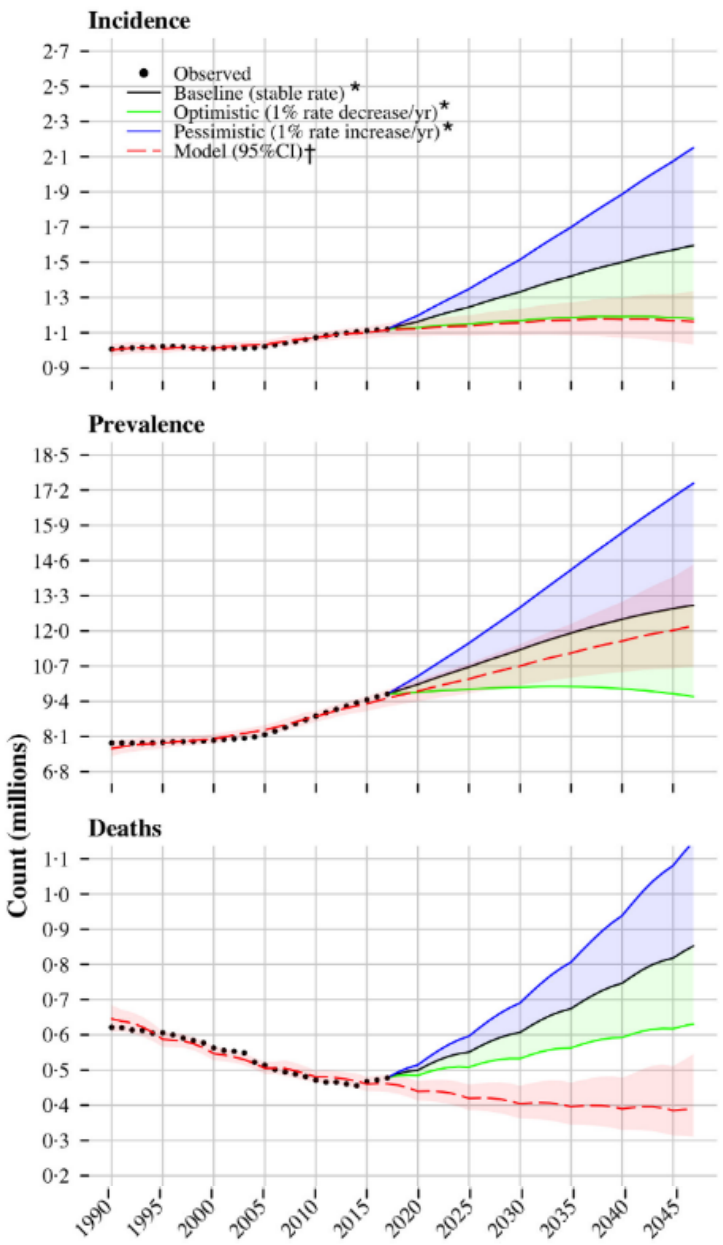

Graphic 2.1. (a) Prevalence; (b) Incidence; and (c) Deaths caused by stroke within the EU (taken from Wafa et. al).[3]

2.1.2. Cell Volume Regulation

As most mammalian cell membranes are highly permeable to water, whenever the osmotic equilibrium of a cell is perturbed, a net transport of water across the plasma membrane is induced and therefore, there are cell volume changes. These changes in cell volume have to be restored to prevent excessive swelling or shrinking, in order not to harm the integrity of the cell and its surrounding tissue, eventually keeping back the homeostasis.[4,5]

Regulatory measures restoring the original cell volume are called regulatory volume decrease (RVD) and regulatory volume increase (RVI), respectively. Cells employ multiple transporters and ion channels in the volume regulation processes, which are responsible for the net transport of ions and organic osmolytes across the plasma membrane. Aiming protection against excessive cell swelling, the VRAC channel is a key player in RVD, since it is activated by cell swelling and mediates efflux of Cl^- and organic osmolytes (including glutamate and aspartate), followed by release of water (Scheme 2.1).[6-8]

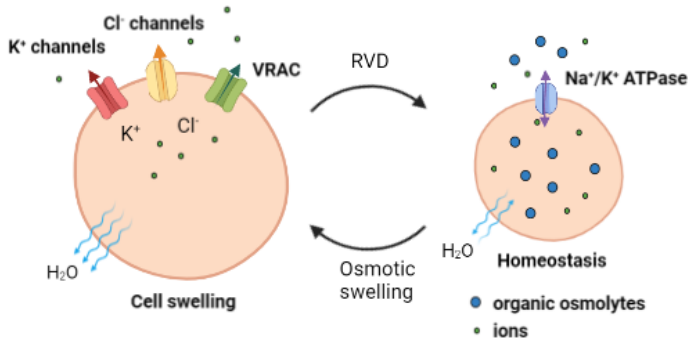

Scheme 2.1. Schematic overview of transporters involved in RVD (created with BioRender.com).

Cell volume changes can be the result of general physiological processes, including cell migration and proliferation, epithelial absorption and secretion, cell differentiation or apoptotic induction; or on the other hand, they can be caused by pathological conditions like hypoxia, ischemia, or intracellular acidosis.[4]

2.1.3. VRAC Channel

Volume-regulated anion channels (VRACs) are channels distributed in the membranes of most mammalian cells. They are ubiquitously expressed in vertebrate systems, so they have multiple roles under physiological conditions. VRACs remain closed under resting conditions but become activated upon increases of cell volume. Thereby, they are deeply involved in cell volume regulation and related processes, playing a part in cell proliferation, migration, apoptosis, cell division, growth, and release of physiologically active molecules. The latter process includes the release of excitatory amino acid neurotransmitters (EAA), like glutamate and aspartate, in the brain, thus promoting astrocyte-neuron signaling. Lately, some articles have uncovered the emergence of unexpected roles beyond volume regulation, such as putative roles in immunological and metabolic processes (Figure 2.1).

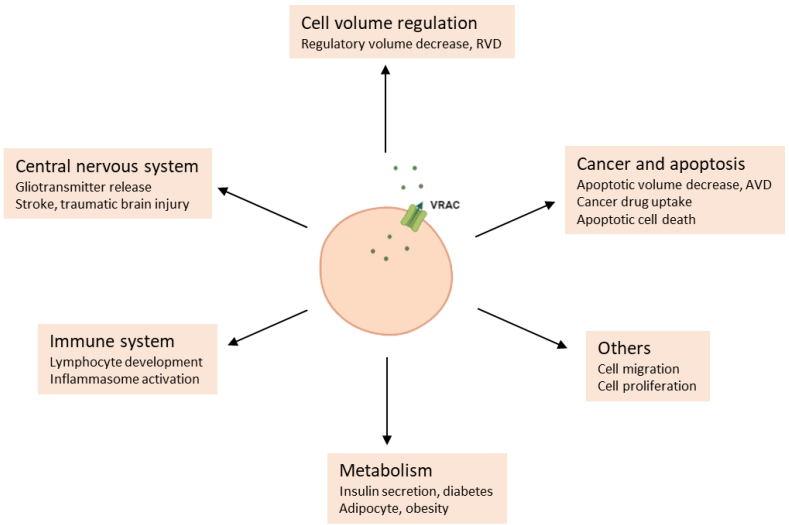

Figure 2.1. Proposed roles of VRAC in cell biology, physiology, and disease (adapted from Osei-Owusu et. al.).[11]

Many significant reviews summarizing the progress in the identification of biophysical properties, molecular structure, physiological and pathological implications, and pharmacology of the channel since it was discovered have been published.[6,9–13]

2.1.4. Considering Astrocytic VRAC as a Therapeutic Target

Pathological Activation of VRAC during Ischemic Episodes

In what concerns us, astrocytic VRACs are rather appealing as they are also involved in pathological processes.[6,8,11,13–17] Astrocytes, which are the most numerous cells within the brain, are known to be profoundly swollen in some brain pathologies. Presence of blood clots and lack of oxygen during stroke cause astrocytes to undergo sustained swelling via yet undefined mechanisms. VRACs become open after detecting such abrupt increases in cell volume leading to compensatory mechanisms as the beforehand mentioned RVD. In the response to this osmotic swelling, VRAC channels aim to restore homeostasis by releasing Cl^- and glutamate, which accumulate in the extracellular space. The excess of glutamate stimulates over activation of neuronal glutamate receptors, in particular the *N*-methyl-D-aspartate (NMDA) receptor, thus persistently depolarizing neurons. This prolonged depolarization causes pathological increases in the intracellular Ca^{2+} levels and ultimately promotes neuronal harm while killing neurons. The whole process of glutamate receptor-dependent cell damage and death is known as excitotoxicity (Figure 2.2).[18,19]

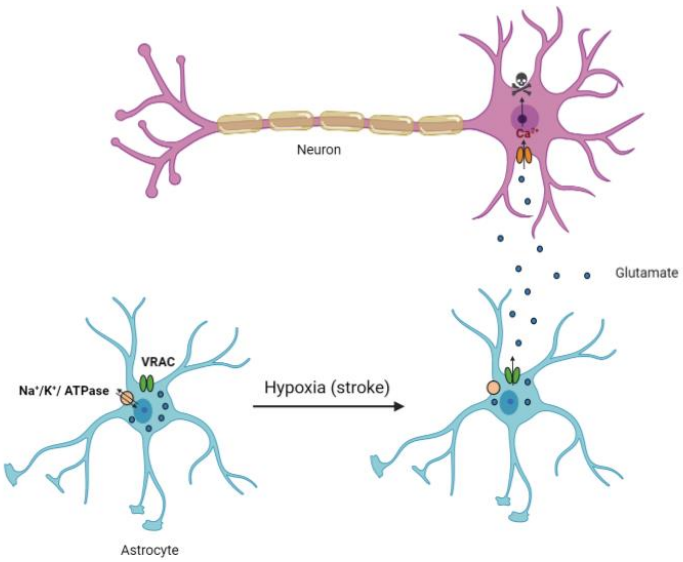

Figure 2.2. Hypothetical representation of the excitotoxicity process involving pathological swelling of astrocytes, which triggers glutamate release via VRAC (in green). Increased glutamate levels cause Ca^{2+} -dependent damage and death of neurons due to excessive activation of neuronal glutamate receptors (in orange) (created with BioRender.com).

Pharmacological Background and Structural Identity of VRAC

Administration of VRAC blockers in rodent models of cerebral ischemia have shown to potently protect the brain against damage, whereas in vitro assays confirmed that such inhibitors suppress the ischemic glutamate release.[20,21] Altogether, those results confirm excitotoxicity as a feasible mechanism after VRAC activation, support the pathological contribution of VRAC to stroke damage, and suggest the channel as a promising therapeutic target in the pathology.

Even though, there are two big challenges when considering VRAC as a therapeutic target in stroke. One obstacle is related to the lack of selective pharmacological agents that block or modulate the VRAC activity. Since there had not been many chemical studies focused on finding new VRAC modulators, a specific class of inhibitors has not been discovered yet. There are broad spectrum Cl^- channel inhibitors such as 5-Nitro-2-(3-phenylpropylamino)benzoic acid (NPPB), 4,4′-Diisothiocyano-2,2′-stilbenedisulfonic acid (DIDS), and 4-[(2-Butyl-6,7-dichloro-2-cyclopentyl-2,3-dihydro-1-oxo-1H-inden-5-yl)oxy]butanoic acid (DCPIB);[22] anti estrogens drugs as tamoxifen and nafoxidine;[23–25] or steroid like derivatives as β-estradiol and carbenoxolone (CBX)[24] that exhibit limited VRAC selectivity and consequently have multiple off-target effects (Figure 2.3). For instance, although tamoxifen is extensively used in the treatment of estrogen-receptor-sensitive breast cancer, over the years it was considered as a quite useful VRAC blocker. However, tamoxifen has also been studied as a Na^+ and K^+ blocker, concluding that it hardly discriminates between anionic and cationic channels.[14]

Among them all, in vitro and in vivo studies support that intracisternal administration of both CBX and DCPIB provide strong neuroprotection in brain ischemic models, but they appear to not cross the blood brain barrier (BBB) as are not effective when given intravenously. However, they still seem to be the most active, potent, and selective VRAC blockers known so far.[26–29]

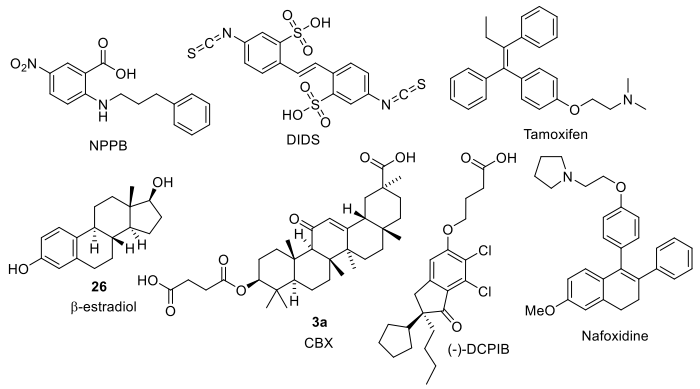

Figure 2.3. VRAC blockers.

The second hurdle is the deficient information regarding the structural identity of the channel and how modulators interact with it. The molecular nature of VRAC remained unknown for several decades, creating therefore difficulties for progressing in the field. Based on the homology of VRAC with pannexins,[30–32] in 2014 two research teams identified leucine-rich repeat-containing family 8 (LRRC8) heteromers as the pore-forming components of VRAC.[33,34] VRAC is composed of hexamers of LRRC8 family proteins, which comprise five members, LRRC8A-E. The LRRC8A unit is essential and must heteromerize with at least one other LRRC8 member to keep the normal physiological function (Figure 2.4a).[35,36] There so, LRRC8A can combine with two or more LRRC8 members in the same complex with a variable subunit stoichiometry; that is to say, the existence of a large number of VRACs with different subunit configurations is conceivable. Such specific subunit combinations may confer alteration on biophysical properties and associated functions of the channel. Besides, the subunit combination promotes substrate specificity. For instance, while subunits LRRC8B and LRRC8E mediate chloride currents in heteromers with LRRC8A, LRRC8D increases the permeability for larger osmolytes as taurine, lysine, or some drugs like cisplatin and the antibiotic blasticidin, thus promoting the uptake of such compounds into cells.[37,38]

More recently, five different research groups have resolved high-resolution cryo-EM structures of LRRC8A complexes, confirming the hexameric composition of the LRRC8/VRAC channel.[39–43] It is worthy to emphasize that these structures are of LRRC8 homomeric channels, which are unclear to exist in vivo (Figure 2.4b,c). One of

the described cryo-EM structures shows LRRC8A homomeric channels blocked by DCPIB, which plugs the channel like a cork in a bottle, sterically occluding ion conduction. The negatively charged butanoic acid group of DCPIB appears to interact with a ring of positively charged arginine residues (R103) located at the *N*-terminus of EH1, while the remainder of the molecule is extracellular to this region (Figure 2.5a,b).[42]

Unexpectedly, in 2021 another cryo-EM structure revealed that the interaction between a special class of synthetic nanobodies (which are small antibodies) and cytoplasmatic LRR domains of LRRC8A was crucial for allosteric modulation of the cannel activity (Figure 2.5c).[44]

Although many efforts are ongoing in this field, the regions and residues involved in the modulators interaction within the binding site of the channel remains ambiguous, as well as the relevance of the LRRC8 combination regarding the behavior of the channel.

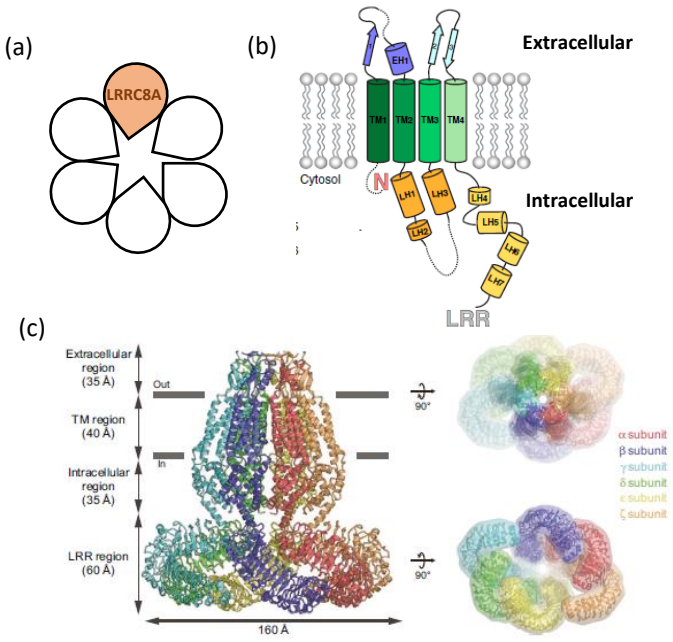

Figure 2.4. Structure of VRAC. (a) Multimeric composition of LRRC8 complexes based on pannexin homology. LRRC8A (in orange) is an obligatory component of the complex and has to be heteromerized with at least one of the other members of the LRRC8 family to form a functional channel. (b) Schematic representation of the structure of a single LRRC8 subunit in a LRRC8 hexamer (taken from Kern et. al.).[42] (c) Structure of an LRRC8A hexamer (PDB 5ZSU) viewed parallel to the membrane (left) and from the intracellular side (right) (adapted from Kasuya et. al.).[39]

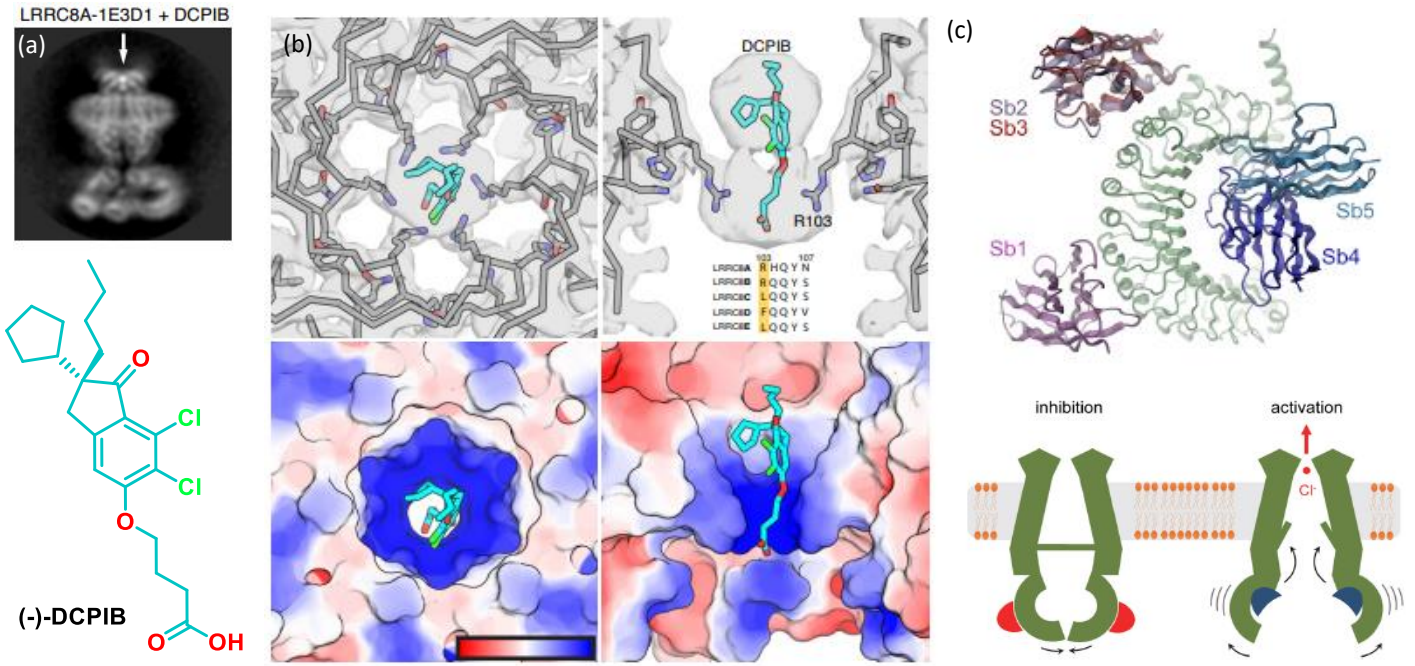

Figure 2.5. VRAC binding sites. (a) Representation of VRAC complexed with DCPIB (marked with an arrow) and DCPIB structure (oxygens are colored red, chlorines green, carbons teal).[42] (b) Views of the DCPIB-binding site (ring of R103 residues). In the upper schemes the atomic model is shown as ribbons and sticks. In the lower representation, the atomic surface is colored by electrostatic potential (color scale drawn on the left panel).[42] (c) Representation of the of antibodies binding sites on the LRR domain of LRRC8A in the upper image. Schematic depiction of the allosteric modulatory mechanisms of synthetic nanobodies (both inhibition and activation) in the lower images.[41]

2.1.5. Bases of Photo-cross-linking: Photoaffinity Labelling (PAL)

Photoaffinity Labelling (PAL) was first developed in the 1960s as a potential photochemical method for mapping the active site of enzymes.[45] Since then, PAL has emerged as a key tool in chemical biology for identifying ligand targets, measuring protein-protein interactions, and investigating protein structures and, indeed, binding site mapping.[46–48]

PAL compounds (commonly known as photoaffinity probes – PAPs) contain a photo-cross-linking unit, which is of fundamental necessity, directly linked to a bioactive motif. The bioactive unit recognizes the binding site of the biological target, while the photo-cross-linker generates a highly reactive intermediate upon irradiation with a specific wavelength.[47] Subsequently, the reactive species reacts irreversibly with the surrounding atoms of the target protein near the binding site residue[45] allowing therefore to identify and map it, likely by proteomic techniques (Scheme 2.2).[49]

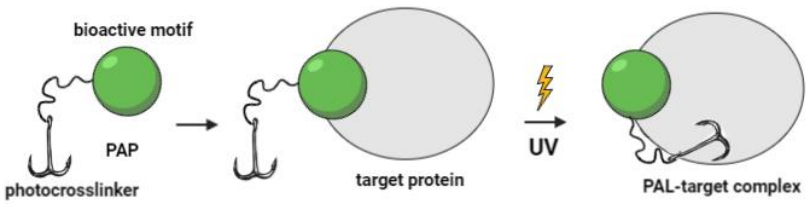

Scheme 2.2. PAP covalently bind to a target protein (created with BioRender.com).

Three usual photoreactive groups are used as photo-cross-linkers in PAL. They are benzophenones, aryl azides, and diazirines, each of them with a specific photoreactive activation mechanism (Scheme 2.3a).[50] While benzophenones generate a reactive diradical, aryl azides and diazirines give raise to nitrenes and carbenes, respectively.

Either way, photoreactive diazirines have several advantages over benzophenones and aryl azides: they are stable at room temperature, stable to nucleophiles, acidic and alkaline conditions, and small (in the case of small molecules, the photophore should be as small as possible in order to generate a suitable mimic of the original ligand); they have a short lifetime upon photoactivation with high subsequent reactivity; and they cross-link upon exposure to longer-wavelengths (360 nm), reducing damage to the targeted proteins (which occurs below 300 nm) (Scheme

2.3b).[46,47,50] The photolabeling mechanism of diazirines exploits the ability of the carbene specie to rapidly form a covalent bond by insertion into the nearest groups of the target molecule, which can be C-H, O-H, S-H and N-H (Scheme 2.4).

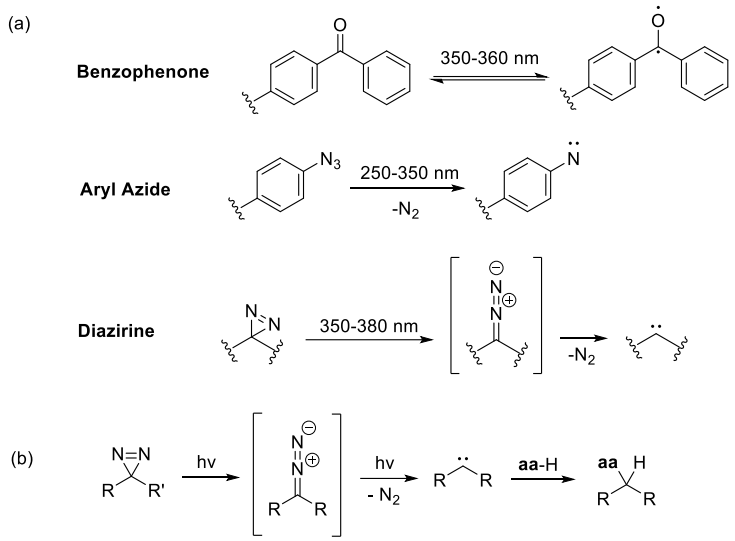

Scheme 1.3. (a) Most common photoreactive groups used as photo-cross-linkers. (b) Photo-activation mechanism of diazirines.

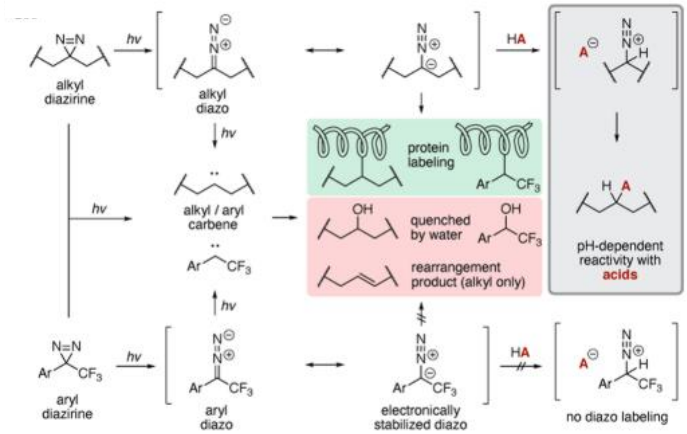

Scheme 2.4. Overview of diazirine reactivity pathways. Alkyl and aryl diazirines form carbene and diazo intermediates upon irradiation. Carbenes label nearby proteins but are rapidly quenched if no protein substrate is around. Alkyl diazo intermediates react selectively with acids, while electronically stabilized aryl diazo intermediates do not.

2.2. Results and Discussion

As a first approach to this new research, we selected two promising hits from the existing pool of compounds exhibiting VRAC blocking activity. Among the blockers regarded beforehand, we decided to focus on the two most active and selective, CBX and DCPIB (Scheme 2.5). As a basic requirement for the initial phase of the project, we aimed to find fast, facile, and easily reproducible synthetic routes for both CBX and DCPIB. Once they were obtained, we wanted to introduce straightforward structural changes to a parent compound that would easily provide us with new families of modified hits. Our main objective, besides finding more potent VRAC blockers, was to improve the BBB permeability of our hit compounds by means of different strategies.

In the context of CNS drug discovery, it is well-stablished that the BBB can be relatively impermeable to negatively charged carboxylates.[51] There so, different approaches are usually required to overcome possible shortcomings and finally target the CNS. Such strategies include chemical modifications as the introduction of isosteres and suitable carboxylic acid surrogates,[52] or the formation of ester and amide prodrugs;[53] but also comprise brain delivery strategies that require physical techniques, like employing nanoparticles or direct brain injections.[54]

First, the steroid-like CBX (**3a**) fitted with our necessities since its parent compound, the well-known glycyrrhetinic acid (**1**), easily admits structural modifications on the lowest alkyl chain. **3a** is the hydrolysis product of **1**, a natural triterpenoid found in liquorice roots (Scheme 2.5a). While **1** has expectorant and antiulcer properties, **3a** has been described as a VRAC blocker after showing evidence of suppressing the release of EAA neurotransmitters induced by hypotonicity in cultured astrocytes.[26] However, the main challenge that **3a** faces due to its acidic nature is the low probability of crossing the BBB. To enhance the BBB permeability of **3a** and derivatives, we decided to employ carboxylic acid surrogates in a new generation of derivatives. Hydroxamic acids are the groups we replaced them with, since they exhibit moderately acidic characteristics (pKa ~ 8-9) compared to the original function (pKa ~ 4-5) (Figure 2.6a).[52]

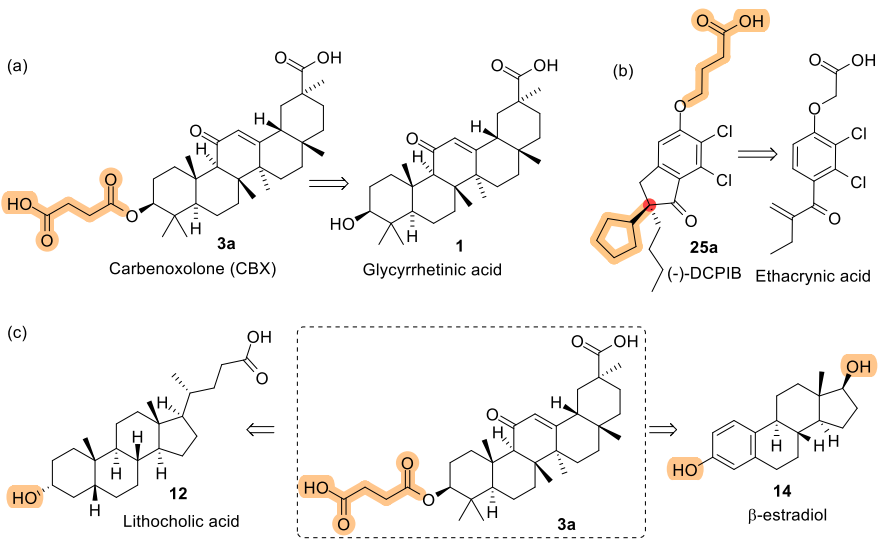

Scheme 2.5. General structures of (a) CBX; (b) DCPIB; and (c) Lithocholic acid and β-estradiol.

The second family of our library involved derivatives of the already known DCPIB (**25a**). **25a** is a derivative of the diuretic drug ethacrynic acid, which is commercially available since the 1960s. In the 80s, a group of chemists designed compounds for the treatment of cerebral edema based on ethacrynic acid derivatives with an indane moiety in their structure, which were free of diuretic activity (Figure 2.5b).[55] In the in vitro assays of the new set of compounds in rat primary astrocyte cultures, they interestingly determined that the derivative **25a** inhibited astrocyte swelling. Some years later, **25a** was confirmed to block the VRAC channel and therefore reduce EAA release involved in astrocyte swelling.[27,29,56,57] Nowadays, DCPIB is the most potent VRAC blocker known to date, even though in high doses it also blocks connexins, glutamate transporters, and proton pumps.[28] Our specific goal for this family was to simplify the preparation of the target **25a**, while improving its BBB permeability and selectivity. On one hand, the obtention of the active enantiomer of DCPIB requires a complex chiral resolution since it has a stereocenter. For that reason, we thought that making a non-chiral compound thus maintaining the blocking activity would facilitate the chemistry work. On the other hand, we considered appropriate to follow an ester prodrug strategy to design a series of compounds capable to cross the BBB. Once across it, these prodrugs would be modified by brain esterases that cleave the ester

function and liberate the active drug. In this case, we decided to use esters, since they have a more ideal hydrolysis rate than amides (Figure 2.6b).[53]

Based on the previously discussed background and inspired by the structure of **3a**, we considered appropriate to complete our library of potential VRAC blockers by checking out the behavior of some new steroid-like derivatives. We chose the steroids lithocholic acid (**12**) and β-estradiol (**14**), since their structures admitted further modifications resembling the original CBX (Scheme 2.5c). So, by simply adding an alkyl chain in the lowest alcohol and phenol functions, respectively, we obtained the last two new derivatives.

In this context, with the aim of enlarging the structural variability, we decided to further modify the scaffolds of DCPIB and CBX, thus obtaining a small new family of hybrid compounds. Diphenyl fragments were proposed as substitutes of the upper alkyl chain of DCPIB derivatives (Figure 2.6c). Likewise, in the synthetic plan of the new hybrid derivatives, ester intermediates were considered as useful prodrugs for enhancing the BBB permeability.

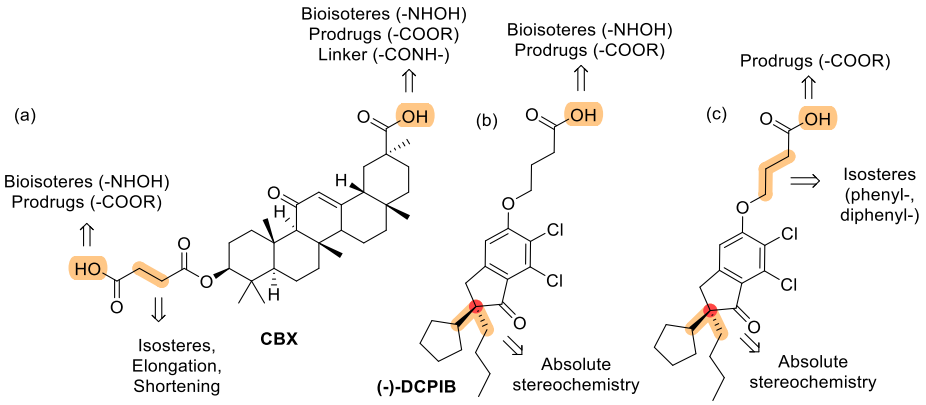

Figure 2.6. Planned modifications for (a) CBX; and (b) DCPIB. (c) Formation of hybrids between CBX and DCPIB structures.

2.2.1. Chemistry

For the preparation of CBX (**3a**) and further derivatives, we started by planning a semisynthetic approach based on the functionalization of **1**. The synthetic pathway of the first generation of derivatives (compounds **3a-f**, **5**, **6**, **7** and **9**) is outlined in Scheme 2.6. It mainly involved simple modifications on the ester chain of the original compound **1**, which included chain elongation, introduction of heteroatoms, and eventually the establishment of isostere groups, such as phenyl- and diphenyl-substitutes.[58] Compounds **3a-f** were prepared in a single step by coupling the subset of selected anhydrides (**2a-f**) with the parent compound **1**.[59,60] Additionally, three inactive controls (**6**, **7** and **9**) were prepared by the simple esterification of **1** and **3a**, respectively.[61] Finally, the dimer **5** was synthesized with a diamino hexane linker,[62] aiming to explore the space availability of the channel pocket or possible proximity effects (Figure 2.6).

With the second generation of CBX-derivatives, we introduced hydroxamic acids as carboxylic acid surrogates to increase the BBB permeability. Since the direct introduction of hydroxamic acids did not work as expected, Scheme 2.7 depicts the strategy we used. Following our approach, final compounds **11b-d** were prepared from the corresponding derivatives **3c**, **3e**, and **3f**. The activation of such precursors with *N*-methylmorpholine and isobutyl chloroformate was followed by the condensation of *O*-benzylhydroxylamine[63] at the less congested acid position, allowing the formation of intermediates **10a-d** (their corresponding structures were well-stablished through NMR spectroscopy, see page S26-28). The benzyl fragment was further removed through catalytic hydrogenation (10 % Pd/C, H_2) to finally yield the free hydroxamic acids **11b-d**. The inactive control **11a** was synthesized by esterifying the original acid **1** with iodomethane. Likewise, the final product **11a** was obtained following the procedure reported above, without relevant modifications (Scheme 2.7).

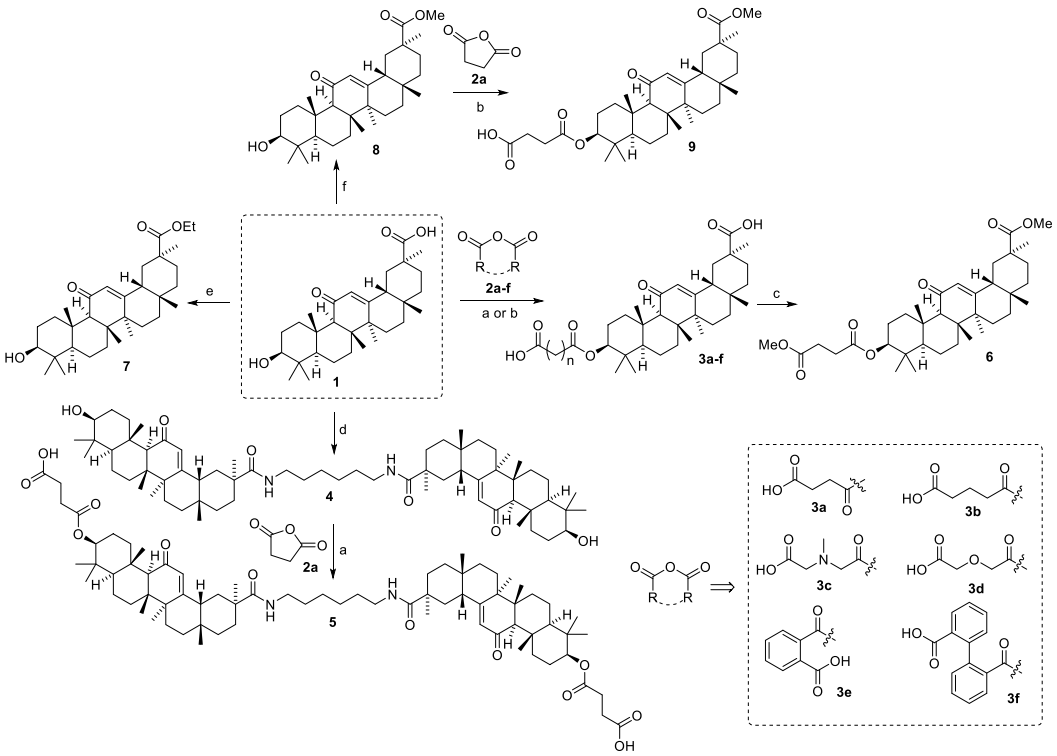

Scheme 2.6. Reagents and conditions: (a): anhydride **2**, DMAP, pyridine, reflux, overnight; (b) anhydride **2**, DMAP, pyridine, 160 °C, 1:30 hours, μW irradiation; (c): $TMSCHN_2$, MeOH/toluene (3:2), rt, 48 hours; (d): hexamethylenediamine, PyBOP, DIEA, DMF, rt, overnight; (e): ethyl iodide, K_2CO_3, DMF, rt, 24 hours; (f): iodomethane, K_2CO_3, DMF, rt, 24 hours.

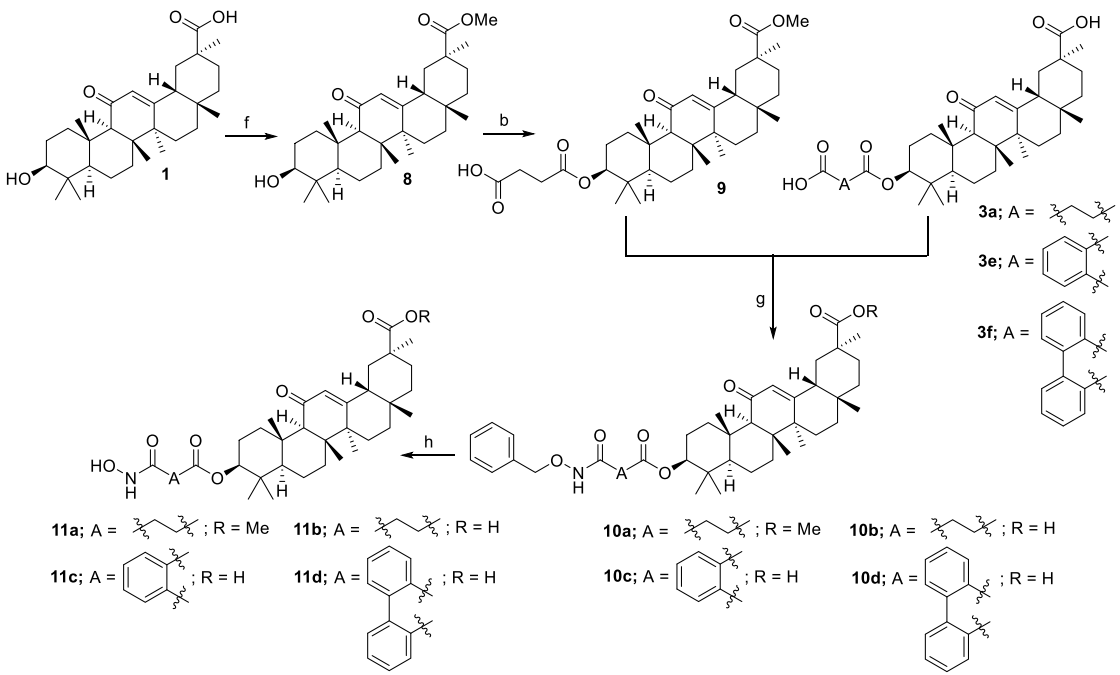

Scheme 2.7. Reagents and conditions: (f): iodomethane, K_2CO_3, DMF, rt, 24 hours; (b) succinic anhydride, DMAP, pyridine, 160 °C, 1:30 hours, μW irradiation; (g): NMM, isobutyl chloroformate, 20 °C, 3 hours; BnO-NH_2 · HCl, DIPEA, DMF, rt, overnight; (h): H_2, Pd/C, CH_2Cl_2, rt, 4 hours.

Interestingly, compound **3f** and related derivatives (intermediate **10d** and hydroxamic acid **11d** bearing the diphenic residue) were still eligible for further pharmacology studies, as we discarded their possibility of displaying a new chirality element at ambient conditions. Even though they have a potential atropoisomeric motif in their structure and follow complex ^{1}H NMR and ^{13}C NMR patterns, ^{1}H NMR experiments at higher temperature (65 ˚C) using DMSO as solvent showed the presence of a single compound (^{1}H NMR experiments were recorded at 25, 45 and 65 ˚C, see full spectroscopy studies at S24).

Finally, the last family of steroid-like derivatives was conveniently prepared from commercially available lithocholic acid (**12**) and β-estradiol (**14**), as shown in Scheme 2.8. First, acid **12** was reacted with succinic anhydride (**2a**) in the same way than before to obtain the ester **13**. On the other hand, the phenol function of compound **14** was involved in a Williamson reaction with ethyl-4-bromobutyrate to yield the intermediate **15**. The ester group was finally hydrolyzed while the upper alcohol position was acetylated in the same acidic media, thus obtaining the final derivative **16** (Scheme 2.8).

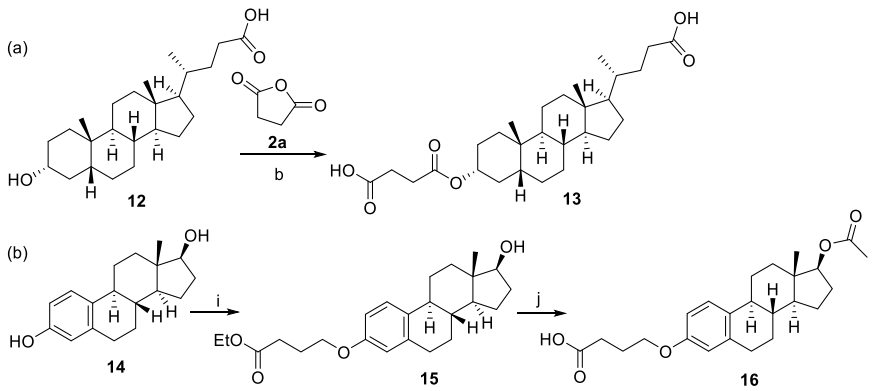

Scheme 2.8. Reagents and conditions: (a): DMAP, pyridine, 160 ºC, 1:30 hours, μW irradiation; (i): K_2CO_3, ethyl-4-bromobutyrate, acetone, reflux, 48 hours; (j): HCl, AcOH, reflux, 7 hours.

As shown in Scheme 2.9a, the *racemic*-DCPIB (**25a**) and the corresponding analog compounds **24a-b** and **25b** were obtained by adapting and improving the original synthetic pathway.[55,64,65] The reported route started with the methoxybenzene derivative **18**; in our case the phenoxy compound **18** was prepared by reacting the

commercially available 2,3-dichlorophenol **17** with an excess of iodomethane. Then, compound **18** was treated with hexanoyl chloride and aluminum chloride to obtain the para-substituted methoxybenzene **19**. The resulting compound **19** underwent a methylenation in the α position of the carbonyl group giving structure **20**, which was later cyclized under acidic conditions through a Nazarov reaction to obtain the fused methoxybenzene cyclopentanone **21**. The α position of the cyclopentanone **21** was further alkylated using the appropriate alkyl halide, either bromocyclopentane or 1-bromobutane yielding derivatives **22a-b**, respectively. Phenols **23a-b** were prepared by using harsh deprotecting conditions. Then, the Williamson reaction to obtain the inactive controls **24a-b** was carried out with ethyl-4-bromobutyrate and, finally, the hydrolysis in acidic media of esters **24a-b** afforded the final compounds **25a-b** bearing a carboxylic acid at the terminal position of the aliphatic chain. Compounds **24a** and **25a** were obtained as a racemic mixture, while **24b** and **25b** were achiral (Scheme 2.9a).

The preparation of the family of hybrid compounds consisted of a convergent synthetic route split into two parts (Scheme 2.9b). First, the obtention of the diphenyl fragment **26** started from the commercially available diphenic anhydride **2f**, which was opened with MeOH, and the corresponding monoester further reduced to the hydroxy derivative. The resulting intermediate **26** was coupled with subsequent hydroxy-indanes **23a-b** (which are common intermediates with the precedent synthesis) by using an adapted Mitsunobu protocol. In the same way than in the previous family of DCPIB derivatives, the esters were hydrolyzed to the corresponding carboxylic functions at the meta positions of the diphenic motif, giving **28b**. In this case, we discarded the preparation of **28a** (R = cyclopentyl) due to synthetic complexity, after checking that the activity values of **25a** were comparable to the ones of **25b** (see below, Scheme 2.9b).

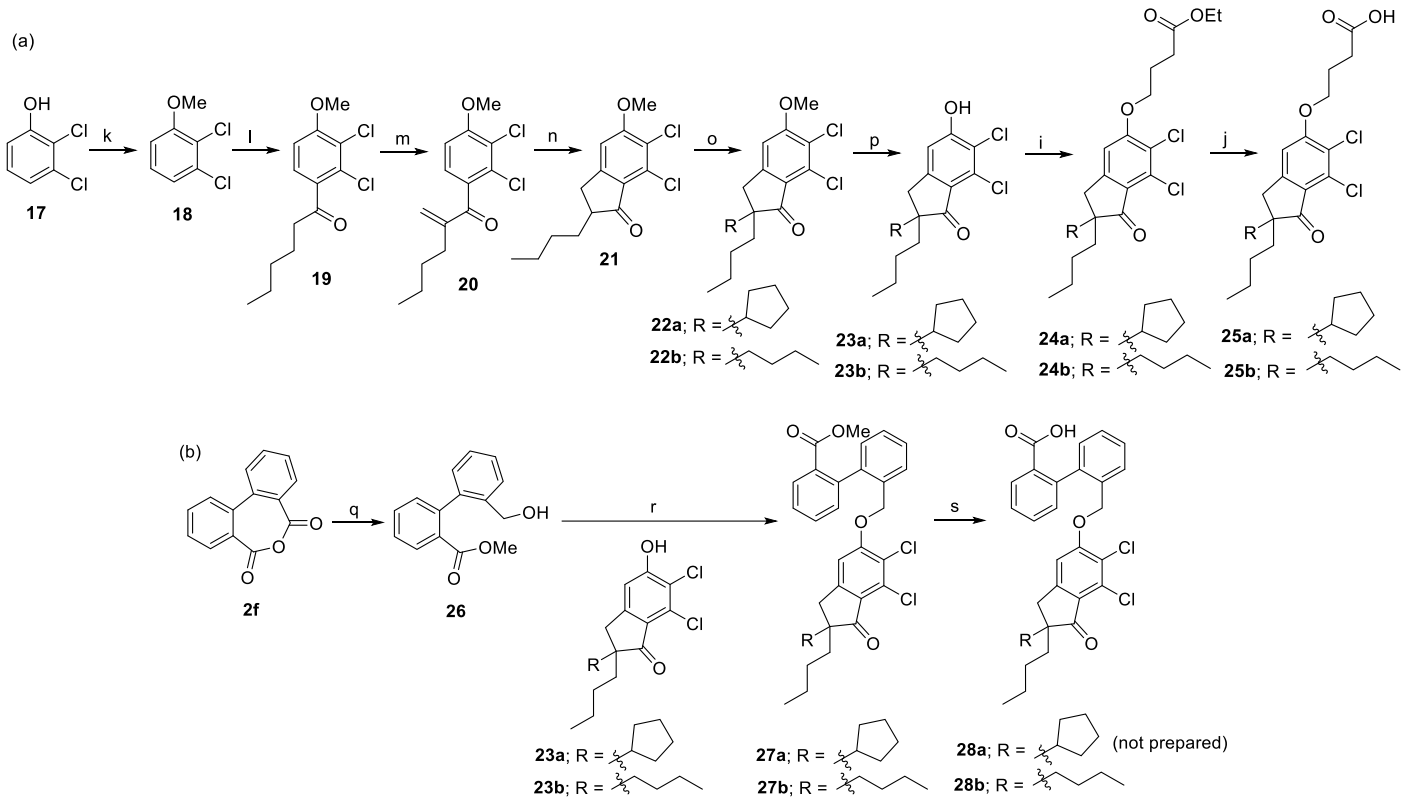

Scheme 2.9. (a) Reagents and conditions: (k): 1) DBU, CH_2Cl_2/toluene, reflux, 1 hour; 2) iodomethane, reflux, overnight; (l): $AlCl_3$, hexanoyl chloride, CH_2Cl_2, rt, overnight; (m): paraformaldehyde, dimethylamine hydrochloride, AcOH, DMF, 80 °C, overnight; (n): H_2SO_4, CH_2Cl_2, rt, overnight; (o): 1) t-BuOK, t-BuOH/toluene, reflux, 30 min; 2) alkyl halide, reflux, 20 min; (p): pyridine · HCl, 195 °C, 3 hours; (i): K_2CO_3, ethyl-4-bromobutyrate, acetone, reflux, 48 hours; (j): HCl, AcOH, reflux, 7 hours.

(b) Reagents and conditions: (q): 1) MeOH, reflux, 48 hours; 2) $BH_3 \cdot SMe_2$, THF, 0 °C to rt, 24 hours; (r): PPh_3, THF, DIAD, 60 °C, 1 hour, μW, (s) LiOH, H_2O_2, 60 °C, 6 hours.

2.2.2. Biological Evaluation

Screening the Inhibitory Activity

Screening evaluation of our set of compounds and further biological experiments were done by our collaborators Dr. Héctor Gaitán and Prof. Raul Estévez (from IDIBELL).

The inhibitory activity of the library was measured using electrophysiology methods, mainly in *Xenopus laevis* oocytes systems expressing green fluorescent protein (GFP)-tagged LRRC8 proteins. In addition, whole-cell patch clamp measurements in two different systems were planned for those CBX derivatives which showed acceptable potency as inhibitors. On one hand, the whole-cell patch clamp technique would be performed in human embryonic kidney 293 cells (HEK293T) LRRC8 knockout cells that specifically express LRRC8 proteins. Secondly, in primary cultures of astrocytes expressing endogenous proteins, which would prove that inhibitors not only inhibit LRRC8 subunits but also astrocytic VRAC current.

Structure-Activity Relationship Study of CBX-family

Up to 14 CBX-derivatives were successfully tested in *Xenopus laevis* oocytes (Figure 2.8) at 20 μM. The graphic in Figure 2.8 presents the channel inhibitory activity of compounds **3a-f**, **5-7**, **9**, and **11a-d**. While compound **3f**, incorporating a biaryl feature replacing the alkyl chain exhibited increased inhibitory activity, compound **3e** displayed an unexpected activating effect on the VRAC current. Inhibitory activities of compounds **3b** (incorporating a longer alkyl chain) and **3c** (featuring an N atom in the alkyl chain) were comparable to the one of **3a**, whereas **3d**, with an electronegative oxygen atom in the alkyl chain, was barely active. Dimer **5** was almost as active as CBX (**3a**), showing so far that great increases in molecular weight are not directly linked to increases of inhibitory activity. As expected, controls **6**, **7** and **11b** did not inhibit the channel, showing that the upper acidic function is fundamental for the inhibitory activity. Compound **9** was not tested after showing low solubility. Compounds **11a**, **11d** and **11e**, featuring hydroxamic acids, exhibited a blocking activity comparable to the one of **3a**. As the activation of the channel did not fit in our initial plan, derivatives

3e and **11e** were discarded as candidates, and their VRAC activation effect remained unexplored.

The most relevant compounds, **3f** and **11d**, were selected to be tested in HEK293T LRRC8 -/- cell-lines overexpressing combination of LRRC8A+8E proteins. Interestingly, both compounds displayed great increase in VRAC inhibition at 10 μM (Figure 2.9a). Afterwards, derivative **11d** at 10 μM was tested in primary cultured astrocytes, inhibiting the activity of endogenous VRAC present in the cells (Figure 2.9b).

Finally, the last two steroid-like derivatives (referred to as compounds **13** and **15**) could not be tested in *Xenopus laevis* oocytes systems, most likely due to low solubility in the media (Figure 2.7).

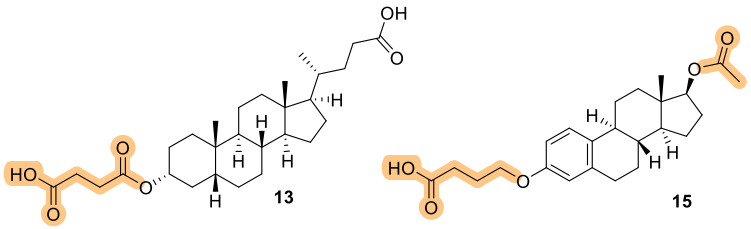

Figure 2.7. Steroid-like derivatives.

(a)

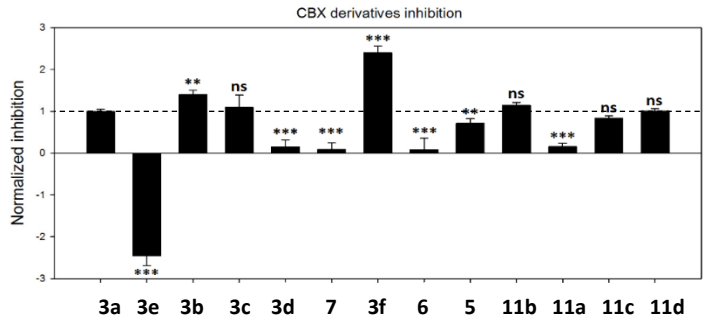

(b)

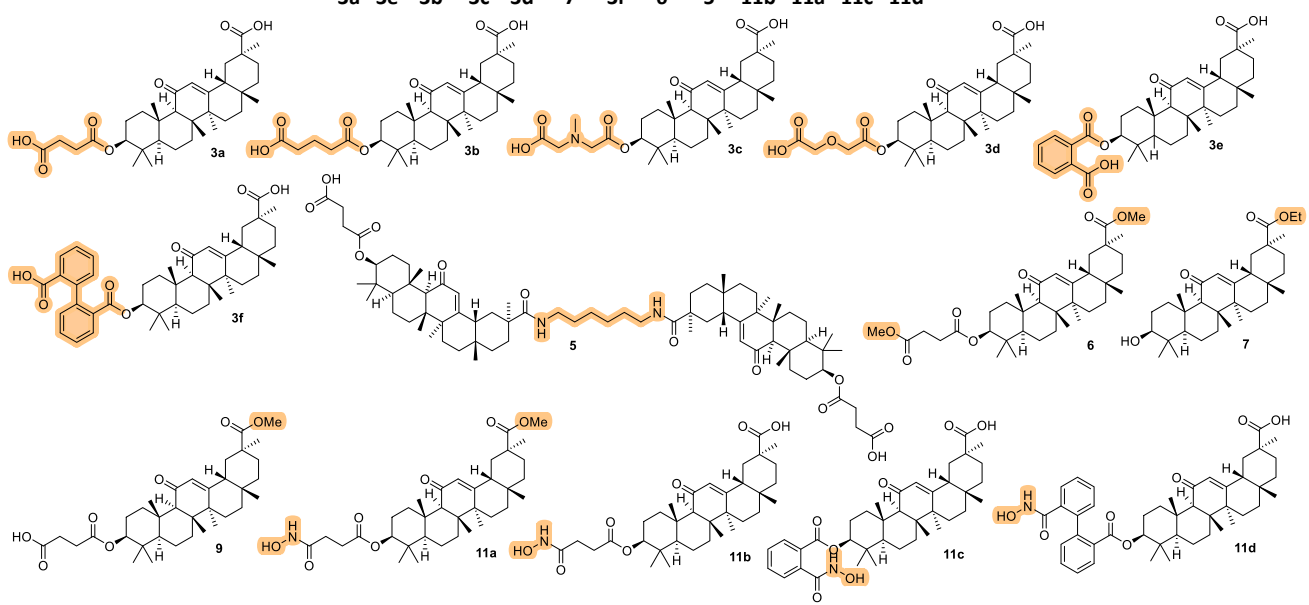

Figure 2.8. (a) Normalized inhibitory activity of CBX derivatives. Depicted values are normalized to **3a**. T-student test was performed to identify statistically significant inhibition differences between each individual derivative vs the original CBX compound. (b) Structures of CBX-derivatives. Orange highlighting shows special features.

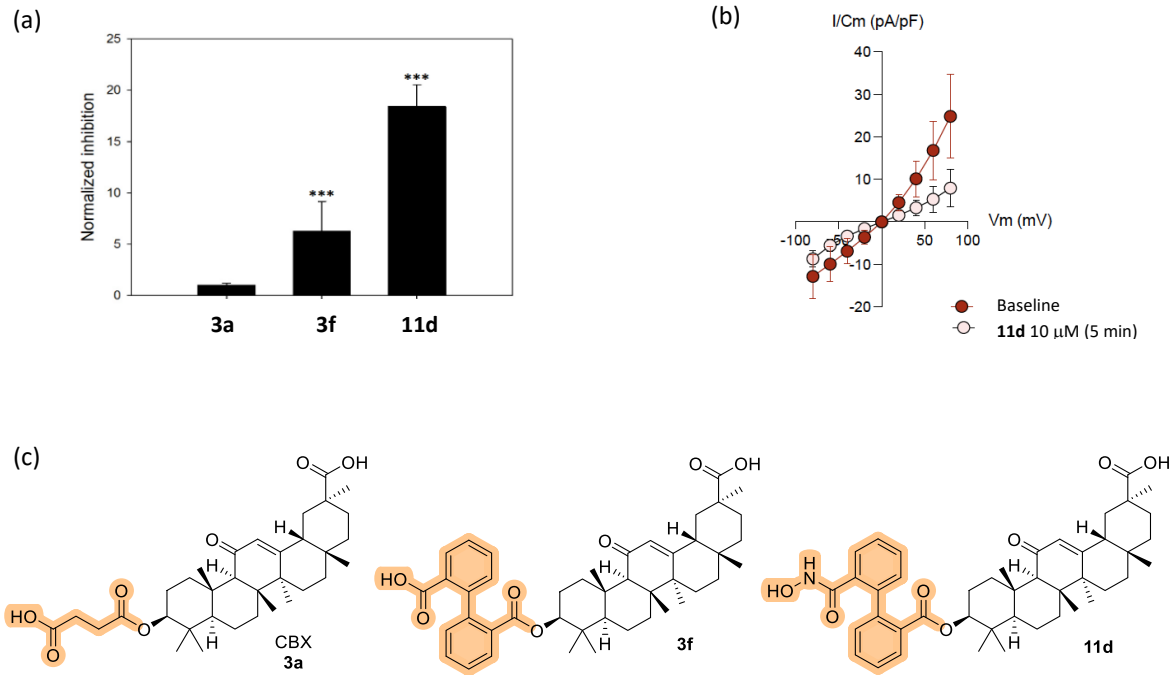

Figure 2.9. VRAC inhibition of **3f** and **11d** in cellular systems. (a) Experiments in HEK293T LRRC8-/- cells overexpressing LRRC8A + LRRC8E. (b) Current-voltage relationship of the VRAC current endogenously expressed in primary astrocytes with or without application of the inhibitor **11d**. (c) Structures of the selected derivatives (**3a**, **3f** and **11d**).

Structure-activity Relationship Study of DCPIB-family

The graphic in Figure 2.10 shows the inhibitory activity of DCPIB and 7 derivatives in *Xenopus laevis* oocytes at 20 μM. The most remarkable data refers to the comparable inhibitory activity of the non-chiral compound **25b** and the *racemic* DCPIB, **25a**, showing that having stereochemistry is not essential for inhibiting the channel. As the preparation of compound **25b** greatly simplified the synthetic chemical procedure, replacing the cyclopentyl motif by a butyl chain was considered for the following group of derivatives, thus discarding the preparation of **28a**. Compounds **24a-b**, featuring ester functions, showed reduced channel inhibition compared to **25a-b**. However, as esters are expected to hydrolyze after accessing the CNS, activity values in these more complex systems should be comparable to the ones of **25a-b** (Figure 2.10).

For the following set of hybrid derivatives, the inhibitory activity of the channel did not follow the expected trend (Figure 2.10). Thus, compounds **27a-b** and **28b**, featuring a DCPIB core and a diphenyl fragment in the upper position, did not improve the inhibitory activity regarding the original **25a**. Compounds **27a-b**, displaying ester functions, were way less active than compound **28b.**

Altogether, the optimized chemical synthesis of compound **24b**, and the chemical modifications improving its BBB permeability, shaped up this derivative as a good hit, likely to be further optimized.

After the preliminary screening of our library of VRAC blockers, we decided to select a specific compound of each family. Being the CBX-derivative **11d** and the DCPIB-derivative **24b** the selected options, we produced them in amounts suitable for in vivo studies.

(a)

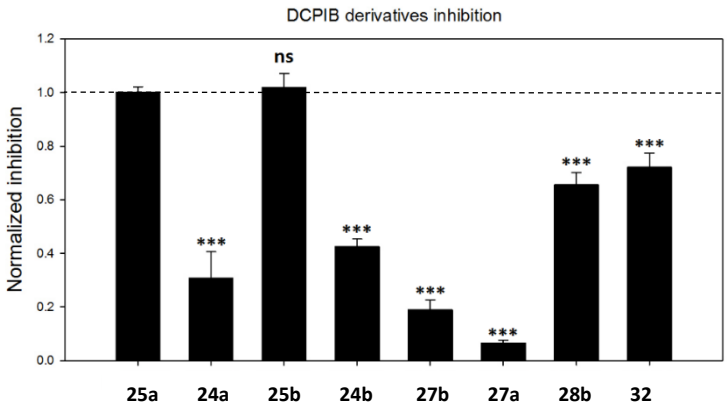

(b)

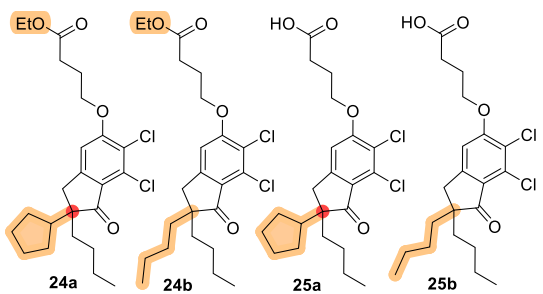

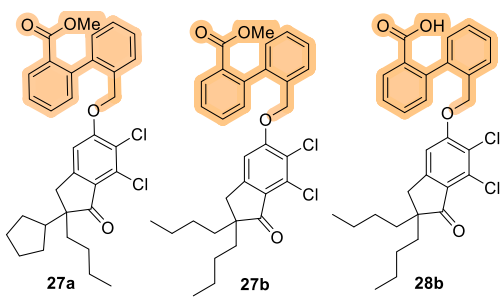

(c)

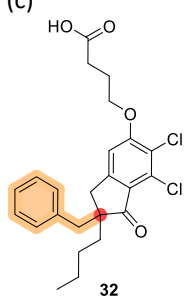

Figure 2.10. (a) Normalized inhibition of DCPIB derivatives. Depicted values are normalized to **24a**. T-student test was performed to identify statistically significant inhibition differences between each individual derivative vs **24a**. (b) Structures of DCPIB-derivatives. Orange highlighting shows special modifications. (c) See detailed information regarding the synthesis and purposes of compound **32** at the section 2.2.3.

In Vivo Studies: Testing the Two Selected Blockers in a Mouse Model of Stroke

For evaluating the protective effect of VRAC blockers during brain ischemia and stroke episodes, our collaborators Carles Justicia and Anna Planas (from CSIC) studied a suitable mouse model of transient occlusion of the middle cerebral artery (MCAO). Such models are obtained by using techniques that occlude the middle cerebral artery (MCA) and its branches, which are the cerebral vessels most affected in human ischemic stroke.

The efficacy of the selected VRAC blockers, **11d** and **24b**, was tested with a negative control containing the media PBS and 2,5 % DMSO (Scheme 2.10). The animals used for the study were mice male of the strain C57BL/6, of about 12 weeks of age. At the beginning of the whole experimental procedure, the average weight was about 25 g.

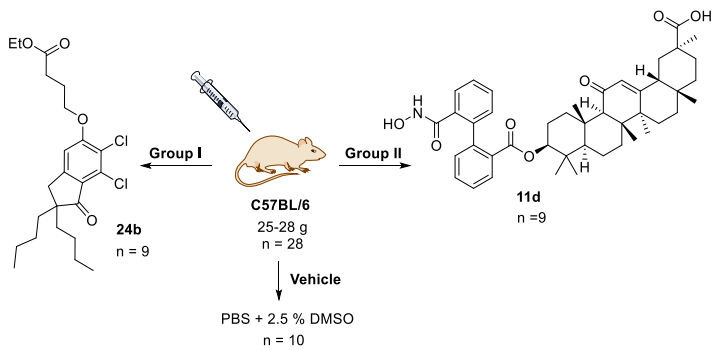

Scheme 2.10. Treatment groups for the in vivo studies.

Mice were randomly distributed within the three treatment groups and were weighted before being intervened. Thirty minutes before the beginning of the arterial occlusion, the corresponding treatment was administered to the animals through an intravenous injection in the tail. The transient intraluminal occlusion of the middle cerebral artery was then induced during 45 minutes in all the animals. Afterwards, the flow of blood was restored and, after 24 hours, the animals were weighted again and the functional affection was evaluated with behavioral tests (Figure 2.11a,b).

Then, mice were sacrificed, and the brain was cut into 1 mm coronal sections. The brain tissue was stained with 2,3,5-Triphenyltetrazolium chloride (TTC) to acquire and

process images that would help in the determination of the volume of the lesion (Figure 2.11c).

After analyzing all the results, no significant differences between the treated groups and the control were detected, neither regarding neurological function nor infarct volume.

It has therefore been concluded that cerebral protective role of **11d** and **24b** has not been demonstrated in this experimental procedure. However, we suggest that the results could be improved by using a method of injection that favored the distribution of the tested compounds in the brain, or by introducing novel brain delivery strategies like liposome administration of the active acids.

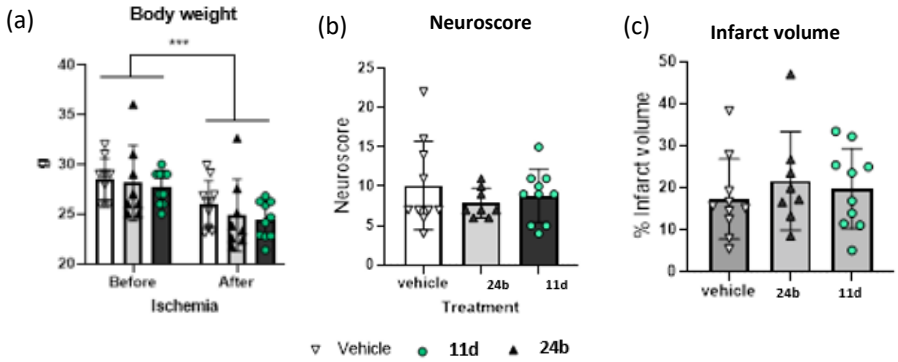

Figure 2.11. (a) Two-way ANOVA comparing the body weight of each group before and after ischemia. Time effect $p < 0.0001$; treatment effect $p=0.56$. (b) Kruskal-Wallis test comparing the functional affection of each group, $p=0.804$. Neuroscore from 0 to 37, more score means more neurological disfunction. (c) One-way ANOVA comparing the volume of the lesion of each group, $p = 0.672$. The volume of the lesion is expressed as % of the volume of the cerebral hemisphere.

2.2.3. Identification of the VRAC Binding Side

Although the resolution of cryo-EM structures of LRRC8 offered the possibility of predicting, calculating and mapping ligands binding sites in the VRAC channel, the only evidence so far is the fitting of DCPIB into the channel pore[42] and the existence of alternative allosteric binding sites in the LRR region.[44] There so, the presence of other several unpredicted binding sites is still not precluded.

In what concern us, together with Dr. Héctor Gaitán and Prof. Raul Estévez (from IDIBELL), we set many efforts on addressing the challenging identification of the binding mode of our compounds. Mainly we used two different strategies based on biological and chemical approximations.

Biological Approximation

The electrophysiology team started by studying the interaction between our set of compounds and the VRAC channel trough a mutated LRRC8A system in *Xenopus laevis* oocytes. Based on precedent investigations,[42] they tested whether exchanging the original arginine 103 residue (R103) by phenylalanine (F) had alterations in the blocking sensitivity of the channel. R103F LRRC8A mutation rendered the channel almost insensitive to ATP outward current inhibition in co-expression with the wild type (WT) LRRC8E subunit in *Xenopus laevis* oocytes (Figure 12a). In agreement with previous studies, these results suggested that the R103 residue is critical for the binding of ATP to LRRC8-VRAC channel. However, neither CBX (**3a**) nor DCPIB (**25a**) inhibition resulted altered in the same mutated system (Figure 2.12). Consequently, whereas the cryo-EM structure of VRAC together with DCPIB proposed R103 as a critical residue for the binding,[42] our results in *Xenopus laevis* oocytes strongly suggested that the same R103 residue would not be directly involved in its binding mode.

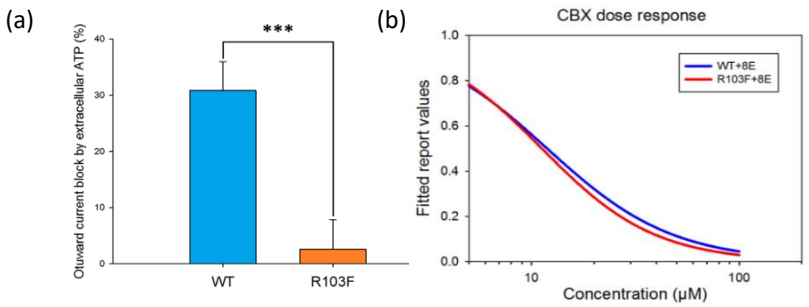

Figure 2.12. Blocking sensitivity of the essential subunit 8A WT/R103F in co-expression with 8E. (a) Quantification from TEVC recordings in *Xenopus* oocytes at an extracellular concentration of 2 mM ATP. (b) Fitted values of the CBX dose-response experiments performed either on the WT 8A (WT) or the R103F 8A mutation (R103F), both in co-expression with 8E. Dose-response experiments were performed at increasing concentrations of CBX in µM: 10, 20, 50, 100.

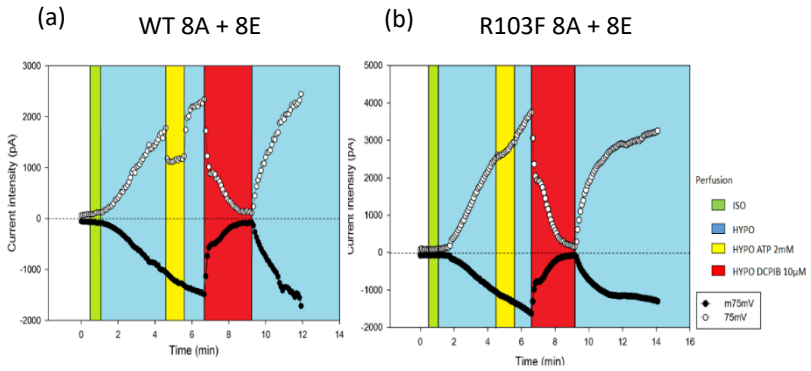

Figure 2.13. Representative recordings showing time course of current activity in different bath solutions including green (isotonic), blue (hypotonic), yellow (hypotonic + 2 mM ATP), and red (hypotonic + 10 µM DCPIB). Dots correspond to measurements at +75 mV (white) and -75 mV (black). (a) WT LRRC8A + LRRC8E VRAC combination. (b) R103F LRRC8A + LRRC8E VRAC combination.

Given that the *Xenopus laevis* oocytes heterologous system has low levels of endogenous LRRC88A protein,[35,36] the electrophysiology team carried out similar experiments in HEK293T LRRC8 -/- cell lines. In concordance with the previous oocyte's experiments, recordings on HEK293T LRRC8 -/- cell-lines overexpressing WT/R103F LRRC8A + LRRC8E followed the same trend than before (Figure 2.13). While WT LRRC8A + LRRC8E outward current was blocked by extracellular ATP (Figure 2.13a, yellow), R103F mutation led to outward current ATP insensitivity (Figure 2.13b, yellow); and WT LRRC8A and R103F LRRC8A mutation were similarly inhibited by both compounds **25a** and **3a** (comparing Figure 2.13a-red vs 2.13b-red).

Overall, the results in both systems demonstrate that R103 LRRC8A residue is only critical for ATP inhibition, since no effect is detected on DCPIB and CBX sensitivity.

Chemical Approximation

Alternatively, we designed a diazirine-based photoaffinity probe[45–47] that would likely shed light on the puzzling VRAC binding site. Based on the DCPIB structure and in parallel with the inactive control **32**, we envisaged the molecular probe **41** (Figure 2.15a). On one hand, the derivative **41** contains a DCPIB core to guarantee suitable affinity levels for the channel interaction, meanwhile a specific functional group is

added to undergo spatioselective photo-cross-linking with the surrounding atoms of the target protein near the binding site.

Before placing the photoaffinity probe on the DCPIB structure, we considered using the CBX core as it admits facile functionalization (Figure 2.14). Among all the possible photo-labeling structures, we prepared an small sized alkyl-amine diazirine[66,67] with the intention of minimizing any significant structural modification of the ligand for its biological activity, thus keeping the physicochemical properties of the original CBX and facilitating a similar accommodation within the binding site to the parent ligand. However, due to undesirable synthetic complications, the preparation of the CBX-probe was never achieved.

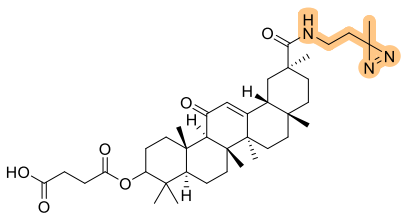

Figure 2.14. Alkyl-diazirine-based photoaffinity probe with the CBX pharmacophore.

In sharp contrast, the DCPIB derivative **25b** seemed promising for suitable derivatization to link the photo-probe unit. We assumed that a DCPIB-derived probe containing a benzyl group may be active and thus, a trifluoromethyl phenyl diazirine (TPD), which is much more stable than an alkyl diazirine, was appended to the pharmacophore unit. We therefore designed the TPD-based probe **41** and prepared it by adapting a reported procedure (Scheme 2.11).[68] The benzylic alcohol of the commercially available iodobenzene **33** was protected and further trifluoroacetylated by Li – halogen exchange using *n*-BuLi at - 78 °C. The resulting trifluoroacetophenone **35** was obtained after addition of ethyl trifluoroacetate, which was confirmed through NMR spectroscopy. A stereoisomeric (E/Z) mixture of tosyl-oximes **36** was yielded after treating **35** with $HONH_2 \cdot HCl$ and TsCl. Upon addition of ammonia in methanol, this mixture was converted to the diaziridine and further oxidized to the corresponding diazirine **37**, without isolating the intermediate. The deprotection of the silyl ether yielded the benzylic alcohol **38**. Differing from the reported synthesis, the benzylic alcohol of **38** was additionally converted to a benzylic bromide and then,

the α-carbon of the cyclopentanone **30** was selectively alkylated using the photo-affinity halide **39** with LDA. The final molecular probe **41** was obtained after a basic hydrolysis (Scheme 2.11).

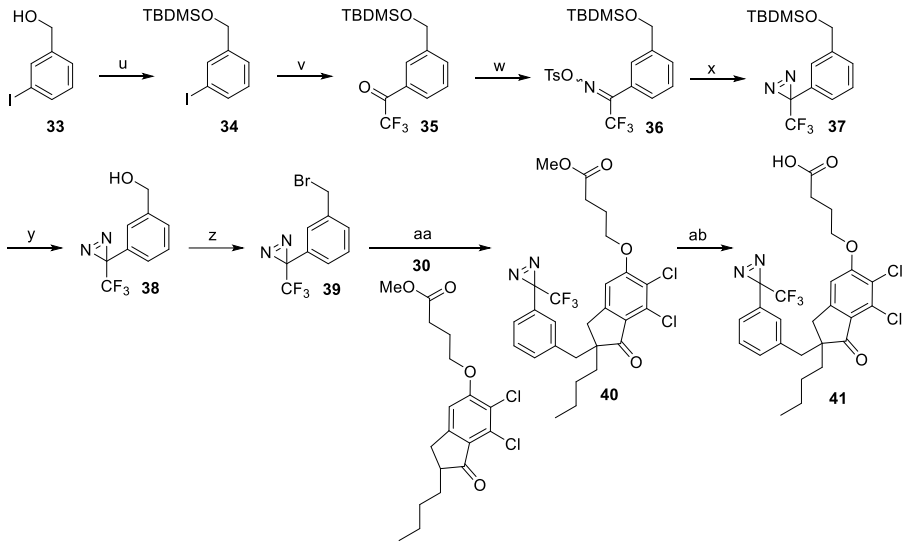

Scheme 2.11. Reagents and conditions: (u): TBDMSCl, imidazole, DMF, rt, 2 hours; (v): 1) *n*-BuLi, THF, - 78 ºC, 15 min; 2) CF_3CO_2Et, THF, - 78 ºC, 1 hour; (w): 1) $HONH_2 \cdot HCl$, EtOH / pyridine, 60 ºC, overnight; 2) TsCl, Et_3N, DMAP, CH_2Cl_2, rt, overnight; (x): 1) NH_3, MeOH, rt, overnight; 2) I_2, Et_3N, MeOH, rt, overnight; (y): TBAF, THF, rt, 1 hour; (z): CBr_4, PPh_3, CH_2Cl_2, rt, 30 min; (aa): 1) LDA, THF, - 78 ºC, 1:30 hours; 2) 3, THF, - 78 ºC, 3 hours; (ab): LiOH 1 M, THF, 1:30 hours.

Since the strategy might have a significant effect on the ligands physicochemical affinity properties, we thereupon prepared the control **32** with a simple benzyl substituent (Scheme 2.12). The phenol **29** was prepared by using harsh deprotecting conditions and was submitted to the Williamson reaction with metyl-4-bromobutyrate to obtain the ester **30**. The α-carbon of the cyclopentanone of **30** was selectively alkylated with benzyl bromide and *t*-BuOK as a base. During the same reaction, compound **30** resulted *tert*-butylated, thus the final acidic hydrolysis allowed the obtention of the control **32** bearing a carboxylic acid at the upper aliphatic chain. In this case, although we based the synthesis of intermediate **30** on the procedure followed for the preparation of DCPIB, some reactions were swap in order to protect diazirines from harsh conditions, due to its known liability and sensitivity.

Compound **41** has been tested as a good inhibitor of the channel, comparable to DCPIB (Figure 2.15b). Likewise, compound **32** showed a blocking activity in the same range to the one of DCPIB (Figure 2.10). Further biochemical and proteomic techniques for the mapping of the residues involved in the binding site are in progress.[49]

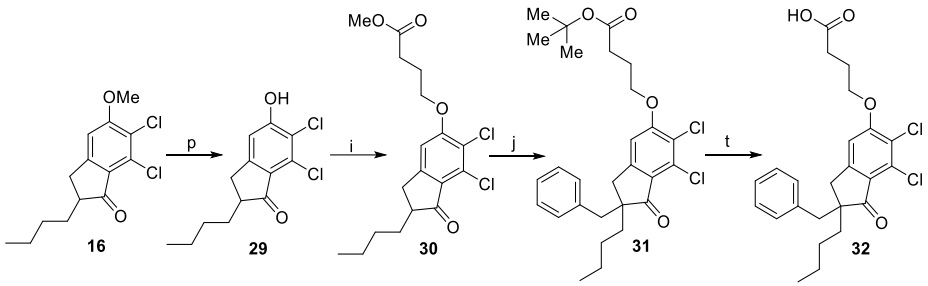

Scheme 2.12. Reagents and conditions: (p): pyridine · HCl, 195 °C, 3 hours; (i): K_2CO_3, methyl-4-bromobutyrate, DMF, reflux, overnight; (j): 1) *t*-BuOK, *t*-BuOH / toluene, reflux, 30 min; 2) benzyl bromide, reflux, 20 min; (t): HCl, dioxane, 40 °C, 5 hours.

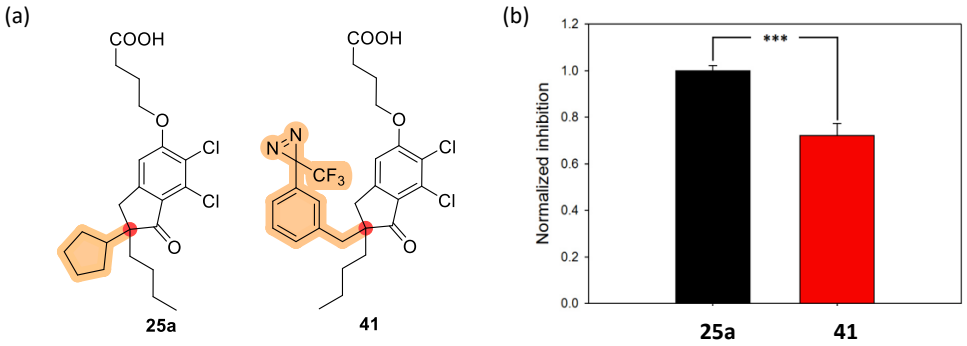

Figure 2.15. (a) DCPIB (**25a**) and photo-affinity probe **41**. (b) Compound **41** is a potent inhibitor of the VRAC channel activity.

Preliminary Docking Studies of Selected Compounds

Since the LRRC8A subunit of VRAC with DCPIB was elucidated for the very first time during the beginning of this project (Figure 2.17), we decided to use its PDB structure to perform preliminary docking studies with a selection of derivatives.[42]

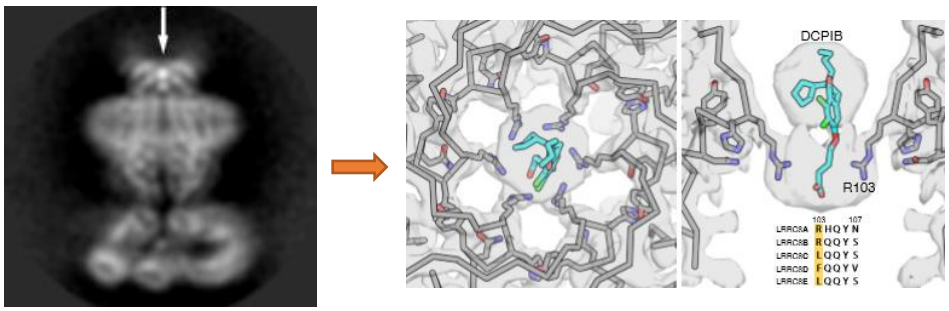

Figure 2.17. Representation of VRAC complexed with DCPIB.[42] (a) Two-dimensional image. An arrow highlights the feature corresponding to DCPIB in the channel pore. (b) View of the DCPIB-binding site.

The molecular docking study of compounds **3b**, **3f** and **25a** with VRAC was carried out by rDock software.[69] The three molecular structures were introduced in the software, and the binding of each ligand was constrained to the active cavity of the channel with a grid box that encompassed the ring of arginine residues (R103) described beforehand. We obtained several predicted docking solutions for each ligand, which were energetically scored. Among all the binding simulations, we selected the most suitable results for every ligand (regarding the energy score) and visually examined the results with the aid of PyMol software.[70]

In Figure 2.18, the selected compounds were docked into the suggested binding site of VRAC using the structure of LRRC8A protein (PDB entry: 6NZW) as a template. In the case of **25a**, the most stable solution referred to the one in which the butyl chain bearing a terminal carboxylic acid function was extended along the pore of the channel, ultimately interacting with the positively charged ring of arginine residues (structures colored in green). The remainder of the molecule was positioned above the arginine ring, and the indane core probably formed π-stacking interactions with the surrounding residues.

Following a similar pattern, compounds **3b** and **3f** were also positioned along the pore of the channel. Their alkyl chain and diphenyl motif -both bearing terminal carboxylic acids- interacted with the ring of arginine residues, while the steroid-like core of the molecule was extracellular to this region, occupying therefore the superior part of the pore, in the same way that **25a** did.

Overall, the results of this preliminary molecular docking study go along with those reported in the original work.[42] Thus, we consider that the study of LRRC8A / **25a**, **3b**, and **3f** complexes strongly support our strategy of designing derivatives with an aliphatic main structure and an appended terminal acidic function, which will expectantly keep the same binding mode than the one reported.

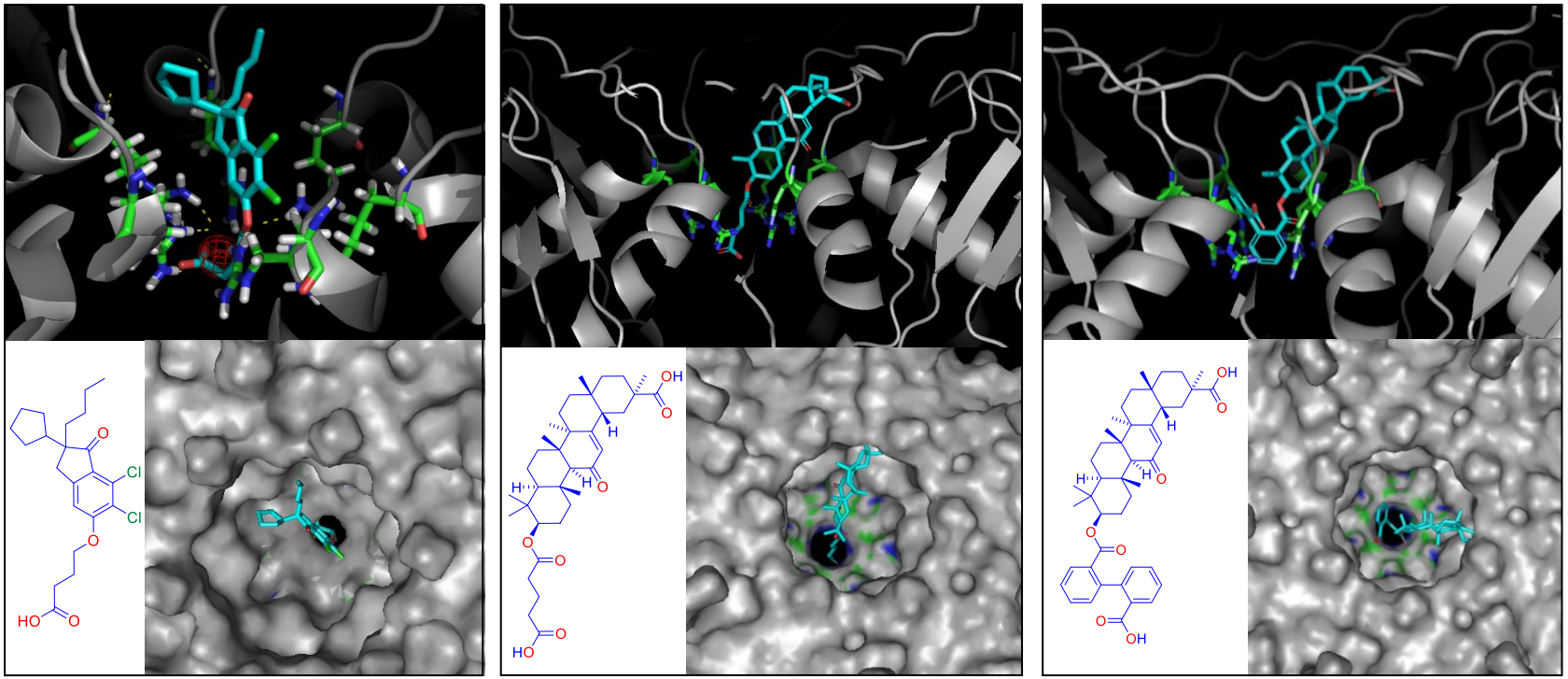

Figure 2.18. Molecular docking of VRAC complexes with: (c) **25a**, (b) **3b** and (c) **3f**. The ring of arginine residues (R103) is colored in green in the three images, while the blockers are colored in blue. Oxygen and nitrogen atoms are highlighted in red and blue, respectively.

2.3. Conclusions and Future Perspectives for the LRRC8/VRAC Research

Considering that VRAC channel is a poorly understood member of the superfamily of chloride channels, it is not surprising that specific families of selective modulators have not been discovered yet. For instance, though several compounds have been studied after showing alteration of the channel current, VRAC is not the main target for any of them, as it is the case of the anticancer drug tamoxifen.

Certainly, one of the reasons why VRAC pharmacology has not been profoundly explored is the unknown molecular interaction of the modulators within the binding site of the channel. While a cryo-EM structure of a homo-hexameric LRRC8A predicted the situation of DCPIB in the channel pore, another cryo-EM with nanobodies suggested allosteric modulation from LRR bindings at alternative sites.

In this work, we have tried to cover the existing gap by rationally designing a series of derivatives based on the structure of the two most active blockers known to date, CBX and DCPIB. After evaluating the inhibitory activity of the set of compounds, we selected the most active derivative of each family and produced them in suitable amounts for the in vivo evaluation.

Besides, we have designed a TPD-based photoaffinity probe with the DCPIB pharmacophore. With this chemical probe, we should be able to settle the interaction of our compounds within the atoms of the VRAC surrounding the binding site. Hopefully, the results will be valuable to determine the nature of the inhibition process by DCPIB and CBX derivatives and will help in the design and synthesis of potent inhibitors with the right physicochemical profile.

Incidentally, a very recent publication has studied the role of VRAC and DCPIB derivatives in metabolic diseases like Type 2 Diabetes (T2D).[71] Such work has opened new and interesting perspectives for our library of compounds beyond targeting astrocytic VRACs.

2.4. Bibliography

[1] Y. Béjot, H. Bailly, J. Durier, M. Giroud, *Press. Medicale* **2016**, *45*, 391–398.

[2] E. Wilkins, L. Wilson, K. Wickramasinghe, P. Bhatnagar, J. Leal, R. Luengo-Fernandez, R. Burns, M. Rayner, N. Townsend, *Eur. Cardiovasc. Dis. Stat.* **2017**, *34*, 3028–3034.

[3] H. A. Wafa, C. D. A. Wolfe, E. Emmett, G. A. Roth, C. O. Johnson, Y. Wang, *Stroke* **2020**, *51*, 2418–2427.

[4] E. K. Hoffmann, I. H. Lambert, S. F. Pedersen, *Physiol. Rev.* **2009**, *89*, 193–277.

[5] I. H. Lambert, E. K. Hoffmann, S. F. Pedersen, *Acta Physiol.* **2008**, *194*, 255–282.

[6] T. J. Jentsch, *Nat. Rev. Mol. Cell Biol.* **2016**, *17*, 293–307.

[7] C. S. Wilson, M. D. Bach, Z. Ashkavand, K. R. Norman, N. Martino, A. P. Adam, A. A. Mongin, *J. Neurochem.* **2019**, *151*, 255–272.

[8] J. Osei-Owusu, J. Yang, M. del C. Vitery, Z. Qiu, in *Curr. Top. Membr.* (Eds.: I. Levitane, E. Delpire, H. Rasgado-Flores), Elsevier Ltd, **2018**, pp. 177–203.

[9] B. Nilius, J. Eggermont, T. Voets, G. Buyse, V. Manolopoulos, G. Droogmans, *Prog. Biophys. Mol. Biol.* **1997**, *68*, 69–119.

[10] Y. Okada, T. Numata, K. Sato-Numata, R. Z. Sabirov, H. Liu, S. ichiro Mori, S. Morishima, *Curr. Top. Membr.* **2019**, *83*, 205–283.

[11] K. Strange, T. Yamada, J. S. Denton, *J. Gen. Physiol.* **2019**, *151*, 100–117.

[12] K. Strange, F. Emma, P. S. Jackson, *Am. J. Physiol.* **1996**, *270*, 711–730.

[13] L. Chen, B. König, T. Liu, S. Pervaiz, Y. S. Razzaque, T. Stauber, *Biol. Chem.* **2020**, *400*, 1481–1496.

[14] A. A. Mongin, *Pflugers Arch. Eur. J. Physiol.* **2016**, *468*, 421–441.

[15] S. F. Pedersen, T. K. Klausen, B. Nilius, *Acta Physiol.* **2015**, *213*, 868–881.

[16] T. Stauber, *Biol. Chem.* **2015**, *396*, 975–990.

[17] X. Elorza-Vidal, H. Gaitán-Peñas, R. Estévez, *Int. J. Mol. Sci.* **2019**, *20*, 1034–1057.

[18] J. W. Olney, *Retina* **1982**, *2*, 341–359.

[19] J. W. Olney, *Science.* **1969**, *164*, 719–721.

[20] H. K. Kimelberg, *Glia* **2005**, *50*, 389–397.

[21] T. W. Lai, S. Zhang, Y. T. Wang, *Prog. Neurobiol.* **2014**, *115*, 157–188.

[22] J. Friard, M. Tauc, M. Cougnon, V. Compan, C. Duranton, I. Rubera, *Front. Pharmacol.* **2017**, *8*, 1–13.

[23] H. K. Kimelberg, P. J. Feustel, Y. Jin, J. Paquette, A. Boulos, J. Keller, B. I. Tranmer, *Neuroreport* **2000**, *11*, 2675–2679.

[24] C. Maertens, G. Droogmans, P. Chakraborty, B. Nilius, *Br. J. Pharmacol.* **2001**, *132*, 135–142.

[25] A. S. Boulos, E. M. Deshaies, J. C. Dalfino, P. J. Feustel, A. J. Popp, D. Drazin, *J. Neurosurg.* **2011**, *114*, 1117–1126.

[26] V. Benfenati, M. Caprini, G. P. Nicchia, A. Rossi, M. Dovizio, C. Cervetto, M. Nobile, S. Ferroni, *Channels* **2009**, *3*, 323–336.

[27] Y. Zhang, H. Zhang, P. J. Feustel, H. K. Kimelberg, *Exp. Neurol.* **2008**, *210*, 514–520.

[28] N. H. Bowens, P. Dohare, Y. H. Kuo, A. A. Mongin, *Mol. Pharmacol.* **2013**, *83*, 22–32.

[29] Q. Han, S. Liu, Z. Li, F. Hu, Q. Zhang, M. Zhou, J. Chen, T. Lei, H. Zhang, *Brain Res.* **2014**, *1542*, 176–185.

[30] Z. Ruan, I. J. Orozco, J. Du, W. Lü, *Nature* **2020**, *584*, 646–651.

[31] K. Michalski, T. Kawate, *J. Gen. Physiol.* **2016**, *147*, 165–174.

[32] F. Abascal, R. Zordoya, *Bioessays* **2012**, *34*, 551–560.

[33] F. K. Voss, F. Ullrich, J. Muňch, K. Lazarow, D. Lutte, N. Mah, M. A. Andrade-Navarro, J. P. Von Kries, T. Stauber, T. J. Jentsch, *Science (80-.).* **2014**, *344*, 634–638.

[34] Z. Qiu, A. E. Dubin, J. Mathur, B. Tu, K. Reddy, L. J. Miraglia, J. Reinhardt, A. P. Orth, A. Patapoutian, *Cell* **2014**, *157*, 447–458.

[35] H. Gaitán-Peñas, M. Pusch, R. Estévez, *Int. J. Mol. Sci.* **2018**, *19*, 719–731.

[36] H. Gaitán-Peñas, A. Gradogna, L. Laparra-Cuervo, C. Solsona, V. Fernández-Dueñas, A. Barrallo-Gimeno, F. Ciruela, M. Lakadamyali, M. Pusch, R. Estévez, *Biophys. J.* **2016**, *111*, 1429–1443.

[37] C. C. Lee, E. Freinkman, D. M. Sabatini, H. L. Ploegh, *J. Biol. Chem.* **2014**, *289*, 17124–17131.

[38] R. Planells-Cases, D. Lutter, C. Guyader, N. M. Gerhards, F. Ullrich, D. A. Elger, A. Kucukosmanoglu, G. Xu, F. K. Voss, S. M. Reincke, T. Stauber, V. A. Blomen, D. J. Vis, L. F. Wessels, T. R. Brummelkamp, P. Borst, S. Rottenberg, T. J. Jentsch, *EMBO J.* **2015**, *34*, 2993–3008.

[39] R. Nakamura, T. Numata, G. Kasuya, T. Yokoyama, T. Nishizawa, T. Kusakizako, T. Kato, T. Hagino, N. Dohmae, M. Inoue, K. Watanabe, H. Ichijo, M. Kikkawa, M. Shirouzu, T. J. Jentsch, R. Ishitani, Y. Okada, O. Nureki, *Commun. Biol.* **2020**, *3*, DOI 10.1038/s42003-020-0951-z.

[40] D. Deneka, M. Sawicka, A. K. M. Lam, C. Paulino, R. Dutzler, *Nature* **2018**, *558*, 254–259.

[41] J. M. Kefauver, K. Saotome, A. E. Dubin, J. Pallesen, C. A. Cottrell, S. M. Cahalan, Z. Qiu, G. Hong, C. S. Crowley, T. Whitwam, W. H. Lee, A. B. Ward, A. Patapoutian, *Elife* **2018**, *7*, DOI 10.1101/323584.

[42] D. M. Kern, S. Oh, R. K. Hite, S. G. Brohawn, *Elife* **2019**, *8*, DOI 10.7554/elife.42636.

[43] G. Kasuya, T. Nakane, T. Yokoyama, Y. Jia, M. Inoue, K. Watanabe, R. Nakamura, T. Nishizawa, T. Kusakizako, A. Tsutsumi, H. Yanagisawa, N. Dohmae, M. Hattori, H. Ichijo, Z. Yan, M. Kikkawa, M. Shirouzu, R. Ishitani, O. Nureki, *Nat. Struct. Mol. Biol.* **2018**, *25*, 797–804.

[44] D. Deneka, S. Rutz, C. A. J. Hutter, M. A. Seeger, M. Sawicka, R. Dutzler, *Nat. Commun.* **2021**, *12*, DOI 10.1038/s41467-021-25742-w.

[45] A. Singh, E. R. Thornton, F. H. Westheimer, *J. Biol. Chem.* **1962**, *237*, 3006–3008.

[46] A. V. West, G. Muncipinto, H. Y. Wu, A. C. Huang, M. T. Labenski, L. H. Jones, C. M. Woo, *J. Am. Chem. Soc.* **2021**, *143*, 6691–6700.

[47] J. R. Hill, A. A. B. Robertson, *J. Med. Chem.* **2018**, *61*, 6945–6963.

[48] E. Smith, I. Collins, *Future Med. Chem.* **2015**, *7*, 159–183.

[49] Y. S. Cheng, T. Zhang, X. Ma, S. Pratuangtham, G. C. Zhang, A. A. Ondrus, A. Mafi, B. Lomenick, J. J. Jones, A. E. Ondrus, *Nat. Chem. Biol.* **2021**, *17*, 1271–1280.

[50] L. Dubinsky, B. P. Krom, M. M. Meijler, *Bioorganic Med. Chem.* **2012**, *20*, 554–570.

[51] H. Pajouhesh, G. R. Lenz, *NeuroRx* **2005**, *2*, 541–553.

[52] B. Carlo, M. H. Donna, L. Amos, B. Smith, *ChemMedChem* **2013**, *8*, 385–395.

[53] A. T. Placzek, S. J. Ferrara, M. D. Hartley, H. S. Sanford-Crane, J. M. Meinig, T. S. Scanlan, *Bioorganic Med. Chem.* **2016**, *24*, 5842–5854.

[54] G. C. Terstappen, A. H. Meyer, R. D. Bell, W. Zhang, *Nat. Rev. Drug Discov.* **2021**, *20*, 362–383.

[55] E. J. Cragoe, N. P. Gould, O. W. Woltersdorf, C. Ziegler, R. S. Bourke, L. R. Nelson, H. K. Kimelberg, J. B. Waldman, A. J. Popp, N. Sedransk, *J. Med. Chem.* **1982**, *25*, 567–579.

[56] N. Decher, H. J. Lang, B. Nilius, A. Brüggemann, A. E. Busch, K. Steinmeyer, *Br. J. Pharmacol.* **2001**, *134*, 1467–1479.

[57] A. Alibrahim, L. Y. Zhao, C. Y. J. Bae, A. Barszczyk, C. Lf Sun, G. L. Wang, H. S. Sun, *Acta Pharmacol. Sin.* **2013**, *34*, 113–118.

[58] M. A. M. Subbaiah, N. A. Meanwell, *J. Med. Chem.* **2021**, *64*, 14046–14128.

[59] G. Xu, J. Li, J. Wu, H. Zhang, J. Hu, M.-H. Li, *ACS Appl. Polym. Mater.* **2019**, *1*, 2577–2581.

[60] D. Chen, X. Huang, H. Zhou, H. Luo, P. Wang, Y. Chang, X. He, S. Ni, Q. Shen, G. Cao, H. Sun, X. Wen, J. Liu, *Eur. J. Med. Chem.* **2017**, *139*, 201–213.

[61] I. Beseda, L. Czollner, P. S. Shah, R. Khunt, R. Gaware, P. Kosma, C. Stanetty, M. C. del Ruiz-Ruiz, H. Amer, K. Mereiter, T. Da Cunha, A. Odermatt, D. Claßen-Houben, U. Jordis, *Bioorganic Med. Chem.* **2010**, *18*, 433–454.

[62] L. H. Lin, L. W. Lee, S. Y. Sheu, P. Y. Lin, *Chem. Pharm. Bull.* **2004**, *52*, 1117–1122.

[63] K. Stenzel, A. Hamacher, F. K. Hansen, C. G. W. Gertzen, J. Senger, V. Marquardt, L.

Marek, M. Marek, C. Romier, M. Remke, M. Jung, H. Gohlke, M. U. Kassack, T. Kurz, *J. Med. Chem.* **2017**, *60*, 5334–5348.

[64] O. W. Woltersdorf, S. J. deSolms, E. M. Schultz, E. J. Cragoe, *J. Med. Chem.* **1977**, *20*, 1400–1408.

[65] S. J. DeSolms, O. W. Woltersdorf, E. J. Cragoe, L. S. Watson, G. M. Fanelli, *J. Med. Chem.* **1978**, *21*, 437–443.

[66] U. K. Shigdel, J. Zhang, C. He, *Angew. Chemie - Int. Ed.* **2008**, *47*, 90–93.

[67] J. Liang, L. Zhang, X. L. Tan, Y. K. Qi, S. Feng, H. Deng, Y. Yan, J. S. Zheng, L. Liu, C. L. Tian, *Angew. Chemie - Int. Ed.* **2017**, *56*, 2744–2748.

[68] K. Nakamoto, Y. Ueno, *J. Org. Chem.* **2014**, *79*, 2463–2472.

[69] *rDOCK;* Version 3.0; Vernalis R&D: Cambridge, United Kingdom, **1998**.

[70] *The PyMOL Molecular Graphics System*; Version 2.0; Schrödinger LLC: New York, NY, USA, **2016**.

[71] S. K. Gunasekar, L. Xie, A. Kumar, J. Hong, P. R. Chheda, C. Kang, D. M. Kern, C. My-Ta, J. Maurer, J. Heebink, E. E. Gerber, W. J. Grzesik, M. Elliot-Hudson, Y. Zhang, P. Key, C. A. Kulkarni, J. W. Beals, G. I. Smith, I. Samuel, J. K. Smith, P. Nau, Y. Imai, R. D. Sheldon, E. B. Taylor, D. J. Lerner, A. W. Norris, S. Klein, S. G. Brohawn, R. Kerns, R. Sah, *Nat. Commun.* **2022**, *13*, DOI 10.1038/s41467-022-28435-0.

2.1. Selected Supporting Information

For a full account see the digital version of the thesis.

1. General Information

Unless otherwise stated, all reactions were carried out under normal atmosphere in dried glassware. Commercially available reactants were used without further purification. Thin-layer chromatography was performed on pre-coated Merk silica gel 60 F_{254} plates and visualized under a UV lamp and/or 1% aqueous solution of $KMnO_4$. Reactions were monitored by HPLC-MS using a HPLC Agilent 1260 Infinity II comprising a pump (Edwards RV12) with degasser, an autosampler and a diode array detector. Flow from the column was split to a MS spectrometer. The MS detector was configured with an electrospray ionization source (micromass ZQ4000) and nitrogen was used as the nebulizer gas. Five microliters of sample 0.5 mg/mL in MeOH:CH_3CN was injected using an Agilent Poroshell 120 EC-C18, 2.7 micrometers, 50 mm x 4.6 mm column at 40 °C. The mobile phase was a mixture of A = water with 0.05% formic acid and B = acetonitrile with 0.05% formic acid, with the method described as follows: flow 0.6 ml/min; gradient: 95% A–5% B to 100% B in 3 min, 100% B 3 min, from 100% B to 95% A–5% B in 1 min, 95% A–5% B 3 min. When stated, the final crude was purified via flash column chromatography with an Isolera Prime Biotage s provided with dual UV detection, with pre-packed RediSep Rf silica gel cartridges. Prepacked normal phase silica or alumina gel columns (12, 24 and 50 g) were used for separation of some products. ^1H, ^{13}C and ^{19}F NMR spectra were recorded on a Varian Mercury 400 or on a Bruker 400 Avance III spectrometers (at 400 MHz, 101 and 376 MHz, respectively). Unless otherwise quoted, NMR spectra were recorded in either $CDCl_3$ or DMSO solution with TMS as an internal reference. Data for ^1H NMR spectra are reported as follows: chemical shift (δ ppm), multiplicity, coupling constants (Hz) and integration. Data for ^{13}C and ^{19}F NMR spectra are reported in terms of chemical shift (δ ppm). High Resolution Mass Spectrometry was performed by the University of Barcelona Mass Spectrometry Service.

2. Experimental Procedures and Characterization Data

2.1. Synthetic Procedures for the Preparation of CBX and Derivatives

A) Modifications on the Ester Chain

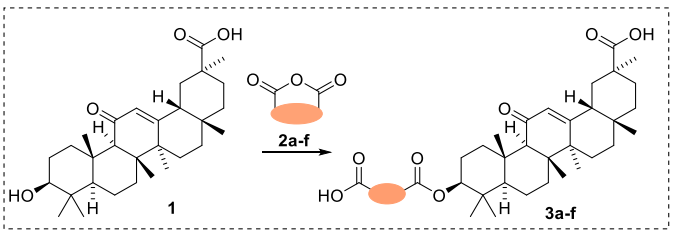

Scheme S2.1. CBX derivatives: condensation of glycyrrhetinic acid (**1**) with anhydrides (**2a-f**).

General Procedure A (synthesis of 3a, 3c, 3e, 3f). A solution of glycyrrhetinic acid (**1**, 0.471 g, 1.0 Eq.) and DMAP (0.246 g, 2.0 Eq.) in dry pyridine (3 mL) was added to a 10-20 mL microwave vial at room temperature. After 10 min of stirring, the suitable anhydride (4.0 Eq.) was added to the reaction mixture and the vial was sealed. The reaction mixture was heated to 160 ^{o}C under microwave irradiation (150 W, 8 bar) for 1:30 hours. After reaction completion confirmed by TLC or LC-MS, the reaction mixture was acidified with 2.0 M HCl (20 mL) and extracted with EtOAc (3 x 20 mL). The organic phase was washed with cold water (50 mL), dried over $MgSO_4$, filtered and the solvent was evaporated under reduced pressure. The pure products **3** were obtained either directly after the work-up or through a further automated flash column chromatography, using CH_2Cl_2/MeOH as eluent.

General Procedure B (synthesis of 2b, 2d). Based on a reported procedures,[1,2] DMAP (0.246 g, 2.0 Eq.) was added in a solution of glycyrrhetinic acid (**1**, 0.471 g, 1.0 mmol, 1.0 Eq.) in dry pyridine (10 mL) at room temperature. After 10 min of stirring, the suitable anhydride (4.0 Eq.) was added to the reaction mixture and heated to reflux overnight. After TLC or HPLC confirmed completion of the reaction, the reaction mixture was acidified with 2.0 M HCl (20 mL) and extracted with EtOAc (3 x 20 mL). The organic phase was washed with cold water (50 mL), dried over $MgSO_4$, filtered and the solvent was evaporated under reduced pressure. The pure products **3** were obtained by flash chromatography, using CH_2Cl_2/MeOH as eluent.

Carbenoxolone (3a)

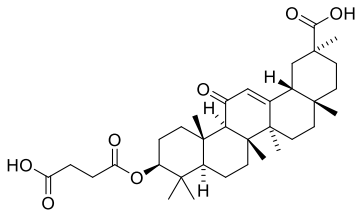

Following the ***General Procedure A*** and using succinic anhydride (**2a**) as starting material, compound **3a** (0.556 g, 97%) was obtained as a pale brown solid directly after the work-up, without any further purification.

^{1}H NMR (400 MHz, DMSO-d_6) δ 12.19 (s, 1H), 5.40 (s, 1H), 4.43 (dd, *J* = 11.8, 4.5 Hz, 1H), 2.66 – 2.59 (m, 1H), 2.40 (d, *J* = 2.3 Hz, 2H), 2.11 – 2.01 (m, 2H), 1.82 – 1.72 (m, 2H), 1.72 – 1.58 (m, 4H), 1.56 – 1.39 (m, 3H), 1.36 (s, 3H), 1.34 – 1.14 (m, 5H), 1.09 (s, 3H), 1.05 (cs, two overlapping s, 6H), 1.01 – 0.86 (m, 3H), 0.82 (cs, two overlapping s, 6H), 0.75 (s, 3H).

^{13}C NMR (101 MHz, DMSO-d_6) δ 198.93, 177.69, 173.43, 171.65, 169.87, 127.22, 79.75, 60.82, 53.73, 48.07, 44.87, 43.08, 42.96, 37.85, 37.66, 37.52, 36.49, 31.91, 31.62, 31.53, 30.36, 29.20, 28.81, 28.39, 27.82, 27.61, 26.10, 25.80, 23.17, 23.01, 18.33, 16.92, 16.57, 16.15.

All HNMR shifts matched to those previously reported.[3,4] See the identification of the most significant HNMR signals at page S19.

m/z: MH^+ 570 at 5.277 min (96%).

10-((2-carboxybenzoyl)oxy)-2,4a,6a,6b,9,9,12a-heptamethyl-13-oxo-1,2,3,4,4a,5,6,6a,6b,7,8,8a,9,10,11,12,12a,12b,13,14b-icosahydropicene-2-carboxylic acid (3e)

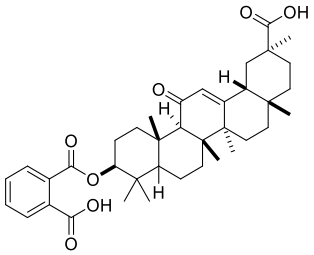

Following the ***General Procedure A*** and using phthalic anhydride (**2e**) as starting material, the pure compound **3e** (0.451 g, 73%) was obtained as a white solid after being purified through automated flash column chromatography using a gradient of CH_2Cl_2/MeOH (from 100:0 to 99.7:0.3, v/v) as eluent.

^{1}H NMR (400 MHz, DMSO-d_6) δ 7.73 – 7.68 (m, 1H), 7.61 (dd, *J* = 6.4, 3.1 Hz, 3H), 5.42 (s, 1H), 4.66 (dd, *J* = 11.5, 4.7 Hz, 1H), 2.67 (d, *J* = 13.3 Hz, 1H), 2.44 (s, 1H), 2.08 (d, *J* = 10.1 Hz, 2H), 1.84 – 1.65 (m, 7H), 1.53 (s, 1H), 1.39 (s, 3H), 1.35 (s, 1H), 1.26 – 1.12 (m, 4H), 1.10 (cs, two overlapping s, 6H), 1.09 (s, 3H), 1.05 (d, *J* = 5.9 Hz, 3H), 0.96 (d, *J* = 11.7 Hz, 2H), 0.92 (s, 3H), 0.84 (s, 3H), 0.76 (s, 3H).

^{13}C NMR (101 MHz, DMSO-d_6) δ 198.92, 177.64, 169.87, 168.20, 167.12, 132.44, 131.64, 130.60 – 130.46, 128.77 (d, J = 19.6 Hz), 128.20 (d, J = 8.2 Hz), 127.23, 81.42, 60.81, 53.83, 52.40, 48.06, 44.88, 43.02 (d, J = 10.1 Hz), 38.29 – 37.94 (m), 37.72 (t, J = 16.9 Hz), 36.53, 31.91, 31.53, 30.35, 28.39, 27.79 (d, J = 4.6 Hz), 26.35 – 26.21, 25.94 (d, J = 30.7 Hz), 23.03, 22.64, 18.33, 16.92, 16.65, 16.13.

The most significant Hs have been identified comparing HNMR spectra of **3e** with **1.** See pages S20-21 for further details.

HRMS: calcd for $C_{38}H_{49}O_7$ 617.3484 ($M\text{-}H^-$); found 617.3477. ***m/z*:** MH^+ 619 at 5.635 min (93%).

10-((2'-carboxy-[1,1'-biphenyl]-2-carbonyl)oxy)-2,4a,6a,6b,9,9,12a-heptamethyl-13-oxo-1,2,3,4,4a,5,6,6a,6b,7,8,8a,9,10,11,12,12a,12b,13,14b-icosahydropicene-2-carboxylic acid (3f)

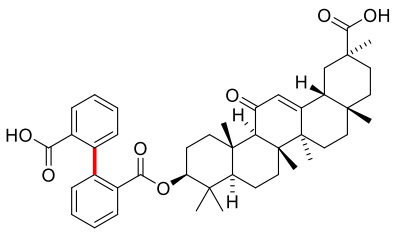

Following the ***General Procedure A*** and using diphenic anhydride (**2f**) as starting material, the pure compound **3f** (0.486 g, 70%) was obtained as a white solid after bien purified through

automated flash column chromatography using a gradient of CH_2Cl_2/MeOH (from 100:0 to 99.8:0.2, v/v) as eluent.

^{1}H NMR (400 MHz, $CDCl_3$) δ 8.04 (dd, *J* = 12.6, 7.8 Hz, 1H), 7.95 (dd, *J* = 12.9, 7.7 Hz, 1H), 7.57 – 7.50 (m, 2H), 7.50 – 7.41 (m, 2H), 7.18 (m, 2H), 5.67 (s, 1H), 4.57 (q, *J* = 9.8 Hz, 1H), 2.69 (m, 1H), 2.30 (s, 1H), 2.15 (d, *J* = 13.5 Hz, 1H), 2.05 – 1.75 (m, 4H), 1.66 – 1.35 (m, 8H), 1.33 (s, 3H), 1.25 (s, 1H), 1.19 (s, 2H), 1.10 (s, 3H), 1.08 (d, *J* = 3.1 Hz, 3H), 1.05 – 0.87 (m, 2H), 0.81 (s, 3H), 0.79 (d, *J* = 2.8 Hz, 3H), 0.70 (d, *J* = 17.6 Hz, 3H).

^{13}C NMR (101 MHz, $CDCl_3$) δ 200.34, 182.30 (d, *J* = 6.8 Hz), 171.39 (d, *J* = 26.2 Hz), 169.43, 167.65 (d, *J* = 27.5 Hz), 163.01, 143.86, 142.65 (d, *J* = 8.1 Hz), 132.20 (d, *J* = 6.6 Hz), 131.38, 131.02 (d, *J* = 10.5 Hz), 130.68, 130.58, 130.38, 129.83, 128.91 (d, *J* = 28.6 Hz), 128.59, 127.39 (d, *J* = 4.6 Hz), 81.48 (d, *J* = 4.0 Hz), 61.76, 55.11, 53.89, 48.28, 45.54, 43.95, 43.28, 40.92, 38.84, 38.27, 37.83, 36.97, 32.79, 31.96, 31.02, 29.83, 28.60 (d, *J* = 7.0 Hz), 28.09 (d, *J* = 9.4 Hz), 26.54 (d, *J* = 5.5 Hz), 23.44, 23.17 (d, *J* = 12.8 Hz), 18.79, 17.43, 16.86 (d, *J* = 9.0 Hz), 16.45 (d, *J* = 2.6 Hz).

HRMS: calcd for $C_{44}H_{53}O_7$ ($M\text{-}H^-$) 693.3797; found 693.3778. ***m/z*:** MH^- 693 at 6.088 min (99%).

Due to the presence of a bond which could originate rotamers (highlighted in red in the molecular structure) and after observing the complexity of signals in NMR spectra (in both ^{1}H and ^{13}C), we considered having a potential mixture of atropisomers. Thus, we used a high temperature HNMR experiment to carefully check out this possibility. HNMR spectra of **3f** in DMSO were recorded at three different temperatures: 25, 45 and 65 ºC. While HNMR-DMSO spectrum at 25 ºC was as complicated as HNMR-$CDCl_3$, HNMR signals at 45 ºC started to be clearer. At 65 ºC, significant simplification of the biaryl and methyl signals were observed. Such experiment allowed us to consider **3f** as a single compound and not as a diastereomeric mixture. See HNMRs at 25, 45 and 65 ºC at page 23.

Double HNMR – CNMR experiments (HSQC and HMBC) have been analyzed for assigning the most significant Cs and Hs of the structure. See pages S22-24 for further details.

B) Synthesis of Hydroxamic Acids

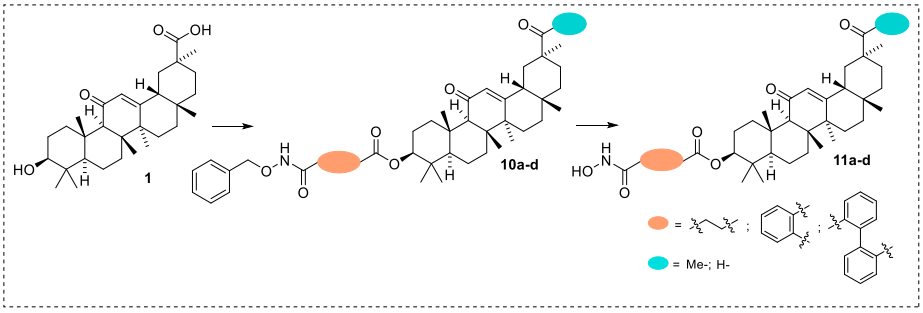

Scheme S2.4. CBX derivatives: introduction of acid carboxylic surrogates to CBX and derivatives.

General Procedure C (10a-d). According to an adapted procedure,[6] O-benzylhydroxylamine derivatives were obtained as followed. A solution of CBX (**1**, 1.0 Eq.) in anhydrous DMF (0.4 M)

was cooled to - 20 ºC. This mixture was treated with NMM (4.0 Eq.), followed by the addition of isobutyl chloroformate (4.0 Eq.) to form the mixed anhydride. After 3 hours, a solution of 4.0 Eq. of BnO-NH_2 · HCl (previously stirred with 6.0 Eq. of DIPEA and minimum amount of DMF for 30 min) was added dropwise. Then, the reaction mixture was then allowed to stir overnight at room temperature. After reaction completion was confirmed by TLC or HPLC, the reaction was stopped and the DMF, evaporated under reduced pressure. The residue was diluted with EtOAc and mixed with water, and extracted with EtOAc (3 x 20 mL). The combined organic layers were washed with $NaHCO_3$ (20 mL) and the organic layer was dried over $MgSO_4$, filtered and the solvent, evaporated under reduced pressure. The pure intermediates **10a-d** were obtained by automated flash column chromatography, using a gradient of CH_2Cl_2/MeOH (from 100:0 to 98:2, v/v) as eluent.

General Procedure D (11a-d). The corresponding compounds **10a-d** (1.0 Eq.) were dissolved in anhydrous CH_2Cl_2 (0.041 M). The resulting solution was purged with argon and then, 10 % Pd/C (0.15 Eq.) was added. The flask was once again purged with argon and then, the argon was removed through a vacuum line. A balloon filled with H_2 was carefully placed on the flask and the reaction mixture was left stirring at room temperature for 4 hours. After reaction completion confirmed by TLC, the flask was purged with argon and the reaction crude was filtered though Celite®. The solvent was evaporated under reduced pressure and the pure compounds **11a-d** bearing hydroxamic acids were obtained by automated flash column chromatography, using a gradient of CH_2Cl_2/MeOH (from 100:0 to 98:2, v/v) as eluent.

10-((2-((benzyloxy)carbamoyl)benzoyl)oxy)-2,4a,6a,6b,9,9,12a-heptamethyl-13-oxo-1,2,3,4,4a,5,6,6a,6b,7,8,8a,9,10,11,12,12a,12b,13,14b-icosahydropicene-2-carboxylic acid (10c)

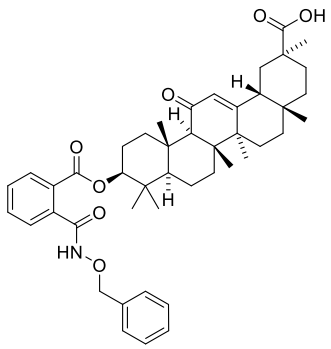

Following the ***General Procedure C***, the intermediate **10c** (0.096 g, 34%) was obtained as a white powder.

^{1}H NMR (400 MHz, DMSO-d_6) δ 12.18 (s, 1H), 11.46 (s, 1H), 7.82 (d, *J* = 7.3 Hz, 1H), 7.65 – 7.55 (m, 2H), 7.47 – 7.35 (m, 6H), 5.41 (s, 1H), 4.94 (s, 2H), 4.67 (dd, *J* = 11.7, 4.5 Hz, 1H), 2.67 (d, *J* = 13.9 Hz, 1H), 2.44 (s, 1H), 2.10 – 2.04 (m, 2H), 1.83 – 1.49 (m, 10H), 1.38 (s, 3H), 1.36 – 1.12 (m, 7H), 1.10 (s, 3H), 1.08 (s, 3H), 1.05 (s, 3H), 0.91 (cs, two overlapping s, 6H), 0.76 (s, 3H). The most significant H signals were assigned to the structure, comparing the HNMR of **10c** to the ones of **3e** and glycyrrhetinic acid **1** (see at page S25).

10-((2'-((((benzyloxy)amino)oxy)carbonyl)-[1,1'-biphenyl]-2-carbonyl)oxy)-2,4a,6a,6b,9,10,12,12a,12b,13,14b-icosahydropicene-2-carboxylic acid (10d)

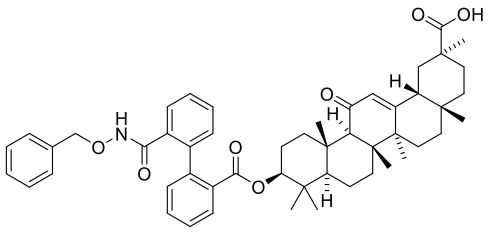

Following the ***General Procedure C***, the intermediate **10d** (0.074 g, 26%) was obtained as a white powder.

^{1}H NMR (400 MHz, $CDCl_3$) δ 9.29 (d, *J* = 47.5 Hz, 1H), 7.67 (cs, two overlapping d, *J* = 8.5 Hz, 2H), 7.50 – 7.33 (m, 5H), 7.27 (s, 3H), 7.12 (dt, *J* = 7.0, 4.2 Hz, 2H), 7.01 (t, *J* = 8.2 Hz, 1H), 5.70 (d, *J* = 2.1 Hz, 1H), 4.71 (t, *J* = 11.6, 1H), 4.53 (td, *J* = 12.6, 4.6 Hz, 1H), 4.35 (d, *J* = 11.5 Hz, 1H), 2.80 – 2.72 (m, 1H), 2.31 (s, 1H), 2.18 (d, *J* = 13.4, 1H), 2.06 – 1.93 (m, 3H), 1.82 (t, *J* = 13.8 Hz, 1H), 1.68 – 1.50 (m, 4H), 1.42 (d, *J* = 9.0 Hz, 5H), 1.35 (d, *J* = 7.0 Hz, 3H), 1.21 (s, 3H), 1.12 (cs, two overlapping s, 6H), 1.06 – 0.91 (m, 2H), 0.83 (cs, two overlapping s, 6H), 0.83 (s, 3H), 0.76 (d, *J* = 8.5 Hz, 3H).

The BnO-NH- substituent has been spotted at the lower acidic position of **3f** after recording and analyzing bidimensional NMR spectra (COSY, HSQC and HMBC). The diagnostic signals and the most significant Cs and correlating Hs are detailed at pages S26-27.

10-((2'-(((hydroxyamino)oxy)carbonyl)-[1,1'-biphenyl]-2-carbonyl)oxy)-2,4a,6a,6b,9,9,12a-heptamethyl-13-oxo-1,2,3,4,4a,5,6,6a,6b,7,8,8a,9,10,11,12,12a,12b,13,14b-icosahydropicene-2-carboxylic acid (11d)

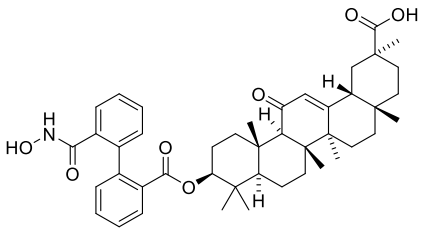

Following the ***General Procedure D***, the pure compound **11d** (0.025 g, 34%) was obtained as a light brown solid.

^{1}H NMR (400 MHz, $CDCl_3$) δ 7.81 – 7.77 (m, 1H), 7.74 – 7.68 (m, 1H), 7.51 – 7.39 (m, 4H), 7.21 (d, *J* = 7.3 Hz, 1H), 7.06 (t, *J* = 7.5 Hz, 1H), 5.69 (s, 1H), 4.65 – 4.56 (m, 1H), 2.77 (d, *J* = 13.6 Hz, 1H), 2.63 (s, 1H), 2.32 (d, *J* = 4.9 Hz, 1H), 2.04 – 1.75 (m, 5H), 1.67 – 1.56 (m, 4H), 1.40 (br s, 4H), 1.34 (d, *J* = 6.9 Hz, 3H), 1.20 (s, 3H), 1.15 (s, 3H), 1.12 (s, 3H), 1.06 – 0.95 (m, 3H), 0.91 (d, *J* = 8.6 Hz, 3H), 0.82 (cs, two overlapping s, 6H), 0.79 – 0.63 (m, 2H).

^{13}C NMR (101 MHz, $CDCl_3$) δ 211.04, 207.26, 200.24, 181.49, 169.66 (d, *J* = 6.2 Hz), 169.30 (d, *J* = 9.9 Hz), 166.58 (d, *J* = 7.3 Hz), 140.66, 140.23, 139.53 (d, *J* = 9.4 Hz), 131.72 (d, *J* = 6.5 Hz), 131.49, 130.73 (d, *J* = 4.5 Hz), 130.47, 129.69 (d, *J* = 12.9 Hz), 129.43, 128.53, 128.12 (d, *J* = 10.9 Hz), 82.80, 69.74, 61.74, 55.18, 53.90, 48.32, 45.54, 43.92, 43.31, 41.01, 38.86, 38.41 (d, *J* = 6.3 Hz), 37.85, 37.02 (d, *J* = 4.1 Hz), 32.77, 31.98, 31.06, 29.83, 29.37, 28.65 (d, *J* = 6.2 Hz), 26.59 (d, *J* = 8.9 Hz), 23.43 (d, *J* = 6.2 Hz), 18.80, 17.46, 17.02 (d, *J* = 15.1 Hz), 16.51.

HRMS: calcd for $C_{44}H_{56}NO_7^+$ ($M+H^+$) 710.4051; found 710.4041. ***m/z:*** MH^+ 710 at 5.201 min (99%).

2.2. Synthetic Procedures for the Preparation of DCPIB and derivatives

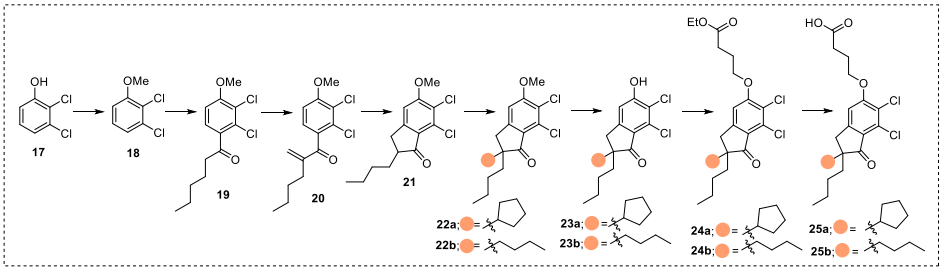

Scheme S2.6. DCPIB derivatives: preparation of the target DCPIB and non-chiral derivatives.

Compounds **18-21**, **22a**, **23a**, **24a** and **25a** were included in the original articles that reported the first synthesis of (-)-DCPIB.[7–9] Thus, for these compounds we have just reported HNMR spectra together with mass evidence or either HPLC data, in the cases where there wasn't molecular ionization.

General Procedure E (22a-b). A solution of **21** (0.600 g, 2.09 mmol, 1.0 Eq.) in dry *t*-BuOH (3.80 mL) and dry toluene (11.61 mL) under inert atmosphere was refluxed for 10 minutes. Then, *t*-BuOK (0.470 g, 4.18 mmol, 2.0 Eq.) in dry *t*-BuOH (14.93 mL) was added to the stirring mixture. The solution was refluxed for 0.5 hour until it turned to brown, cooled to room temperature, and treated with the corresponding alkyl halide (5.0 Eq.). The reaction mixture was refluxed for 20 minutes until it turned to green and cooled to room temperature. The crude was diluted with H_2O (30 mL) and EtOAc (30 mL) and washed with brine (3 x 50 mL). The combined organic phases were dried over $MgSO_4$, filtered, and concentrated under reduced pressure. The resulting crude mixture was purified through automated flash column chromatography, using a gradient of CH_2Cl_2/hexane (from 0:100 to 10:90, v/v) as eluent to obtain the pure compound **22a-b.**

2-butyl-6,7-dichloro-2-cyclopentyl-5-methoxy-2,3-dihydro-1*H*-inden-1-one (22a)

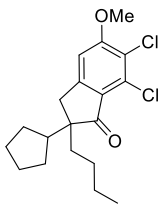

Following the ***General Procedure E*** and using 1-bromocyclopentane as alkyl halide, compound **22a** (0.233 g, 38%) was obtained as pale-yellow crystals.

^{1}H NMR (400 MHz, $CDCl_3$) δ 6.86 (s, 1H), 4.00 (s, 3H), 2.90 (d, *J* = 17.9 Hz, 1H), 2.81 (d, *J* = 17.8 Hz, 1H), 2.33 – 2.20 (m, 1H), 1.87 – 1.72 (m, 2H), 1.53 – 1.45 (m, 4H), 1.27 – 1.18 (m, 4H), 1.06 – 0.97 (m, 2H), 0.92 – 0.87 (m, 2H), 0.80 (d, *J* = 7.4 Hz, 3H).

***m/z*:** MH^+ 355 at 5.992 min.

General Procedure F (23a-b). Pyridine hydrochloride (29.4 Eq.) was melted by heating at 195 °C in a sealed tube, and **22a-b** (1.0 Eq.) was added with stirring. The mixture was heated for 3 hours. After reaction completion confirmed by LC-MS, the reaction mixture was poured into ice-water and the resulting suspension was extracted with Et_2O. The organic layer was washed with water (3 x 20 mL), dried over $MgSO_4$ and the solvent removed under reduced pressure. The resulting crude mixture was purified through automated flash column chromatography, using a gradient of CH_2Cl_2/hexane (from 100:0 to 80:20, v/v) as eluent to obtain the pure compound **23a-b**.

2,2-dibutyl-6,7-dichloro-5-hydroxy-2,3-dihydro-1*H*-inden-1-one (23b)

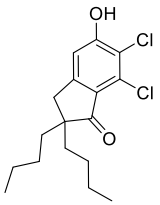

Following the ***General Procedure F***, compound **23b** (0.250 g, 67%) was obtained as a white powder.

^{1}H NMR (400 MHz, $CDCl_3$) δ 7.00 (s, 1H), 6.38 (s, 1H), 2.90 (s, 2H), 1.66 – 1.50 (m, 4H), 1.29 – 1.19 (m, 4H), 1.19 – 0.97 (m, 4H), 0.83 (t, *J* = 7.3 Hz, 6H).

^{13}C NMR (101 MHz, $CDCl_3$) δ 206.76, 157.19, 155.25, 130.89, 127.39, 120.41, 111.30, 53.94, 37.76, 36.99, 26.57, 23.40, 14.06.

HRMS: calcd for $C_{17}H_{23}Cl_2O_2^+$ 329.1071 ($M+H^+$); found 329.1068.

General Procedure G (24a-b). To a solution of **23a-b** (1.0 Eq.) and K_2CO_3 (3.0 Eq.) in acetone (1.5 mL) was added ethyl-4-bromobutyrate (1.2 Eq.). The mixture was heated at 50 °C for 48 hours. After reaction completion confirmed by LC-MS, the reaction mixture was quenched with saturated Na_2SO_4 aq. solution. The organic layer was extracted with CH_2Cl_2 (3 x 20 mL) and washed with water (3 x 20 mL), dried over $MgSO_4$, filtered and the solvent removed under reduced pressure. The resulting crude mixture was purified through automated flash column chromatography, using a gradient of CH_2Cl_2/hexane (from 0:100 to 40:60, v/v) as eluent to obtain the pure compounds **24a-b**.

Ethyl 4-((2-butyl-6,7-dichloro-2-cyclopentyl-1-oxo-2,3-dihydro-1*H*-inden-5-yl)oxy)butanoate (24a)

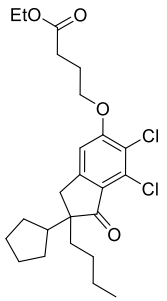

Following the ***General Procedure G,*** compound **24a** (0.1515 g, 76%) was obtained as colorless oil.

^{1}H NMR (400 MHz, $CDCl_3$) δ 6.85 (s, 1H), 4.22 – 4.07 (cs, t and q overlapped, 4H), 2.85 (d, *J* = 17.9 Hz, 1H), 2.77 (d, *J* = 17.8 Hz, 1H), 2.56 (t, *J* = 7.1 Hz, 2H), 2.28 – 2.11 (m, 3H), 1.84 – 1.66 (m, 2H), 1.58 – 1.40 (m, 6H), 1.23 (t, *J* = 7.1 Hz, 3H), 1.19 – 1.08 (m, 3H), 1.06 – 0.90 (m, 2H), 0.91 – 0.83 (m, 1H), 0.77 (t, *J* = 7.3 Hz, 3H).

^{13}C NMR (101 MHz, $CDCl_3$) δ 206.33, 172.94, 159.90, 155.50, 127.68, 107.32, 107.30, 68.56, 60.61, 56.14, 46.73, 37.84, 34.50, 30.36, 28.09, 27.14, 26.47, 25.48, 25.22, 24.25, 23.35, 14.25, 13.93.

HRMS: calcd for $C_{24}H_{33}Cl_2O_4^+$ 455.1750 ($M+H^+$); found 455.1756. ***m/z:*** MH^+ 455 at 6.176 min (90%).

Ethyl 4-((2,2-dibutyl-6,7-dichloro-1-oxo-2,3-dihydro-1*H*-inden-5-yl)oxy)butanoate (24b)

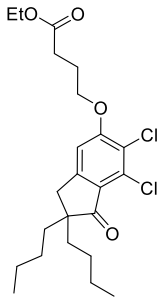

Following the ***General Procedure G,*** compound **24b (**0.268 g, 80%) was obtained as colorless oil.

^{1}H NMR (400 MHz, $CDCl_3$) δ 6.84 (s, 1H), 4.22 – 4.09 (cs, t and q overlapped, 4H), 2.89 (s, 2H), 2.59 (t, *J* = 7.1 Hz, 2H), 2.20 (p, *J* = 6.6 Hz, 2H), 1.63 – 1.52 (m, 5H), 1.31 – 1.24 (m, 6H), 1.17 – 1.00 (m, 4H), 0.83 (t, *J* = 7.3 Hz, 6H).

^{13}C NMR (101 MHz, $CDCl_3$) δ 206.52, 173.10, 160.06, 155.09, 131.61, 127.17, 123.05, 107.47, 68.62, 60.75, 53.78, 37.78, 37.19, 30.45, 29.84, 26.57, 24.34, 23.40, 14.35, 14.06.

HRMS: calcd for $C_{23}H_{33}Cl_2O_4^+$ 443.1750 ($M+H^+$); found 443.1752. ***m/z:*** MH^+ 443 at 5.786 min (98%).

General Procedure H (25a-b). To a solution of AcOH and 6 N HCl (3:1) was added **24a-b** (1.0 Eq.), and the mixture was allowed to stir at reflux for 7 hours. After reaction completion confirmed by LC-MS, the reaction mixture was poured into H_2O and mixed with Et_2O. The organic layer was separated and washed with water (3 x 20 mL), dried over $MgSO_4$, filtered and the solvent removed under reduced pressure. The resulting crude mixture was purified through automated flash column chromatography, using a gradient of CH_2Cl_2/MeOH (from 100:0 to 98:2, v/v) as eluent to obtain the pure compounds **25a-b**.

4-((2-butyl-6,7-dichloro-2-cyclopentyl-1-oxo-2,3-dihydro-1*H*-inden-5-yl)oxy)butanoic acid – *rac*DCPIB (25a)

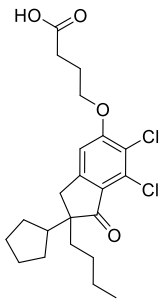

Following the ***General Procedure H,*** the racemic mixture **25a** (0.019 g, 91%) was obtained as a clear oil.

^{1}H NMR (400 MHz, $CDCl_3$) δ 6.84 (s, 1H), 4.19 (t, *J* = 5.9 Hz, 2H), 2.87 (d, *J* = 17.9 Hz, 1H), 2.79 (d, *J* = 17.7 Hz, 1H), 2.67 (t, *J* = 7.0 Hz, 2H), 2.27-2.18 (m, 3H), 1.86 – 1.70 (m, 2H), 1.60 – 1.43 (m, 6H), 1.29 – 1.12 (m, 3H), 1.04-0.95 (m, 2H), 0.92 – 0.84 (m, 1H), 0.80 (t, *J* = 7.3 Hz, 3H).

^{13}C NMR (101 MHz, $CDCl_3$) δ 206.49, 178.55, 159.87, 155.56, 131.49, 127.92, 123.04, 107.27, 68.42, 56.29, 46.82, 37.94, 34.61, 30.32, 28.21, 27.25, 26.57, 25.59, 25.32, 24.17, 23.45, 14.04.

HRMS: calcd for $C_{22}H_{27}Cl_2O_4^-$ 425.1292 ($M\text{-}H^-$); found 425.1300. ***m/z:*** MH^+ 427 at 4.741 min (88%).

4-((2,2-dibutyl-6,7-dichloro-1-oxo-2,3-dihydro-1*H*-inden-5-yl)oxy)butanoix acid (25b)

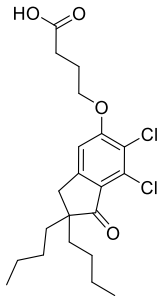

Following the ***General Procedure H***, compound **25b** (0.025 g, 93%) was obtained as a clear oil.

^{1}H NMR (400 MHz, $CDCl_3$) δ 6.84 (s, 1H), 4.19 (t, *J* = 5.9 Hz, 2H), 2.90 (s, 2H), 2.67 (t, *J* = 7.0 Hz, 2H), 2.23 (p, *J* = 6.5 Hz, 2H), 1.70 – 1.48 (m, 4H), 1.26 – 1.19 (m, 4H), 1.14 – 0.99 (m, 4H), 0.83 (t, *J* = 7.3 Hz, 6H).

^{13}C NMR (101 MHz, $CDCl_3$) δ 206.56, 178.45, 159.95, 155.11, 131.66, 127.26, 123.07, 107.44, 68.44, 53.81, 37.77, 37.21, 30.31, 26.56, 24.17, 23.40, 14.05.

HRMS: calcd for $C_{21}H_{27}Cl_2O_4^-$ 413.1292 (M-H$^-$); found 413.1300. ***m/z:*** MH^- 411 at 5.541 min (97%).

2.3. Synthetic Procedures for the Preparation of Hybrid Derivatives

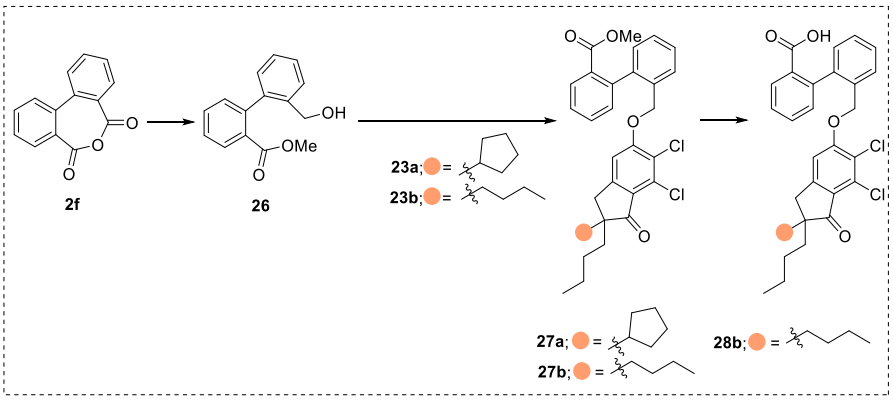

Scheme S2.7. Synthesis of hybrid derivatives merging structural features of both **CBX-3f** and DCPIB (**25a**).

General Procedure H (27a-b). Compounds **27a-b** were prepared by modifying an existing Mitsunobu reaction procedure, where we swapped sonication for microwave irradiation.[11] To a 0.5 – 10 mL microwave vial was added **23a-b** (1.0 Eq., 0.200 g, 0.61 mmol), **26** (1.1 Eq., 0.162 g, 0.67 mmol) and triphenyl phosphine (1.1 Eq., 0.176 g, 0.67 mmol) in 0.2 mL of THF (3.0 M regarding **23a-b**). The vial was stirred at room temperature for several minutes, giving a exothermic solution. While stirring, DIAD (1.1 Eq., 0.13 mL, 0.67 mmol) was added dropwise to the reaction mixture. The vial was then sealed and heated at 60 °C under microwave irradiation for 90 min. After reaction completion was detected by LC-MS, the reaction mixture was concentrated to dryness. The resulting crude mixture was purified through automated flash column chromatography, using a gradient of CH_2Cl_2/hexane (from 0:100 to 20:80, v/v) as eluent to obtain the pure compounds **27a-b**.

Methyl 2'-(((2-butyl-6,7-dichloro-2-cyclopentyl-1-oxo-2,3-dihydro-1*H*-inden-5-yl)oxy)methyl)-[1,1'-biphenyl]-2-carboxylate (27a)

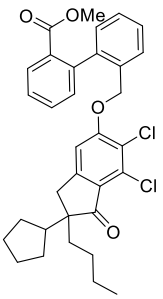

Following ***General Procedure H,*** compound **27a** (0.015 g, 58%) was obtained as a clear oil.

^{1}H NMR (400 MHz, $CDCl_3$) δ 7.99 (dd, *J* = 7.8, 1.4 Hz, 1H), 7.62 (d, *J* = 7.4, 1H), 7.55 (tt, *J* = 7.5, 1.3 Hz, 1H), 7.49 – 7.34 (m, 4H), 7.15 (dd, *J* = 7.6, 1.5 Hz, 1H), 6.69 (s, 1H), 5.00 – 4.95 (m, 2H), 3.64 (s, 3H), 2.83 – 2.65 (m, 2H), 2.28 – 2.17 (m, 1H), 1.80-1.66 (m, 2H), 1.55 – 1.43 (m, 6H), 1.27 – 1.09 (m, 4H), 1.02 – 0.93 (m, 2H), 0.79 (td, *J* = 7.3, 1.9 Hz, 3H).

^{13}C NMR (101 MHz, $CDCl_3$) δ 206.46, 167.68, 159.72, 157.08, 155.63, 155.43, 140.99, 140.73, 132.87, 131.88, 131.33 (d, *J* = 5.8 Hz), 130.34 (d, *J* = 4.4 Hz), 129.18, 128.02 (d, *J* = 3.3 Hz), 127.81, 127.66 (d, *J* = 4.0 Hz), 123.01, 111.12, 107.79, 69.75, 56.20, 52.20, 46.75 (d, *J* = 6.2 Hz), 37.93 (d, *J* = 4.2 Hz), 34.53, 28.18, 27.22, 26.53, 25.56 (d, *J* = 2.9 Hz), 25.30 (d, *J* = 3.8 Hz), 23.44. One C quaternary signal not detected.

HRMS: calcd for $C_{33}H_{35}Cl_2O_4^+$ 565.1907 ($M+H^+$); found 565.1895. ***m/z:*** MH^+ 565 at 6.073 min (93%).

Methyl 2'-((2,2-dibutyl-6,7-dichloro-1-oxo-2,3-dihydro-1*H*-inden-5-yl)oxy)methyl-[1,1'-biphenyl]-2-carboxylate (27b)

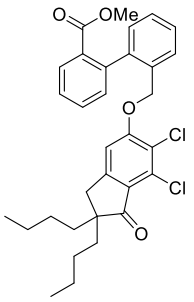

Following the ***General Procedure H,*** compound **27b** (0.199 g, 59%) was obtained as a clear oil.

^{1}H NMR (400 MHz, $CDCl_3$) δ 7.99 (dd, *J* = 7.8, 1.5 Hz, 1H), 7.61 (d, *J* = 5.8 Hz, 1H), 7.55 (td, *J* = 7.5, 1.5 Hz, 1H), 7.49 – 7.33 (m, 4H), 7.15 (dd, *J* = 7.4, 1.2 Hz, 1H), 6.69 (d, *J* = 0.9 Hz, 1H), 4.98 (d, *J* = 2.8 Hz, 2H), 3.65 (s, 3H), 2.80 (d, *J* = 3.4 Hz, 1H), 1.62 – 1.46 (m, 5H), 1.27-1.17 (m, 4H), 1.15 – 0.97 (m, 4H), 0.82 (td, *J* = 7.3, 1.7 Hz, 6H).

^{13}C NMR (101 MHz, $CDCl_3$) δ 206.50, 167.67, 159.78, 154.96, 140.97, 140.72, 132.86, 131.87, 131.45, 131.34, 130.36, 130.33, 129.18, 128.03, 128.01, 127.64, 127.13, 123.02, 108.00, 69.74, 53.71, 52.19, 37.67 (d, *J* = 3.9 Hz), 37.12, 26.53, 23.38, 14.04. One C quaternary signal not detected.

HRMS: calcd for $C_{32}H_{35}Cl_2O_4^+$ 553.1907 ($M+H^+$); found 553.1902. ***m/z:*** MH^+ 553 at 6.083 min (88%).

2'-(((2,2-dibutyl-6,7-dichloro-1-oxo-2,3-dihydro-1*H*-inden-5-yl)oxy)methyl)-[1,1'-biphenyl]-2-carboxylic acid (28b)

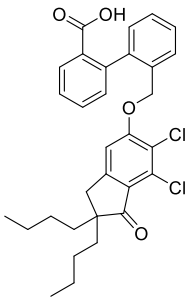

Compounds **28b** was prepared according to an adapted procedure[12] To a small vial was dissolved **27b** (1.0 Eq., 0.054 mmol, 0.030 g) in a mixture of H_2O:THF (1:1, 3.0 mL). An excess of 30% H_2O_2 (20.0 Eq., 1.08 mmol, 0.11 mL) was added before heating the solution to 60 °C for 4 hours. After reaction completion was detected by TLC, the reaction mixture was acidified with HCl 1M and diluted with Et_2O. The organic layer was separated, and the aqueous phase was extracted with Et_2O (3 x 10 mL). The combined organic layers were dried over $MgSO_4$, filtered and the solvent evaporated. The resulting crude was purified through automated flash column chromatography, using a gradient of CH_2Cl_2/MeOH (from 100:0 to 99:1) as eluent to obtain the pure compounds **28b** (0.011 g, 38%) as colourless oil.

^{1}H NMR (400 MHz, $CDCl_3$) δ 8.05 (dd, *J* = 7.9, 1.4 Hz, 1H), 7.61-7.54 (m, 2H), 7.47 (td, *J* = 7.7, 1.4 Hz, 1H), 7.44 – 7.39 (m, 1H), 7.40 – 7.32 (m, 2H), 7.16 (dd, *J* = 7.5, 1.5 Hz, 1H), 6.66 (s, 1H), 4.97 (d, *J* = 3.1 Hz, 2H), 2.79 (s, 2H), 1.59 – 1.44 (m, 4H), 1.26 – 1.14 (m, 4H), 1.11 – 0.94 (m, 4H), 0.80 (td, *J* = 7.3, 1.7 Hz, 6H).

^{13}C NMR (101 MHz, $CDCl_3$) δ 206.57, 170.56, 159.72, 154.99, 141.56, 140.53, 132.76, 132.69, 131.64, 131.49, 131.12, 129.23, 128.95, 128.13, 128.11, 127.78, 127.14, 123.00, 107.93, 69.76, 53.71, (d, *J* = 3.9 Hz), 37.11, 26.52, 23.39, 14.07. One C quaternary signal not detected.

HRMS: calcd for $C_{31}H_{33}Cl_2O_4^+$ 539.1750 ($M+H^+$); found 539.1742. ***m/z:*** MH^+ 539 at 6.401 min (96%).

2.4. Synthetic Procedure for the Preparation of the Photo-cross-linkable Inactive Control

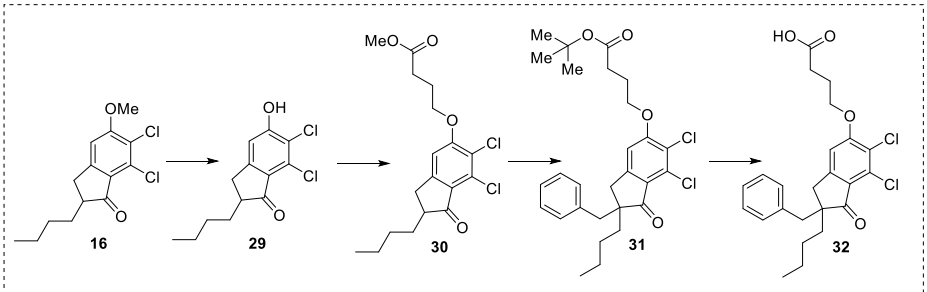

SchemeS2.8. DCPIB derivatives: synthesis of the negative control of the photo-cross-linkable DCPIB.

2-butyl-6,7-dichloro-5-hydroxy-2,3-dihydro-1*H*-inden-1-one (29)

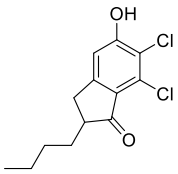

Pyridine hydrochloride (20.88 g, 180.70 mmol, 29.4 Eq.) was melted by heating at 195 ºC in an opened flask, and compound **16** (1.77 g, 6.15 mmol, 1.0 Eq.) was added with stirring. The mixture was heated for 4 hours. After reaction completion confirmed by LC-MS, the reaction mixture was poured into ice-water and the resulting suspension was extracted with Et_2O. The organic layer was washed with water (3 x 20 mL), dried over $MgSO_4$ and the solvent removed under reduced pressure. The resulting crude mixture was purified through automated flash column chromatography, using a gradient of CH_2Cl_2/hexane (from 100:0 to 90:10, v/v) as eluent to obtain the pure compound **29** (1.276 g, 76%) as beige powder.

^{1}H NMR (400 MHz, $CDCl_3$) δ 6.83 (s, 1H), 3.32 (br s, 1H), 3.17 – 3.05 (m, 1H), 2.67 – 2.53 (m, 2H), 1.34 –1.26 (m, 5H), 1.90 – 1.82 (m, 1H), 0.84 (t, J = 7.2 Hz, 3H).

^{13}C NMR (101 MHz, $CDCl_3$ and one drop of MeOD) δ 204.78, 159.24, 155.51, 131.45, 125.83, 121.19, 111.19, 48.40, 31.97, 31.36, 29.41, 22.67, 13.92.

HRMS: calcd for $C_{13}H_{15}Cl_2O_2^+$ ($M+H^+$) 273.0444; found 273.0443.

Methyl 4-((2-butyl-6,7-dichloro-1-oxo-2,3-dihydro-1H-inden-5-yl)oxy)butanoate (30)

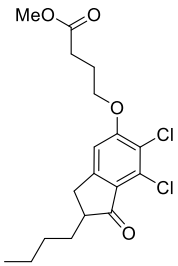

To a solution of **29** (1.28 g, 4.68 mmol, 1.0 Eq.) and K_2CO_3 (1.94 g, 14.04 mmol, 3.0 Eq.) in DMF (50 mL) was added methyl-4-bromobutyrate (0.709 mL, 5.60 mmol, 1.2 Eq.). The mixture was heated at 50 ºC for overnight. After reaction completion confirmed by LC-MS, the reaction mixture was poured into 2M NaOH solution. The organic layer was extracted with EtOAc (3 x 20 mL) and washed with water (3 x 20 mL), dried over $MgSO_4$, filtered and the solvent removed under reduced pressure. The resulting crude mixture was purified through automated flash column chromatography, using a gradient of CH_2Cl_2/hexane (from 0:100 to 50:50, v/v) as eluent to obtain the pure compounds **30** (0.821 g, 47%) as pale-yellow solid.

^{1}H NMR (400 MHz, $CDCl_3$) δ 6.84 (s, 1H), 4.17 (t, *J* = 6.0 Hz, 2H), 3.69 (s, 3H), 3.25 – 3.12 (m, 1H), 2.74 – 2.63 (m, 2H), 2.59 (t, *J* = 7.1 Hz, 2H), 2.25 – 2.16 (m, 2H), 1.98 – 1.88 (m, 1H), 1.42 – 1.24 (m, 5H), 0.90 (t, *J* = 7.1 Hz, 3H).

^{13}C NMR (101 MHz, $CDCl_3$) δ 203.60, 173.17, 159.66, 155.13, 131.43, 126.45, 122.75, 107.31, 68.28, 51.58, 48.09, 32.13, 31.18, 29.88, 29.23, 23.98, 22.51, 13.79.

HRMS: calcd for $C_{18}H_{23}Cl_2O_4^+$ (M+H$^+$) 373.0968; found 373.0966.

***Tert*-butyl 4-((2-benzyl-2-butyl-6,7-dichloro-1-oxo-2,3-dihydro-1*H*-inden-5-yl)oxy)butanoate (31)**

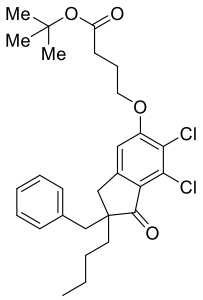

A solution of **30** (0.050 g, 0.134 mmol, 1.0 Eq.) in dry *t*-BuOH (0.25 mL) and dry toluene (0.75 mL) flask under inert atmosphere was refluxed for 10 minutes. Then, *t*-BuOK (0.030 g, 0.27 mmol, 2.0 Eq.) in dry *t*-BuOH (0.50 mL) was added to the stirring mixture, turning it to a deep yellow mixture. The solution was refluxed for 0.5 hour until it turned to brown, cooled to room temperature, and treated with benzyl bromide (0.160 mL, 1.34 mmol, 10.0 Eq.). The reaction mixture was refluxed for 20 minutes and cooled to room temperature. The crude was diluted with H_2O (30 mL) and EtOAc (30 mL) and washed with Brine (3 x 50 mL). The combined organic phases were dried over $MgSO_4$, filtered and concentrated under reduced pressure. The resulting crude mixture was purified through automated flash column chromatography, using a gradient of CH_2Cl_2/hexane (from 0:100 to 20:80, v/v) as eluent to obtain the pure compound **31** (0.011 g, 18%) as colorless oil.

^{1}H NMR (400 MHz, $CDCl_3$) δ 7.20 – 7.06 (m, 5H), 6.69 (s, 1H), 4.09 (t, *J* = 5.4 Hz, 2H), 3.10 (d, *J* = 13.4 Hz, 1H), 3.01 (d, *J* = 16.6 Hz, 1H), 2.84 – 2.71 (m, 2H), 2.46 (t, *J* = 7.2 Hz, 2H), 2.15 – 2.08 (m, 2H), 1.81-1.75 (m, 1H), 1.57 (s, 1H), 1.44 (s, 9H), 1.26-1.20 (m, 2H), 1.12-1.04 (m, 2H), 0.83 (t, *J* = 7.3 Hz, 3H).

^{13}C NMR (101 MHz, $CDCl_3$) δ 205.83, 172.41, 160.05, 154.95, 137.54, 131.48, 130.28, 128.24, 127.07, 126.58, 122.95, 107.32, 80.80, 68.69, 55.03, 43.30, 38.61, 35.58, 31.56, 28.26, 26.65, 24.43, 23.37, 14.06.

HRMS: calcd for $C_{28}H_{35}Cl_2O_4^+$ (M+H$^+$) 505.1907; found 505.1833. ***m/z:*** MH$^+$ 505 at 4.791 min (90%).

4-((2-benzyl-2-butyl-6,7-dichloro-1-oxo-2,3-dihydro-1*H*-inden-5-yl)oxy)butanoic acid (32)

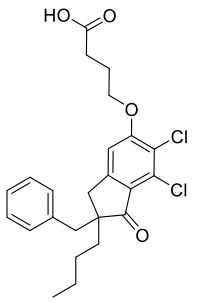

According to a reported procedure,[13] compound **31** (0.010 g, 0.020 mmol, 1.0 Eq.) was dissolved in 4 M HCl in dioxane (0.33 mL) and the resulting solution was stirred at 40 °C for 5 hours. After checking the reaction completion by TLC, the reaction mixture was concentrated under reduced pressure to yield the pure final product **32** (8.8 mg, 99%) as colorless oil.

^{1}H NMR (400 MHz, $CDCl_3$ and one drop of dioxane) δ 7.21 – 7.05 (m, 5H), 6.69 (s, 1H), 4.11 (t, *J* = 5.8 Hz, 2H), 3.11 (d, *J* = 13.4 Hz, 1H), 3.02 (d, *J* = 17.5 Hz, 1H), 2.77 (t, *J* = 15.4, 2H), 2.57 (t, *J* = 7.0 Hz, 2H), 2.20 – 2.09 (m, 2H), 1.82 – 1.74 (m, 1H), 1.59 – 1.50 (m, 1H), 1.34 – 1.20 (m, 2H), 1.16 – 0.99 (m, 2H), 0.83 (t, *J* = 7.3 Hz, 3H).

^{13}C NMR (101 MHz, $CDCl_3$ and one drop of dioxane) δ 205.82, 173.49, 159.93, 154.95, 137.52, 131.50, 130.28, 128.24, 127.12, 126.57, 122.91, 107.30, 55.03, 51.89, 43.28, 38.62, 35.57, 30.16, 26.64, 24.28, 23.36, 14.05.

HRMS: calcd for $C_{24}H_{27}Cl_2O_4^+$ ($M+H^+$) 449.1281; found 449.1252. ***m/z:*** MH^+ 449 at 5.983 min (88%).

2.5. Synthetic Procedures for the Preparation of the Photo-cross-linkable DCPIB

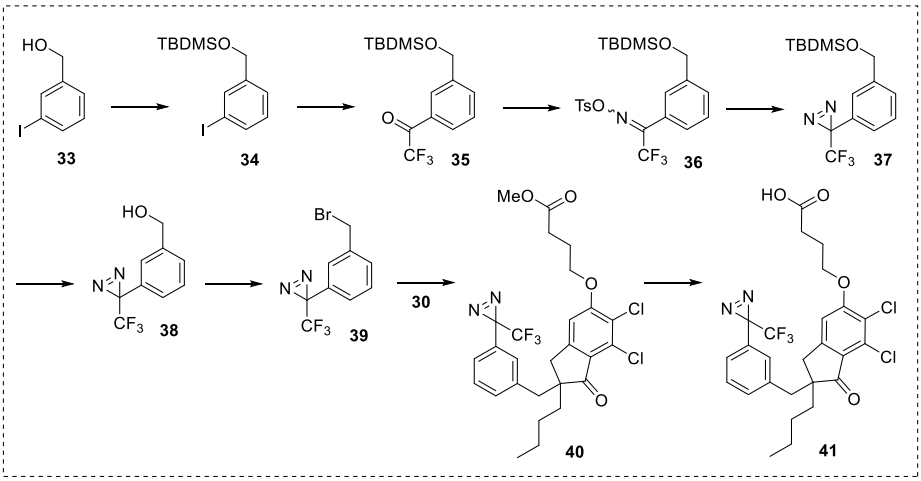

Scheme S2.9. DCPIB derivatives: synthesis of the photo-cross linkable derivative **41**.

The synthetic route of **41** has been adapted from reported procedures.[14] Hence, we just present complete characterization data for the not previously described compounds (**39-41**).

3-(3-(bromomethyl)phenyl)-3-(trifluoromethyl)-3*H*-diazirine (39)

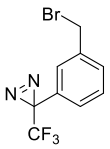

According to an adapted procedure,[15] PPh_3 (0.705 g, 2.69 mmol, 1.25 Eq.) was added in portions to a solution of **38** (0.465 g, 2.15 mmol, 1.0 Eq.) and CBr_4 (0.892 g, 2.69 mmol, 1.25 Eq.) in anhydrous CH_2Cl_2 (10.6 mL) at 0 °C. The resulting mixture was stirred for 30 minutes at room

temperature. After reaction completion checked by TLC, the reaction crude was evaporated under reduced pressure. The pure compound **39** (0.570 g, 95%) was obtained as colorless oil by a quick wash of EtOAc through packed silica.

^{1}H NMR (400 MHz, $CDCl_3$) δ 7.46 (d, *J* = 7.8 Hz, 1H), 7.44 – 7.35 (m, 1H), 7.22 – 7.13 (m, 2H), 4.46 (s, 2H).

^{13}C NMR (101 MHz, $CDCl_3$) δ 138.92, 130.46, 129.95, 129.55, 127.02, 126.64, 122.16 (q, $J_{C\text{-}F}$ = 270.5 Hz), 32.29, 28.63 (d, $J_{C\text{-}F}$ = 40.3 Hz).

^{19}F NMR (376 MHz, $CDCl_3$) δ -65.15**.**

HRMS: calcd for $C_9H_7BrF_3N_2^+$ ($M+H^+$) 278.9739; found 279.0806.

Methyl 4-((2-butyl-6,7-dichloro-1-oxo-2-(3-(3-(trifluoromethyl)-3*H*-diazirin-3-yl)benzyl)-2,3-dihydro-1*H*-inden-5-yl)oxy)butanoate (40)

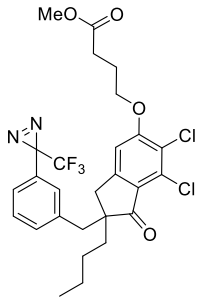

Following a reported LDA alkylation protocol,[16] to a solution of **39** (0.095 g, 0.255 mmol, 1.0 Eq.) in anhydrous THF (2.5 mL) was rapidly added LDA (1.0 M in hexanes, 0.280 mL, 0.280 mmol, 1.100 Eq.) at - 78 ˚C, and the resulting solution was stirred for 1h 30 min at the same temperature. A solution of **25** (0.213 g, 0.764 mmol, 3.0 Eq.) in anhydrous THF (1.5 mL) was then added at - 78 ºC. After maintaining the solution at - 78 ˚C for 3 hours, it was then warmed to room temperature and stirred overnight. After reaction completion check by HPLC-MS, the crude was mixed with saturated NH_4Cl solution and extracted with Et_2O (3 x 20 mL). The combined organic layers were dried over $MgSO_4$, and the solvent was removed under reduced pressure. The pure compound 40 (0.056 g, 39%, yellowish oil) was obtained through automated flash column chromatography, using a gradient of CH_2Cl_2/hexane (gradient from 0:100 to 50:50, v/v) as solvent system.

^{1}H NMR (400 MHz, $CDCl_3$) δ 7.18 (t, *J* = 7.7 Hz, 1H), 7.12 (d, *J* = 7.8 Hz, 1H), 6.94 (d, *J* = 7.8 Hz, 1H), 6.87 (s, 1H), 6.68 (s, 1H), 4.11 (t, *J* = 6.1 Hz, 2H), 3.69 (s, 3H), 3.10 (d, *J* = 13.4 Hz, 1H), 2.88 (d, *J* = 17.5 Hz, 1H), 2.81 (d, *J* = 17.2 Hz, 1H), 2.74 (d, *J* = 13.4 Hz, 1H), 2.57 (t, *J* = 7.1 Hz, 2H), 2.21 – 2.14 (m, 2H), 1.79-1.70 (m, 1H), 1.57-1.48 (m, 1H), 1.25 – 1.20 (m, 2H), 1.14 – 1.03 (m, 2H), 0.83 (t, *J* = 7.3 Hz, 3H).

^{13}C NMR (101 MHz, $CDCl_3$) δ 205.26, 173.47, 160.07, 154.62, 138.43, 131.60, 131.54, 128.95, 128.82, 128.03, 126.98, 124.81, 123.08, 122.20 (q, $J_{C\text{-}F}$ = 271.7 Hz), 107.19, 68.55, 54.87, 51.87, 43.18, 38.43, 35.59, 30.15, 28.42 (q, $J_{C\text{-}F}$ = 40.3 Hz), 26.59, 24.26, 23.30, 14.00. The C coupled with F, with chemical shift of 28.23 ppm, should be a quadruplet just like the signal at 122.20. However, the small signals were not detected as are probably overlapped within the noise.

^{19}F NMR (376 MHz, $CDCl_3$) δ -65.22.

HRMS: calcd for $C_{27}H_{28}Cl_2F_3N_2O_4^+$ ($M+H^+$) 571.1373; found 571.1421.

4-((2-butyl-6,7-dichloro-1-oxo-2-(3-(3-(trifluoromethyl)-3*H*-diazirin-3-yl)benzyl)-2,3-dihydro-1*H*-inden-5-yl)oxy)butanoate (41)

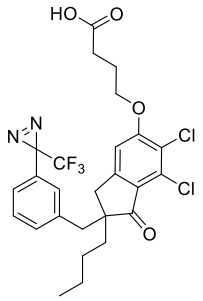

According to a reported procedure,[17] the corresponding amount of 1M LiOH (0.196 mL, 0.196 mmol, 2.0 Eq.) was added to a solution of **40** (0.056 g, 0.098 mmol, 1.0 Eq.) in THF (0.196 mL) over 20 minutes. After stirring the mixture for 1 hour, reaction completion was confirmed by TLC. The resulting solution was cooled to 0 °C and acidified with 1M HCl aq. solution. The suspension was extracted with EtOAc and the combined organic layers were washed with brine and dried over $MgSO_4$. The crude was purified through automated flash column chromatography, using a gradient of CH_2Cl_2/MeOH (from 100:0 to 99:1, v/v) as solvent system, to afford the pure compound **41** (0.048 g, 88%) as yellowish oil.

^{1}H NMR (400 MHz, $CDCl_3$) δ 7.18 (t, *J* = 7.7 Hz, 1H), 7.12 (d, *J* = 8.1 Hz, 1H), 6.94 (d, *J* = 7.8 Hz, 1H), 6.88 (s, 1H), 6.67 (s, 1H), 4.12 (t, *J* = 5.9 Hz, 2H), 3.10 (d, *J* = 13.4 Hz, 1H), 2.89 (d, *J* = 17.6 Hz, 1H), 2.81 (d, *J* = 17.6 Hz, 1H), 2.75 (d, *J* = 13.4 Hz, 1H), 2.63 (t, *J* = 7.0 Hz, 2H), 2.24-2.15 (m, 2H), 1.81-1.71 (m, *J* = 13.3, 11.2, 5.4 Hz, 1H), 1.59 – 1.48 (m, 1H), 1.32 – 1.25 (m, 2H), 1.14-1.05 (m, 2H), 0.84 (t, *J* = 7.3 Hz, 3H).

^{13}C NMR (101 MHz, $CDCl_3$) δ 205.30, 178.51, 159.98, 154.62, 138.41, 131.64, 131.55, 128.93, 128.83, 128.03, 127.06, 124.82, 122.80 (d, $J_{C\text{-}F}$ = 61.2 Hz), 122.20 (d, *J* = 274.8 Hz), 107.15, 68.41, 54.90, 43.20, 38.39, 35.60, 30.25, 28.43 (d, $J_{C\text{-}F}$ = 40.4 Hz), 26.59, 24.08, 23.30, 14.01. The two C atoms coupled with F, with chemical shifts of 120.84 and 28.23 ppm respectively, should follow the quadruplet pattern 1:3:3:1 as if in compound **25**. However, the small signals were not detected.

^{19}F NMR (376 MHz, $CDCl_3$) δ -65.22.

HRMS: calcd for $C_{26}H_{24}Cl_2F_3N_2O_4^-$ ($M-H^-$) 555.1071; found 555.1746.

3. Selected NMR spectra

Carbenoxolone (3a)

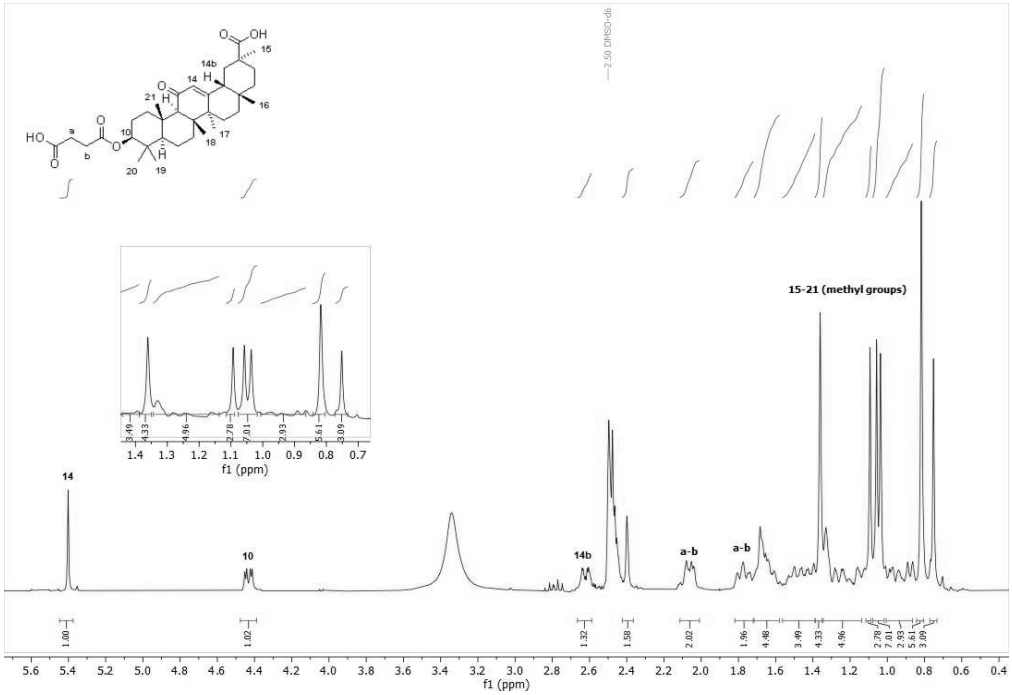

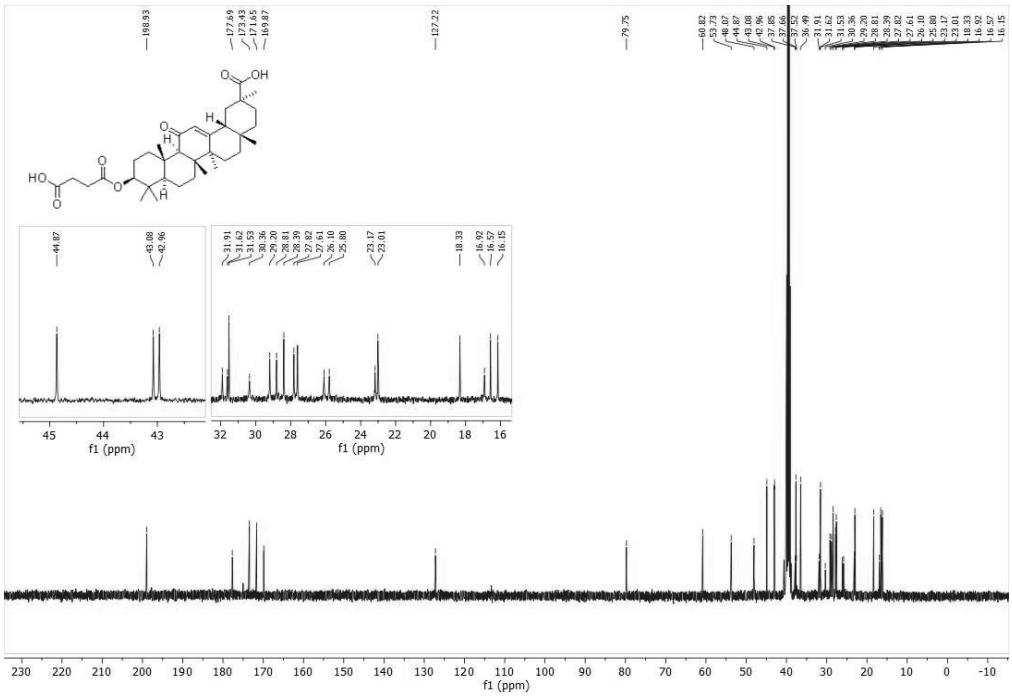

10-((2-carboxybenzoyl)oxy)-2,4a,6a,6b,9,9,12a-heptamethyl-13-oxo-1,2,3,4,4a,5,6,6a,6b,7,8,8a,9,10,11,12,12a,12b,13,14b-icosahydropicene-2-carboxylic acid (3e) and comparison with ^{1}H NMR spectrum of compound 1.

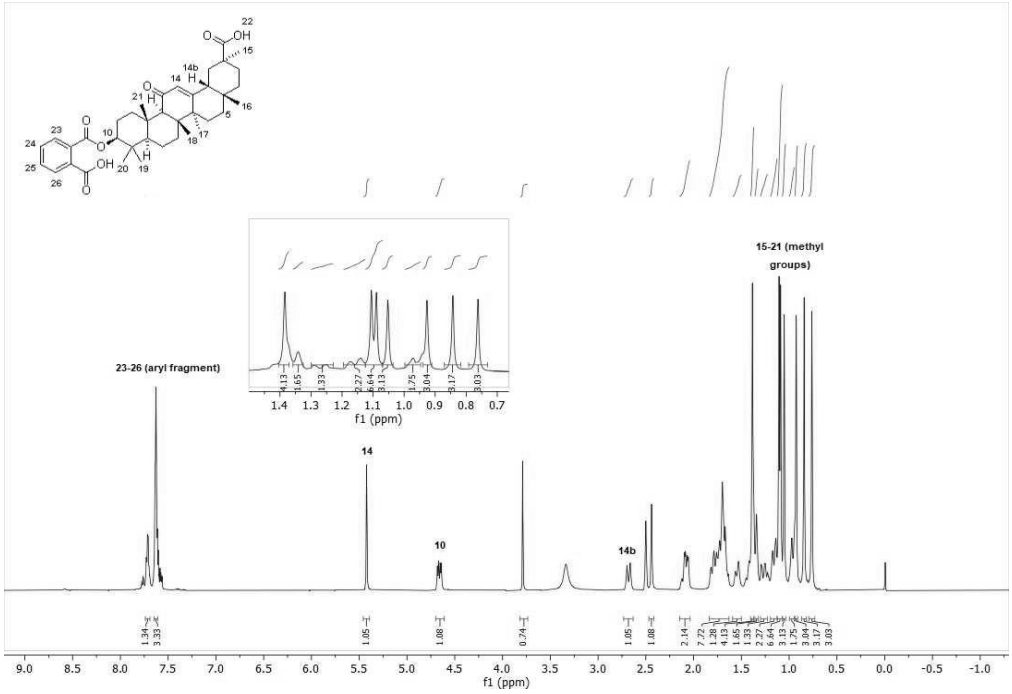

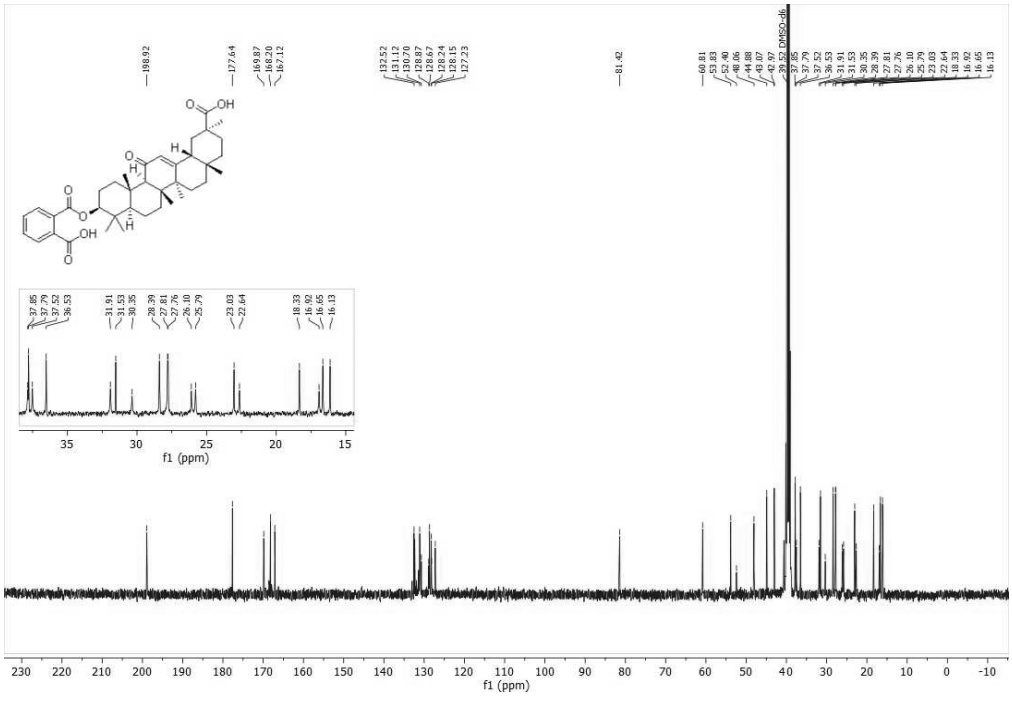

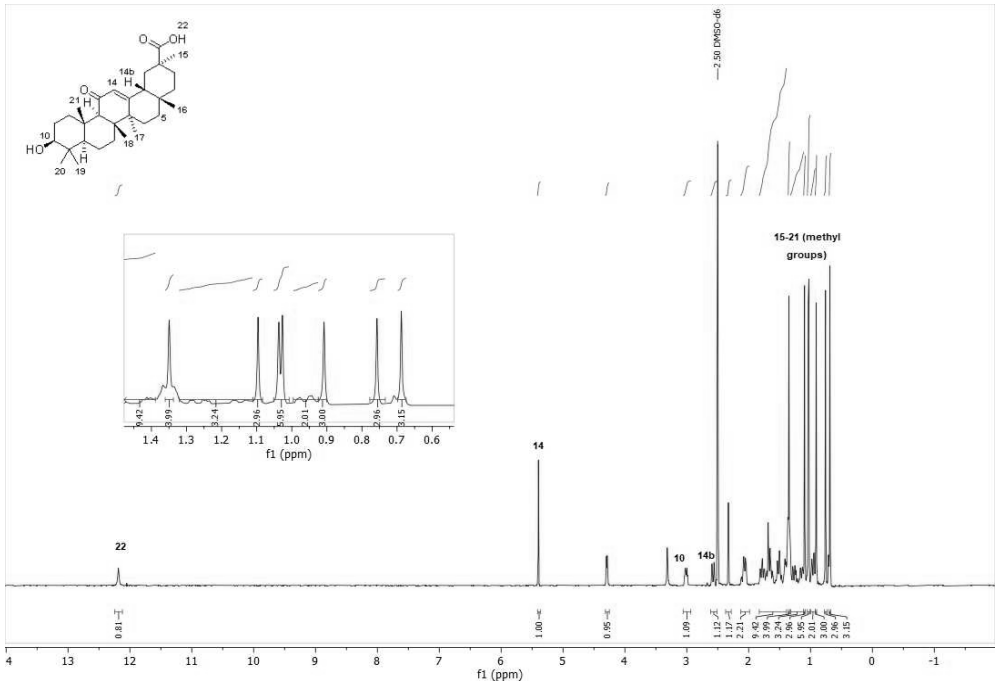
22
OH
15
14b
H
14
O
21
H
16
5
10
HO
18
17
H
20
19
2.50 DMSO-d6
15-21 (methyl groups)
14
22
10
14b
f1 (ppm)

10-((2'-carboxy-[1,1'-biphenyl]-2-carbonyl)oxy)-2,4a,6a,6b,9,9,12a-heptamethyl-13-oxo-1,2,3,4,4a,5,6,6a,6b,7,8,8a,9,10,11,12,12a,12b,13,14b-icosahydropicene-2-carboxylic acid (3f)

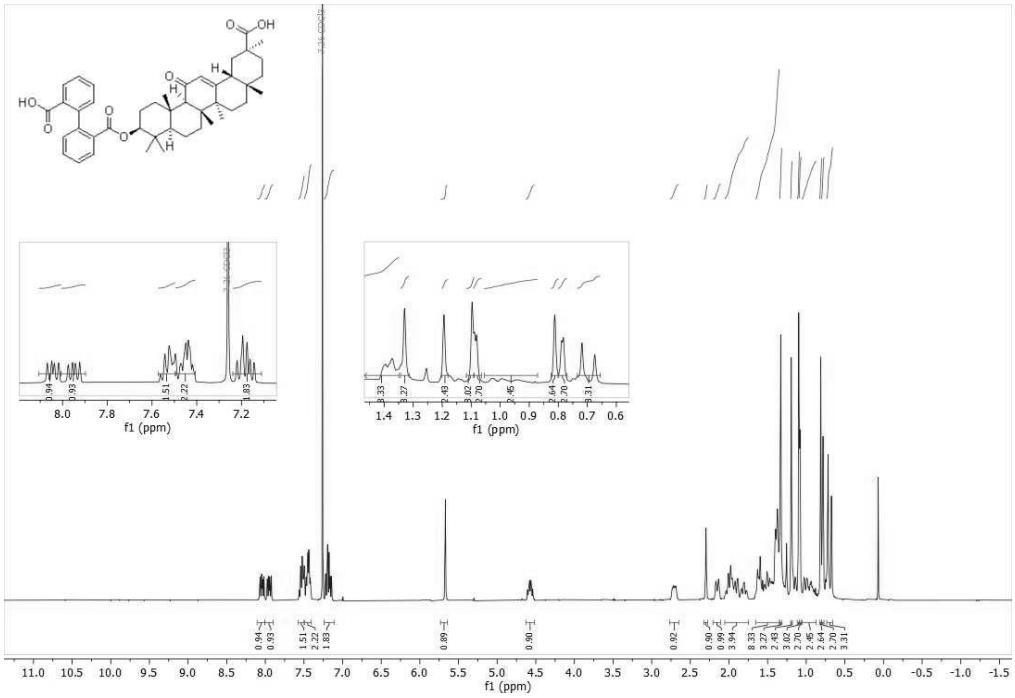

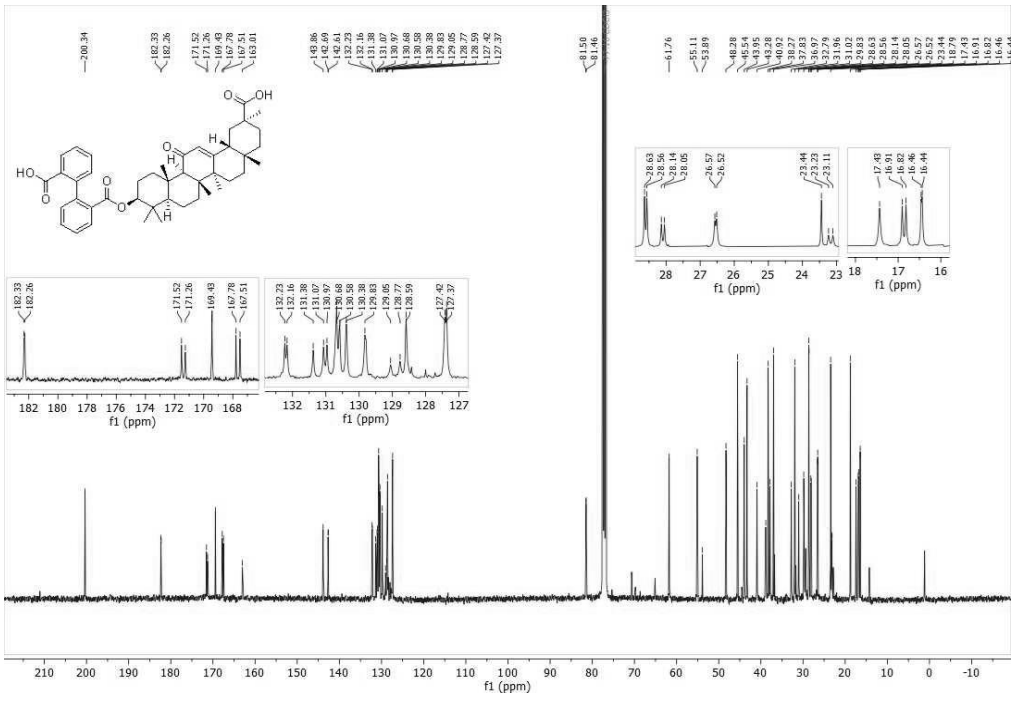

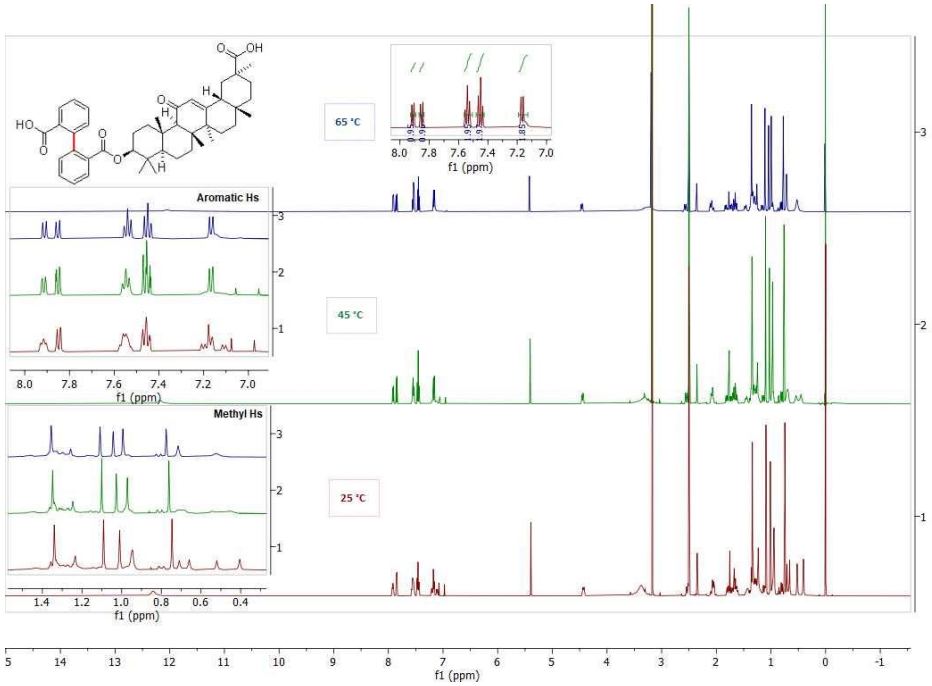

Figure S1. Variable temperature NMR experiments. The same sample of **3f** was recorded at 25, 45 and 65 ˚C, respectively.

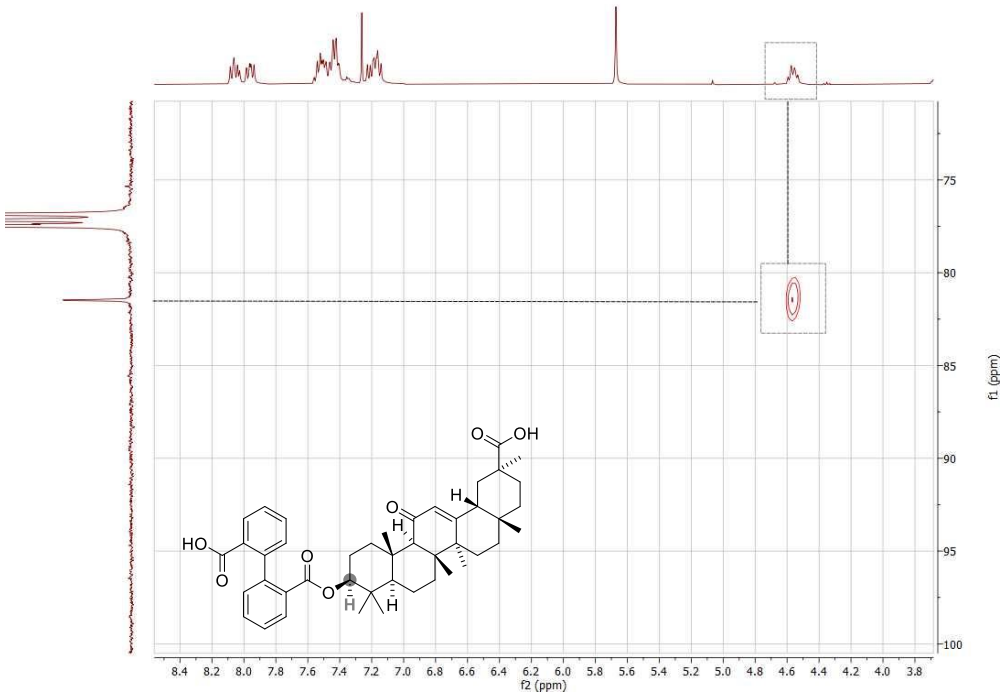

Figure S2. Identification of the C-OCO- (highlighted in gray) through HSQC.

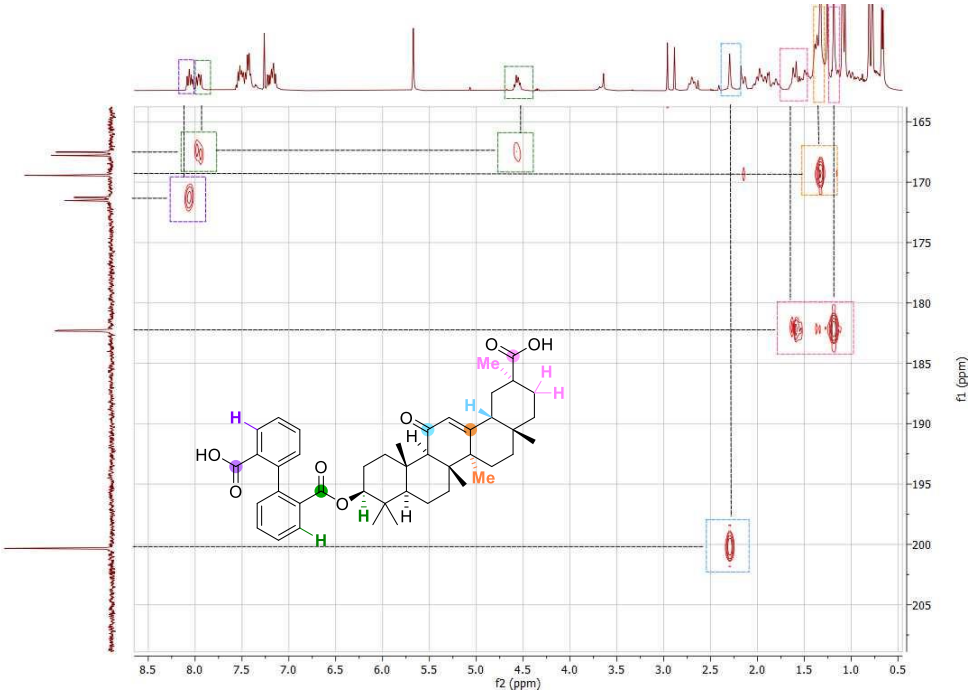

Figure S3. Assignation of all C atoms from C=O presents in the molecule through HMBC. Each C atom is highlighted in the same color than the correlating Hs.

10-((2-((benzyloxy)carbamoyl)benzoyl)oxy)-2,4a,6a,6b,9,9,12a-heptamethyl-13-oxo-1,2,3,4,4a,5,6,6a,6b,7,8,8a,9,10,11,12,12a,12b,13,14b-icosahydropicene-2-carboxylic acid (10c)

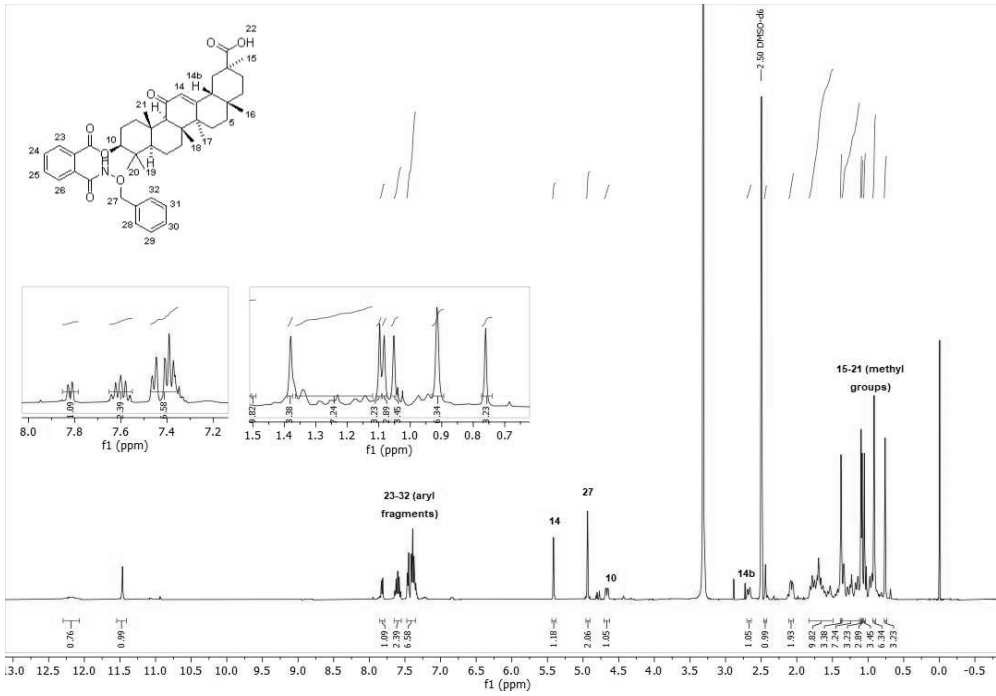

10-((2'-((((benzyloxy)amino)oxy)carbonyl)-[1,1'-biphenyl]-2-carbonyl)oxy)-2,4a,6a,6b,9,10,12,12a,12b,13,14b-icosahydropicene-2-carboxylic acid (10d)

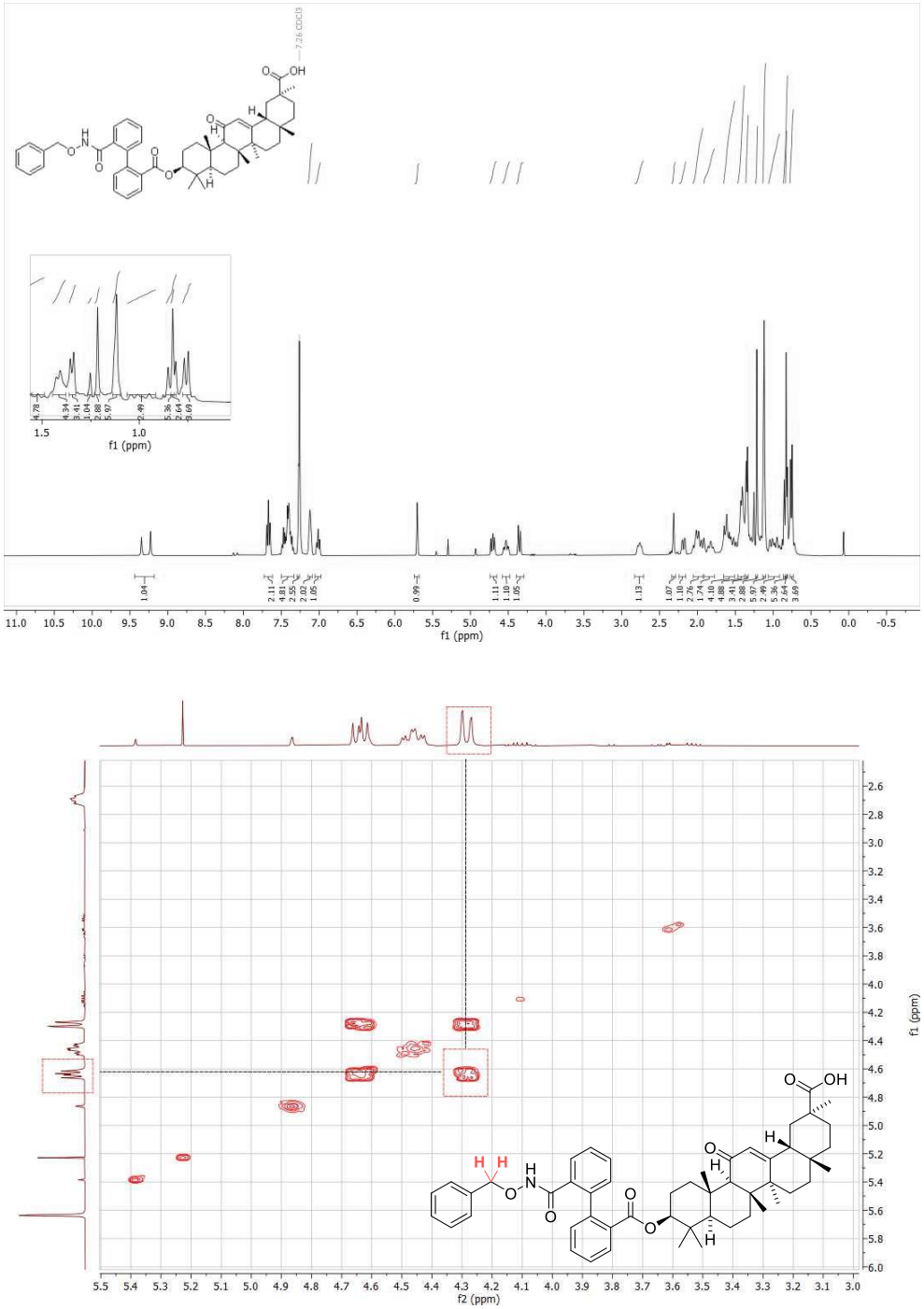

Figure S4. Identification of the benzylic protons (-CH_2-, highlighted in red) through COSY.

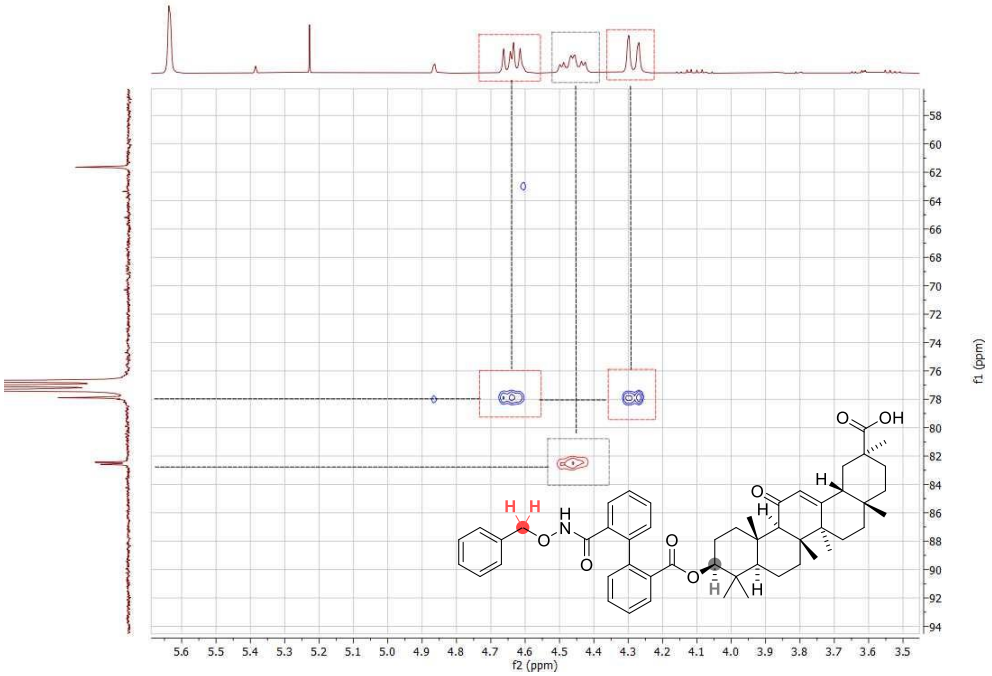

Figure S5. Identification of the benzylic C (highlited in red) and the C-OCO- (highlighted in gray) through HSQC.

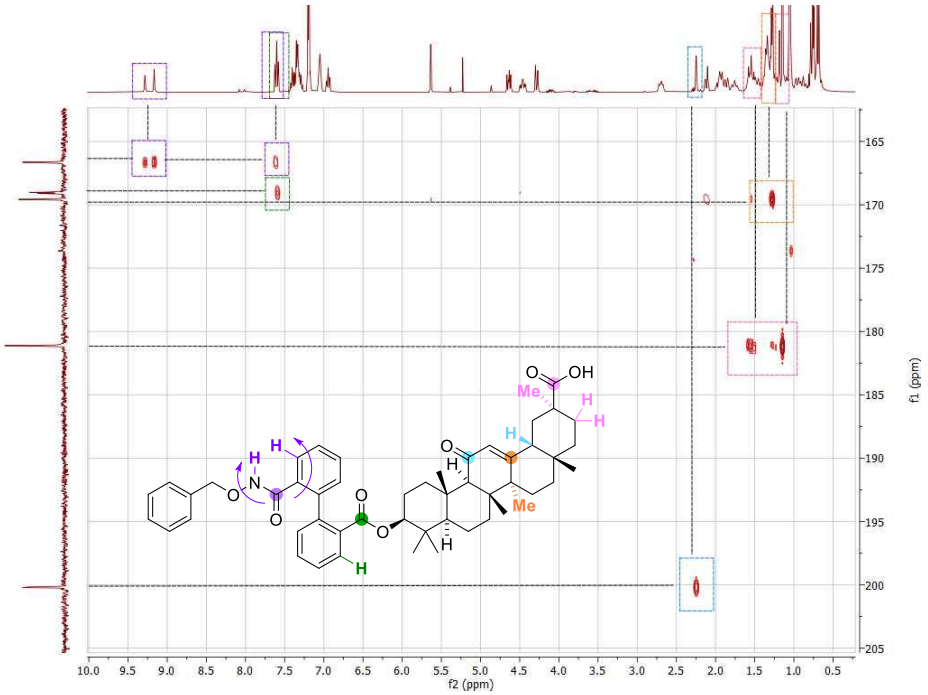

Figure S6. Assignation of all C atoms from C=O presents in the molecule through HMBC. Each C atom is highlighted in the same color than the correlating Hs. The correlation between the C belonging to the -CONH- fragment and a H of the biaryl- and the NH the *O*-benzylhydroxylamine is considered a diagnostic signal.

10-((2'-(((hydroxyamino)oxy)carbonyl)-[1,1'-biphenyl]-2-carbonyl)oxy)-2,4a,6a,6b,9,9,12a-heptamethyl-13-oxo-1,2,3,4,4a,5,6,6a,6b,7,8,8a,9,10,11,12,12a,12b,13,14b-icosahydropicene-2-carboxylic acid (11d)

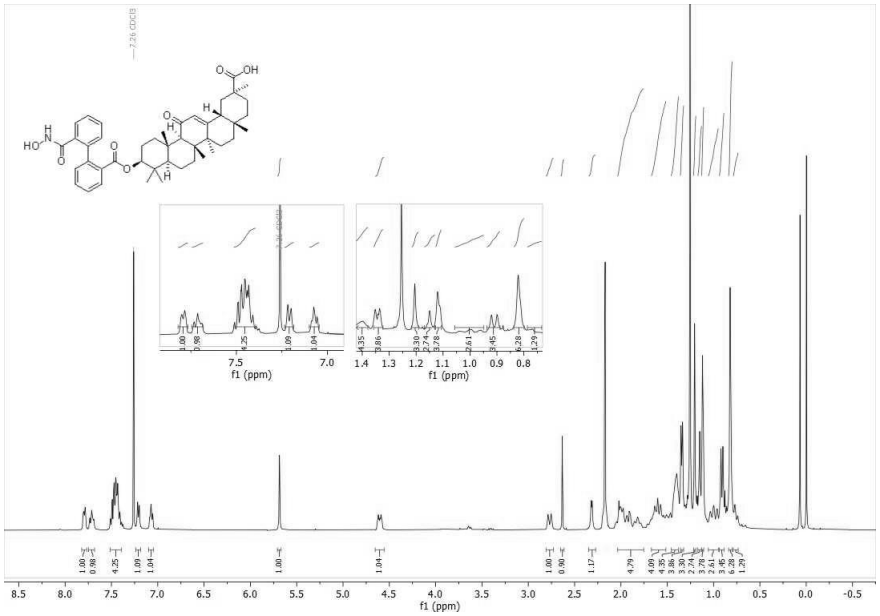

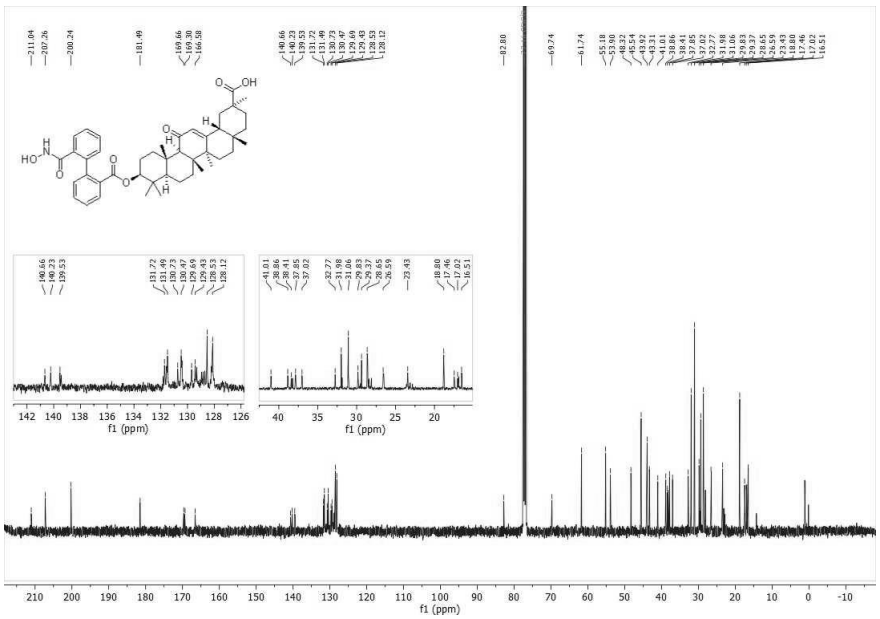

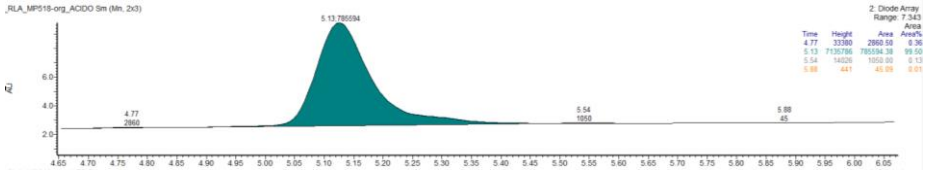

2,2-dibutyl-6,7-dichloro-5-methoxy-2,3-dihydro-1*H*-inden-1-one (22b)

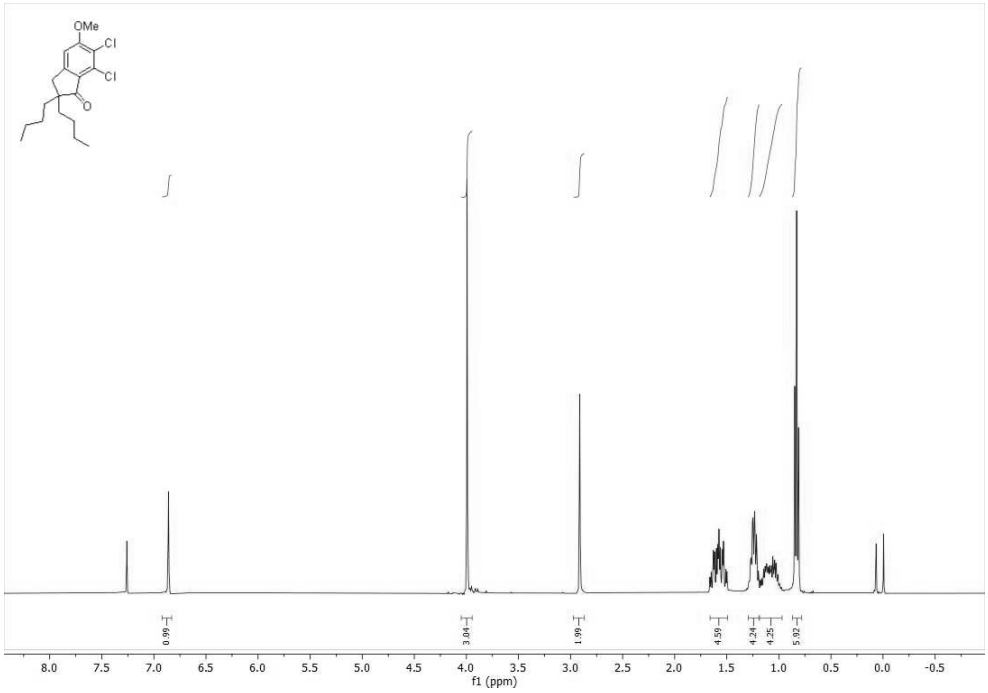

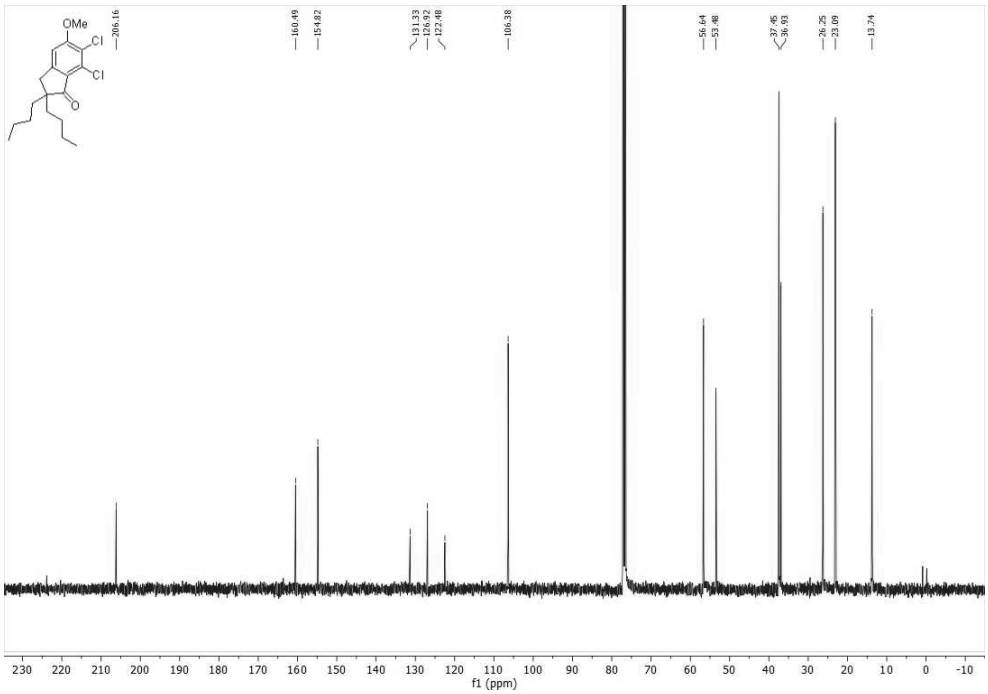

2,2-dibutyl-6,7-dichloro-5-hydroxy-2,3-dihydro-1*H*-inden-1-one (23b)

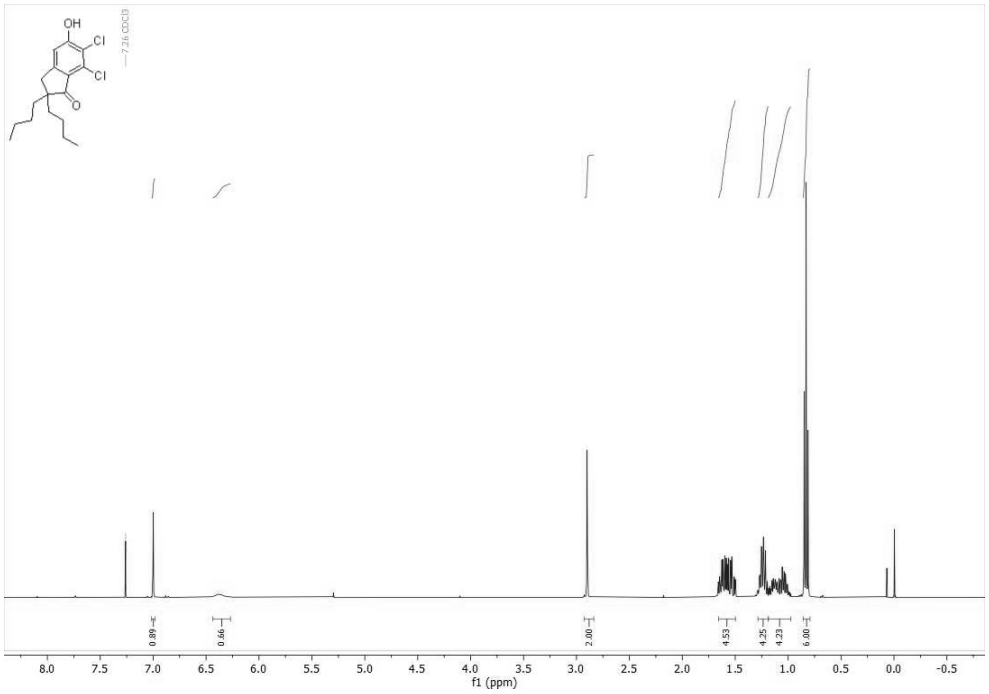

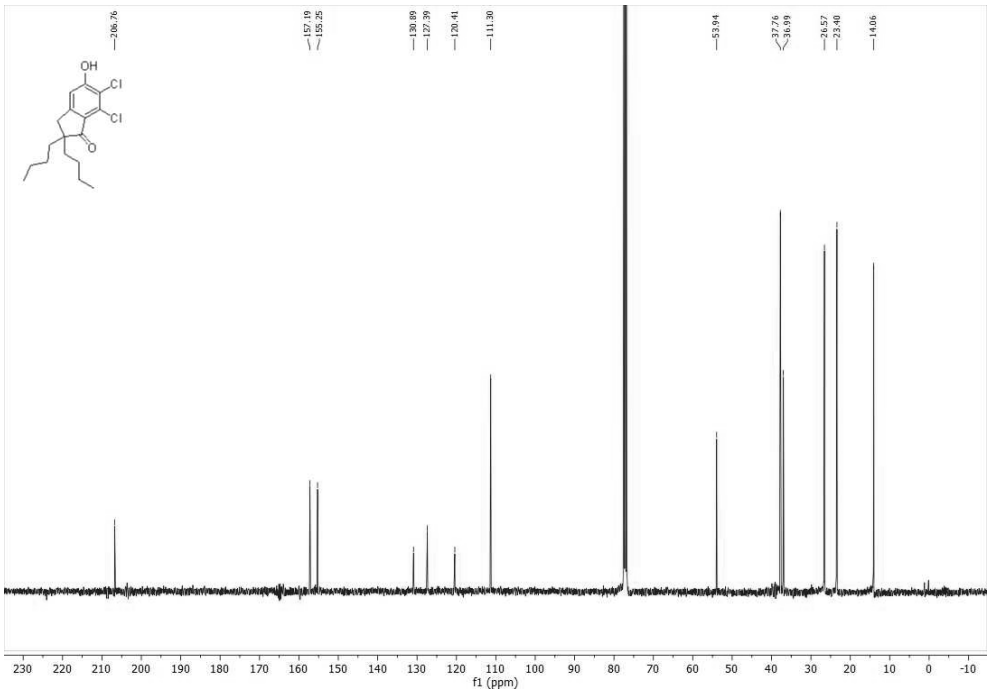

Ethyl 4-((2-butyl-6,7-dichloro-2-cyclopentyl-1-oxo-2,3-dihydro-1*H*-inden-5-yl)oxy)butanoate (24a)

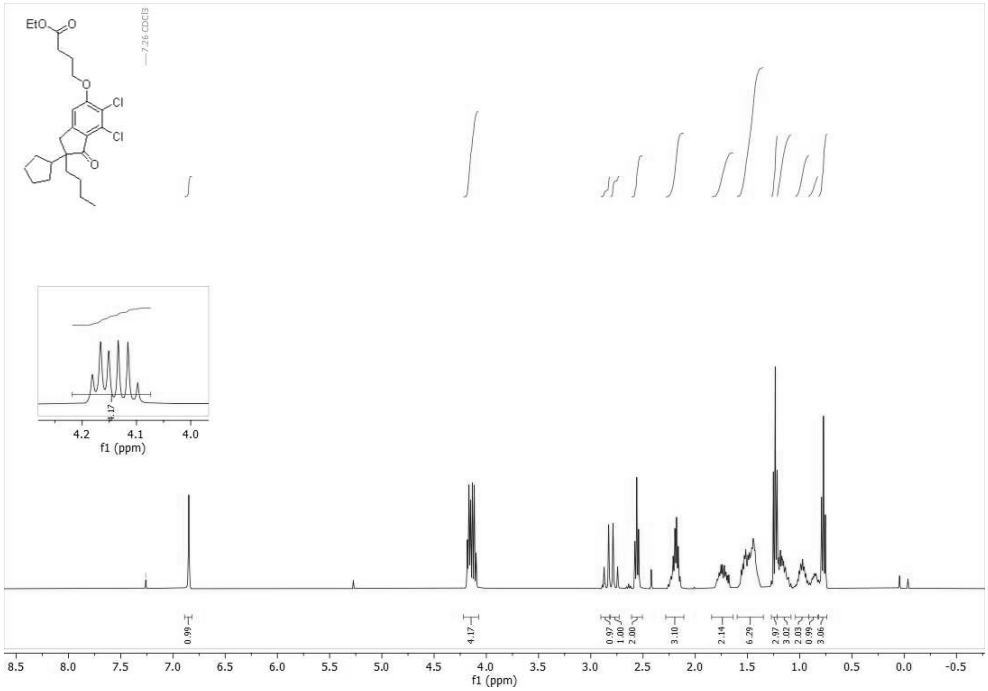

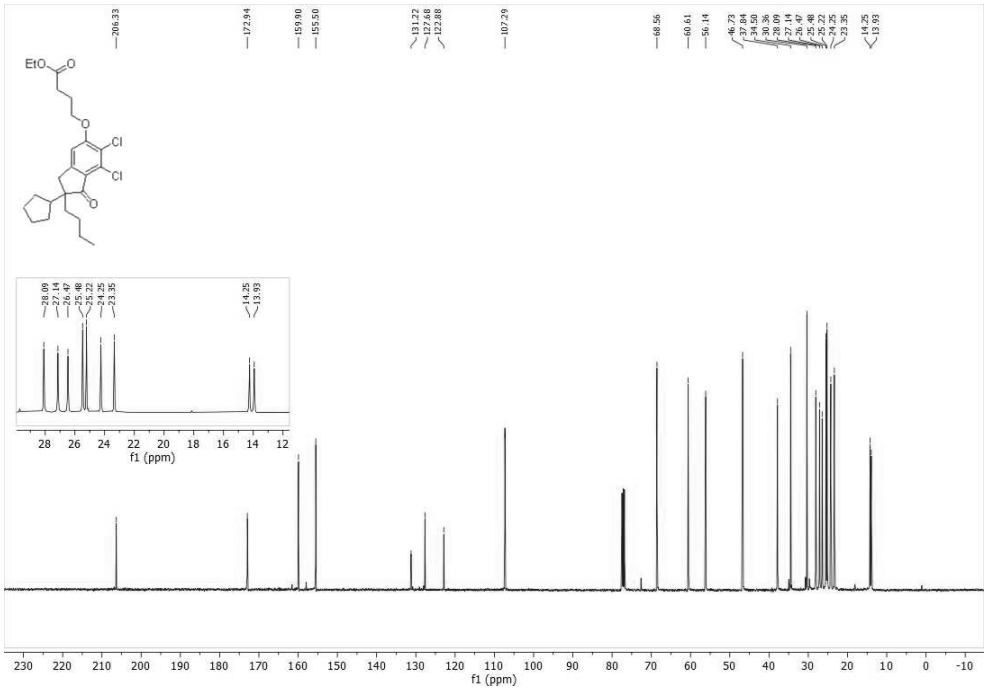

Ethyl 4-((2,2-dibutyl-6,7-dichloro-1-oxo-2,3-dihydro-1*H*-inden-5-yl)oxy)butanoate (24b)

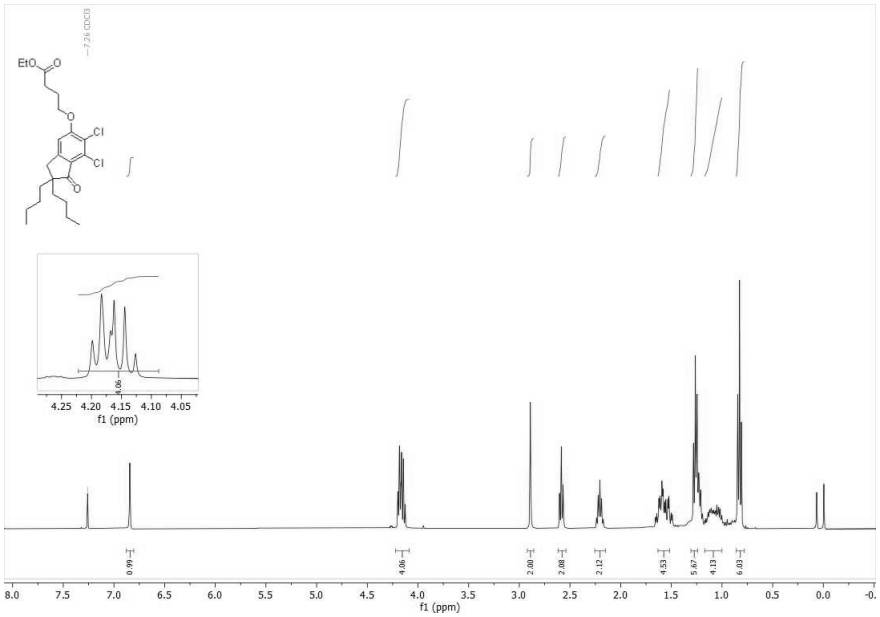

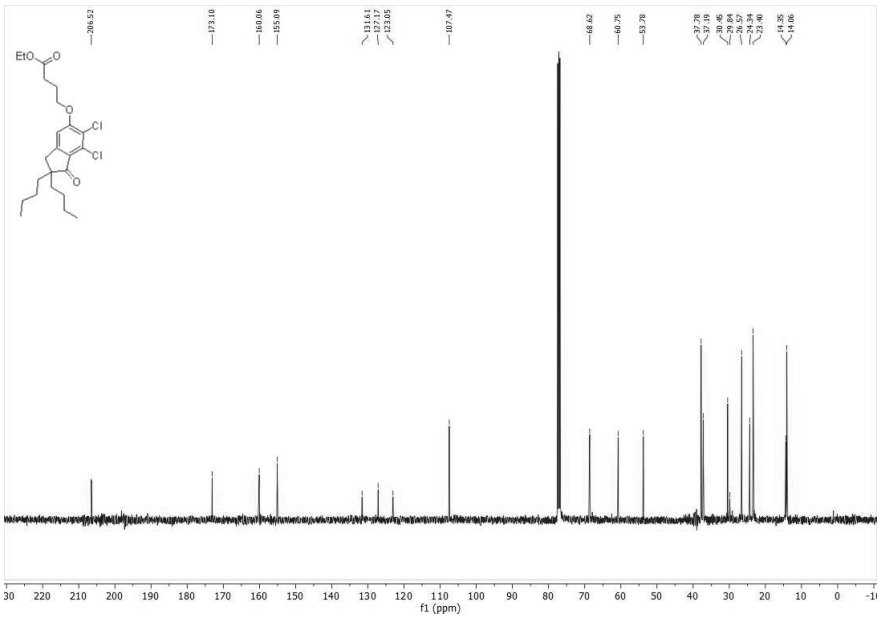

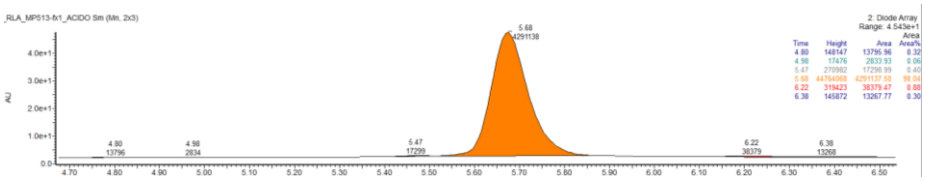

4-((2-butyl-6,7-dichloro-2-cyclopentyl-1-oxo-2,3-dihydro-1*H*-inden-5-yl)oxy)butanoic acid (25a) – *rac*-DCPIB

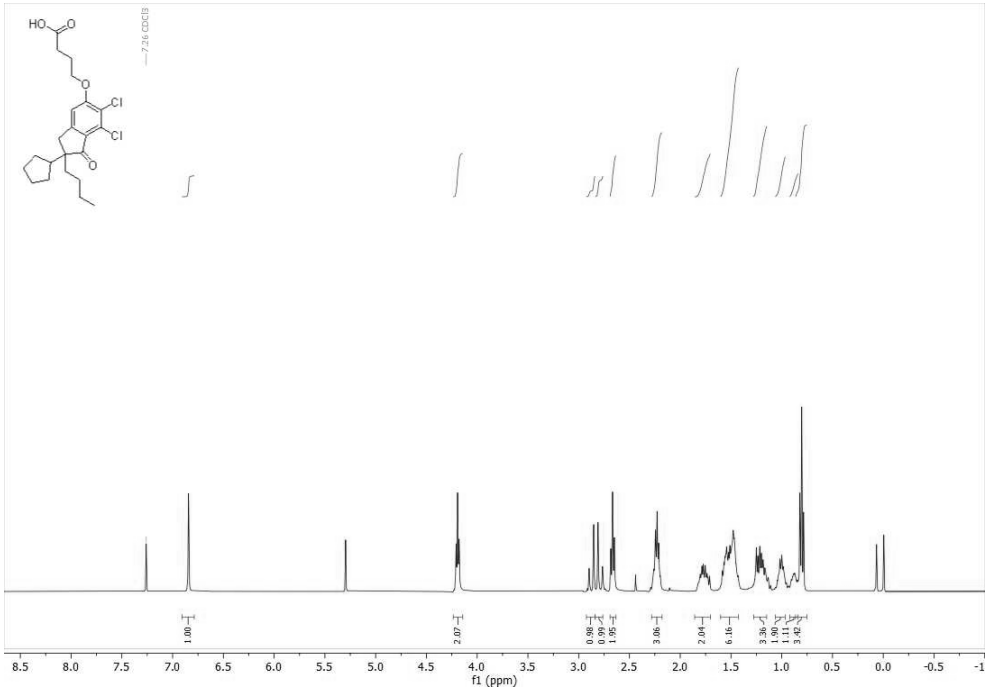

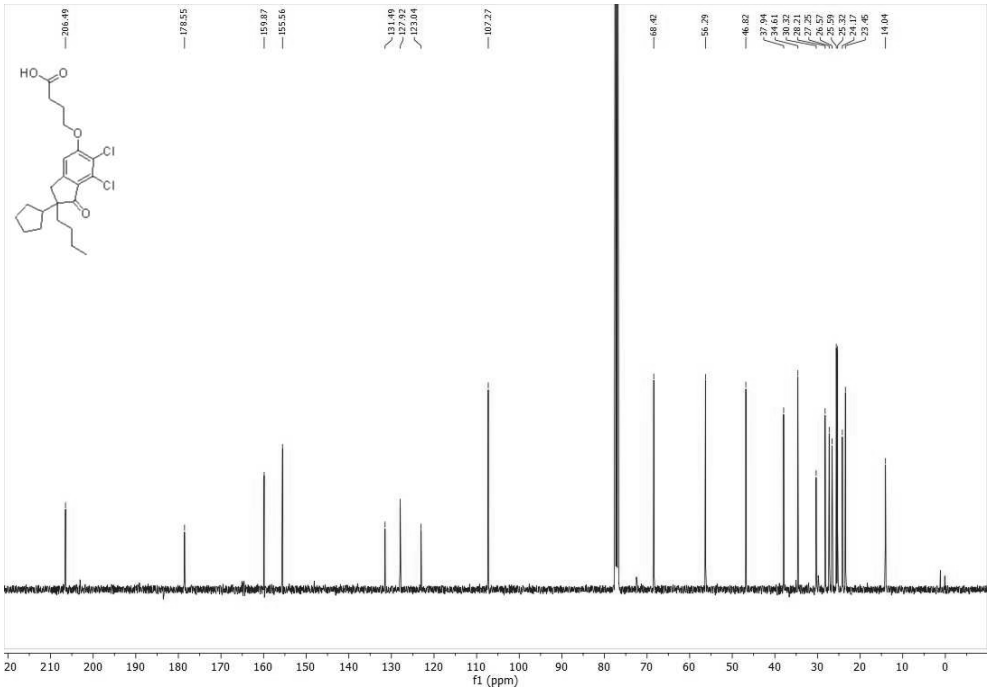

4-((2,2-dibutyl-6,7-dichloro-1-oxo-2,3-dihydro-1*H*-inden-5-yl)oxy)butanoix acid (25b)

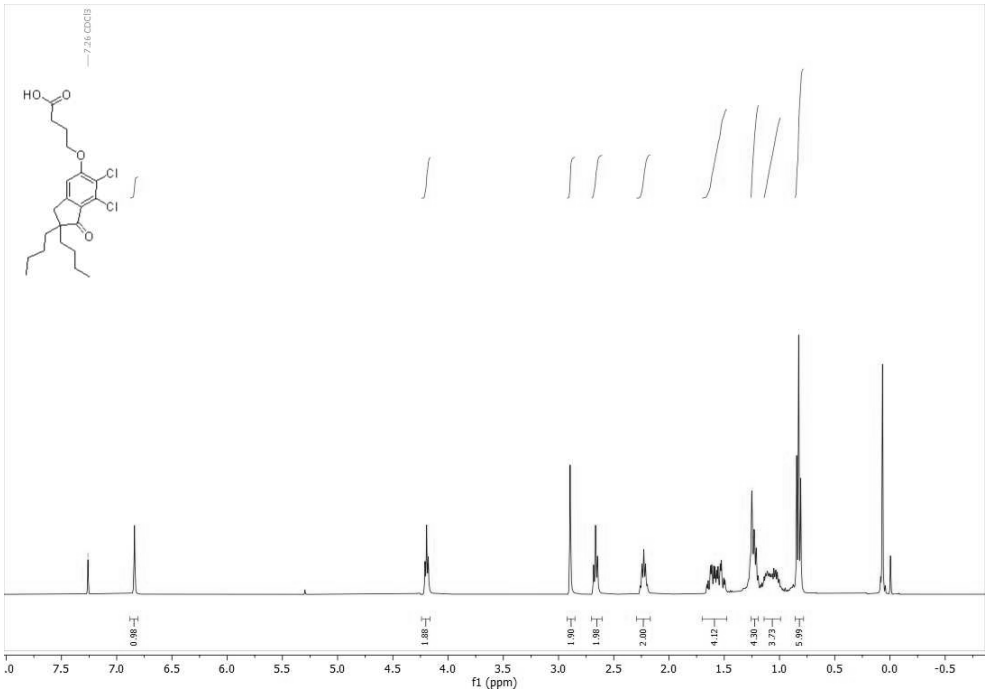

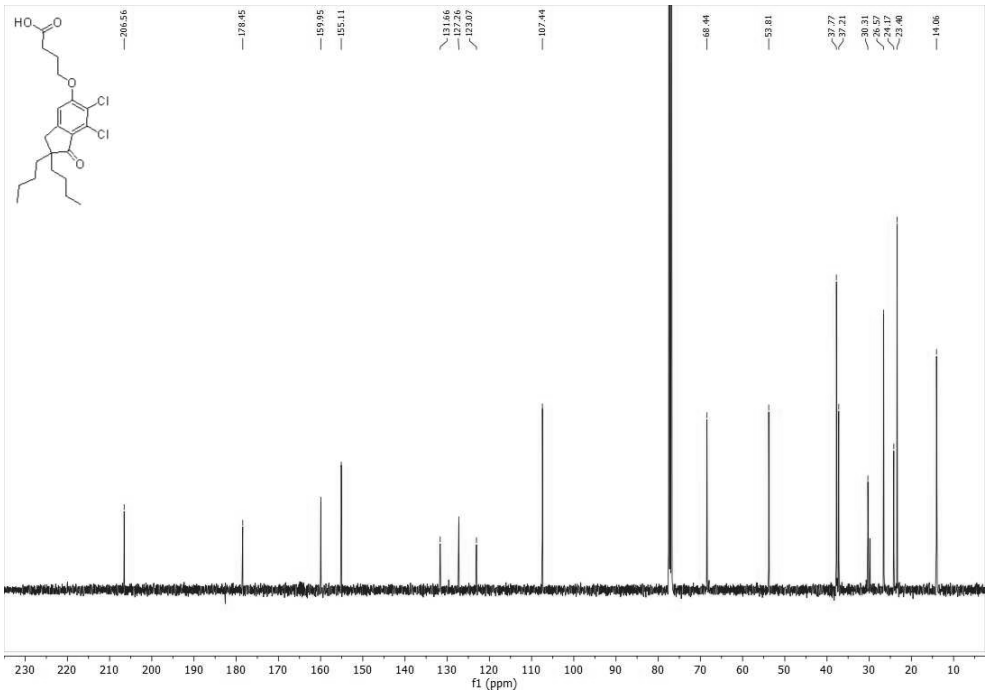

Methyl 2'-(((2-butyl-6,7-dichloro-2-cyclopentyl-1-oxo-2,3-dihydro-1*H*-inden-5-yl)oxy)methyl)-[1,1'-biphenyl]-2-carboxylate (27a)

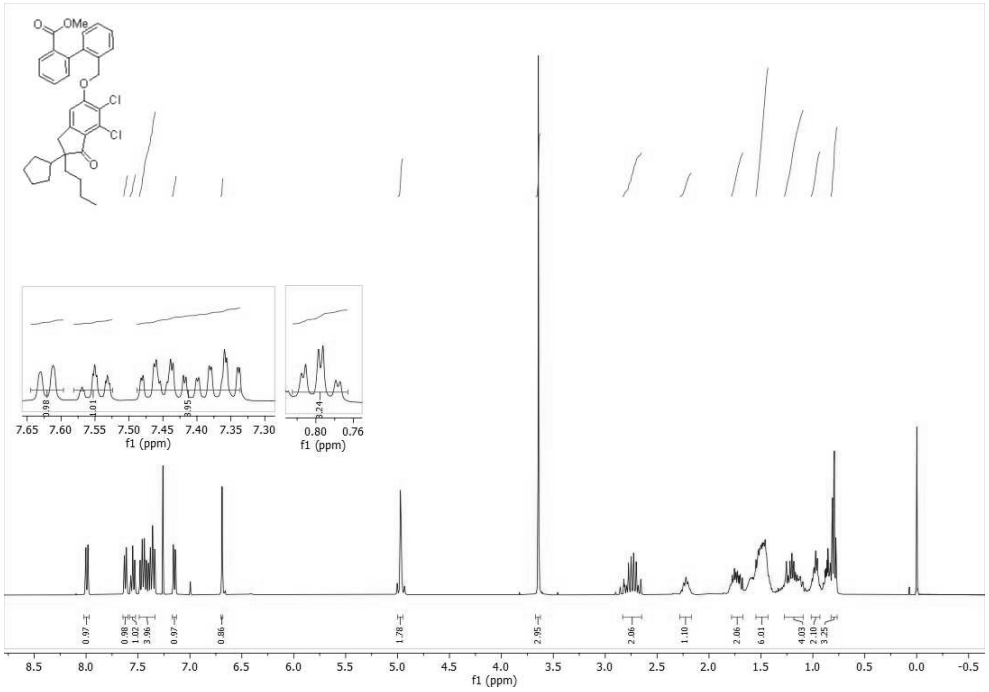

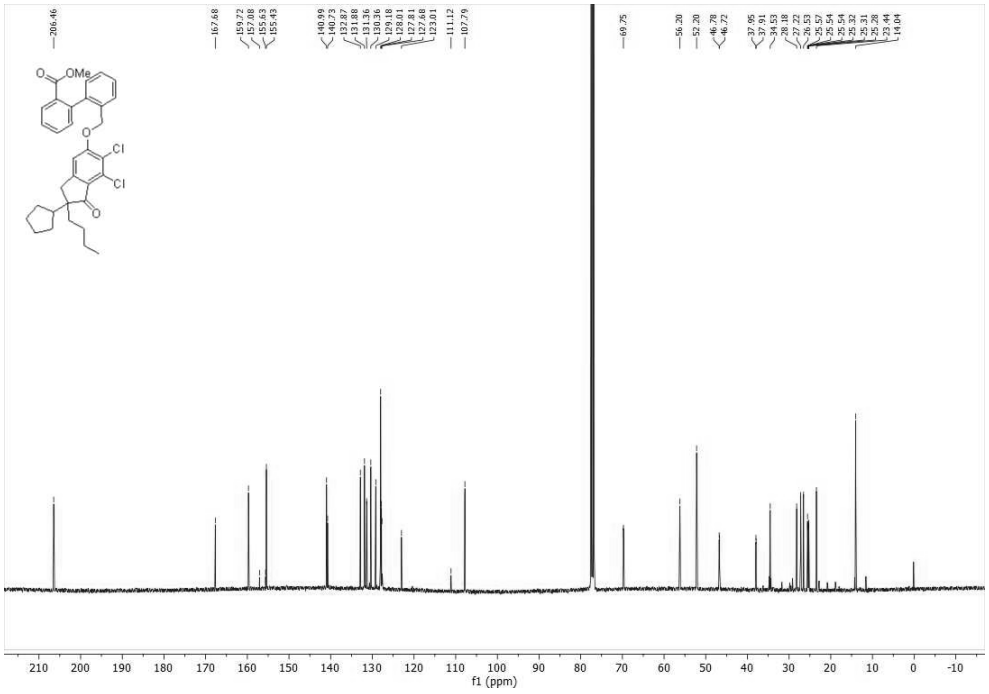

Methyl 2'-((2,2-dibutyl-6,7-dichloro-1-oxo-2,3-dihydro-1*H*-inden-5-yl)oxy)methyl-[1,1'-biphenyl]-2-carboxylate (27b)

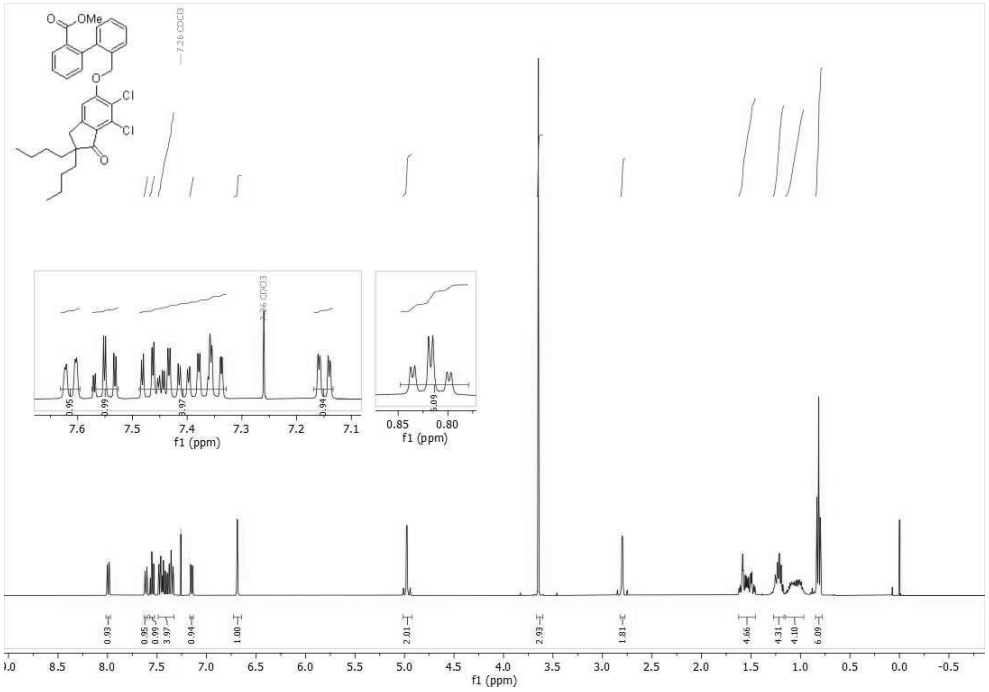

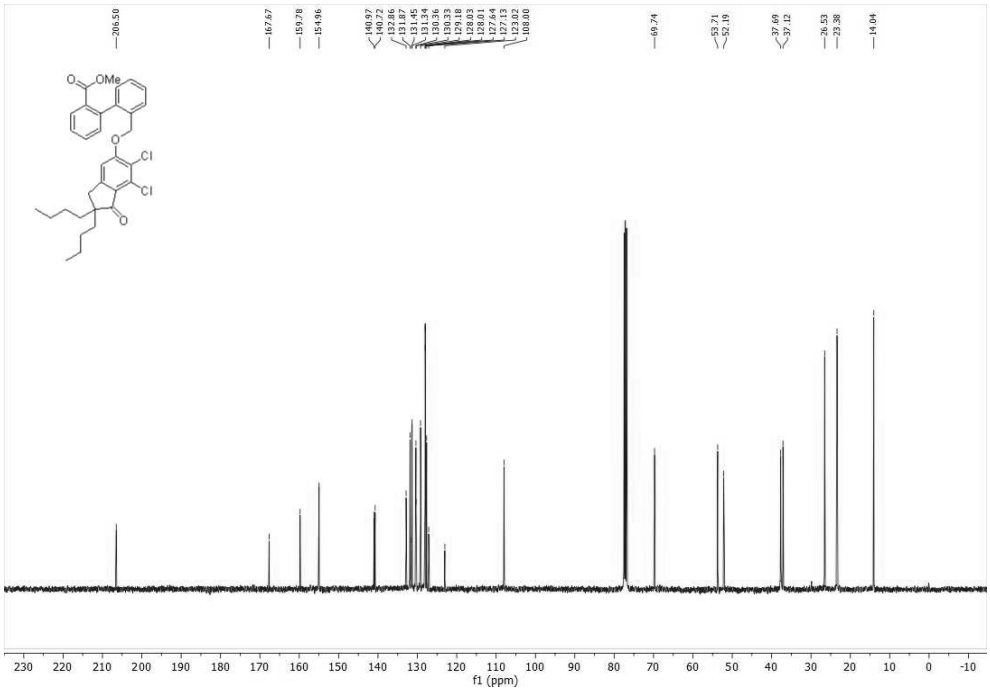

2'-(((2,2-dibutyl-6,7-dichloro-1-oxo-2,3-dihydro-1*H*-inden-5-yl)oxy)methyl)-[1,1'-biphenyl]-2-carboxylic acid (28b)

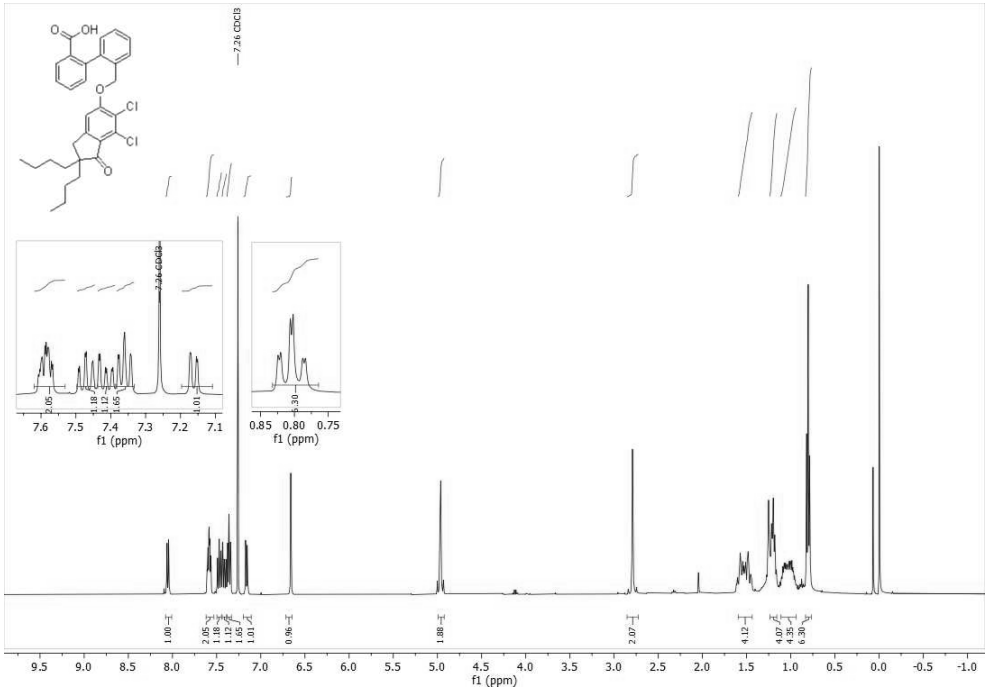

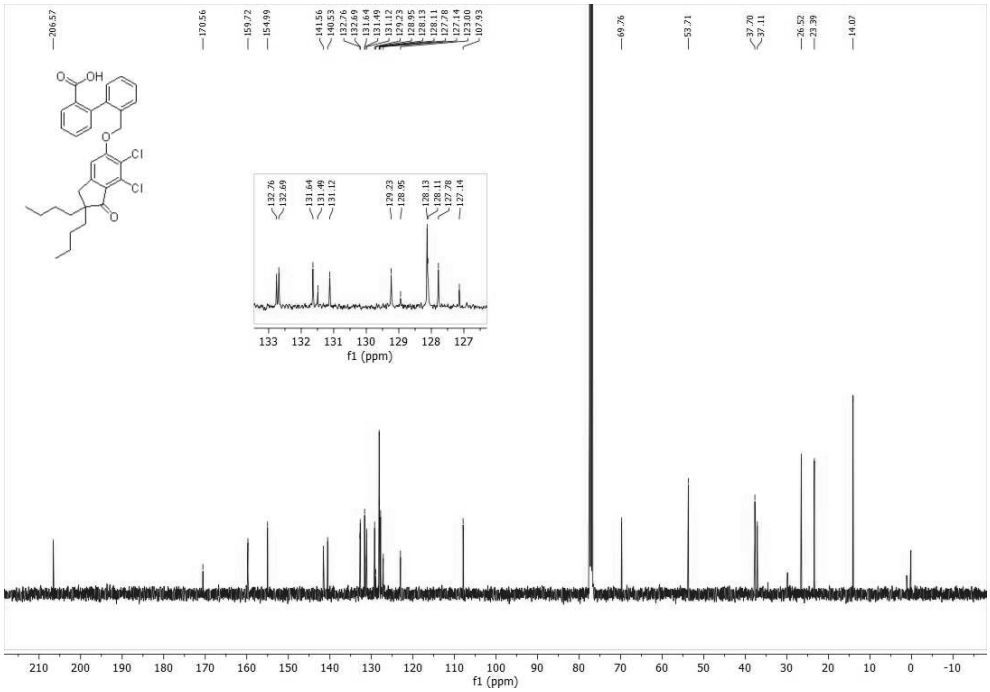

2-butyl-6,7-dichloro-5-hydroxy-2,3-dihydro-1*H*-inden-1-one (29)

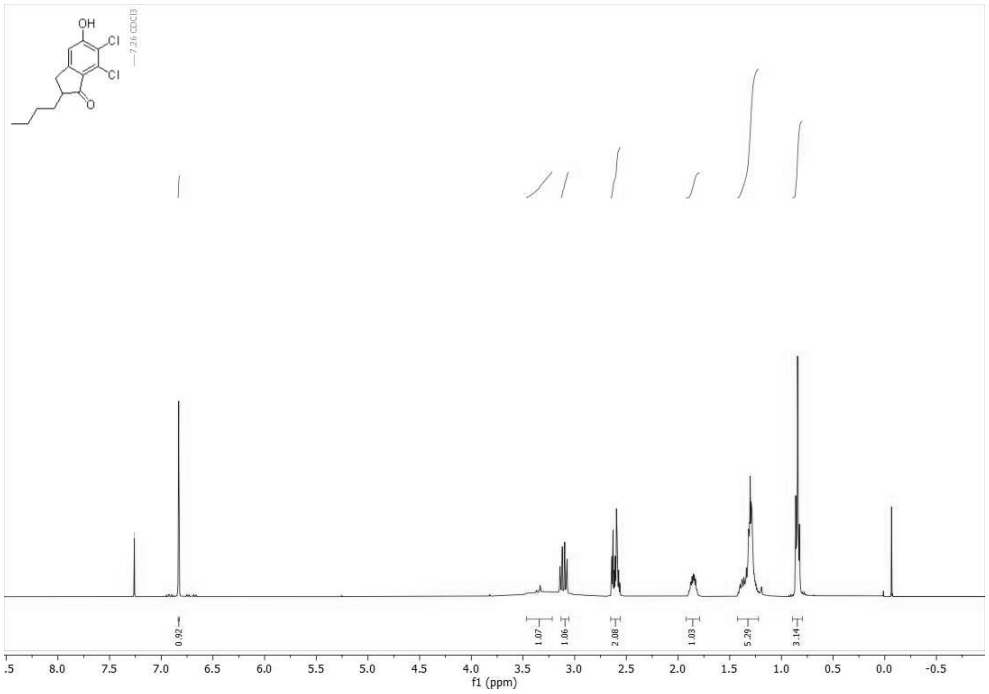

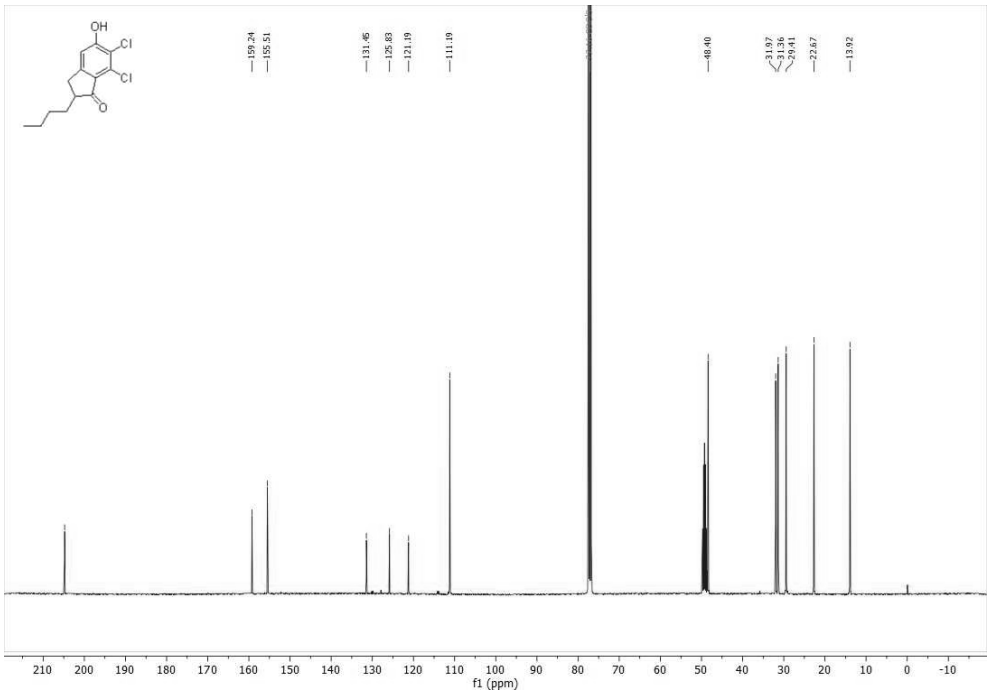

Methyl 4-((2-butyl-6,7-dichloro-1-oxo-2,3-dihydro-1H-inden-5-yl)oxy)butanoate (30)

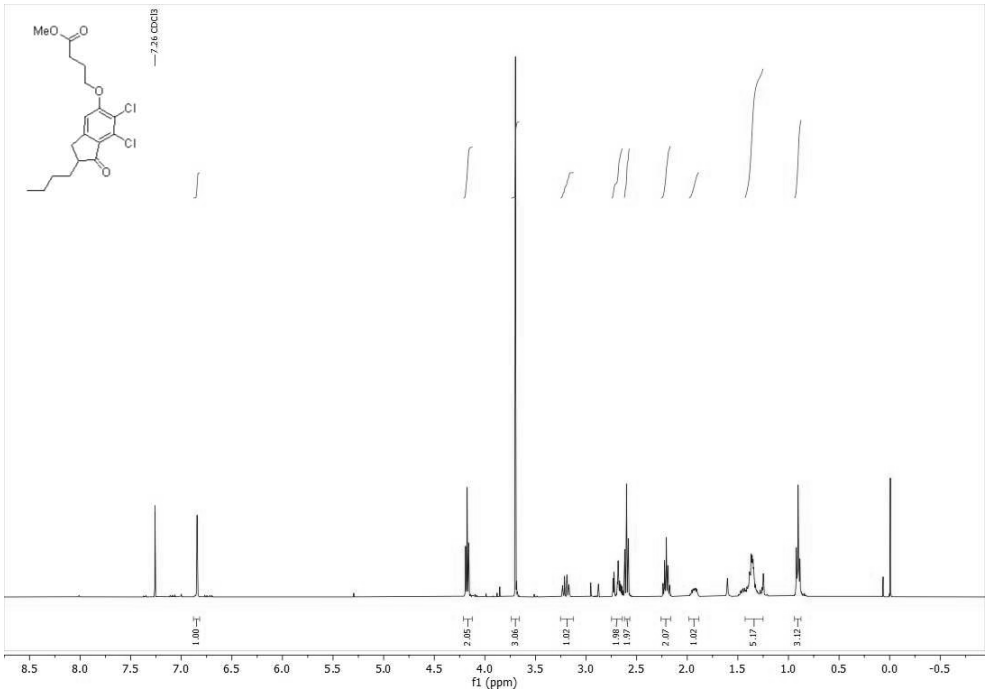

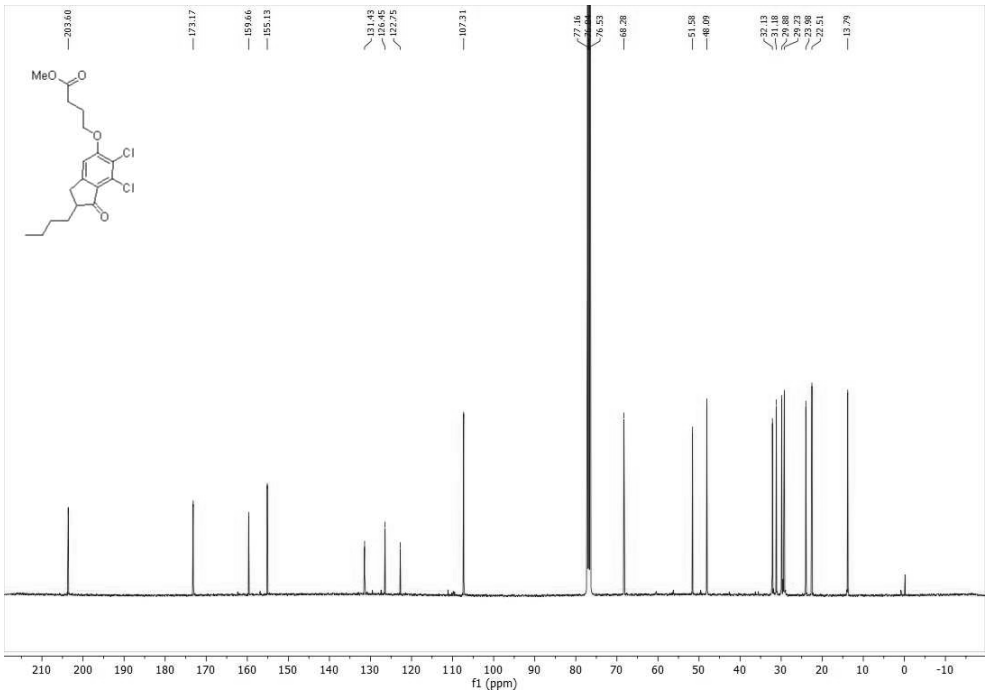

***Tert*-butyl 4-((2-benzyl-2-butyl-6,7-dichloro-1-oxo-2,3-dihydro-1*H*-inden-5-yl)oxy)butanoate (31)**

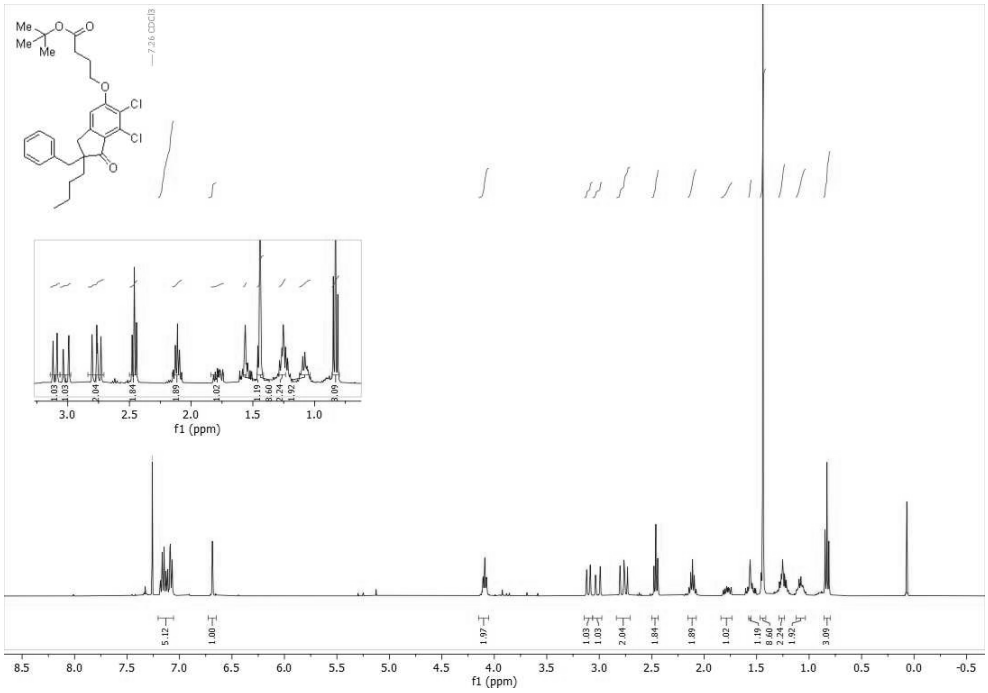

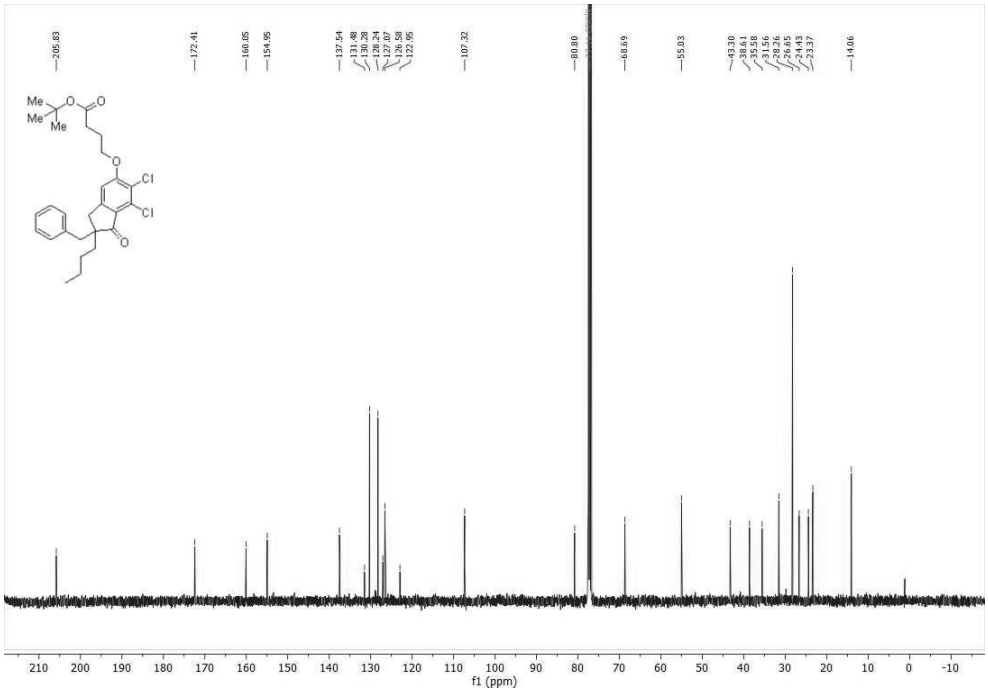

4-((2-benzyl-2-butyl-6,7-dichloro-1-oxo-2,3-dihydro-1*H*-inden-5-yl)oxy)butanoic acid (32)

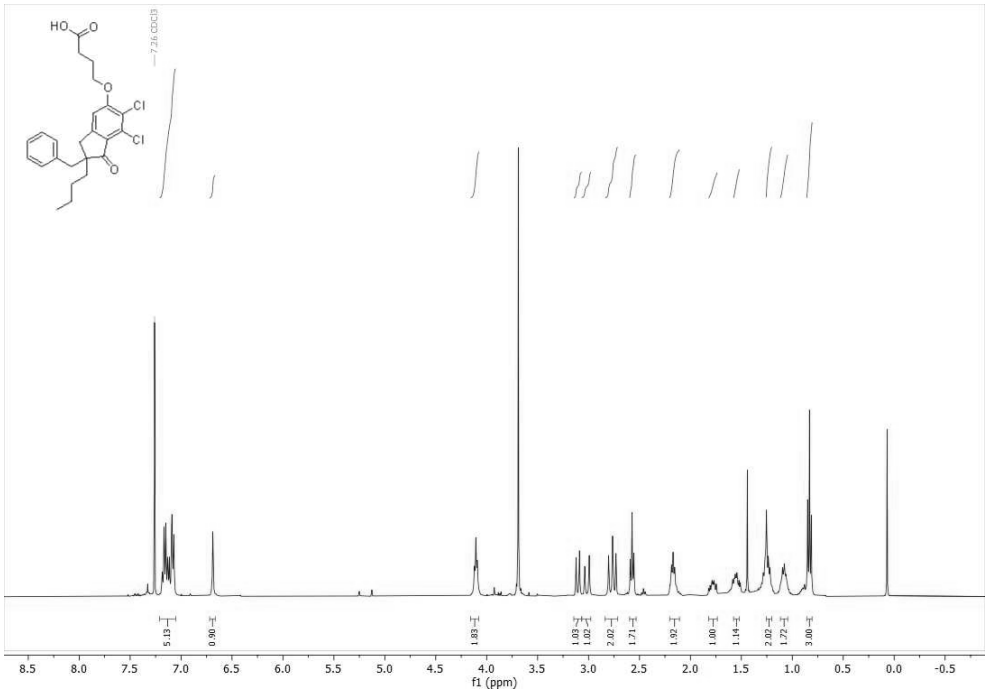

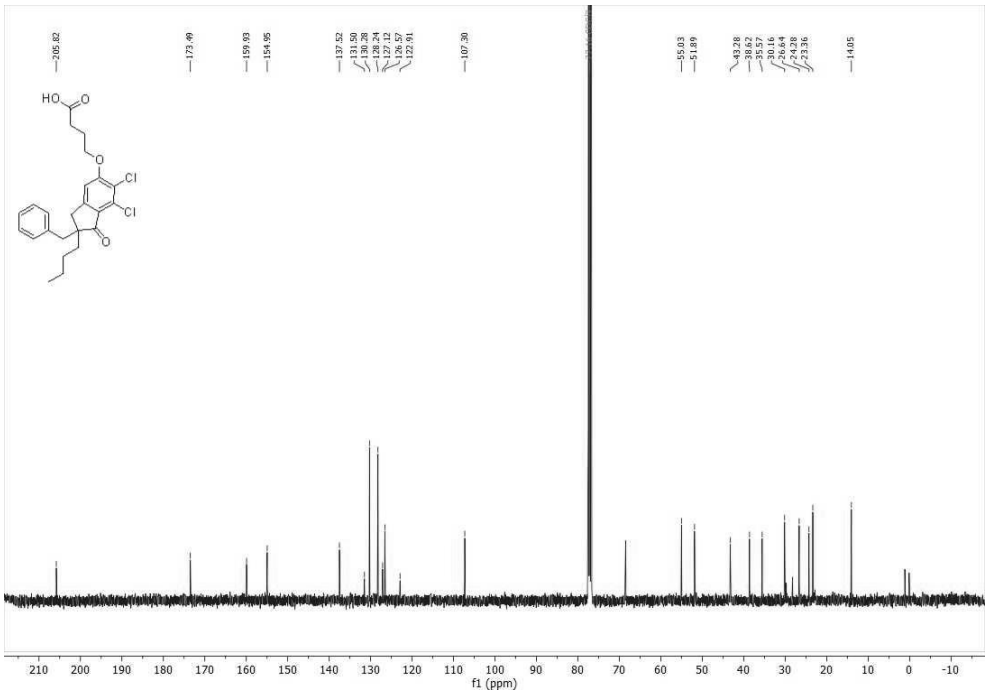

3-(3-(bromomethyl)phenyl)-3-(trifluoromethyl)-3*H*-diazirine (39)

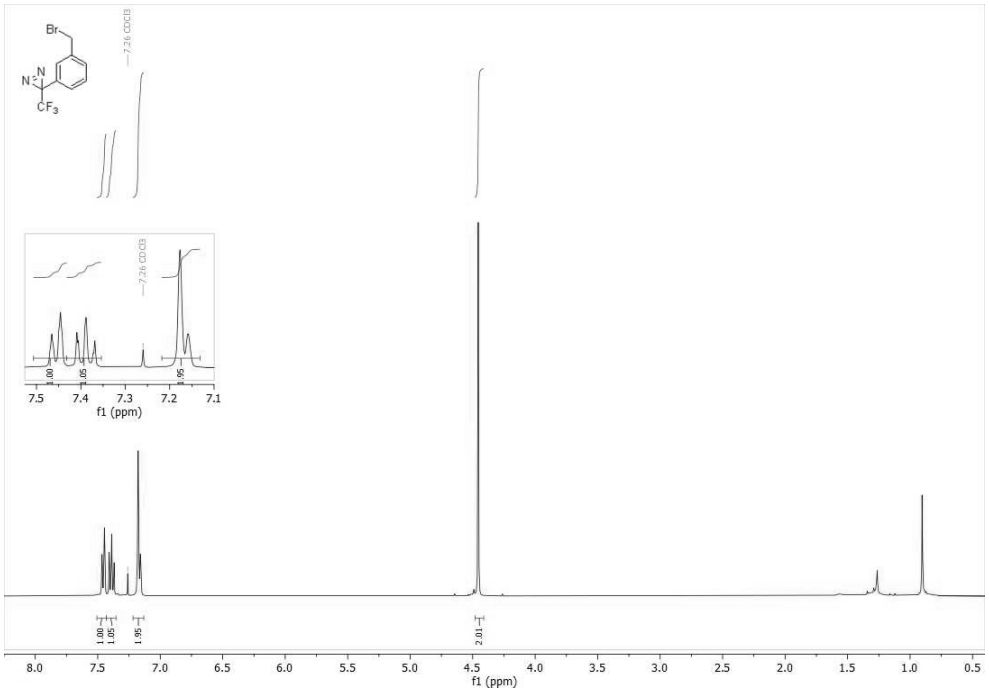

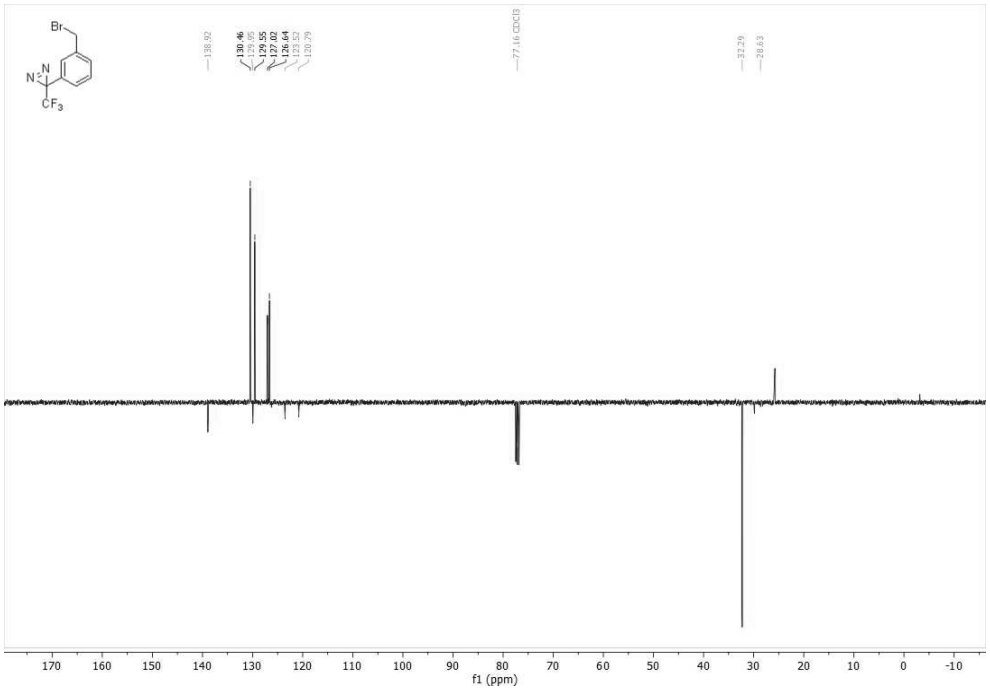

Methyl 4-((2-butyl-6,7-dichloro-1-oxo-2-(3-(3-(trifluoromethyl)-3*H*-diazirin-3-yl)benzyl)-2,3-dihydro-1*H*-inden-5-yl)oxy)butanoate (40)

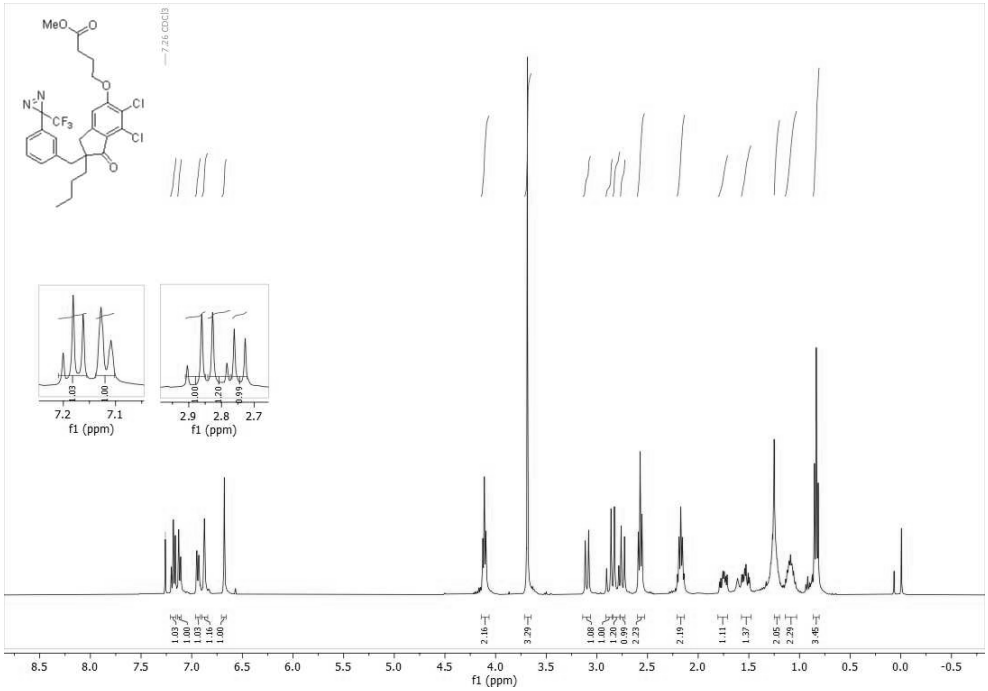

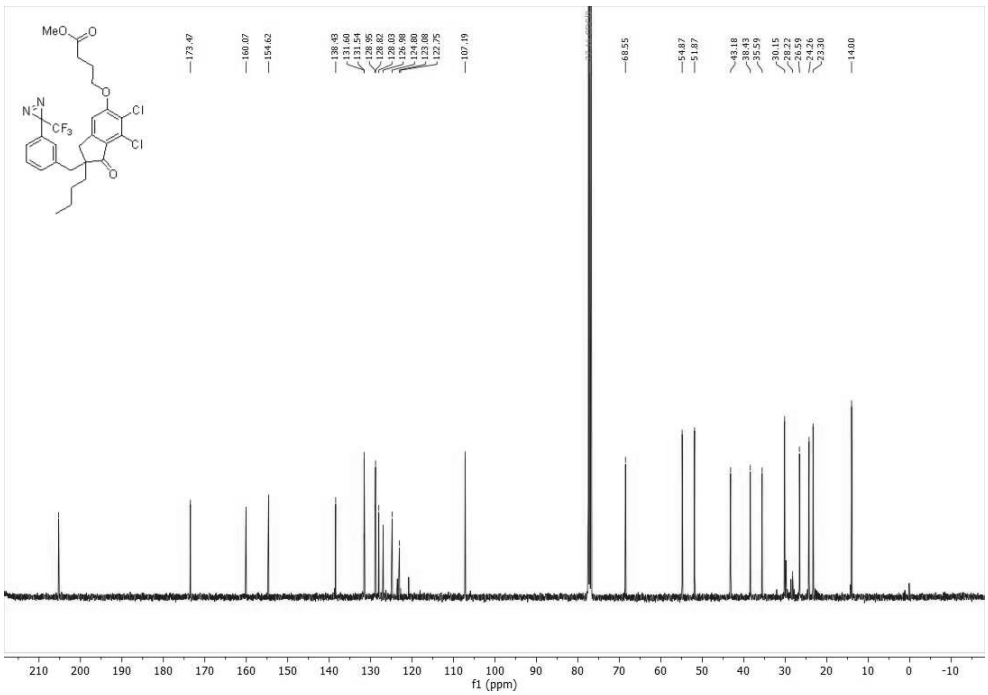

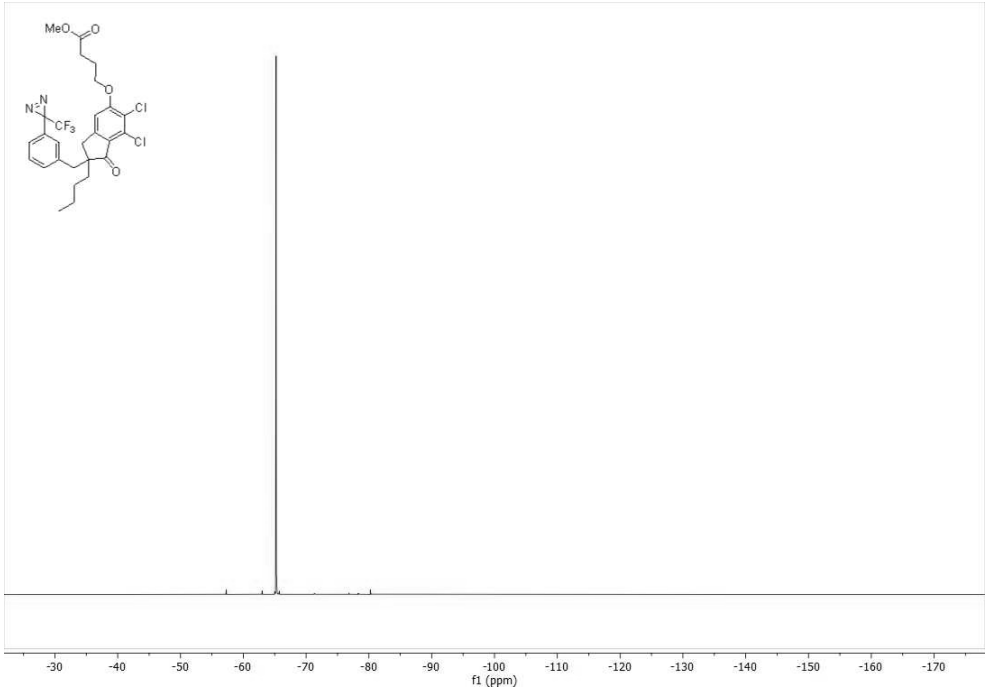
MeO
O
O
N
N
CF3
Cl
Cl
O
-30
-40
-50
-60
-70
-80
-90
-100
-110
-120
-130
-140
-150
-160
-170
f1 (ppm)

4-((2-butyl-6,7-dichloro-1-oxo-2-(3-(3-(trifluoromethyl)-3*H*-diazirin-3-yl)benzyl)-2,3-dihydro-1*H*-inden-5-yl)oxy)butanoate (41)

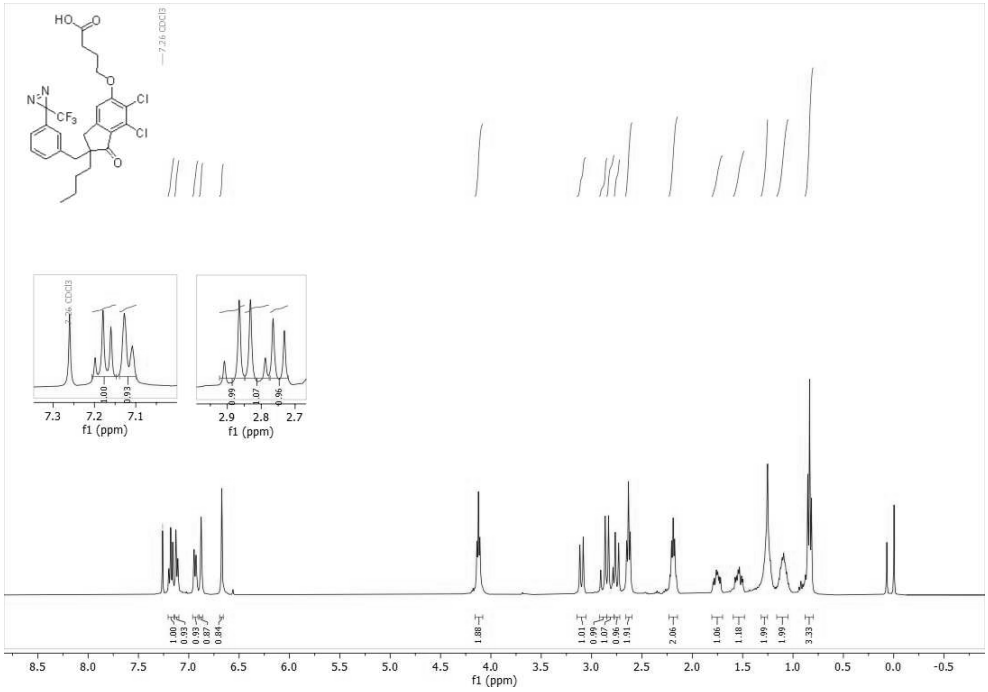

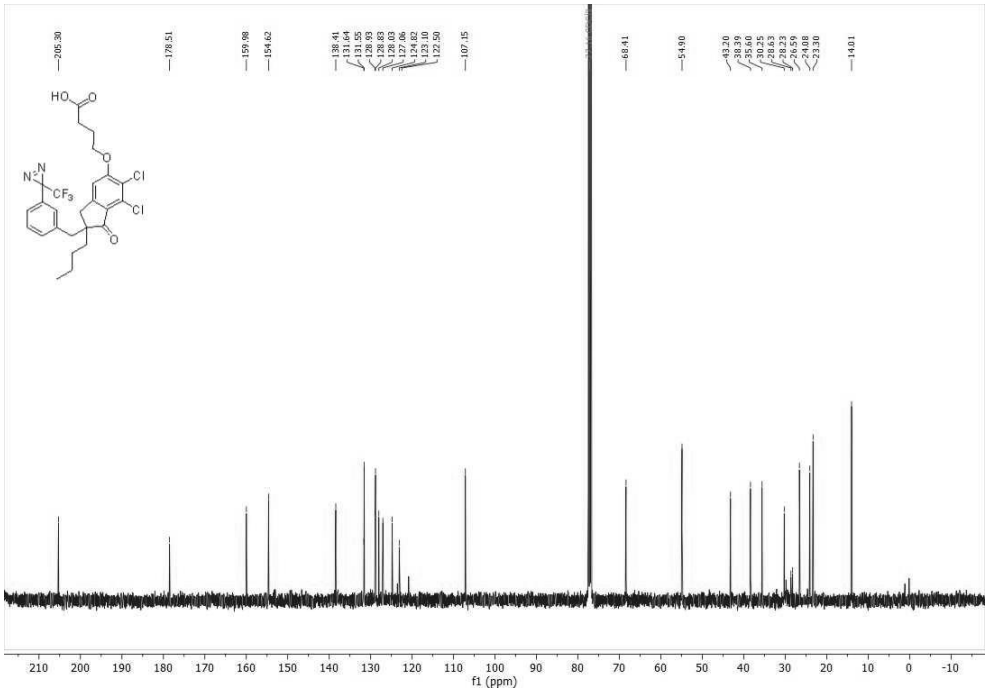

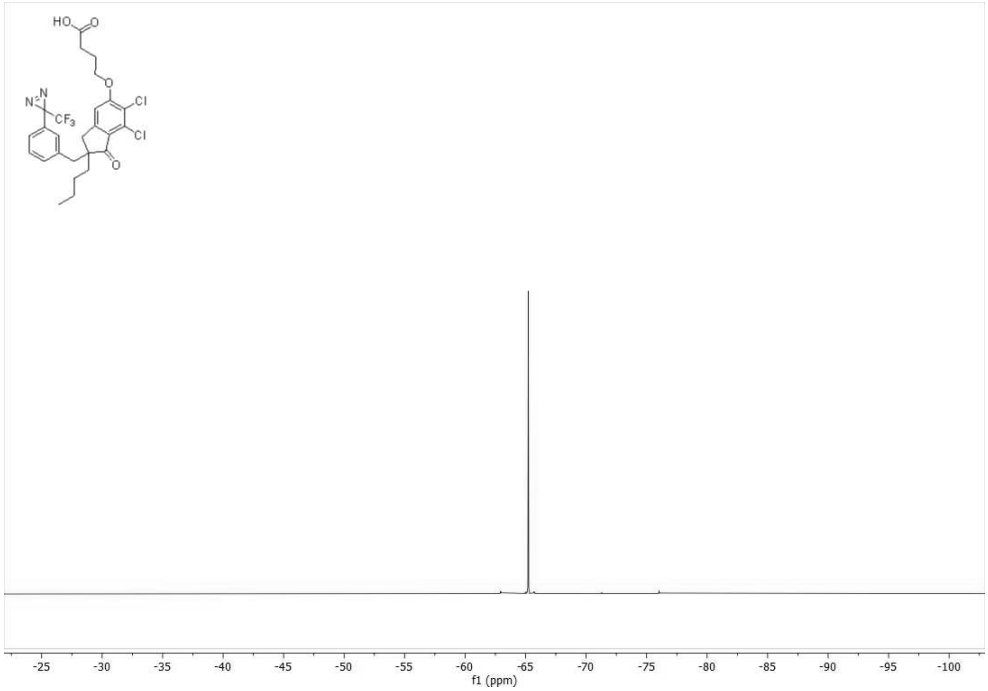
HO
O
O
N
N
CF3
Cl
Cl
O
-25
-30
-35
-40
-45
-50
-55
-60
-65
-70
-75
-80
-85
-90
-95
-100
f1 (ppm)

4. Bibliography

[1] X. Su, H. Lawrence, D. Ganeshapillai, A. Cruttenden, A. Purohit, M. J. Reed, N. Vicker, B. V. L. Potter, *Bioorganic Med. Chem.* **2004**, *12*, 4439–4457.

[2] D. Chen, X. Huang, H. Zhou, H. Luo, P. Wang, Y. Chang, X. He, S. Ni, Q. Shen, G. Cao, H. Sun, X. Wen, J. Liu, *Eur. J. Med. Chem.* **2017**, *139*, 201–213.

[3] I. Beseda, L. Czollner, P. S. Shah, R. Khunt, R. Gaware, P. Kosma, C. Stanetty, M. C. del Ruiz-Ruiz, H. Amer, K. Mereiter, T. Da Cunha, A. Odermatt, D. Claßen-Houben, U. Jordis, *Bioorganic Med. Chem.* **2010**, *18*, 433–454.

[4] G. Xu, J. Li, J. Wu, H. Zhang, J. Hu, M.-H. Li, *ACS Appl. Polym. Mater.* **2019**, *1*, 2577–2581.

[5] L. H. Lin, L. W. Lee, S. Y. Sheu, P. Y. Lin, *Chem. Pharm. Bull.* **2004**, *52*, 1117–1122.

[6] K. Stenzel, A. Hamacher, F. K. Hansen, C. G. W. Gertzen, J. Senger, V. Marquardt, L. Marek, M. Marek, C. Romier, M. Remke, M. Jung, H. Gohlke, M. U. Kassack, T. Kurz, *J. Med. Chem.* **2017**, *60*, 5334–5348.

[7] O. W. Woltersdorf, S. J. deSolms, E. M. Schultz, E. J. Cragoe, *J. Med. Chem.* **1977**, *20*, 1400–1408.

[8] S. J. deSolms, O. W. Woltersdorf, E. J. Cragoe, L. S. Watson, G. M. Fanelli, *J. Med. Chem.* **1978**, *21*, 437–443.

[9] E. J. Cragoe, N. P. Gould, O. W. Woltersdorf, C. Ziegler, R. S. Bourke, L. R. Nelson, H. K. Kimelberg, J. B. Waldman, A. J. Popp, N. Sedransk, *J. Med. Chem.* **1982**, *25*, 567–579.

[10] D. J. Edwards, D. House, H. M. Sheldrake, S. J. Stone, T. W. Wallace, *Org. Biomol. Chem.* **2007**, *5*, 2658–2669.

[11] S. D. Lepore, Y. He, *J. Org. Chem.* **2003**, *68*, 8261–8263.

[12] D. A. Evans, P. H. Carter, C. J. Dinsmore, J. C. Barrow, J. L. Katz, D. W. Kung, *Tetrahedron Lett.* **1997**, *38*, 4535–4538.

[13] W. Nguyen, J. Jacobson, K. E. Jarman, H. Jousset Sabroux, L. Harty, J. McMahon, S. R. Lewin, D. F. Purcell, B. E. Sleebs, *J. Med. Chem.* **2019**, *62*, 5148–5175.

[14] K. Nakamoto, Y. Ueno, *J. Org. Chem.* **2014**, *79*, 2463–2472.

[15] L. Feng, K. Lv, M. Liu, S. Wang, J. Zhao, X. You, S. Li, J. Cao, H. Guo, *Eur. J. Med. Chem.* **2012**, *55*, 125–136.

[16] C. Charrier, J. Roche, J. P. Gesson, P. Bertrand, *Bioorganic Med. Chem. Lett.* **2007**, *17*, 6142–6146.

[17] T. Yang, X.-M. Li, X. Bao, Y. man Eva Fung, X. D. Li, *Nat. Chem. Biol.* **2016**, *12*, 70–72.

Chapter III

Multicomponent Reactions towards the Synthesis of Bioactive Compounds

3.1. Introduction and Background

3.1.1. Multicomponent Reactions (MCRs)

MCRs are reactions in which three or more starting materials are combined to form a product in a one-pot approach, incorporating essentially most of the atoms of the components into the final adduct (Scheme 3.1a).[1,2]

Differing from linear and divergent multistep approaches (Scheme 3.1b), in MCRs all the components are added simultaneously at the onset of the reaction. However, they do not react at once in one step, but they combine in an ordered manner and rather react in a sequence of mono- and bimolecular events that proceed consecutively until the product is originated, usually after a final irreversible step.[3,4]

(a) Multicomponent Reaction

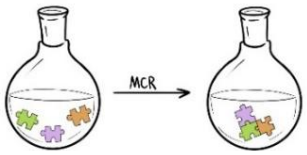

(b) Linear Multistep Reaction

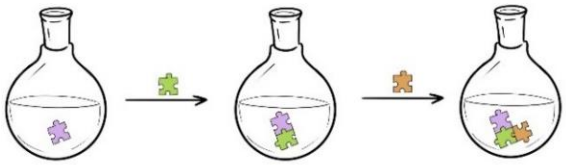

Scheme 3.1. Representation of MCRs vs linear multistep reactions.

Besides generating structural complexity in a single step, MCRs have other advantages compared to classical chemical methods, which are summarized as followed:

- They are experimentally *simpler* over conventional reactions involved in multistep sequences, as all the reagents and catalysts are added one-pot and just require a single isolation procedure.
- They are *convergent* since several starting materials assemble to generate complex products under the same reaction conditions.
- They are *atom economic*, as the product incorporates structural features of each reagent.
- They have a very *high bond-forming efficiency* (BFE).

Thus, MCRs come close towards the concept of "ideal synthesis", which include a reduction of intermediate steps, functional group manipulations and/or protective group strategies. Overall, this led to a simple, efficient, safe, economically acceptable, and sustainable synthesis.[5]

The first MCR was reported by Strecker in the 1850s. This reaction involves the interaction between an aldehyde and ammonia in the presence of potassium cyanide, ultimately yielding natural and/or unnatural amino acids. In the original Strecker reaction, acetaldehyde, ammonia, and potassium cyanide reacted together to form alanine, after the acid-mediated hydrolysis of the α-aminonitrile intermediate (Scheme 3.2).[6]

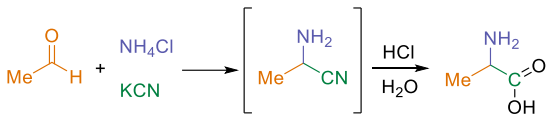

Scheme 3.2. Strecker reaction.

3.1.2. Isocyanide-based Multicomponent Reactions: Passerini, Ugi and Groebke-Blackburn-Bienaymé (GBB) Reactions

An important subclass of MCRs are the isocyanide-based multicomponent reactions (IMCRs). Isocyanides, also known as isonitriles, have a great potential for the development of MCRs, due to their exceptional reactivity. They are described by two resonance structures (Scheme 3.3a) and its formal carbene character enhances the terminal carbon to react as electrophile and/or as nucleophile (Scheme 3.3b).[3] In most of the IMCR approaches, isocyanides participate as nucleophiles to generate a nitrilium–intermediate, later trapped by an external nucleophilic attack, although other mechanistic variations are known.

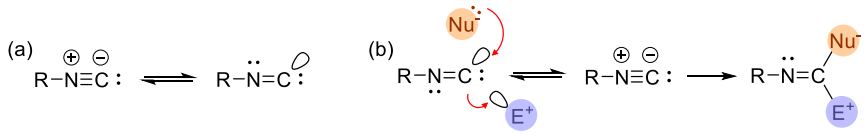

Scheme 3.3. (a) Resonant structure of isocyanides. (b) Reactivity of isocyanides towards nucleophiles and electrophiles.

Even though isocyanide's reactivity was first exploited by Passerini,[7] in 1921, it is the Ugi reaction (1959)[8] which has received much more attention to date. The Passerini reaction is a 3-CR between a ketone or aldehyde, a carboxylic acid, and an isocyanide to obtain α-acyloxy amides (Scheme 3.4a), whereas in the Ugi reaction the carbonyl component is replaced by an imine (resulting from the interaction of a carbonyl group and amine). The Ugi reaction finally results in the formation of a α-amino acyl amides (Scheme 3.4b) with peptide-like structure, which can be highly diverse due to the wide variety of starting materials that it admits. Consequently, the Ugi approach has resulted very useful for the preparation of screening libraries of multifunctional peptide-like compounds.

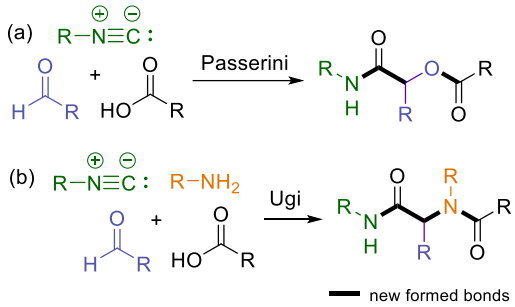

Scheme 3.4. (a) Passerini reaction. (b) Ugi reaction.

Afterwards, in the late 1990s, a heterocyclic variant of the Ugi reaction was simultaneously discovered by three different chemists: Groebke, Blackburn and Bienaymé. Subsequently, this transformation, usually referred as the Groebke, Blackburn and Bienaymé MCR reaction (GBB),[9–11] has had an enormous impact in medical chemistry. The reaction involves the interaction between heterocyclic amidines with aldehydes and isocyanides to yield nitrogen-based heterocycles (Scheme 3.5). Differing from the Passerini and the Ugi reactions, the GBB reaction comprises the additional reactivity of the endocyclic nitrogen in the amidine component, whereas the acid component is not incorporated in the final product and serves only for catalytic purposes instead, leading to improved reaction kinetics.

As depicted in Scheme 3.5, the GBB-3CR proceeds with the *in-situ* formation of the imine intermediate **I**, as in the Ugi reaction. This imine **I** is activated by acid and follows an isocyanide-based formal [4+1] cycloaddition sequence, giving the nitrilium ion **II**,

then undergoing intramolecular trapping by the nucleophilic azine *N* atom and concluding with aromatization via a 1,3-H shift to form the *N*-fused bicyclic imidazo-azine **III**. The reaction is catalyzed by a wide range of acid species (organic and inorganic acids, metal cations, Lewis acids, etc.).

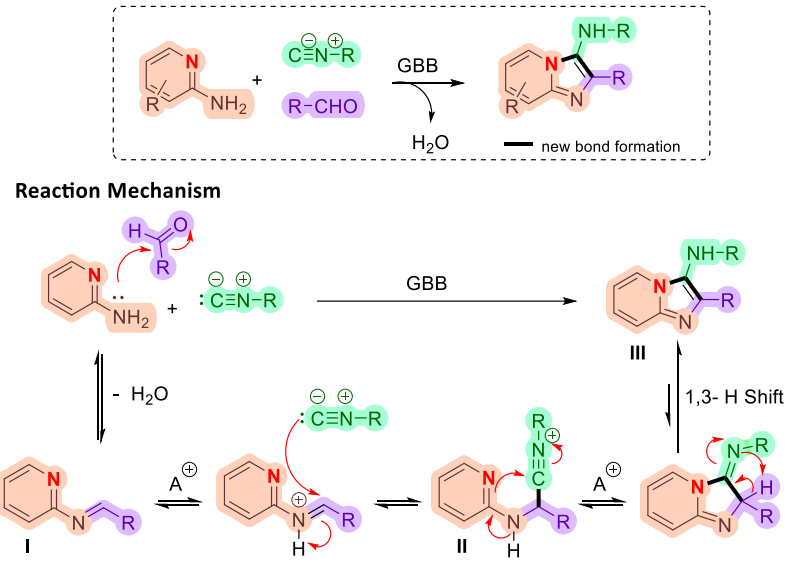

Scheme 3.5. GBB reaction mechanism.

Interestingly, substituted *N*-fused bicyclic imidazole systems are of biological and therapeutic relevance. They are found in several bioactive compounds and many marketed drugs, showing diverse activities such as analgesic, sedative, anti-inflammatory, anticonvulsant, anxiolytic, cardiotonic, etc. (Scheme 3.6). Thus, the GBB reaction is a powerful tool employed in drug discovery and medicinal chemistry.[12–15]

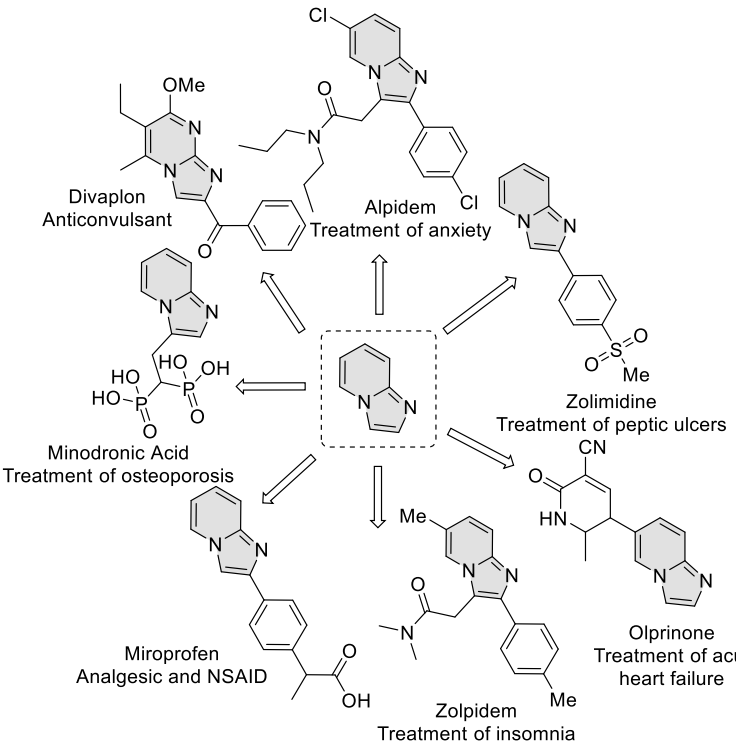

Scheme 3.6. Example of commercially available drugs with *N*-fused bicyclic imidazole scaffolds.

3.1.3. Post-MCR Transformations

In general, MCRs allow a high variability of the feasible substituents, since these processes are compatible with a wide range of functional groups. However, the formed adducts usually comprise the same kind of structures, being linear diamide and imidazole-fused heterocyclic scaffolds in the cases of the Ugi and the GBB reactions, respectively. With the aim of increasing the skeletal diversity of the IMCR scaffolds, the adducts are amenable to undergo further diversification *via* secondary transformations or domino post-condensation modifications. These approaches lead to adducts of higher molecular complexity and structural diversity, and may involve just the functional groups in the peripheral substituents (Scheme 3.7a) or all the backbone of the initial adduct (Scheme 3.7b).

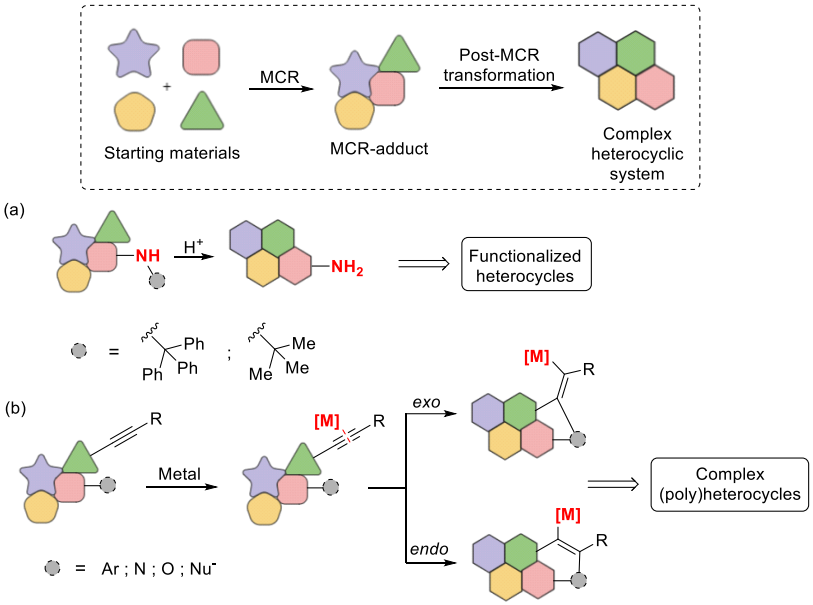

Scheme 3.7. Examples of post-MCR transformations.

Remarkable approaches modifying peripheral functional groups are the use of convertible reagents such as trityl[16] or *tert*-butyl[17] isocyanides, and subsequent deprotection and/or derivatization of the formed group. Thus, the development of a tandem dealkylation of a GBB adduct, and the *in-situ* cyclization of the generated primary amine functionality with a tethered internal functional group is a useful approach for the preparation of diverse (poly)-*N*-fused imidazoles (Scheme 3.8).[17]

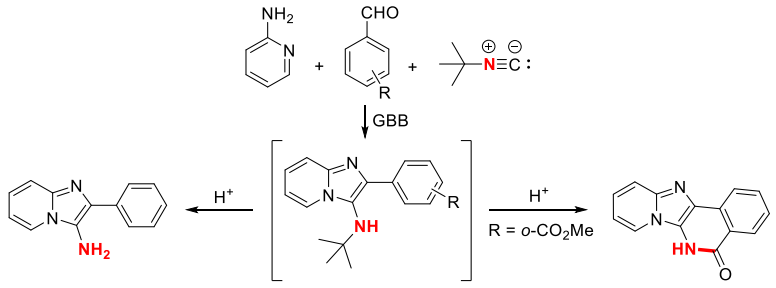

Scheme 3.8. Post de-*tert*-butylation and derivatization of *tert*-butyl GBB adducts.

Moreover, the use of substituents suitable for post-nucleophilic substitutions, metal-catalyzed cross-coupling, or alkylation reactions deal with the formation of complex (poly)heteroaromatic products, which are quite relevant in materials science and bioimaging.[18]

More recently, metal-catalyzed post-modifications have come to play a significant role expanding structural frameworks.[19–21] For instance, a Pd-catalyzed domino polycyclization strategy that involves a Buchwald-Hartwig/aldol reaction uses an acyclic Ugi adduct for the generation of complex (spiro)polyheterocyclic scaffolds. In this case, the obtention of rather one of both possible products is controlled by a ligand-switch (Scheme 3.9).[22]

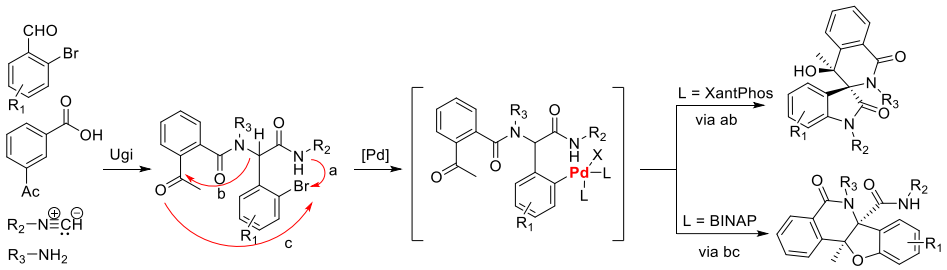

Scheme 3.9. Pd-catalyzed domino polycyclization of Ugi adducts.

A related cyclization reaction promoted by Au-catalysis assembles a complex bridged indole alkaloid-like heterocyclic scaffold. In this case, an alkyne-Ugi adduct is subjected to an Au-catalyzed intramolecular dearomative cascade cyclization followed by a concerted [4+2] cyclization (Scheme 3.10a).[23]

Finally, in the case of a specific alkyne-containing GBB adduct obtained from *tert*-butyl isocyanide, there is a similar Au-catalyzed cyclization. It happens through a 6-*exo*-dig cyclization/retro-ene reaction, but the approach is limited to those adducts with a *tert*-butyl substituent (Scheme 3.10b).[24]

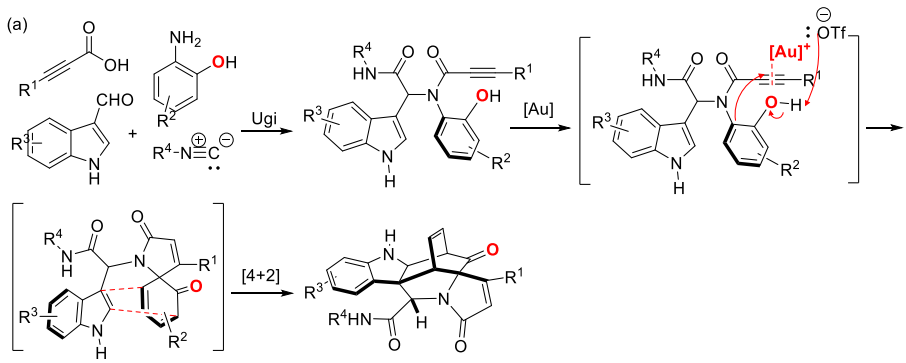

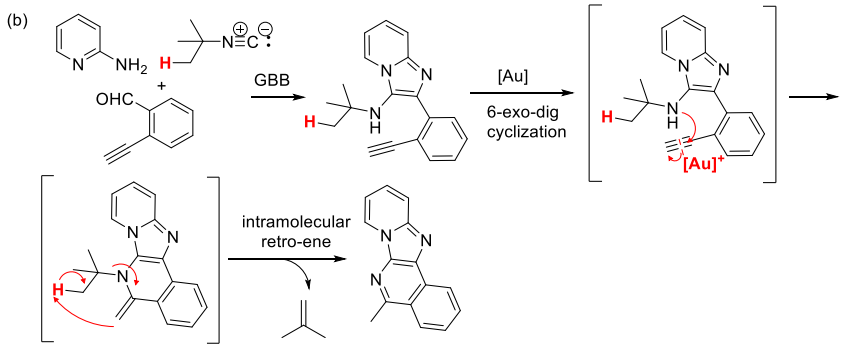

Scheme 3.10. Au-catalyzed post-MCR transformations.

Whereas domino post-condensation modifications of Ugi adducts have been widely explored to deliver novel and complex heterocyclic scaffolds, and many examples of framework exploration have been described, such a strategy appears to be much less applied to GBB adducts.

3.1.4. Domino Reactions

Since domino processes are described as transformations of two or more bond-forming reactions under identical reaction conditions, MCRs are considered a subclass of domino reactions that occurs intermolecularly.

In a domino reaction, the overall transformation is initiated at one site and the first reaction intermediate evolves by generating new intermediates that keep reacting in a similar way, forming bonds along the structure of the substrate; and finally, a terminator ends the process. As a requisite, the substrates must have several functionalities of comparable reactivity and must react in a fixed chronological order.[25,26]

In Nature there are many examples of domino reactions. The biosynthesis of lanosterol from (*S*)-2,3-oxidosqualene is of special interest since the transformation is catalyzed by a single enzyme, the oxidosqualene-lanosterol cyclase (Scheme 3.11). This enzyme enforces a specific conformation of its substrate, being a highly stereoselective process.[27]

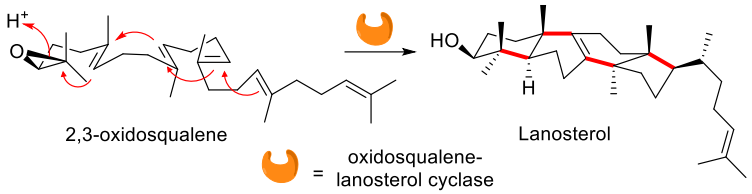

Scheme 3.11. Biosynthesis of lanosterol.

Besides biosynthesis, domino reactions have a remarkable impact in biomimetic approaches of natural products. Historically, the chemical community has paid much attention to the preparation of numerous compounds mimicking the way Nature would biosynthesize them. For instance, the synthesis of progesterone was deeply studied in the 70's and was efficiently improved when the trienyol **I** was proposed as one possible substrate to undergo the domino cyclization that would lead to the natural product (Scheme 3.12).[28]

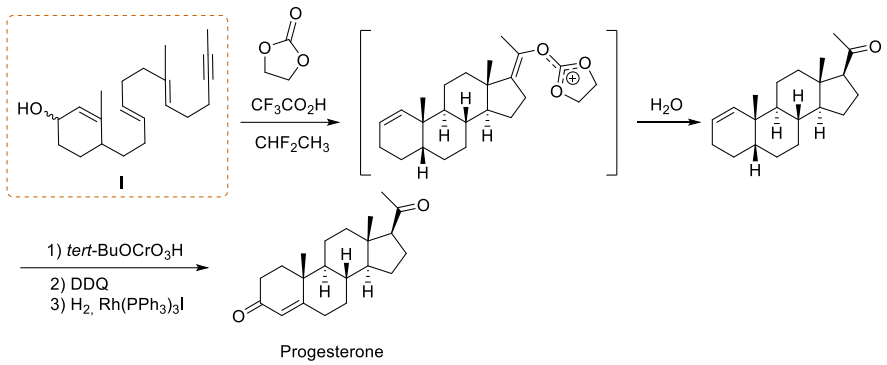

Scheme 3.12. Synthesis of progesterone.

However, the main disadvantage of such approach is the preparation of the substrate **I** as it requires a challenging and long synthetic sequence. The multistep preparation of **I** starts with a commercially available ester and involve 6 synthetic steps plus the convergent synthesis of compound **7**. Both synthetic routes are detailed in the following Scheme 3.13.

In summary, substrates susceptible to undergo domino reactions usually have complex structures with a specific conformation and different functionalities. Thus, the main obstacles of this elegant and efficient approach are the multistep synthetic

procedures behind the preparation of such substrates. This drawback prevents the use of domino reactions in practical synthetic protocols.

3.1.5. Application of MCRs in Drug Discovery

Although the Strecker reaction was the very first developed MCR, it was not until more than one century later, when Ivar Ugi discovered his 4-CR, that the scientific community recognized the enormous potential of MCRs in applied chemistry.[2]

Because of their advantages compared to traditional ways of synthesizing target molecules over multiple sequential steps (previously described at 3.1.1), MCRs may be regarded as a powerful tool in medicinal chemistry and drug discovery processes because their capacity to:

- Rapidly elaborate chemsets for efficient SAR studies.[29] All the different moieties are introduced at selected diversification points in one step instead of sequentially, avoiding extra reaction and isolation steps.

- Access to a huge structural diversity, molecular complexity, and a wide variety of relevant scaffolds, due to the nature of the existing MCRs and the easy diversification by systematic variation of each input or post-modification reactions.[30]

- Exploit the potential of DOS[31] and BIOS[32] design strategies.

Overall, MCRs allow the preparation of effective and functional libraries of small molecules, uncovering therefore the discovery of novel bioactive structures from the very large biological chemical space.

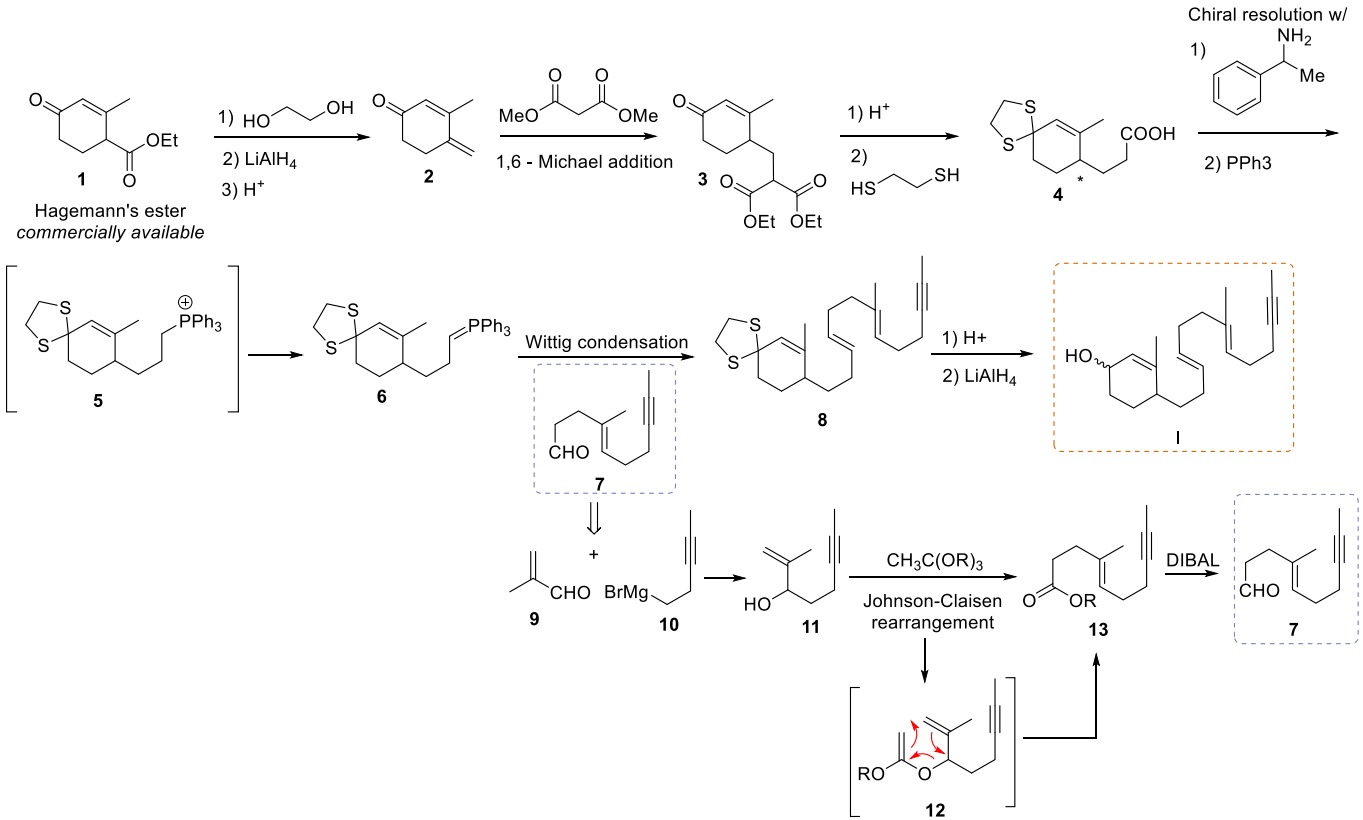

Scheme 3.13. Preparation of the domino substrate **I**.

3.1.6. Advances in MCRs Discovery

Nowadays, the choice of synthetic methods is so overwhelming that it is possible to rationally design a retrosynthetic approach for almost any feasible chemical structure. However, this is not the case for MCR approaches. Ever since the beginning of organic chemistry, advances have been mainly focused on the discovery of new bimolecular reactivity, and only few research groups occasionally investigated MCRs.[2]

Only in the last 50 years, MCRs have been increasingly appreciated as efficient synthetic tools to rapidly access complex products,[4,30] but only a few new MCRs have been described over this time, such as the GBB reaction, and little efforts are currently being dedicated to this area of research. In fact, as for MCRs, reaching the general use and acceptation of multistep synthesis remains far from reality.

In recent years, rational design strategies have been explored for filling this existing gap in the discovery of new MCRs.[2,33] Those strategies are mainly based on the following entries, which are summarized on Scheme 3.14.

- *Replacing a single reactant* (SRR) in an already known MCR (Scheme 3.14a).[34] The new component (D-x) should mimic the chemical reactivity or property necessary for the interaction with the other components (A and B). Like Ugi did in his 4-CR approach, replacing the carbonyl component of the Passerini reaction by an imine brought a different outcome and expanded the structural framework regarding the original reaction.

- *Modulating reaction sequences* (MRS, Scheme 3.14b). This approach involves an intermediate that is generated by a previous MCR and is then reacted *in situ* with different reagents. Such intermediate displays divergent reactivity modes depending on the reagent, thus generating scaffold diversity.

- Changing reaction conditions to create *condition-based divergence* (CBD, Scheme 3.14c). As simple as applying a different catalyst, solvent, or heating mode, this can modify the reactivity pattern of the MCR inputs and generate novel scaffolds.

- *Combining two (or more) different types of MCRs* (MCR^2) in a one-pot process (Scheme 3.14d). The product of the primary MCR should have orthogonal reactive groups that would allow the further reactivity of the secondary MCR. The generation of complex and variable structures is achieved by varying the successive MCR.

Overall, we consider that due to their intrinsic advantages and the rational design possibilities that they might allow, MCRs offer a large area for relevant new discoveries in many areas of research.

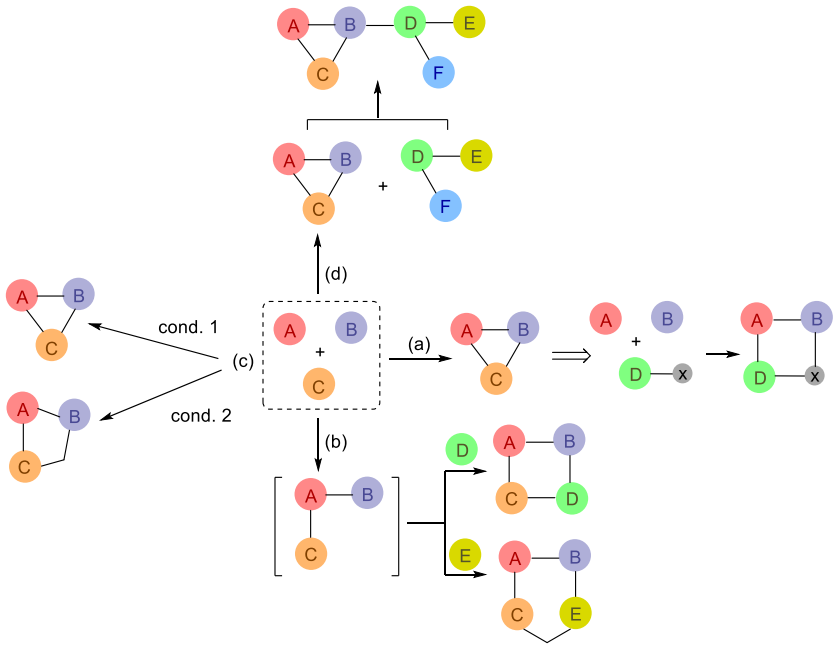

Scheme 3.14. (a) Single reactant replacement; (b) modular reaction sequences; (c) condition-based divergence in MCRs; and (d) union of MCRs.

3.2. Results and Discussion

The present chapter is divided into three sections, and each section includes one or two publications.

To begin with, we introduce an unusual approach in which marketed drugs are used as substrates in MCRs. Complex adducts that frame novel heterocyclic scaffolds with a relevant degree of chemical diversity at selected positions are obtained as final products. The products keep the same kind of activity than the original drug, but display modifications on the binding mode and/or enhance kinetic profiles and properties of the parent compound.

In the second part, while exploring new reactivity to expand our current knowledge of chemical and reaction space, we came with the idea of developing a novel methodology linking the concepts of MCRs and domino reactions. The main inconvenient that domino approaches present is the high complexity of the domino substrates, which most of the times require long synthetic routes. Here, instead of starting from a typical domino substrate, we introduce a MCR product to different domino processes, being able to obtain several domino prolonged MCRs that lead to unprecedented polyheteroaromatic systems reliable as AhR ligands.

In the last part, more than 120 articles about the reactivity of basic heterocycles as inputs in MCRs have been reviewed in a chapter belonging to the book *Multicomponent Reactions towards Heterocycles: Concepts and Applications*. With the intention of presenting the current state of the topic, we have selected the most relevant work in the field since the publication of our last bibliographic revisions.[35,36] The articles reviewed are comprised between the years 2015 and 2021, approximately, and show a notable expansion of the field.

3.3. Bibliography

[1] J. Zhu, H. Bienaymé, *Multicomponent Reactions*, Wiley-VCH, Weinheim, **2005**.

[2] J. Zhu, Q. Wang, M.-X. Wang, *Multicomponent Reactions in Organic Synthesis*, Wiley-VCH, Weinheim, **2014**.

[3] A. Dömling, I. Ugi, *Angew. Chem. Int. Ed.* **2000**, *39*, 3168–3210.

[4] A. Dömling, *Chem. Rev.* **2006**, *106*, 17–89.

[5] P. A. Wender, B. L. Miller, *Nature* **2009**, *460*, 197–201.

[6] A. Strecker, *Ann. der Chemie und Pharm.* **1854**, *91*, 349–351.

[7] M. Passerini, L. Simone, *Gazz. Chim. Ital.* **1921**, *51*, 169–129.

[8] I. Ugi, *Angew. Chem. Int. Ed.* **1959**, *71*, 386.

[9] K. Groebke, L. Weber, F. Mehlin, *Synlett* **1998**, *1998*, 661–663.

[10] C. Blackburn, B. Guan, P. Fleming, K. Shiosaki, S. Tsai, *Tetrahedron Lett.* **1998**, *39*, 3635–3638.

[11] H. Bienaymé, K. Bouzid, *Angew. Chem. Int. Ed.* **1998**, *37*, 2234–2237.

[12] N. Devi, R. K. Rawal, V. Singh, *Tetrahedron* **2015**, *71*, 183–232.

[13] K. Pericherla, P. Kaswan, K. Pandey, A. Kumar, *Synthesis (Stuttg).* **2015**, *47*, 887–912.

[14] S. Shaaban, B. F. Abdel-Wahab, *Mol. Divers.* **2016**, *20*, 233–254.

[15] A. Boltjes, A. Dömling, *European J. Org. Chem.* **2019**, *2019*, 7007–7049.

[16] R. C. Cioc, H. D. Preschel, G. Van Der Heijden, E. Ruijter, R. V. A. Orru, *Chem. Eur. J.* **2016**, *22*, 7837–7842.

[17] S. K. Guchhait, C. Madaan, *Org. Biomol. Chem.* **2010**, *8*, 3631–3634.

[18] O. Ghashghaei, S. Caputo, M. Sintes, M. Reves, N. Kielland, C. Estarellas, F. J. Luque, A. Aviñó, R. Eritja, A. Serna-Gallego, J. A. Marrugal-Lorenzo, J. Pachon, J. Sanchez-Cespedes, R. Treadwell, F. de Moliner, M. Vendrell, R. Lavilla, *Chem. Eur. J.* **2018**, *24*, 14513–14521.

[19] U. K. Sharma, N. Sharma, D. D. Vachhani, E. V. Van Der Eycken, *Chem. Soc. Rev.* **2015**, *44*, 1836–1860.

[20] U. K. Sharma, G. Tian, L. G. Voskressensky, E. V. Van der Eycken, *Drug Discov. Today Technol.* **2018**, *29*, 61–69.

[21] J. Bariwal, R. Kaur, L. G. Voskressensky, E. V. Van der Eycken, *Front. Chem.* **2018**, *6*, 1–21.

[22] Z. Li, N. Sharma, U. K. Sharma, J. Jacobs, L. Van Meervelt, E. V. Van Der Eycken, *Chem. Commun.* **2016**, *52*, 5516–5519.

[23] Y. He, Z. Liu, D. Wu, Z. Li, K. Robeyns, L. Van Meervelt, E. V. Van Der Eycken, *Org. Lett.* **2019**, *21*, 4469–4474.

[24] T. Shao, Z. Gong, T. Su, W. Hao, C. Che, *Beilstein J. Org. Chem.* **2017**, *13*, 817–824.

[25] L. F. Tietze, G. Brasche, K. M. Gericke, *Domino Reactions in Organic Synthesis*, Wiley-VCH, Weinheim, **2006**.

[26] L. F. Tietze, G. Brasche, K. M. Gericke, *Chem. Rev.* **1996**, *96*, 115–136.

[27] K. U. Wendt, G. E. Schulz, E. J. Corey, D. R. Liu, *Angew. Chem. Int. Ed.* **2000**, *39*, 2812–2833.

[28] W. S. Johnson, *Angew. Chem. Int. Ed.* **1976**, *15*, 9–17.

[29] A. Dömling, *Chem. Rev.* **2006**, *106*, 17–89.

[30] A. Dömling, W. Wang, K. Wang, *Chem. Rev.* **2012**, *112*, 3083–3135.

[31] S. L. Schreiber, *Science.* **2000**, *287*, 1964–1969.

[32] A. Nören-Müller, I. Reis-Corrêa, H. Prinz, C. Rosenbaum, K. Saxena, H. J. Schwalbe, D. Vestweber, G. Cagna, S. Schunk, O. Schwarz, H. Schiewe, H. Waldmann, *Proc. Natl. Acad. Sci. U. S. A.* **2006**, *103*, 10606–10611.

[33] E. Ruijter, R. Scheffelaar, R. V. A. Orru, *Angew. Chem. Int. Ed.* **2011**, *50*, 6234–6246.

[34] B. Ganem, *Acc. Chem. Res.* **2009**, *42*, 463–472.

[35] N. Isambert, R. Lavilla, *Chem. - A Eur. J.* **2008**, *14*, 8444–8454.

[36] E. Vicente García, N. Kielland, R. Lavilla, in *Multicomponent React. Org. Synth.* (Eds.: J. Zhu, Q. Wang, M.-X. Wang), Wiley-VCH, Wheinheim, **2015**, pp. 159–182.

From Drugs to Drugs: towards Improved Antibiotics

Publication I: Multicomponent Reactions Upon the Known Drug Trimethoprim as a Source of Novel Antimicrobial Agents

frontiers in Chemistry

ORIGINAL RESEARCH
published: 04 July 2019
doi: 10.3389/fchem.2019.00475

Multicomponent Reactions Upon the Known Drug Trimethoprim as a Source of Novel Antimicrobial Agents

Marina Pedrola[1†], Marta Jorba[2,3†], Eda Jardas[1], Ferran Jardi[1], Ouldouz Ghashghaei[1], Miguel Viñas[2,3] and Rodolfo Lavilla[1*]*

[1] Laboratory of Medicinal Chemistry, Faculty of Pharmacy and Food Sciences and Institute of Biomedicine (IBUB), University of Barcelona, Barcelona, Spain, [2] Laboratory of Molecular Microbiology & Antimicrobials, Department of Pathology & Experimental Therapeutics, Medical School, Hospitalet de Llobregat, University of Barcelona, Barcelona, Spain, [3] Bellvitge Institute for Biomedical Research (IDIBELL), Barcelona, Spain

OPEN ACCESS

Edited by:
Jonathan G. Rudick,
Stony Brook University, United States

Reviewed by:
Jean-François Brière,
UMR6014 Chimie Organique, Bioorganique Réactivité et Analyse (COBRA), France
Andrea Trabocchi,
University of Florence, Italy
Fabio De Moliner,
University of Edinburgh, United Kingdom

***Correspondence:**
Miguel Viñas
mvinyas@ub.edu
Rodolfo Lavilla
rlavilla@ub.edu

[†] These authors have contributed equally to this work

Specialty section:
This article was submitted to Organic Chemistry, a section of the journal Frontiers in Chemistry

Received: 04 April 2019
Accepted: 20 June 2019
Published: 04 July 2019

Citation:
Pedrola M, Jorba M, Jardas E, Jardi F, Ghashghaei O, Viñas M and Lavilla R (2019) Multicomponent Reactions Upon the Known Drug Trimethoprim as a Source of Novel Antimicrobial Agents. Front. Chem. 7:475. doi: 10.3389/fchem.2019.00475

Novel antibiotic compounds have been prepared through a selective multicomponent reaction upon the known drug Trimethoprim. The Groebke-Blackburn-Bienaymé reaction involving this α-aminoazine, with a range of aldehydes and isocyanides afforded the desired adducts in one-step. The analogs display meaningful structural features of the initial drug together with relevant modifications at several points, keeping antibiotic potency and showing satisfactory antimicrobial profile (good activity levels and reduced growth rates), especially against methicillin-resistant *Staphylococcus aureus*. The new products may open new possibilities to fight bacterial infections.

Keywords: antibiotics, drugs, isocyanides, multicomponent reactions, resistant bacteria

INTRODUCTION

Trimethoprim (TMP, **1**, **Figure 1A**) is a well-known antibiotic, present in the *Model List of Essential Medicines* from the World Health Organization. TMP is usually used in combinationwith Sulfamethoxazole (SMX) to treat lower urinary tract infections and acute invasive diarrhea/bacterial dysentery as first and second choice, respectively (WHO, 2017), respiratory infections in cystic fibrosis patients caused by *Staphylococcus aureus*, among other many infections. Lately, it has also been used for preventing infections from the opportunistic pathogen *Pneumocystis carinii* (Urbancic et al., 2018), which normally causes pneumonia in patients with AIDS. Both drugs act on the folic acid biosynthetic route by inhibiting two enzymes: dihydrofolate reductase (DHFR) and dihydropteroate synthetase, respectively. Folate needs to be synthesized by bacteria and it is crucial in the biosynthetic pathway of thymidine, essential in DNA synthesis. Hence, when used in combination, these antibiotics display a synergistic effect in inhibiting bacterial growth and leading to eventual cell death (**Figure 1B**) (Torok et al., 2009; Katzung et al., 2012).

The combination of sulfonamides and DHFR inhibitors has been clinically used since 1968 when it was first approved in the UK (Cody et al., 2008; Torok et al., 2009). Unfortunately, resistance emerged soon and has become widespread (Huovinen et al., 1995; Ventola, 2015). Nowadays, antibiotic resistance is one of the world's most pressing public health problems with high morbidity and mortality rates (Centers for Disease Control and Prevention, 2017). Furthermore, finding active drugs to fight both multidrug resistant infections and organisms is becoming extremely challenging, as is often the case of methicillin-resistant *Staphylococcus aureus* (MRSA) and multidrug resistant *Pseudomonas aeruginosa*. In this context, the co-therapy with TMP and SMX turns out to be

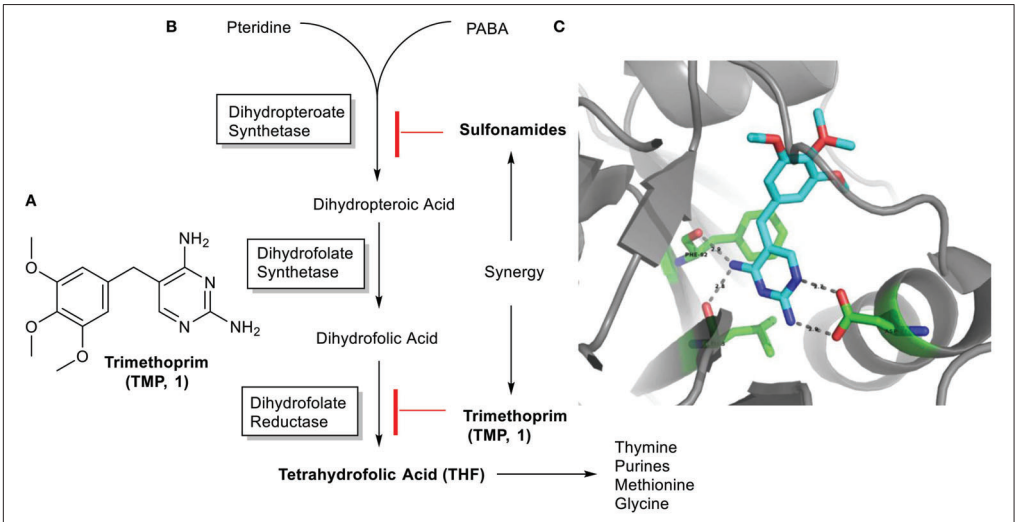

FIGURE 1 | (A) TMP (**1**) structure. **(B)** Folic acid biosynthetic route. **(C)** Interactions of the TMP (**1**, in blue) with key amino acid residues at the DHFR binding site. Representation based on the 2W9H PDB file, with a resolution of 1.48 A (Heaslet et al., 2009).

ineffective to treat infections of a subset of bacteria with TMP-resistant DHFR enzymes (Heaslet et al., 2009).

Thus, the exploration of new synthetic compounds mimicking the structure and mechanism of action of conventional antimicrobial agents can be regarded as a main goal of this field of research. Such chemical entities would open new perspectives to reduce secondary effects and to enhance antimicrobial action and/or spectrum. Moreover, interaction between new molecules and conventional antimicrobials should be explored with the aim to find eventual synergistic activity.

So far, some research groups have introduced chemical variability at the trimethoxybenzyl residue of the TMP in order to optimize the drug and improve its properties, overall activity and tackle TMP-resistance issues (**Scheme 1**) (Zhou et al., 2013; Lombardo et al., 2016; Rashid et al., 2016), being able to find promising potent compounds against *S. aureus* and *E. coli*. However, in this work we will focus our efforts on modifying the 2,4-diaminopyrimidine moiety, through a selective multicomponent reaction (MCR), the Groebke-Blackburn-Bienaymé reaction (GBBR). In the past, changes at this part of the molecule have not been considered, as they involve key interactions in the recognition of the natural substrate at the DHFR active site; however, the situation could be otherwise in mutated enzymes. Furthermore, inspection of the PDB of the crystal structure of a TMP-DHFR complex shows room for structural changes at the pyrimidine moiety (**Figure 1C**) (Heaslet et al., 2009). These GBBR-type modifications will change the heterocyclic core of the drug into a more complex di- or tricyclic azine, and up to four diversity points, which will be introduced in a regioselective manner (**Scheme 1**). These transformations, involving a relevant structural change on the TMP original framework, strictly speaking cannot be considered as drug late stage functionalizations (Cernak et al., 2016), although share the same philosophy of the approach.

MCRs represent an alternative to the usual sequential multistep synthesis. They involve the reaction of three or more starting materials in a convergent way to yield an adduct, whose structure embodies the major part of the reactive materials in a one-pot reaction through a unified mechanism (Zhu et al., 2014). Specifically, these reactions bring high efficiency, simplicity and both atom and step economy. Thus, they are of interest in medicinal chemistry to assemble relevant, complex heterocycles with remarkable bioactivities and to speed up the Structure-Activity Relationship studies (Hulme, 2005; Akritopoulou-Zanze and Djuric, 2010; Domling et al., 2012; Slobbe et al., 2012; Zarganes-Tzitzikas and Doemling, 2014).

The GBBR (**Scheme 2**) is an isocyanide-based MCR yielding azine-fused imidazoles from readily available aldehydes (**2**), isocyanides (**3**) and amidine-type building blocks (**1**) (Bienaymé and Bouzid, 1998; Blackburn et al., 1998; Groebke et al., 1998). Several reviews have abstracted the main features of this MCR (Devi et al., 2015; Pericherla et al., 2015). This important transformation is massively used in medicinal chemistry, especially in drug discovery, because of the drug like character of the adduct (imidazo-azine), together with the power to decorate it with a wide range of structural diversity (Shaaban and Abdel-Wahab, 2016). These *N*-fused bicyclic imidazo-azines represent a special class of privileged scaffold found in several bioactive compounds and commercially available drugs, such as Zolpidem, Alpidem, Necopidem, Zolimidine, Divaplon, and

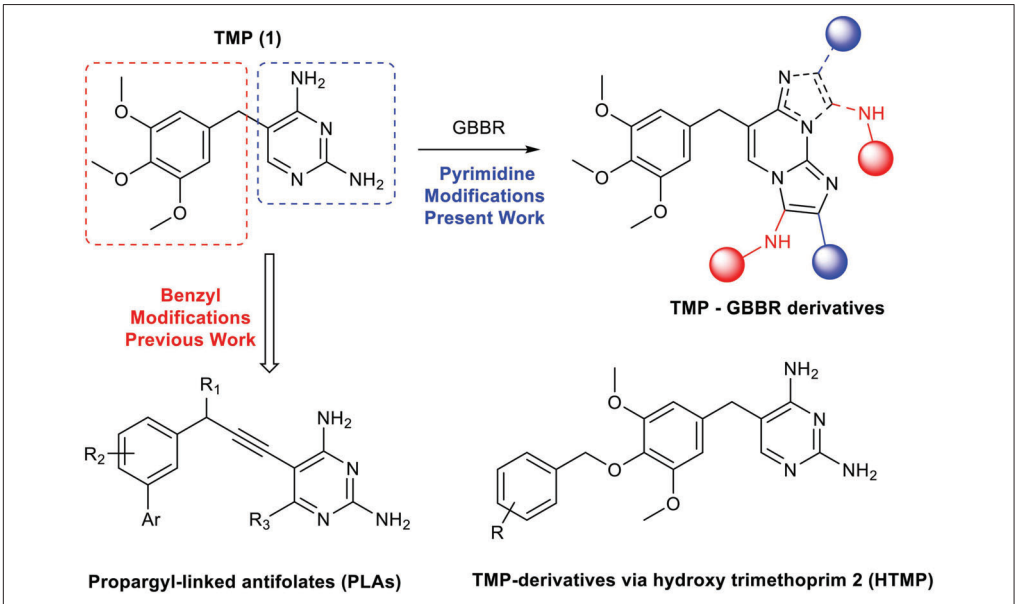

SCHEME 1 | TMP-GBBR derivatives and precedent modifications on the benzyl moiety.

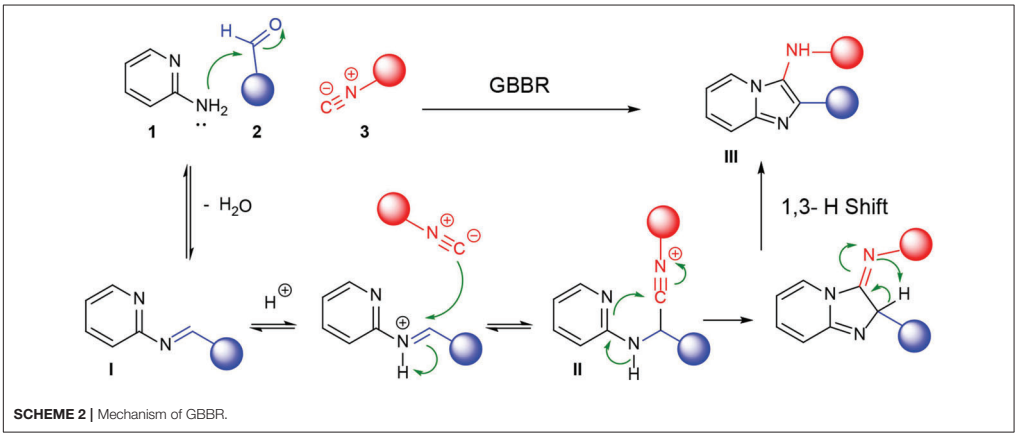

SCHEME 2 | Mechanism of GBBR.

Minodronic acid (approved for treatments of insomnia, anxiety, peptic ulcers, epilepsy, osteoporosis, etc.) (**Figure 2**). It is also well-known that α-polyamino-polyazines are important aromatic polyheterocycles present in a wide variety of clinical drugs, such as the antibacterial drug Trimethoprim, the anticonvulsant drug Lamotrigine and the anticancer drug Methotrexate. Furthermore, specific GBBR adducts have been identified as active antibiotics through phenotypic analyses, addressing a variety of targets (Al-Tel and Al-Qawasmeh, 2010; Shukla et al., 2012; Semreen et al., 2013; Kumar et al., 2014). These facts back our project to modify TMP via GBBR processes to deliver potentially useful novel antibiotics, either improving the activity of the original drug upon DHFR or acting through independent mechanisms.

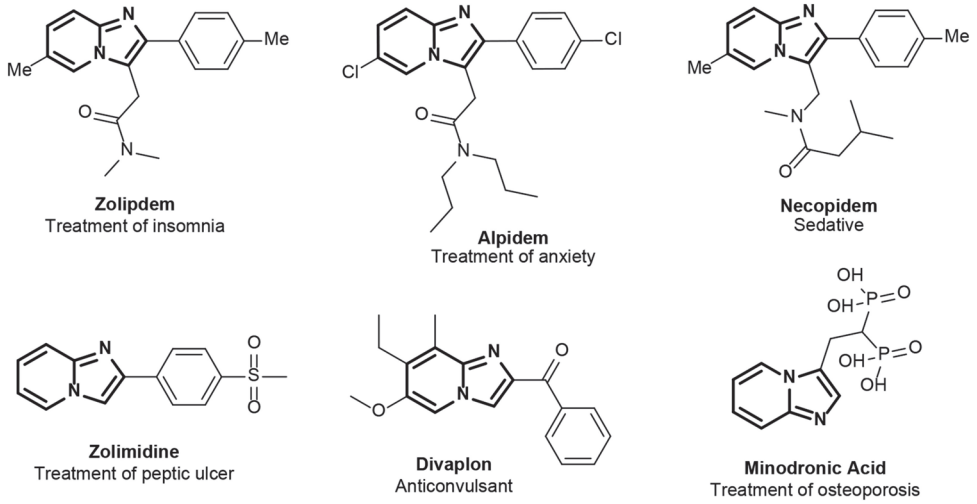

FIGURE 2 | Example of commercial drugs with *N*-fused bicyclic imidazo-azines. The imidazo-azine core is highlighted in bold.

RESULTS AND DISCUSSION

Chemical Synthesis

In this context, we planned to develop a series of TMP derivatives through the GBBR by interaction of the original drug (TMP, **1**) with a range of aldehydes (**2**) and isocyanides (**3**), and analyse the resulting MCR adducts as novel antibiotics, determining their potency, and efficiency, also considering their potential impact on resistant bacteria (**Scheme 3**).

The chemical modifications on TMP are based in our recent discoveries on GBBRs upon diaminopyrimidines, involving selective and multiple MCRs (Ghashghaei et al., 2018). In this way, the preparation of TMP analogs consisted in a regioselective mono-GBBR with an aldehyde/isocyanide pair, to yield derivatives **4**; it is worth mentioning that a kinetic control justifies the preferential formation of the observed isomer. Furthermore, double GBBR processes upon TMP yield doubly substituted derivatives **5**, with two equivalents of each reactant class (**Scheme 3**). The participation of a variety of Lewis acids catalyst is required to suitably generate and activate the imine intermediate and to achieve a moderate yield. In addition, standard flash chromatography purification was normally needed to afford the pure product. The designed analogs featured the *N*-fused bicyclic imidazo-azine scaffolds from the TMP reactant and displayed the variability points at substituents R^1, derived from the isocyanide input (**3**) and R^2 arising from the aldehyde reactant (**2**).

The processes worked in our TMP system as expected, yielding the corresponding products, showing the same reactivity and selectivity trends that were described in the unsubstituted diaminopyrimidine studies (Ghashghaei et al., 2018). For the initial screening, we prepared a series of TMP analogs featuring a variety of substituents on the imidazole amino group (R^1, being *tert*-butyl, 4-methoxyphenyl, cyclohexyl, and ethoxycarbonylmethyl) whereas at its carbon position a range of aromatic or alkyl substituents were introduced (R^2 being 4-chlorophenyl, α-, β-, or γ-pyridinyl, α-thienyl, methyl, and isopropyl). All the reactions were successful, yielding the mono-GBBR derivatives **4** and the doubly substituted-GBBR adducts **5** in acceptable yields (unoptimized). In this way, 12 new products (**4a**-**4j** and **5a**-**b**) arising from the corresponding aldehyde/isocyanide combinations were suitably prepared as pure materials (**Figure 3**).

The connectivity of the first analog synthesized (**4a**) was assigned through two-dimensional NMR experiments: HSQC, HMBC and NOESY spectra (see **Supplementary Material**) and matched with the expected structure, displaying the regioselectivity previously described (Ghashghaei et al., 2018). The rest of derivatives showed the same spectroscopical trends and their structures were assigned by analogy. Furthermore, the doubly substituted GBBR adducts **5** synthetically derived from the corresponding precursors **4**, then securing their identity.

We planned to incorporate an unsubstituted amino group in the imidazole ring of the novel derivatives **4** and **5** in order to favor their recognition by the DHFR active site, in line with the natural substrate. Then, we tackled the preparation of such compounds through the acidic removal of a *tert*-butyl group from a suitable precursor adduct coming from MCRs involving *tert*-butyl isocyanide. Precedent work by Krasavin et al. (2008) demonstrated that this transformation is feasible in GBBR

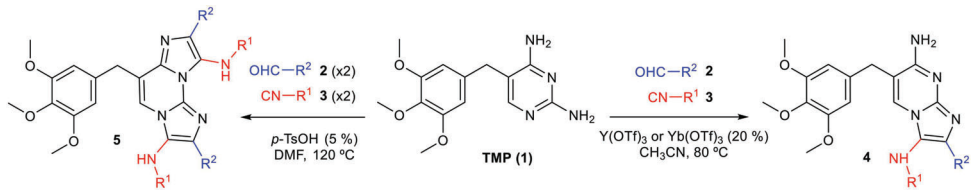

SCHEME 3 | Synthesis of mono- (**4**) and double- (**5**) TMP GBBR adducts.

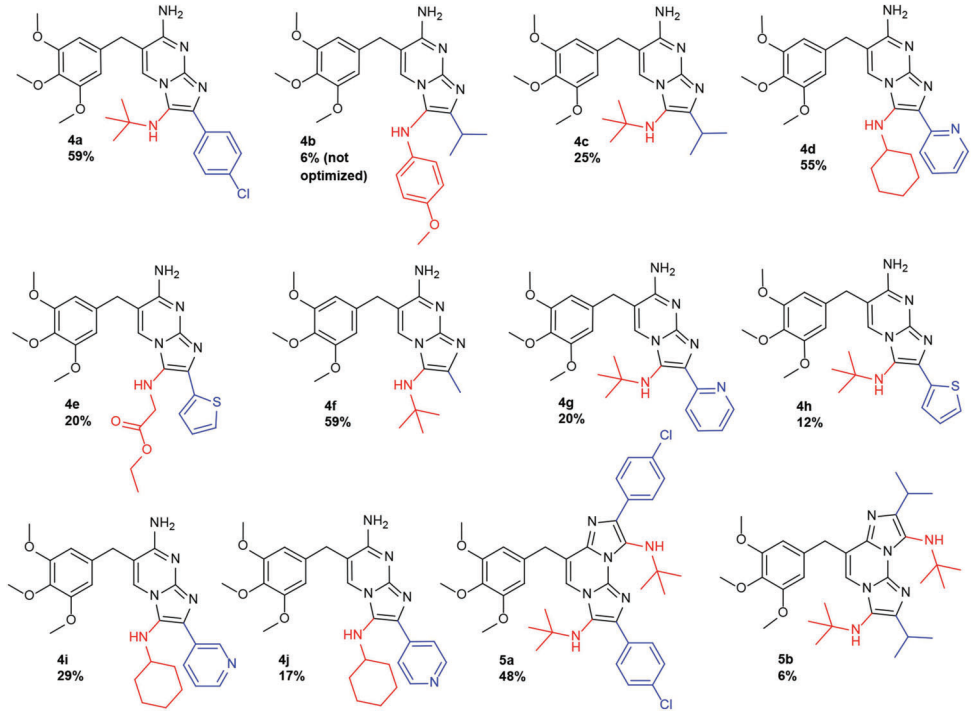

FIGURE 3 | TMP mono- (**4**) and double-GBBR (**5**) adducts.

adducts. In this way, compounds **6a-6b** and **7a** were obtained as pure unsubstituted amino derivatives form *tert*-butyl precursors **4** and **5**, after HBF_4 treatment (**Scheme 4**). All the synthesized compounds were suitably obtained in pure form, characterized and forwarded to microbiological analyses.

Biological Analyses

The Minimum Inhibitory Concentration (MIC) values of the 15 TMP analogs against control strains are shown in **Table 1** (for details, see the **Supplementary Material**). Although all the compounds showed MIC values against *E. coli* ATCC 25922 and *S. aureus* ATCC 29213 higher than TMP, some of them were almost as potent as TMP (**4c**, **4f**, **4h, 4i, 4j** and **6a**). *P. aeruginosa* PAO1 was found to be fully resistant to TMP, as well as to all new compounds. A preliminary inspection of the results showed that double GBBR adducts **5** lacked activity, probably meaning that they were unsuitable for binding to the target sites. Whereas for derivatives **4** some combinations were unproductive

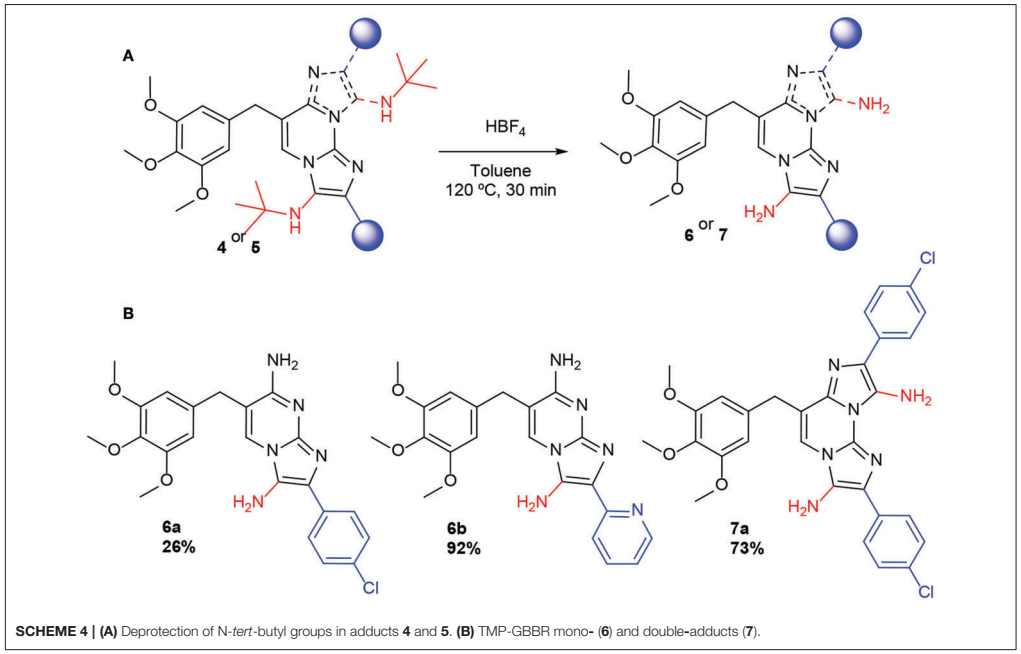

SCHEME 4 | (A) Deprotection of N-*tert*-butyl groups in adducts **4** and **5**. **(B)** TMP-GBBR mono- (**6**) and double-adducts (**7**).

(especially the ones with aromatic and acetate R^1 substituents and *p*-chlorophenyl group at R^2 position), those featuring *tert*-butyl groups at R^1 and isopropyl, methyl, β-, γ- (but not α-) pyridyl, and α-thienyl groups at R^2 were particularly favored. Moreover, comparing compounds **4d**, **4g** and **6b**, we are able to confirm that the reduction of R^1 substituents size allowed to decrease the MIC. It is also worthy to emphasize that all compounds resulted to be more active on *E. coli* than on *S. aureus*; **4i**, **4c**, and **4f** being the most potent ones. Thus, chemical modifications do not seem to limit the ability of the different new compounds to penetrate the outer membrane in Gram negative bacteria.

Almost all the new compounds acted synergistically with SMX as the control drug TMP did, against *E. coli* ATCC 25922 and *S. aureus* ATCC 29213 (**Table 2**); the latter species being much more sensitive to the SMX combination than to the treatment with the TMP-GBBR analogs alone. It also becomes apparent that nearly all the new compounds presented high activity against a set of clinical isolates of MRSA isolated from hospitalized or Cystic fibrosis (CF) patients. In CF patients, *Staphylococcus aureus* (and particularly MRSA) infection is the main challenge of antibiotic therapy, since the persistent infection caused by this bacterium is strongly associated with increased rates of decline in respiratory function and high mortality (Dolce et al., 2019). Thus, new approaches to fight this kind of bacterium are mandatory and should be based on new antimicrobials, most probably combined with conventional ones (Lo et al., 2018; Xhemali et al., 2019).

Again, derivatives **4c**, **4f**, **4h**, **4i**, **4j**, and **6b** were the most potent, but interestingly, some adducts which were not meaningful acting alone (**Table 1**), on SMX combination displayed a relevant potency (**4a**, **4d**, **4e**, **4g**, and **6a**). Disappointingly, no effect either of adducts alone or in combination with SMX was observed on *Pseudomonas aeruginosa* in any case, in line with the detected TMP activity. Particularly interesting are the activities against MRSA isolates as can be seen in **Table 2**, with many derivatives being as active as the TMP reference.

A relevant feature in the use of an antibiotic is its kinetic profile. Specifically, a fast reduction of the growth rates of the infective microorganism is of capital interest in therapeutics, arguably as important or more than the effective dose. Thus, the effect of TMP analogs in combination with SMX on the growth curves of *E. coli* ATCC 25922 and *S. aureus* ATCC 29213 was studied for the most interesting compounds (**Figure 4** and **Supplementary Material**). Some differences were observed at subinhibitory concentrations of the antimicrobials (1/2 MIC and 1/4 MIC). In both tested bacteria, full inhibition occurred for derivatives **4g** and **4i** with SMX (1:20) at 1/2 the MIC value (**Figures 4A,C,D**). On the other hand, compounds **4g** and **4f**, at a concentration of 1/4 MIC, gave similar results than

TMP at 1/2 MIC against *E. coli* ATCC 25922 (**Figures 4A,B**). In all the cases, significant reductions in the growth rates were observed when compared with the antimicrobial-free control, being comparatively better for some conditions than the TMP reference, especially compound **4i** for long culture times (**Figure 4D**).

TABLE 1 | Minimum Inhibitory Concentration (MIC, μM) of TMP and the new GBBR analogs against *E. coli* ATCC 25922, *S. aureus* ATCC 29213, and *P. aeruginosa* PAO1.

	MIC (μM)		
	***E. coli* ATCC 25922**	***S. aureus* ATCC 29213**	***P. aeruginosa* PAO1**
TMP 1	0.43	13.78	> 110.22
4a	16.13	> 64.52	> 64.52
4b	> 67.01	> 67.01	> 67.01
4c	1.17	18.71	> 74.85
4d	8.19	> 65.50	> 65.50
4e	5.19	> 83.07	> 83.07
4f	1.25	80.10	> 80.10
4g	17.30	> 69.18	> 69.18
4h	2.14	> 68.44	> 68.44
4i	1.02	65.50	> 65.50
4j	2.05	65.50	> 65.50
5a	> 45.60	> 45.60	> 45.60
5b	> 56.66	> 56.66	> 56.66
6a	4.55	> 72.75	> 72.75
6b	2.46	78.73	> 78.73
7a	> 54.29	> 54.29	> 54.29

CONCLUSION

The marketed antibiotic TMP (**1**) has been succesfully modified by a GBB MCR with a range of commercially available aldehydes and isocyanides in selective processes yielding mono- or double- imidazo-azine adducts **4** and **5**. A short synthetic (one or two steps) protocol allowed access to a focused library of 15 TMP analogs featuring a novel heterocyclic scaffold with a relevant degree of chemical diversity at selected positions, including hydrogen atoms, small alkyl groups, aromatic and heteroaromatic rings. Incidentally, this work shows the possibility of using known drugs as substrates for MCRs and, in this manner, opens new ways to develop novel chemical entities of biological interest from this unusual origin. Antimicrobial activity of the novel analogs has been assayed in Grampositive (*S. aureus*) and Gramnegative (*E. coli*) microorganisms as well as on a bacterium considered the paradigm of resistance (*P. aeruginosa*). Despite the latter was resistant to all the new compounds, several mono-adducts **4** displayed MICs in the micromolar range against *E. coli* and *S. aureus*, what make us think that the TMP-derivatives bind to DHFR as well. The observed impact on growth kinetics allows us to conclude that the association of these new products with SMX exert a very similar effect than TMP itself. It is worthy to emphasize the excellent activities detected against MRSA strains. Given the reduced size of the focused chemset analyzed, and the relevant results found, we can conclude that the novel scaffold synthesized has potential to become a source for novel antibiotics. Further on going studies along these

TABLE 2 | Minimum Inhibitory Concentration (MIC, μM) of TMP and the new GBBR analogs in combination with Sulfamethoxazole (1:20) against *E. coli* ATCC 25922, *S. aureus* ATCC 29213, *P. aeruginosa* PAO1, *S. aureus* 8125304770, *S. aureus* 8139265926, *S. aureus* 8125255044, and *S. aureus* 8124825998.

	MIC (μM)						
	***E. coli* ATCC 25922**	***S. aureus* ATCC 29213**	***P. aeruginosa* PAO1**	***S. aureus* 8125304770**	***S. aureus* 8139265926**	***S. aureus* 8125255044**	***S. aureus* 8124825998**
TMP 1	0.11	0.43	13.78	0.431	0.86	0.22	0.43
4a	2.02	8.06	> 64.52	4.03	8.06	1.01	4.03
4b	67.01	> 67.01	> 67.01	67.01	> 67.01	67.01	> 67.00
4c	1.17	4.68	37.42	4.68	9.36	0.292	1.17
4d	2.05	4.09	> 65.50	4.09	4.093	1.02	4.09
4e	1.30	5.19	> 83.07	1.298	2.60	0.65	1.30
4f	0.63	5.01	40.05	0.63	2.50	0.63	1.25
4g	0.54	4.32	> 69.18	2.16	8.65	1.08	4.32
4h	0.27	2.14	34.22	1.07	1.07	0.27	1.07
4i	0.13	2.05	32.75	0.51	1.02	0.51	1.02
4j	0.26	2.05	32.75	1.02	2.05	0.51	1.02
5a	> 45.60	> 45.60	> 45.60	> 45.60	> 45.60	> 45.60	> 45.60
5b	28.33	> 56.66	> 56.66	28.331	> 56.66	14.17	56.66
6a	2.27	9.09	> 72.75	2.27	4.55	1.14	4.55
6b	0.31	2.46	78.73	1.23	2.46	0.62	2.46
7a	> 54.29	> 54.29	> 54.29	> 54.9	> 54.29	> 54.29	> 54.29

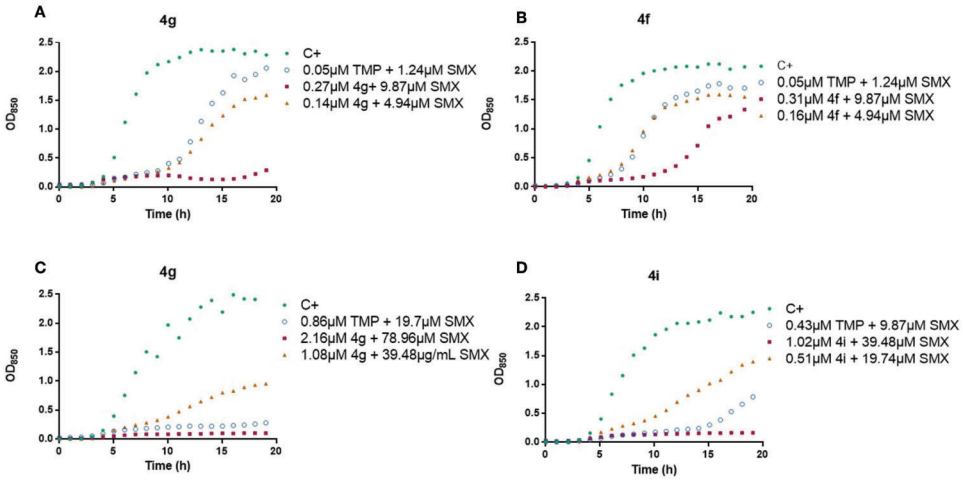

FIGURE 4 | Effect of the analogs **4f**, **4g**, **4i** and TMP in combination with sulfamethoxazole (1:20) on the growth curve of *E. coli* (**4g**, **4f**; **A,B**) and *S. aureus* (**4g**, **4i**; **C,D**).

lines tackle toxicity, the mechanism of action and bacterial resistance issues.

DATA AVAILABILITY

All datasets generated for this study are included in the manuscript and/or the **Supplementary Files**.

AUTHOR CONTRIBUTIONS

MP was responsible for designing and performing the initial experiments. EJ, FJ, OG, and RL performed the rest of the experimentation of the chemical section and analyzed the results. MJ designed and performed the microbiological experiments. MJ and MV analyzed the results of this section. All authors discussed the whole project and wrote the publication.

FUNDING

Financial support from the Ministerio de Economía y Competitividad-Spain (MINECO, CTQ2015-67870-P) and Generalitat de Catalunya (2017 SGR 1439) is gratefully acknowledged. The Microbiology group was financed by the Generalitat de Catalunya (GGC2017A-SGR-1488) and Marató TV3 (201C/2018) and its own funding.

ACKNOWLEDGMENTS

We thank Dr. Josep M. Sierra (U. Barcelona, IDIBELL) for useful suggestions and discussions. MV is a member of JIPAMR (Joint Programming Initiative on Antimicrobial Resistance) translocation-transfer and of ENABLE consortia. Clinical strains were kindly supplied by Servei de Microbiologia Hospital Vall d'Hebron (Barcelona).

SUPPLEMENTARY MATERIAL

The Supplementary Material for this article can be found online at: https://www.frontiersin.org/articles/10.3389/fchem.2019.00475/full#supplementary-material

REFERENCES

Akritopoulou-Zanze, I., and Djuric, S. W. (2010). "Applications of MCR-derived heterocycles in drug discovery," in *Topics in Heterocyclic Chemistry*, eds. B. U. W. Maes, R. V. A. Orru, and E. Ruitjer (Berlin: Springer), 231–287. doi: 10.1007/7081_2010_46

Al-Tel, T. H., and Al-Qawasmeh, R. A. (2010). Post Groebke-Blackburn multicomponent protocol: synthesis of new polyfunctional imidazo[1,2-a]pyridine and imidazo[1,2-a]pyrimidine derivatives as potential antimicrobial agents. *Eur. J. Med. Chem.* 45, 5848–5855. doi: 10.1016/j.ejmech.2010.09.049

Bienaymé, H., and Bouzid, K. (1998). A new heterocyclic multicomponent reaction for the combinatorial synthesis of fused 3-aminoimidazoles. *Angew. Chemie Int. Ed.* 37, 2234–2237. doi: 10.1002/(SICI)1521-3773(19980904)37:16<2234::AID-ANIE2234>3.0.CO;2-R

Blackburn, C., Guan, B., Fleming, P., Shiosaki, K., and Tsai, S. (1998). Parallel synthesis of 3-aminoimidazo[1,2-a]pyridines

and pyrazines by a new three-component condensation. *Tetrahedron Lett.* 39, 3635–3638. doi: 10.1016/S0040-4039(98)00653-4

Centers for Disease Control and Prevention (2017). *Facts about Antibiotic Resistance and Antibiotic Prescribing: Attitudes, Behaviors, Trends and Cost*. Available at: http://www.cdc.gov/getsmart/community/about/fast-facts.html (accessed March 10, 2019).

Cernak, T., Dykstra, K. D., Tyagarajan, S., Krskab, P. V., and Shane, W. (2016). The medicinal chemist's toolbox for late stage functionalization of drug-like molecules. *Chem. Soc. Rev.* 45, 456–576. doi: 10.1039/C5CS00628G

Cody, V., Pace, J., Chisum, K., and Rosowsk, A. (2008). New insights into DHFR interactions: analysis of *Pneumocystis carinii* and mouse DHFR complexes with NADPH and two highly potent 5-x-carboxy(alkyloxy) trimethoprim derivatives reveals conformational correlations with activity and novel parallel ring stack. *Proteins* 70, 311–319. doi: 10.1002/prot.21131

Devi, N., Rawal, R. K., and Singh, V. (2015). Diversity-oriented synthesis of fused-imidazole derivatives via Groebke-Blackburn-Bienayme reaction: a review. *Tetrahedron* 71, 183–232. doi: 10.1016/j.tet.2014.10.032

Dolce, D., Neri, S., Grisotto, L., Campana, S., Ravenni, N., Miselli, F., et al. (2019). Methicillin-resistant *Staphylococcus aureus* eradication in cystic fibrosis patients: a randomized multicenter study. *PLoS ONE* 14, 1–15. doi: 10.1371/journal.pone.0213497

Domling, A., Wang, W., and Wang, K. (2012). Chemistry and biology of multicomponent reactions. *Chem. Rev.* 112, 3083–3135. doi: 10.1021/cr100233r

Ghashghaei, O., Caputo, S., Sintes, M., Reves, M., Kielland, N., Estarellas, C., et al. (2018). Multiple multicomponent reactions: unexplored substrates, selective processes, and versatile chemotypes in biomedicine. *Chem. Eur. J.* 24, 14513–14521. doi: 10.1002/chem.201802877

Groebke, K., Weber, L., and Mehlin, F. (1998). Synthesis of imidazo[1,2-a] annulated pyridines, pyrazines and pyrimidines by a novel three-component condensation. *Synlett* 1998, 661–663. doi: 10.1055/s-1998-1721

Heaslet, H., Harris, M., Fahnoe, K., Sarver, R., Putz, H., Chang, J., et al. (2009). Structural comparison of chromosomal and exogenous dihydrofolate reductase from *Staphylococcus aureus* in complex with the potent inhibitor trimethoprim. *Proteins* 76, 706–717. doi: 10.1002/prot.22383

Hulme, C. (2005). "Applications of multicomponent reactions in drug discovery—lead generation to process development," in *Multicomponent Reactions*, eds. J. Zhu and H. Bienayme (Weinheim: Wiley-VCH), 311–341. doi: 10.1002/3527605118.ch11

Huovinen, P., Sundstrom, L., Swedberg, G., and Skold, O. (1995). Trimethoprim and sulfonamide resistance. *Antimicrob. Agents Chemother.* 39, 279–289. doi: 10.1128/AAC.39.2.279

Katzung, B. G., Masters, S. B., and Trevor, A. J. (2012). *Basic and Clinical Pharmacology. 12th Edn*. Oxford; San Francisco, CA: McGraw-Hill.

Krasavin, M., Tsirulnikov, S., Nikulnikov, M., Sandulenko, Y., and Bukhryakov, K. (2008). Tert-Butyl isocyanide revisited as a convertible reagent in the Groebke-Blackburn reaction. *Tetrahedron Lett.* 49, 7318–7321. doi: 10.1016/j.tetlet.2008.10.046

Kumar, M., Makhal, B., Gupta, V. K., and Sharma, A. (2014). *In silico* investigation of medicinal spectrum of imidazo-azines from the perspective of multitarget screening against malaria, tuberculosis and chagas disease. *J. Mol. Graph. Model.* 50, 1–9. doi: 10.1016/j.jmgm.2014.02.006

Lo, D., Muhlebach, M., and Smyth, A. (2018). Interventions for the eradication of meticillin-resistant *Staphylococcus aureus* (MRSA) in people with cystic fibrosis. *Cochrane Database Syst. Rev.* 21, 1–58. doi: 10.1002/14651858.CD009650.pub4

Lombardo, M. N., G-dayanandan, N., Wright, D. L., and Anderson, A. C. (2016). Crystal structures of trimethoprim-resistant DfrA1 rationalize potent inhibition by Propargyl-linked antifolates. *Infect. Dis.* 2, 149–156. doi: 10.1021/acsinfecdis.5b00129

Pericherla, K., Kaswan, P., Pandey, K., and Kumar, A. (2015). Recent developments in the synthesis of imidazo[1,2-a]pyridines. *Synthesis* 47, 887–912. doi: 10.1055/s-0034-1380182

Rashid, U., Ahmad, W., Hassan, S. F., Qureshi, N. A., Niaz, B., Muhammad, B., et al. (2016). Design, synthesis, antibacterial activity and docking study of some new trimethoprim derivatives. *Bioorganic Med. Chem. Lett.* 26, 5749–5753. doi: 10.1016/j.bmcl.2016.10.051

Semreen, M. H., El-Awady, R., Abu-Odeh, R., Saber-Ayad, M., Al-Qawasmeh, R. A., Chouaib, S., et al. (2013). Tandem multicomponent reactions toward the design and synthesis of novel antibacterial and cytotoxic motifs. *Curr. Med. Chem.* 20, 1445–1459. doi: 10.2174/0929867311320110007

Shaaban, S., and Abdel-Wahab, B. F. (2016). Groebke-Blackburn-Bienaymé multicomponent reaction: emerging chemistry for drug discovery. *Mol. Divers.* 20, 233–254. doi: 10.1007/s11030-015-9602-6

Shukla, N. M., Salunke, D. B., Yoo, E., Mutz, C. A., Balakrishna, R., and David, S. A. (2012). Antibacterial activities of Groebke–Blackburn–Bienaymé-derived imidazo[1,2-a]pyridin-3-amines. *Bioorg. Med. Chem.* 20, 5850–5863. doi: 10.1016/j.bmc.2012.07.052

Slobbe, P., Ruijter, E., and Orru, R. V. A. (2012). Recent applications of multicomponent reactions in medicinal chemistry. *Med. Chem. Commun.* 3, 1189–1218. doi: 10.1039/c2md20089a

Torok, E., Moran, E., and Cooke, F. (2009). *Oxford Handbook of Infectious Diseases and Microbiology*. Oxford: Oxford University.

Urbancic, K. F., Ierino, F., Phillips, E., Mount, P., Mahony, A., and Trubiano, J. (2018). Taking the challenge: a protocolized approach to optimize *Pneumocystis pneumonia* prophylaxis in renal transplant recipients. *Am. J. Transpl.* 18, 462–466. doi: 10.1111/ajt.14498

Ventola, C. L. (2015). The antibiotic resistance crisis: causes and threats. *Pharm. Ther.* 40, 277–283.

WHO (2017). *20th WHO Model List of Essential Medicines*. Essential Medicines and Health Products. Available online at: https://www.who.int/medicines/publications/essentialmedicines/20th_EML2017.pdf?ua=1 (accessed March 10, 2019).

Xhemali, X., Smith, J., Kebriaei, R., Rice, S., Stamper, K., Compton, M., et al. (2019). Evaluation of dalbavancin alone and in combination with β-lactam antibiotics against resistant phenotypes of *Staphylococcus aureus*. *J. Antimicrob. Chemother.* 74, 82–86. doi: 10.1093/jac/dky376

Zarganes-Tzitzikas, T., and Doemling, A. (2014). Modern multicomponent reactions for better drug synthesis. *Org. Chem. Front.* 1, 834–837. doi: 10.1039/C4QO00088A

Zhou, W., Scocchera, E. W., Wright, D. L., and Anderson, A. C. (2013). Antifolates as effective antimicrobial agents: new generations of trimethoprim analogs. *Med. Chem. Commun.* 4, 908–915. doi: 10.1039/c3md00104k

Zhu, J., Wang, Q., and Wang, M. (2014). *Multicomponent Reactions in Organic Synthesis. 1st Edn*. Weinheim: Wiley-VCH.

Conflict of Interest Statement: The authors declare that the research was conducted in the absence of any commercial or financial relationships that could be construed as a potential conflict of interest.

The reviewer FD declared a past co-authorship with one with the authors OG, RL to the handling editor.

frontiers

Supplementary Material

Multicomponent Reactions upon the Known Drug Trimethoprim as a Source of Novel Antimicrobial Agents

Marina Pedrola [1], Marta Jorba [2], Eda Jardas [1], Ferran Jardi [1], Ouldouz Ghashghaei [1], Miguel Viñas[2] and Rodolfo Lavilla[1]

[1]Laboratory of Medicinal Chemistry, Faculty of Pharmacy and Food Sciences and Institute of Biomedicine (IBUB), University of Barcelona, Av. de Joan XXIII, 27-31, 08028 Barcelona, Spain

[2]Laboratory of Molecular Microbiology & Antimicrobials, Dept. Pathology & Experimental Therapeutics. Medical School. University of Barcelona and IDIBELL, Feixa Llarga, s/n. 08907 Hospitalet de Llobregat, Barcelona, Spain

Contents

Chemistry

General Information

Unless otherwise stated, all reactions were carried out under normal atmosphere in dried glassware. Commercially available reactants were used without further purification. Thin-layer chromatography was performed on pre-coated Merk silica gel 60 F_{254} plates and visualized under a UV lamp. Reactions were monitored by HPLC-MS using a HPLC Waters Alliance HT comprising a pump (Edwards RV12) with degasser, an autosampler and a diode array detector. Flow from the column was split to a MS spectrometer. The MS detector was configured with an electrospray ionization source (micromass ZQ4000) and nitrogen was used as the nebulizer gas. Data acquisition was performed with MassLynx software. When stated, the final crude was purified via flash column chromatography with a Combi Flash ISCO RF provided with dual UV detection. Prepacked normal phase silica or alumina gel columns (4, 12 and 24 g) were used for separation of products. ^{1}H and ^{13}C NMR spectra were recorded on a Varian Mercury 400 (at 400 MHz and 100 MHz, respectively). Unless otherwise quoted, NMR spectra were recorded in either $CDCl_3$ or DMSO solution with TMS as an internal reference. Data for ^{1}H NMR spectra are reported as follows: chemical shift (δ ppm), multiplicity, coupling constants (Hz) and integration. Data for ^{13}C NMR spectra are reported in terms of chemical shift (δ ppm). High Resolution Mass Spectrometry was performed by the University of Barcelona Mass Spectrometry Service. Yields correspond to the isolated pure compounds and the processes were not optimized.

Experimental Procedures for the Synthesis of Trimethoprim GBB Adducts and Related Compounds

Synthesis of Trimethoprim Mono GBBR Adducts

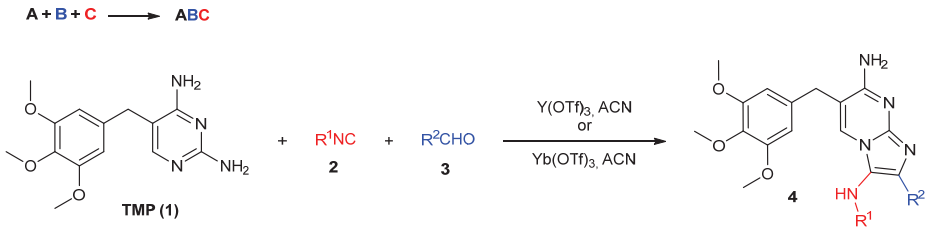

***General Procedure A (for synthesis of products 4a-4f)*:** A solution of trimethoprim (**1**, 1 mmol, 1 eq.) and aldehyde (**2**, 1 mmol, 1 eq.) in ACN (25 mL) was added into a Schlenk vessel followed by the addition of $Y(OTf)_3$ or $Yb(OTf)_3$ (0.2 mmol, 0.2 eq.) at room temperature. After 10 min, the suitable isocyanide (**3**, 1 mmol, 1 eq.) was added to the stirring reaction mixture; the vessel was closed and heated to 80 ºC overnight. After reaction completion was confirmed by TLC or HPLC, ACN was evaporated and DCM was added until everything was dissolved. The mixture was treated with saturated $NaHCO_3$ aqueous solution to basic pH. The organic layer was separated, dried over $MgSO_4$, filtered and evaporated under reduced pressure. The pure product **4** was obtained from the crude residue by flash chromatography with DCM/MeOH as eluent.

Synthesis of Trimethoprim Double GBBR Adducts

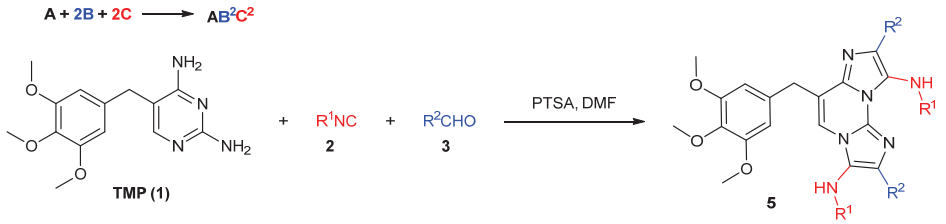

***General Procedure B (for synthesis of products 5a-5b)*:** A solution of trimethoprim (**1**, 1 mmol, 1 eq.) and aldehyde (**2**, 2 mmol, 2 eq.) in DMF (25 mL) was transferred to a Schlenk vessel followed by the addition of PTSA (0.2 mmol. 0.2 eq.) at room temperature. After 10 min, the suitable isocyanide (**3**, 2 mmol, 2 eq.) was added to the stirring reaction mixture, the vessel sealed and heated to 120 °C overnight. After reaction completion was confirmed by TLC or HPLC, solvent was evaporated and the mixture was treated with saturated $NaHCO_3$ aqueous solution to basic pH and extracted with DCM. The organic phase was dried over $MgSO_4$, filtered and evaporated under reduced pressure. The pure product **5** was obtained from the crude residue by flash chromatography with DCM/MeOH as eluent.

The tert-Butyl Removal from Trimethoprim GBBR Adducts

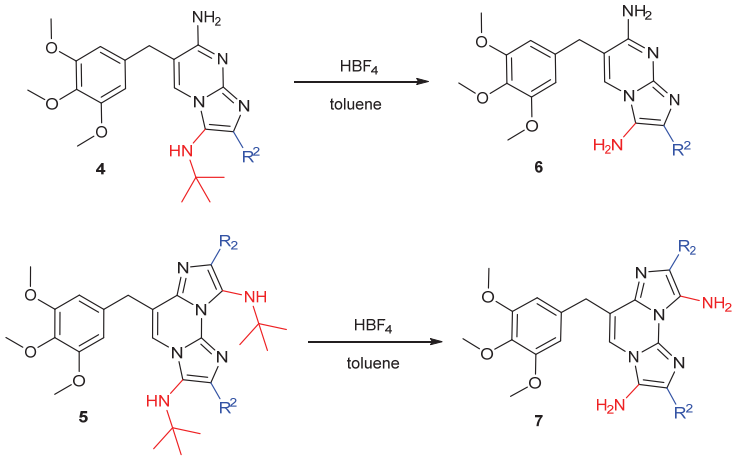

***General Procedure C (for synthesis of products 6)*:** To a solution of compound **4** (0.3 mmol, 1 eq.) in toluene (1.5 mL), tetrafluoroboric acid diethyl ether complex (0.15 mL, 1 mmol, 3 eq.) was added and reaction mixture was heated to 120 °C for 30 minutes. After reaction completion, confirmed by TLC or HPLC, the reaction mixture was cooled down to room temperature, treated with saturated $NaHCO_3$ aqueous solution to basic pH and extracted with ethyl acetate. The organic phase was dried over $MgSO_4$, filtered and evaporated under reduced pressure. The pure product **6** was obtained from the crude residue by flash chromatography with DCM/MeOH as eluent.

***General Procedure D (for synthesis of product 7)*:** To a solution of compound **5** (0.2 mmol, 1 eq.) in toluene (1.5 mL), tetrafluoroboric acid diethyl ether complex (0.5mL, 3.6 mmol, 18 eq.) was added and reaction mixture was heated to 120 °C for 30 minutes. After reaction completion, confirmed by TLC or HPLC, the reaction mixture was cooled down to room temperature, treated with saturated $NaHCO_3$ aqueous solution to basic pH and extracted with ethyl acetate. The organic phase was dried over $MgSO_4$, filtered and evaporated under reduced pressure. The pure product **7** was obtained by precipitation with dichloromethane.

Characterization Data for the Isolated Compounds

***N*^{3}-(tert-butyl)-2-(4-chlorophenyl)-6-(3,4,5-trimethoxybenzyl)imidazo[1,2-*a*]pyrimidine-3,7-diamine (4a)**

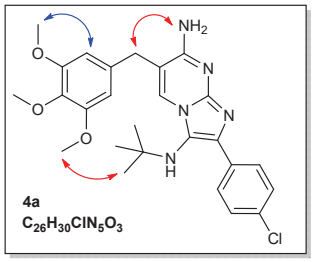

Following the *General Procedure A* with $Yb(OTf)_3$ as Lewis Acid, compound **4a** was obtained as a yellow solid, 59%. ^{1}H NMR (400 MHz, DMSO-d_6) δ 8.08 (d, J = 8.7 Hz, 2H), 7.81 (s, 1H), 7.38 (d, J = 8.7 Hz, 2H), 6.76 (s, 1H), 6.64 (s, 2H), 4.43 (s, 1H), 3.75 (s, 2H), 3.71 (s, 6H), 3.63 (s, 3H), 0.91 (s, 9H). ^{13}C NMR (101 MHz, DMSO-d_6) δ 157.76, 153.36, 145.21, 136.54, 134.44, 133.92, 131.18, 130.56, 129.26, 128.20, 121.30, 111.79, 106.83, 60.42, 56.21, 55.58, 34.04, 30.36. One C signal was not detected. HRMS: calcd for $C_{26}H_{31}ClN_5O_3$ 496.2110 ($M+H^+$); found 496.2125. For this molecule, NOESY, HMBC and HSQC spectra were analyzed: positive control crosspeak is marked in blue, diagnostic interactions are marked in red.

***N*^{3}-(*tert*-butyl)-2-methyl-6-(3,4,5-trimethoxybenzyl)imidazo[1,2-*a*]pyrimidine-3-7-diamine (4f)**

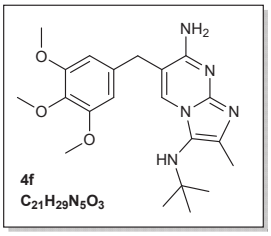

Following the *General Procedure A* with $Yb(OTf)_3$ as Lewis Acid, compound **4f** was obtained as a white powder, 59%. ^{1}H NMR (400 MHz, DMSO- d_6) δ 7.11 (s, 1H), 6.62 (s, 2H), 6.46 (s, 1H), 3.71 (s, 8H), 3.64 (s, 3H), 3.38 (s, 2H), 2.12 (s, 3H), 1.00 (s, 9H). ^{13}C NMR (101 MHz, DMSO-d_6) δ 156.70, 153.30, 144.83, 136.45, 134.34, 133.12, 130.13, 120.67, 110.32, 106.74, 60.40, 56.18, 54.87, 34.00, 30.18, 14.07. HRMS: calcd for $C_{21}H_{30}N_5O_3$ 400.2270 ($M+H^+$); found 400.2338.

***N*^{3}-cyclohexyl-2-(pyridin-3-yl)-6-(3,4,5-trimethoxybenzyl)imidazo[1,2-*a*]pyrimidine-3,7-diamine (4i)**

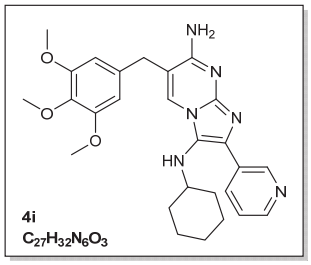

Following the *General Procedure A* with $Yb(OTf)_3$ as Lewis Acid, compound **4i** was obtained as a pale yellow solid, 29%. ^{1}H NMR (400 MHz, DMSO-d_6) δ 9.26 (d, J = 1.8 Hz, 1H), 8.38 (dd, J = 4.8, 1.5 Hz, 1H), 8.37 – 8.34 (m, 1H), 7.73 (s, 1H), 7.38 (dd, J = 7.9, 4.8 Hz, 1H), 6.72 (s, 2H), 6.68 (s, 2H), 4.61 (d, J = 5.2 Hz, 1H), 3.76 (d, J = 4.0 Hz, 2H), 3.75 (s, 6H), 3.66 (s, 3H), 2.68 (d, J = 4.3 Hz, 1H), 1.71 – 1.43 (m, 5H), 1.20 – 0.99 (m, 5H). ^{13}C NMR (101 MHz, DMSO-d_6) δ 157.04, 152.89, 147.14, 146.74, 144.84, 136.04, 133.43, 132.65, 130.83, 129.38, 129.23, 123.25, 123.00, 111.59, 106.35, 59.88, 56.63, 55.72, 33.59, 33.43, 25.35, 24.34. HRMS: calcd for $C_{27}H_{33}N_6O_3$ 489.2536 ($M+H^+$); found 489.2603.

N^3,N^9-di-tert-butyl-2,8-bis(4-chlorophenyl)-6-(3,4,5-trimethoxybenzyl)diimidazo[1,2-*a*:1',2'-*c*]pyrimidine-3,9-diamine (5a)

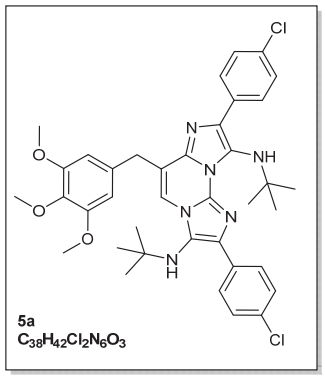

Following the *General Procedure B*, compound **5a** was obtained as an orange solid, 48%. ^{1}H NMR (400 MHz, $CDCl_3$) δ 8.18 (d, *J* = 8.5 Hz, 2H), 7.90 (d, *J* = 8.5 Hz, 2H), 7.37 (dd, *J* = 8.5, 6.4 Hz, 4H), 7.14 (s, 1H), 6.64 (s, 2H), 4.17 (s, 2H), 3.86 (s, 3H), 3.84 (s, 6H), 1.26 (s, 1H), 1.14 (s, 9H), 1.00 (s, 9H). ^{13}C NMR (101 MHz, $CDCl_3$) δ 153.51, 137.75, 136.99, 134.92, 134.31, 133.82, 133.68, 133.06, 132.89, 132.70, 132.34, 129.21, 128.61, 128.46, 128.35, 123.04, 118.49, 116.75, 106.77, 61.03, 58.10, 56.22, 56.05, 34.25, 30.55, 30.18. One C signal not detected. HRMS: calcd for $C_{38}H_{43}Cl_2N_6O_3$ 701.2768 ($M+H^+$); found 701.2785.

2-(4-chlorophenyl)-6-(3,4,5-trimethoxybenzyl)imidazo[1,2-*a*]pyrimidine-3,7-diamine (6a)

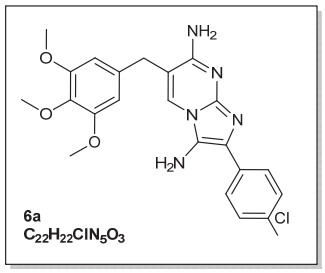

Following the *General Procedure C*, compound **6a** was obtained as a yellow solid, 26%. ^{1}H NMR (400 MHz, DMSO-d_6) δ 8.01 (s, 1H), 7.99 (d, *J* = 8.7 Hz, 2H), 7.39 (d, *J* = 8.7 Hz, 2H), 6.65 (s, 2H), 4.72 (s, 2H), 3.77 (s, 2H), 3.74 (s, 6H), 3.64 (s, 3H). HRMS: calcd for $C_{22}H_{23}ClN_5O_3$ 440.1484 ($M+H^+$); found 440.1483.

2,8-bis(4-chlorophenyl)-6-(3,4,5-trimethoxybenzyl)diimidazo[1,2-*a*:1',2'-*c*]pyrimidine-3,9-diamine (7a)

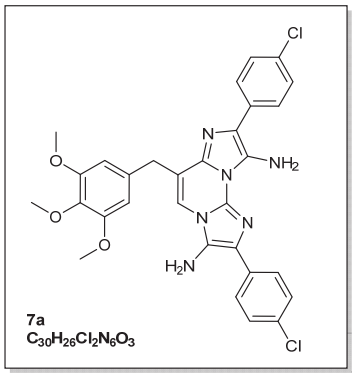

Following the *General Procedure D*, compound **7a** was obtained as light yellow solid, 73%. ^{1}H NMR (400 MHz, DMSO-d_6) δ 7.97 (dd, *J* = 9.7, 8.9 Hz, 4H), 7.76 (s, 1H), 7.46 (dd, *J* = 9.7, 8.8 Hz, 4H), 6.86 (s, 2H), 6.38 (s, 2H), 5.28 (s, 2H), 4.02 (s, 2H), 3.76 (s, 6H), 3.62 (s, 3H). ^{13}C NMR (101 MHz, DMSO-d_6) δ 152.63, 136.04, 134.67, 133.56, 133.40, 133.24, 132.39, 131.74, 129.38, 129.23, 128.35, 128.27, 126.91, 126.57, 126.15, 119.90, 118.91, 116.66, 115.04, 106.54, 59.92, 55.79, 54.90. HRMS: calcd for $C_{30}H_{27}Cl_2N_6O_3$ 589.1516 ($M+H^+$); found 589.1539.

Copies of the NMR Spectra

N^3-(tert-butyl)-2-(4-chlorophenyl)-6-(3,4,5-trimethoxybenzyl)imidazo[1,2-*a*]pyrimidine-3,7-diamine (4a)

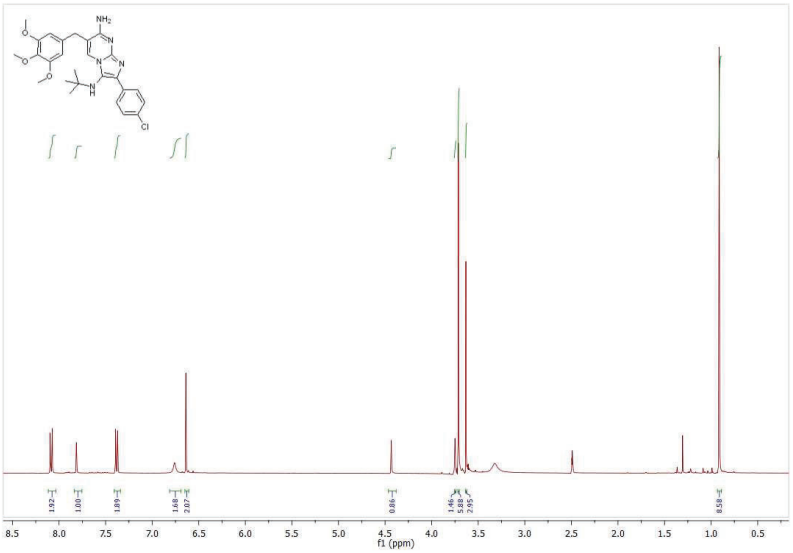

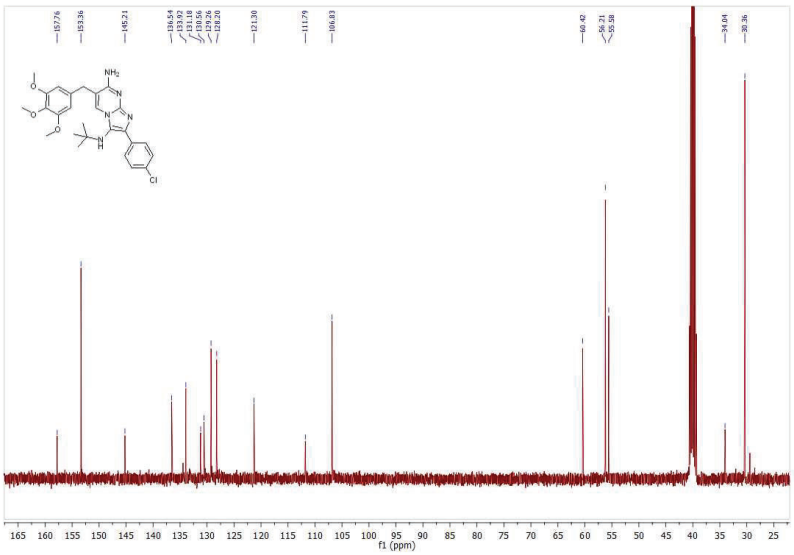

HMBC:

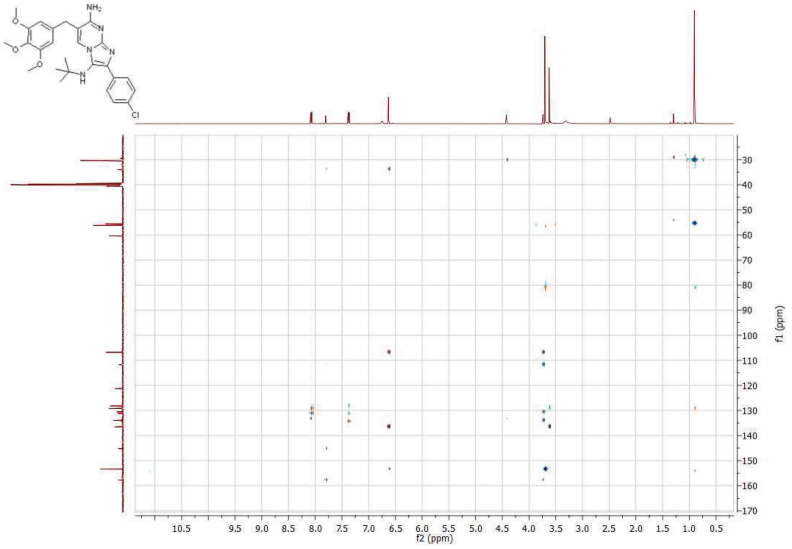

HSQC:

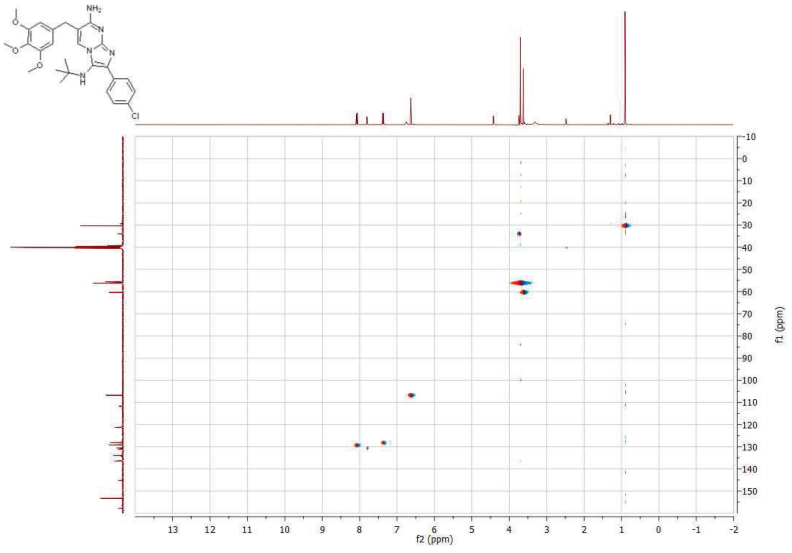

NOESY: Positive control is marked in blue, while diagnostic interactions are marked in red.

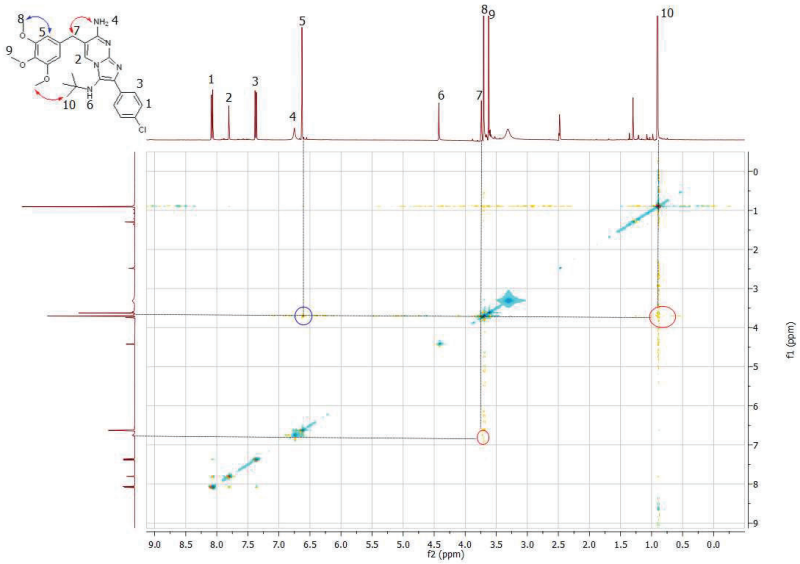

:

N^3-(*tert*-butyl)-2-methyl-6-(3,4,5-trimethoxybenzyl)imidazo[1,2-*a*]pyrimidine-3-7-diamine (4f)

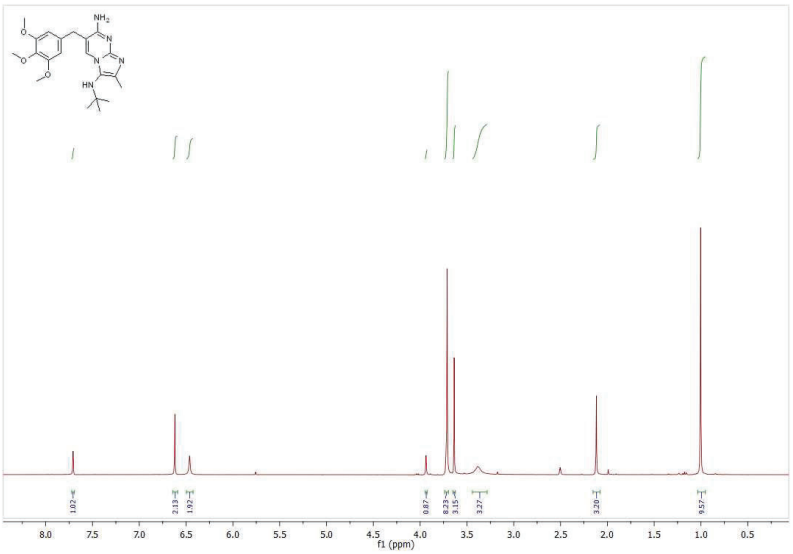

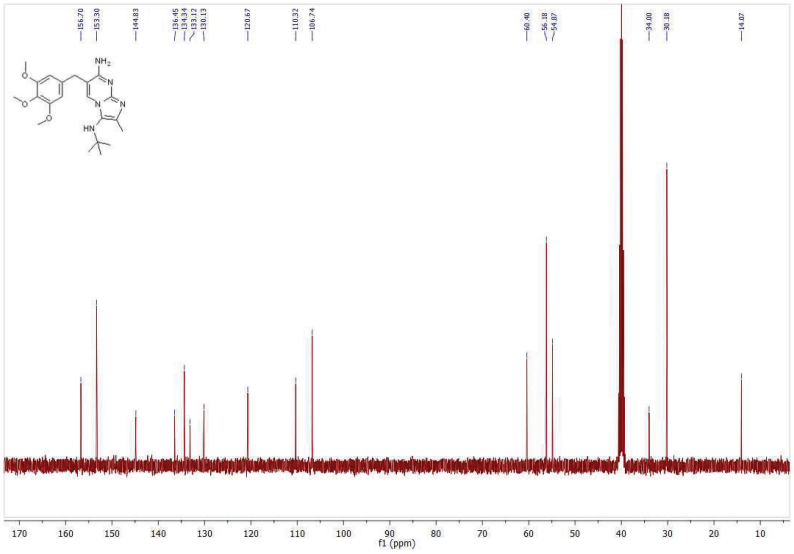

N^3-cyclohexyl-2-(pyridin-3-yl)-6-(3,4,5-trimethoxybenzyl)imidazo[1,2-*a*]pyrimidine-3,7-diamine (4i)

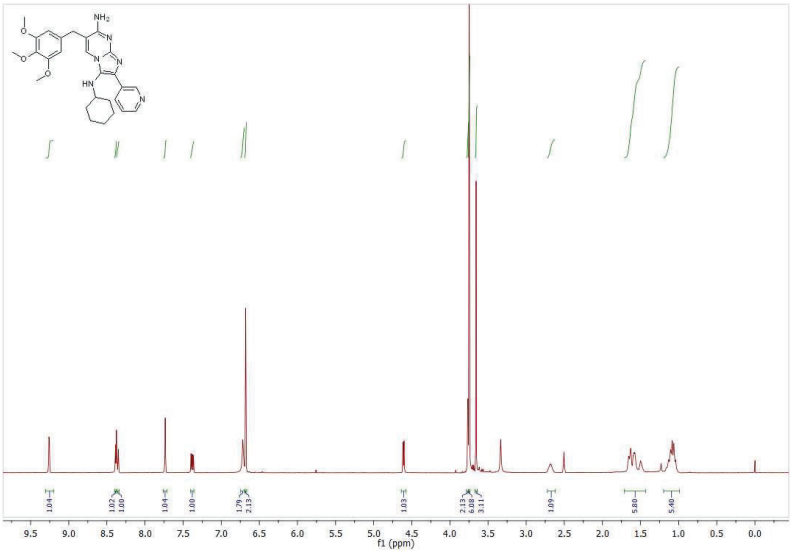

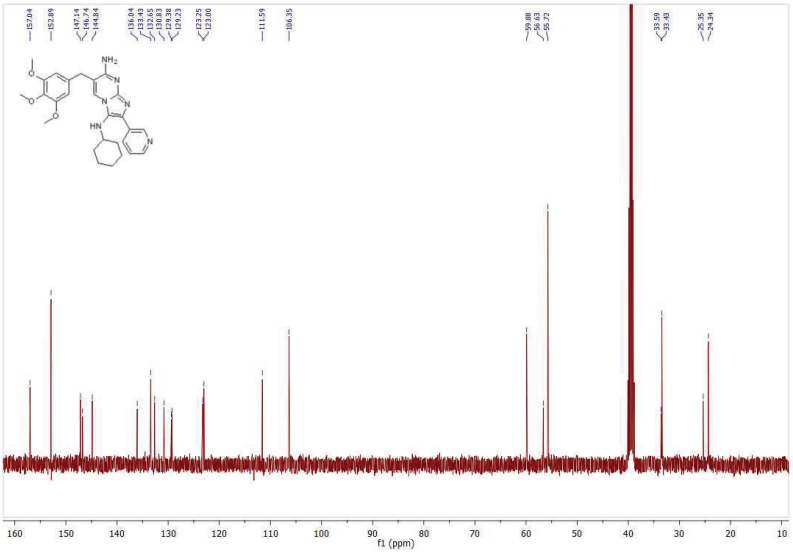

N^3,N^9-di-tert-butyl-2,8-bis(4-chlorophenyl)-6-(3,4,5-trimethoxybenzyl)diimidazo[1,2-*a*:1',2'-*c*]pyrimidine-3,9-diamine (5a)

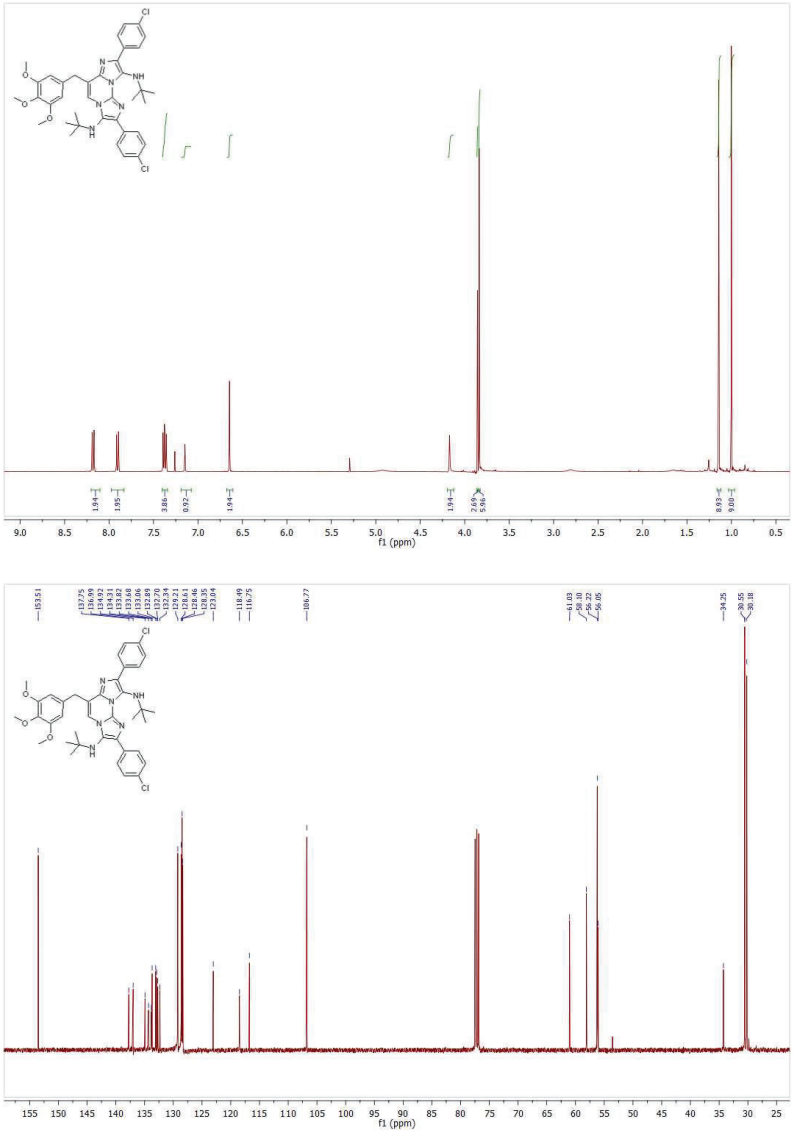

2-(4-chlorophenyl)-6-(3,4,5-trimethoxybenzyl)imidazo[1,2-*a*]pyrimidine-3,7-diamine (6a)

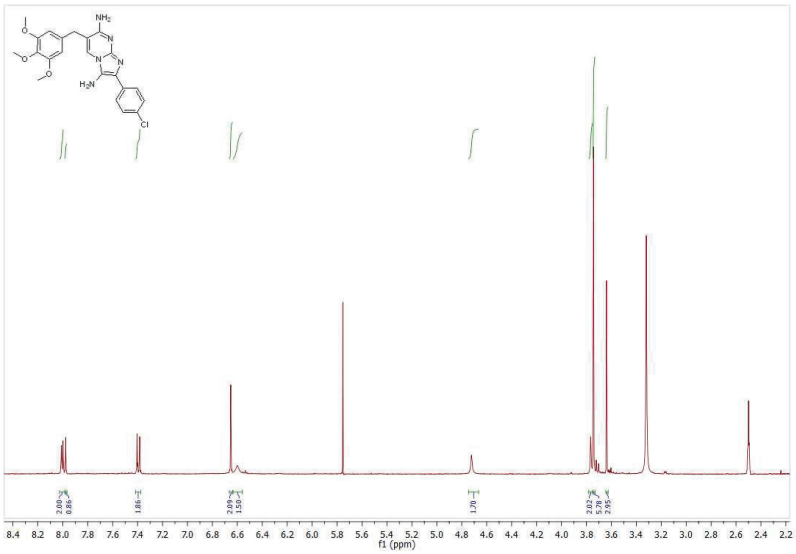

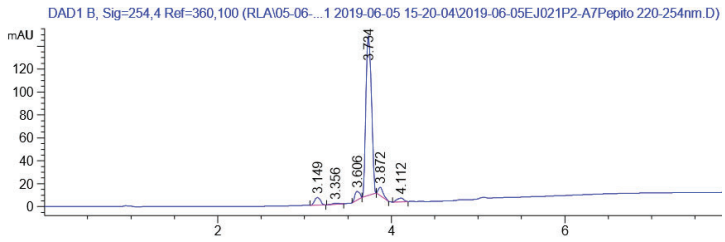

2,8-bis(4-chlorophenyl)-6-(3,4,5-trimethoxybenzyl)diimidazo[1,2-*a*:1',2'-*c*]pyrimidine-3,9-diamine (7a)

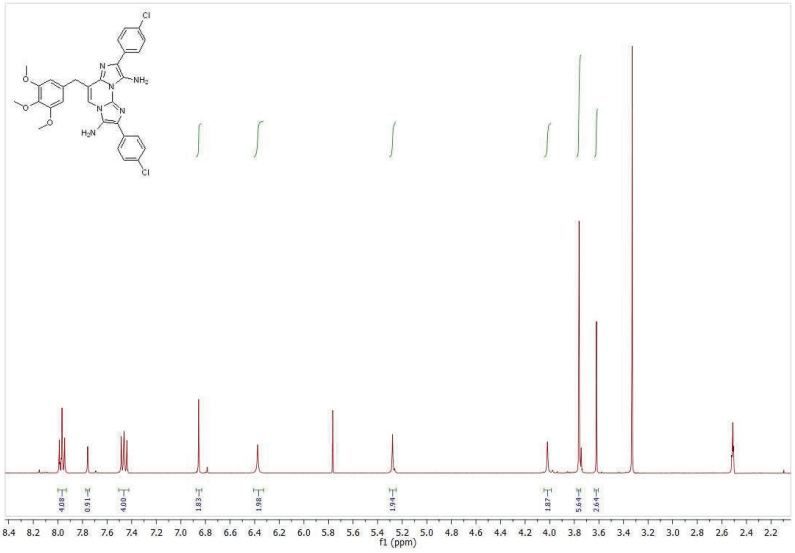

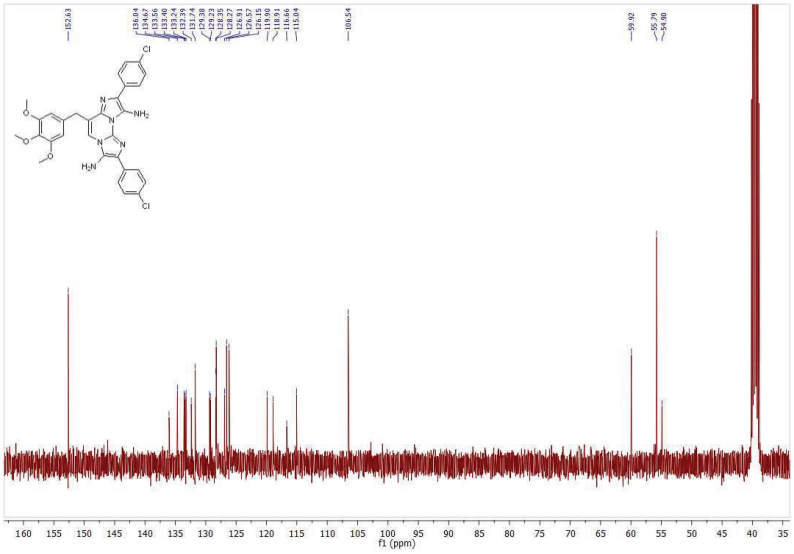

Microbiology

Material and Methods

Bacterial strains, bacteriological media and antimicrobials

Three different control strains were selected; *Escherichia coli* ATCC 25922, *Staphylococcus aureus* ATCC 29213 and *Pseudomonas aeruginosa* PAO1. Four clinical isolates of methicillin-resistant *S. aureus* from nasal and wound smear were used (*S. aureus* 8125304770, *S. aureus* 8139265926, *S. aureus* 8125255044, *S. aureus* 8124825998).

Tryptic soy broth (TSB, Scharlau Microbiology, Sentmenat, Spain) was used to determine the minimum inhibitory concentrations (MICs) and in the growth curves. Sulfamethoxazole and Trimethoprim were purchased from Sigma-Aldrich (St. Louis, USA).

Susceptibility testing

Determination of the Minimum Inhibitory Concentrations (MIC)

MIC values were determined by the broth microdilution method and interpreted according to the European Committee on Antimicrobial Susceptibility Testing (EUCAST) guidelines.[1] Briefly, the strains were grown overnight at 37 ^{o}C with orbital shaking at 200 rpm in Tryptone Soy Broth (TSB). After doing a refresh of 2 h in the same conditions, the bacterial cultures were adjusted to OD_{625nm} of 0.08–0.1 (10^8 CFUs/mL) in fresh TSB medium. 5 µL of each suspension was added to 96-well plates previously filled with TSB and serially diluted TMP analogues. Concentrations assayed were 32, 16, 8, 4, 2, 1, 0.5, 0.25, 0.125 and 0.062 µg/ml. The plates were incubated at 37 ºC for 24 h, after which the MIC was determined macroscopically, based on the visually turbidity of the wells by placing the plates on top of a viewing device in form of a stand with an enlarging mirror.

The antimicrobial activity of these 15 new Trimethoprim (TMP) analogues was evaluated against *Escherichia coli* ATCC 25922, *Staphylococcus aureus* ATCC 29213, *Pseudomonas aeruginosa* 01. Moreover, susceptibility was examined using the new compounds alone and in combination with Sulfamethoxazole in a 1:20 ratio in the three previous strains and also in *S. aureus* 8125304770, *S. aureus* 8139265926, *S. aureus* 8125255044 and *S. aureus* 8124825998. Serial dilutions of the antimicrobials starting from 32 µg/mL were tested.

Minimal inhibitory concentrations were determined in triplicate in at least three different experiments. Values resulted to be repetitive with undetectable differences by this method.

[1] EUCAST. European Committee on Antimicrobial Susceptibility Testing Breakpoint Tables for Interpretation of MICs and Zone Diameters European Committee on Antimicrobial Susceptibility Testing Breakpoint tables for Interpretation of MICs and Zone Diameters 0–99. Available online: http://www.eucast.org/fileadmin/src/media/PDFs/EUCAST_files/Breakpoint_tables/v_9.0_Breakpoint_Tables.pdf (accessed on 10 March 2019).

Effect of TMP-SMX and the GBBR analogues on bacterial growth curves

The combination of some of the most active analogues and Sulfamethoxazole (1:20) was assayed for their effect on the growth curve. A Gram-negative (*E. coli* ATCC 25922) and a Gram-positive (*S. aureus* ATCC 29213) were used to examine the effect of these new compounds in real time.

Volumes of 10 mL TSB liquid cultures with 1-5×10^8 CFU/mL in logarithmic-phase were adjusted. Antimicrobials were then added at sublethal concentrations (½ MIC and ¼ MIC). Trimethoprim was also evaluated as a control.

The incubation was performed in RTS-1C real-time cell growth loggers (Biosan) for 20h at 37 °C and 2000 rpm. Growth was measured as optical density (OD 850 nm) every 10 minutes.

Growth Curves

Effect of the analogues **4c**, **4d**, **4e**, **4f**, **4h**, **4j**, **6b** and **TMP** in combination with sulfamethoxazole (1:20) on the growth curve of *S. aureus*.

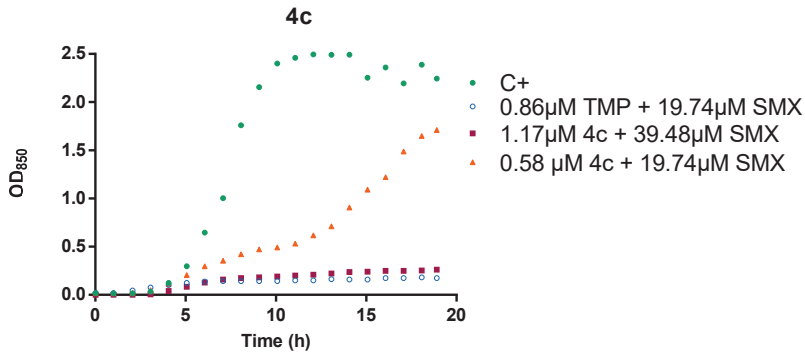

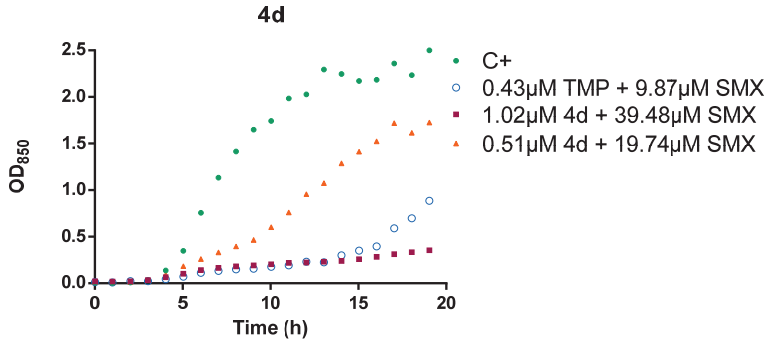

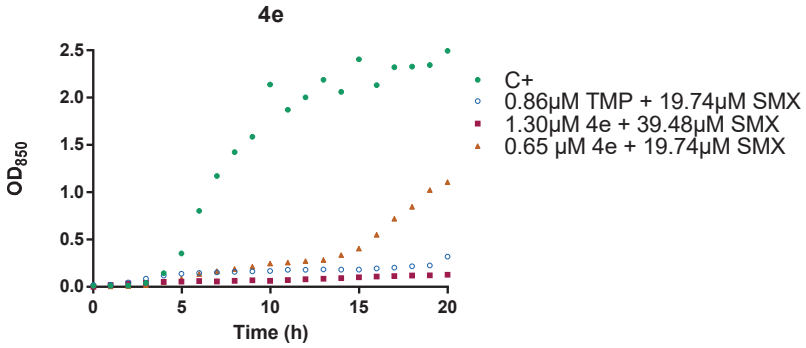
4e
OD850
2.5
2.0
1.5
1.0
0.5
0.0
0
5
10
15
20
Time (h)
C+
0.86μM TMP + 19.74μM SMX
1.30μM 4e + 39.48μM SMX
0.65 μM 4e + 19.74μM SMX

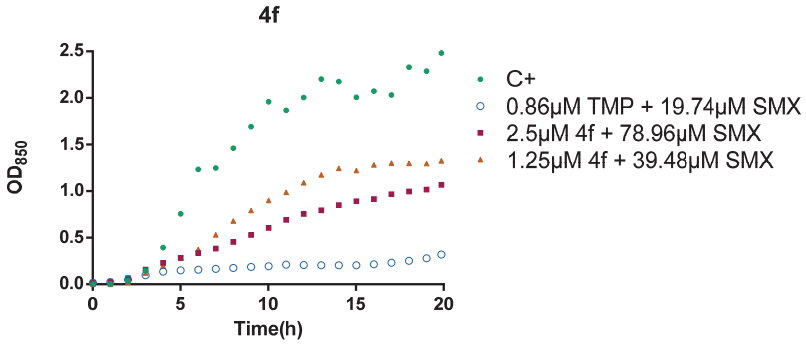
4f
OD850
2.5
2.0
1.5
1.0
0.5
0.0
0
5
10
15
20
Time(h)
C+
0.86μM TMP + 19.74μM SMX
2.5μM 4f + 78.96μM SMX
1.25μM 4f + 39.48μM SMX

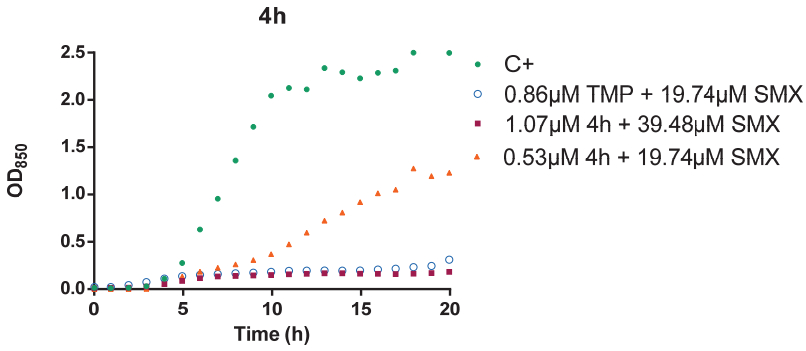
4h
OD850
2.5
2.0
1.5
1.0
0.5
0.0
0
5
10
15
20
Time (h)
C+
0.86μM TMP + 19.74μM SMX
1.07μM 4h + 39.48μM SMX
0.53μM 4h + 19.74μM SMX

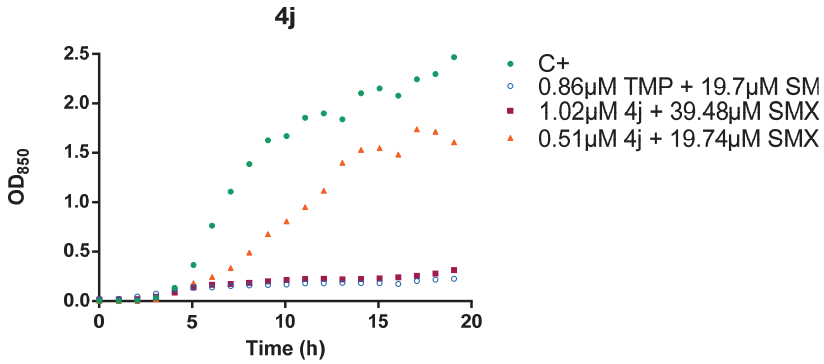
4j
OD850
2.5
2.0
1.5
1.0
0.5
0.0
0
5
10
15
20
Time (h)
C+
0.86µM TMP + 19.7µM SM
1.02µM 4j + 39.48µM SMX
0.51µM 4j + 19.74µM SMX

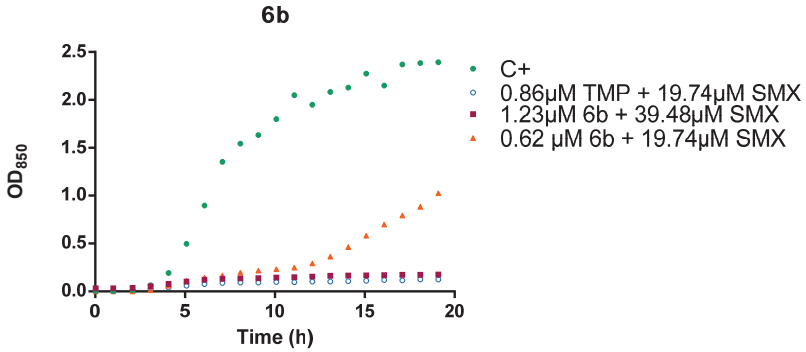
6b
OD850
2.5
2.0
1.5
1.0
0.5
0.0
0
5
10
15
20
Time (h)
C+
0.86µM TMP + 19.74µM SMX
1.23µM 6b + 39.48µM SMX
0.62 µM 6b + 19.74µM SMX

Effect of the analogues **4h** and **4i** and TMP in combination with sulfamethoxazole (1:20) on the growth curve of *E. coli*.

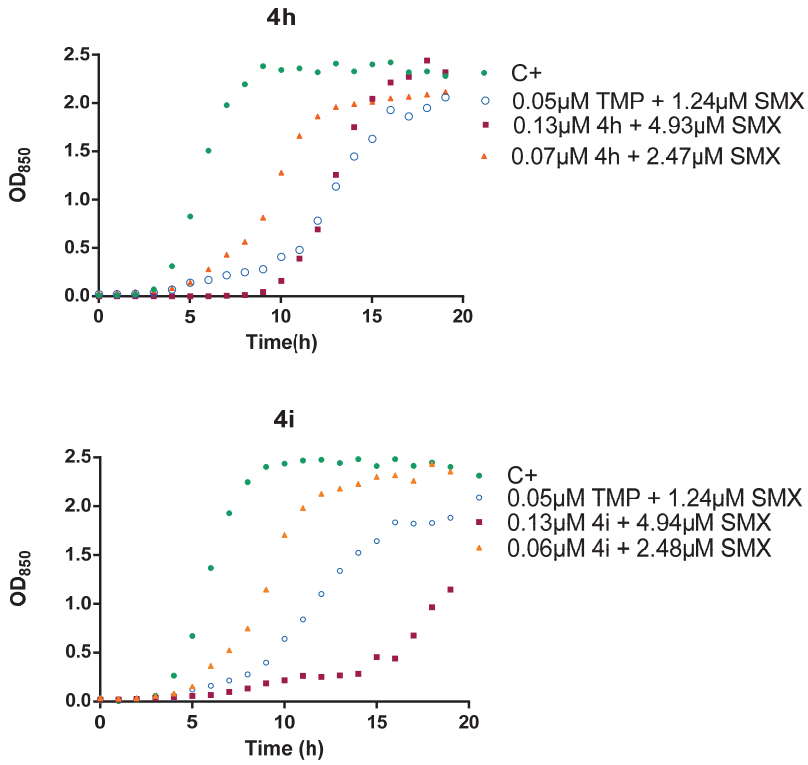

From Drugs to Drugs: towards Improved Antibiotics

Publication II: New Trimethoprim-like Molecules: Bacteriological Evaluation and Insights into their Action

antibiotics

MDPI

Article

New Trimethoprim-Like Molecules: Bacteriological Evaluation and Insights into Their Action

Marta Jorba [1], Marina Pedrola [2], Ouldouz Ghashghaei [2], Rocío Herráez [1], Lluis Campos-Vicens [3,4], Francisco Javier Luque [3], Rodolfo Lavilla [2] and Miguel Viñas [1,*]

[1] Laboratory of Molecular Microbiology & Antimicrobials, Department of Pathology & Experimental Therapeutics, Medical School, University of Barcelona, Bellvitge Institute for Biomedical Research (IDIBELL), Hospitalet de Llobregat, 08907 Barcelona, Spain; mjorba@ub.edu (M.J.); rherraez@ub.edu (R.H.)
[2] Laboratory of Medicinal Chemistry, Faculty of Pharmacy and Food Sciences and Institute of Biomedicine (IBUB), University of Barcelona, 08028 Barcelona, Spain; mpedrola@ub.edu (M.P.); ghashghaei@ub.edu (O.G.); rlavilla@ub.edu (R.L.)
[3] Department of Nutrition, Food Science and Gastronomy, Faculty of Pharmacy and Food Sciences, Institute of Biomedicine (IBUB), Institute of Theoretical and Computational Chemistry (IQTC-UB), University of Barcelona, Av. Prat de la Riba 171, 08921 Santa Coloma de Gramenet, Spain; lluis.campos@pharmacelera.com (L.C.-V.); fjluque@ub.edu (F.J.L.)
[4] Pharmacelera, Torre R, 4a planta, Despatx A05, Parc Científic de Barcelona, Baldiri Reixac 8, 08028 Barcelona, Spain
* Correspondence: mvinyas@ub.edu

Abstract: This work reports a detailed characterization of the antimicrobial profile of two trimethoprim-like molecules (compounds **1a** and **1b**) identified in previous studies. Both molecules displayed remarkable antimicrobial activity, particularly when combined with sulfamethoxazole. In disk diffusion assays on Petri dishes, compounds **1a** and **1b** showed synergistic effects with colistin. Specifically, in combinations with low concentrations of colistin, very large increases in the activities of compounds **1a** and **1b** were determined, as demonstrated by alterations in the kinetics of bacterial growth despite only slight changes in the fractional inhibitory concentration index. The effect of colistin may be to increase the rate of antibiotic entry while reducing efflux pump activity. Compounds **1a** and **1b** were susceptible to extrusion by efflux pumps, whereas the inhibitor phenylalanine arginyl β-naphthylamide (PAβN) exerted effects similar to those of colistin. The interactions between the target enzyme (dihydrofolate reductase), the coenzyme nicotinamide adenine dinucleotide phosphate (NADPH), and the studied molecules were explored using enzymology tools and computational chemistry. A model based on docking results is reported.

Keywords: trimethoprim; multidrug-resistant (MDR) bacteria; mechanisms of action; dihydrofolate reductase

Citation: Jorba, M.; Pedrola, M.; Ghashghaei, O.; Herráez, R.; Campos-Vicens, L.; Luque, F.J.; Lavilla, R.; Viñas, M. New Trimethoprim-Like Molecules: Bacteriological Evaluation and Insights into Their Action. *Antibiotics* **2021**, *10*, 709. https://doi.org/10.3390/antibiotics10060709

Academic Editor: Carlos M. Franco

Received: 18 May 2021
Accepted: 10 June 2021
Published: 12 June 2021

1. Introduction

Unlike eukaryotes, prokaryotes must produce their own nucleotides. In bacteria, a prerequisite for the biosynthesis of thymidine is the production of folate. Trimethoprim (TMP), included in the World Health Organization's Model List of Essential Medicines, was first used in 1962 and remains a first-line antibiotic in many countries, usually in combination with sulfamethoxazole (SMX), with which it acts synergistically. TMP and SMX target two key enzymes of the folate pathway, acting as inhibitors of dihydrofolate reductase (DHFR) and dihydropteroate synthetase (DHPS), respectively (Figure 1).

Antimicrobial resistance remains a major challenge for microbiologists and public health officials, as infections by multidrug-resistant bacteria have reached worrisome levels. Resistant bacteria include: (i) multi-resistant strains, which are resistant to antimicrobials from at least three different families, (ii) extremely resistant strains, which are resistant

to all antimicrobials except colistin, and (iii) pan-drug-resistant strains, resistant to all available antimicrobials [1].

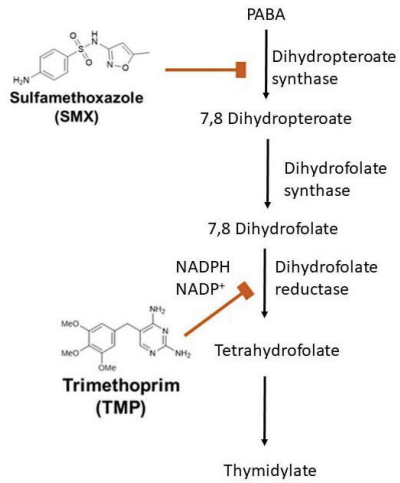

Figure 1. Folic acid biosynthesis pathway.

Among the lines of research aimed at overcoming antimicrobial resistance are: (i) the "green" approach, based on innovative eco-friendly antimicrobials [2], and (ii) the chemical approach, based on the synthesis of new molecules with antimicrobial action, including: (a) inhibitors of the resistance mechanisms to potentiate already existing antimicrobials [3]; (b) bioactive peptides [4], (c) the conjugation of different molecules to generate new ones with improved properties [5], and (d) a combination of two or more of these strategies. The interests of our laboratories include the synthesis of molecules whose active sites resemble those of already known antibiotics [6], the improvement of molecular delivery, such as the use of nanoparticles as antibiotics carriers in nano-medical devices [7], and the modification of natural molecules such that they acquire antimicrobial properties [8].

In this article we examine two TMP-like molecules that have been recently reported [6], focusing on their antibacterial effects and their mechanisms of action. TMP acts directly on dihydrofolate reductase (DHFR, EC 1.5.1.3), which catalyzes the reduction of 7,8-dihydrofolate (H_2F) to 5,6,7,8-tetrahydrofolate (H_{1a}) using NADPH as a cofactor. The conversion requires the transfer of a hydride from C4 of the NADPH cofactor to C6 of the pterin ring of H_2F, accompanied by the protonation of dihydrofolate on N5. This reaction is essential in the de novo synthesis of purines, thymidine, and certain amino acids [9,10]. Given the important role of DHFR, which is ubiquitously expressed by all kingdoms of life, the enzyme may be an effective therapeutic target in cells with a rapid DNA turnover and therefore both in bacteria and the treatment of cancer [11,12].

Based on the straightforward synthesis of compounds **1a** and **1b**, which were readily prepared through a Groebke-Blackburn-Bienaymé (GBBR) multicomponent reaction (Scheme 1), and the preliminary bacteriological profiles, which combine suitable antibiotic potency and kinetics [6], compounds **1a** and **1b** are explored in this study with respect to their mechanism of action and possible synergistic effects when used in combination with other antibacterial agents.

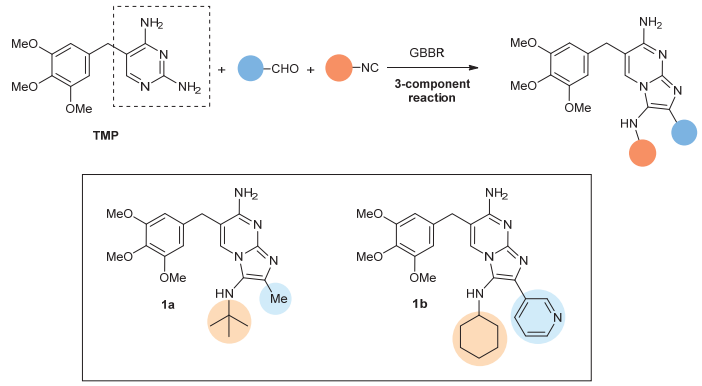

Scheme 1. Multicomponent access to new trimethoprim (TMP) derivatives.

2. Results and Discussion

2.1. Antimicrobial Susceptibility of Planktonic Bacteria

The minimum inhibitory concentrations (MICs) of TMP, **1a** and **1b**, both alone and in combination with SMX and colistin, are shown in Table 1. The *E. coli* ATCC 25922 strain was susceptible to TMP, **1a** and **1b**, and the activity was enhanced when the compounds were combined with SMX. The *P. aeruginosa* PAO1 strain was resistant to TMP, **1a** and **1b**, but susceptible to colistin. On the contrary, S. *marcescens* was colistin-resistant, but susceptible to the combined treatment of the compounds with SMX. Finally, **1a** and **1b** were also tested in TMP-resistant strains (*E. coli* 220560529 and *S. epidermidis* 220560752) but no significant effect was observed, suggesting that these compounds should share the target with TMP (data not shown).

Table 1. Minimum inhibitory concentration (MIC, μM) of trimethoprim (TMP) and compounds **1a** and **1b** tested alone and in combination with sulfamethoxazole (SMX) and colistin against *Escherichia coli* ATCC 25922, *Pseudomonas aeruginosa* PAO1, and *Serratia marcescens* NIMA. Data for *P. aeruginosa* PAO1 and *E. coli* ATCC 25922 were already reported [6].

Antimicrobial	MIC (μM)		
	E. coli **ATCC 25922**	***P. aeruginosa*** **PA01**	***S. marcescens*** **NIMA**
TMP	0.43	>110.22	13.78
TMP (SMX)	0.11 (2.37)	13.78 (315.86)	0.86 (19.74)
1a	1.25	>80.10	80.10
1a (SMX)	0.63 (19.74)	40.05 (1263.43)	2.5 (78.96)
1b	1.02	>65.50	16.37
1b (SMX)	0.13 (3.95)	32.75 (1263.43)	1.02 (39.48)
Colistin	0.43	1.73	>886.23

2.2. Antimicrobial Susceptibility of Sessile Bacteria

Many microorganisms that cause infectious diseases normally grow attached to a surface or an interface, thus forming biofilms. These structured communities contain bacterial cells of one or more species, attached to a living or inert surface and immersed in a hydrated polymeric matrix [13]. Within the biofilm, bacteria grow as part of complex and dynamic systems that result in their ability to tolerate antimicrobials [14], leading to persistent infections. Thus, the efficacy of new antibiotics requires both conventional antimicrobial susceptibility tests against planktonic cells (e.g., MIC determinations) and tests against bacteria residing in biofilms. In this work, the activity of **1a** and **1b** was

measured under both conditions and then compared with the corresponding activity of TMP.

The minimum biofilm eradication concentration (MBEC) and biofilm prevention concentration (BPC) for TMP and compounds **1a** and **1b**, alone and in combination with SMX (1:20), are shown in Table 2. Antimicrobials that exhibited antibiofilm activity had higher MBECs than BPCs. This result reflects the fact that the MBEC is a measure of the antimicrobial activity on mature biofilms, while the BPC is the concentration at which biofilm formation is blocked by the antimicrobial. Compound **1b** was highly active in biofilm prevention, whereas neither TMP nor compounds **1a** and **1b** were able to fully eradicate *Staphylococcus aureus* biofilms (neither *S. aureus* ATCC 29213 nor *S. aureus* 8124825998).

Table 2. The minimum biofilm eradication concentration (MBEC, μM) and biofilm prevention concentration (BPC, μM) of TMP and the GBBR analogues **1a** and **1b** when tested alone and in combination with SMX (1:20) against *E. coli* ATCC 25922, S. aureus ATCC 29213, and S. aureus 8124825998.

Antimicrobial	*E. coli* ATCC 25922		*S. aureus* ATCC 29213		*S. aureus* 8124825998	
	MBEC (μM)	BPC (μM)	MBEC (μM)	BPC (μM)	MBEC (μM)	BPC (μM)
TMP (SMX)	275.56 (6317.14)	275.56 (6317.14)	>2204.46 (50,537.15)	1102.23 (25,268.58)	>2204.46 (50,537.15)	>2204.46 (50,537.15)
1a (SMX)	>1602.06 (50,537.15)	200.26 (6317.14)	>1602.06 (50,537.15)	801.03 (25,268.58)	>1602.06 (50,537.15)	>1602.06 (50,537.15)
1b (SMX)	163.74 (6317.14)	81.87 (3158.57)	>1309.91 (50,537.15)	163.74 (6317.14)	>1309.91 (50,537.15)	327.48 (12,634.29)

2.3. Synergism Studies

Table 3 shows the results of TMP-SMX checkerboard assays in combination with colistin when tested in four clinical strains: *E. coli* 220560529, *P. aeruginosa* SJD 536, *P. aeruginosa* SJD VH023, and *P. aeruginosa* SJD 481. Synergistic effects between the two drugs were not found, as noted in the values of the fractional inhibitory concentration index (FICi), which is $\geq$0.5 and <4, in any of the studied strains.

Table 3. Fractional inhibitory concentration index (FICi) of TMP-SMX (1:20) with colistin.

Strains	FICi
E. coli 220560529	2.0019
P. aeruginosa SJD536	1
P. aeruginosa VH023	1
P. aeruginosa SJD481	1.003

By contrast, a strong synergism was observed with these drugs in TMP-susceptible/colistin-resistant *S. marcescens* (Table 4). This suggests that the susceptibility to TMP and TMP-like molecules in some gram-negative bacteria is due to limitations in TMP transport through the bacterial outer membrane. Colistin is unable to kill *S. marcescens* but it does adversely impact prodigiosin biosynthesis [15]. Effects on both the entry of antimicrobials as well as drug extrusion by efflux pumps have also been described [16]. Thus, as reported for antimicrobials such as linezolid and rifampin [17], colistin could be used to enhance bacterial susceptibility to TMP and TMP-like compounds. The use of very low concentrations of these drugs would limit their toxicity. It should be noted that in preliminary plate experiments, positive effects between colistin and TMP-SMX were observed in *E. coli* and *P. aeruginosa* (Figure 2), in agreement with the relatively low FICi (close to 1). In colistin-susceptible bacteria, however, the lethality of colistin masked any possible synergy.

Table 4. FICi of TMP and compounds **1a** and **1b** with SMX (1:20) when tested with colistin.

	FICi		
Antimicrobial	***E. coli* ATCC 25922**	***P. aeruginosa* PA01**	***S. marcescens* NIMA**
TMP + SMX	1.02	1.25	0.13
1a + SMX	1.02	1.00	0.25
1b + SMX	1.02	1.01	0.25

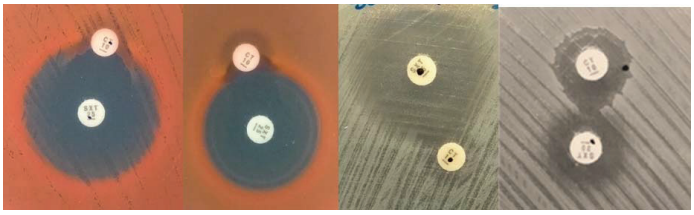

(**a**) (**b**) (**c**)

Figure 2. Interaction between colistin and TMP-SMX in (**a**) *S. marcescens* NIMA; (**b**) *E. coli* ATCC 25922, and (**c**) *P. aeruginosa* PAO1.

The effect of combining TMP, **1a** and **1b** with SMX and colistin in real-time were determined by plotting growth curves for *E. coli* ATCC 25922, *P. aeruginosa* PAO1, and *S. marcescens* NIMA using concentrations at which these strains were fully resistant (Figure 3). When TMP, **1a** and **1b** were used in combination with colistin, bacterial growth was nearly abolished, thus demonstrating synergism between these antibiotics. In the kinetics profile of *E. coli* (Figure 3a), although 0.11 μM colistin provoked a 10 h delay in growth, growth had resumed to the same level as the control at the end of the experiment. Following the addition of TMP + SMX (0.05 μM + 1.22 μM), however, growth was delayed for 20 h.

A similar effect was observed in *P. aeruginosa*, both with TMP and with compounds **1a** and **1b** (Figure 3b). At a colistin dose of 0.87 μM, the growth was delayed for 2 h and then reached the same level as the control. Similar curves were obtained with TMP + SMX (6.89 μM + 157.93 μM), whereas the growth delay was 4 h with **1a** + SMX (10.01 μM + 315.86 μM) and **1b** + SMX (8.19 μM + 315.86 μM). The addition of 0.87 μM colistin to **1a** + SMX and **1b** + SMX resulted in a delay of 10 h, whereas the addition of 0.87 μM colistin to TMP + SMX completely abolished the growth for 23 h after the start of the experiment. The results from the agar plates and the growth curves suggested an additive effect, even though it was not clearly reflected in the FICi values.

The effects of the antibiotics were also explored in *S. marcescens* (Figure 3c), which is intrinsically fully resistant to colistin. Thus, while colistin severely alters the bacterium's outer membrane, it does not affect bacterial viability, as the cytoplasmic membrane remains intact. The effect of colistin on the outer membrane of Serratia can be readily seen by transmission electron microscopy [18]. The growth curve of *S. marcescens* in the presence of TMP + SMX and colistin exhibited a longer delay (up to 10 h) in the start of detectable growth compared to the delay observed in the presence of TMP + SMX. Similar results were obtained with **1a**. Moreover, when testing **1b**, a complete abolition of growth was obtained in the presence of colistin.

The nearly complete abolition or prolonged delay of growth in the studied bacteria suggested that colistin alters the hydrophobic permeability barrier of the lipopolysaccharide outer membrane and thus facilitates the internalization of the DHFR inhibitors, which then inhibit the bacterial growth. The demonstration of these synergistic effects in gram-negative bacteria should renew the interest for the use of TMP and TMP-like molecules.

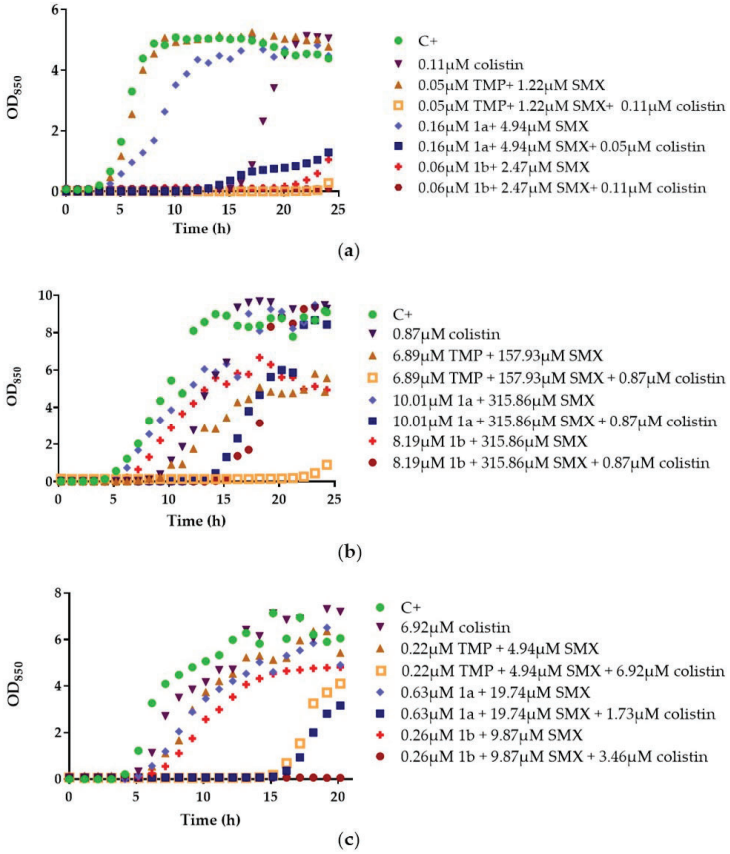

Figure 3. Effects of TMP, **1a** and **1b** when tested in combination with SMX (1:20) and in the presence of sublethal concentrations of colistin on the growth curve of (**a**) *E. coli* ATCC 25922, (**b**) *P. aeruginosa* PAO1, and (**c**) *S. marcescens* NIMA.

2.4. The Role of Efflux Pumps

The TMP analogues were tested in combination with SMX (1:20) in the presence of 20 μg/mL of the efflux pump inhibitor phenylalanine arginyl ß-naphthylamide (PAßN). At this point, it is worth noting that previous studies demonstrated that they have no detectable effect on bacterial growth when used at concentrations up to 40 μg/mL [19]. The MIC values are shown in Table 5. Lower MIC values were obtained in the presence of PAßN compared to the assays performed in the absence of the efflux pump inhibitor.

A recent study demonstrated that colistin, even at low concentrations, has a direct effect on efflux pump functionality [16]. In the present study, the addition of 20 μg PAßN/mL resulted in a 16-fold reduction in the MICs of TMP and its analogues (Table 5). These results are consistent with the critical role of efflux pumps in bacterial susceptibility to these antimicrobials.

Table 5. MIC values of TMP and compounds **1a** and **1b** in combination with SMX (1:20) as well as colistin in *P. aeruginosa* PAO1 in the presence or absence of the efflux pump inhibitor PAßN (20 μg/mL).

Antimicrobial	MIC (μM)	
	With PAßN	Without PAßN
TMP (SMX)	1.72 (39.48)	27.56 (631.71)
1a (SMX)	5.01 (157.93)	80.10 (2526.86)
1b (SMX)	2.05 (78.96)	32.76 (1263.43)
Colistin	1.73	1.73

This work examined possible synergisms between colistin and TMP, **1a** and **1b** in enhancing the antimicrobial activity, following the positive results in preliminary experiments on Petri dishes (Figure 2). The synergistic effects of colistin and all three TMP molecules were confirmed (Figure 3 and Table 4) and a possible mechanism involving bacterial efflux pumps was demonstrated. Our findings suggest that DHFR inhibitors can be used in combination with low concentrations of colistin or similar molecules as a new approach for the treatment of infections caused by multidrug-resistant variants of gram-negative bacteria. The synergism between colistin and the TMP molecules in *S. marcescens* further suggested that peptides with the ability to facilitate antibiotic penetration by altering the bacteria outer membrane and inhibiting bacterial efflux pumps can be used to sensitize bacteria to a wide range of otherwise ineffective antimicrobials.

2.5. Enzymatic Assays

Like TMP, compounds **1a** and **1b** are potent inhibitors of DHFR. Both analogues inhibited the activity of this enzyme by >80%. All three inhibitors were then tested in *E. coli* supplied with increased concentrations of the DHFR cofactor NADPH and the substrate H_2F. The reaction without inhibitors served as the reference (100% activity). In the reactions with TMP or its analogues, increasing concentrations of NADPH resulted in the increased enzyme activity (Figure 4). The enzyme activity was the highest at the highest tested concentration of NADPH (240 μM).

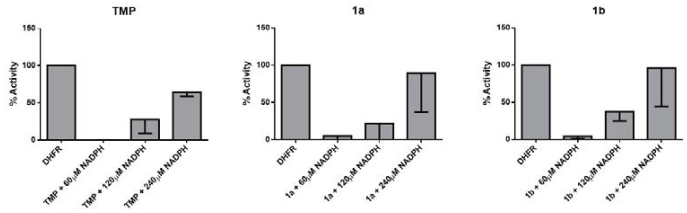

(**a**) (**b**) (**c**)

Figure 4. Activity (%) of *E. coli* dihydrofolate reductase (DHFR) after a 30-min incubation with substrate in the presence of the inhibitors (**a**) TMP, (**b**) **1a** and (**c**) **1b**, each at a concentration of 5 μM, and different concentrations of NADPH. The data are expressed as a percentage with respect to the control.

Similar results were obtained for the three antibiotics tested in the presence of increasing concentrations of H_2F (Figure 5) When the enzymatic assays were performed using a substrate concentration four times higher than the concentration used in the first assay (i.e., 50 μM H_2F), the inhibition was nearly reversed. Thus, as the concentrations of NADPH or H_2F were increased, the enzymatic activity was recovered as well, regardless of the presence of the antibiotics.

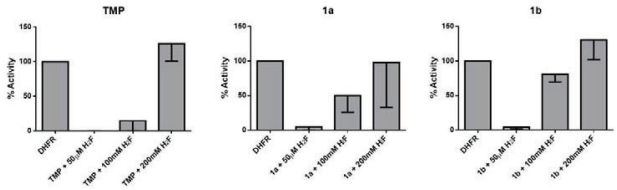

(**a**) (**b**) (**c**)

Figure 5. Percentage of activity of *E. coli* DHFR after a 30-min incubation. Each histogram represents the activity of DHFR in the presence of different concentrations of H_2F and 5 μM of the inhibitors (**a**) TMP, (**b**) **1a** and (**c**) **1b**. The data are expressed as a percentage with respect to the control.

To explore the molecular basis of these results, we examined the binding of **1a** to *E. coli* DHFR. According to the docking model, the heterocyclic ring of **1a** fills the pocket occupied by the nicotinamide ring of NADPH, whereas the trimethoxybenzene ring overlaps the same moiety present in TMP (Figure 6A). Accordingly, the binding of **1a** would compete with the substrate but would also affect the correct alignment of NADPH in its binding pocket.

This binding model is supported by the following experimental evidence. First, a comparison of the arrangements adopted by TMP in its interaction with human and *E. coli* DHFR showed the similar orientation of the diaminopyrimidine ring, which involves the formation of several hydrogen bonds with residues in the binding pocket (Asp27, Ile5, Ile94). By contrast, the position of the trimethoxybenzene ring is more variable and, in fact, it can adopt multiple arrangements, which often would sterically collide with NADPH when bound to the enzyme. Indeed, the most severe steric hindrance (PDB entry 2W9H; TMP, shown as blue sticks in Figure 6B) would occur in an X-ray structure that did not include NADPH. Furthermore, accommodation of compounds **1a** and **1b** was facilitated by the flexibility of the loops that shape the binding pocket. This was seen in the superposition of the X-ray structures 3DAU (*E. coli*) [20] and 4KM2 (M. tuberculosis) [21], which revealed the altered arrangement of loops Met20 and F-G (Figure 6C), as described in previous studies [22,23]. On the basis of this conformational flexibility, compound **1b** was docked using a structural model of *E. coli* DHFR built using the open structure of the enzyme (PDB entry 4KM2) as a template. The open structure enabled the proper accommodation of **1b** in the binding pocket of *E. coli* DHFR (Figure 6D), which would lead to steric hindrance with the nicotinamide ring of NADPH.

2.6. Cytotoxicity

At concentrations as high as 32 μg/mL, which was the maximal concentration considered in these assays, the cytoxicity of TMP, as well as compounds **1a** and **1b** in HepG2 and L-929 cells, was almost negligible (Table 6). A drug is considered toxic when its cytotoxicity level exceeds 20% [24]. For all three compounds, the IC_{50} (the drug concentration needed to inhibit cell growth by 50%) was >32 μg/mL.

Table 6. Cytotoxicity (%) of TMP, **1a** and **1b** in HepG2 and L-929 cells. The data are presented as the percentage of dead cells at maximal concentration tested of the compounds studied (32 μg/mL).

Compound	Cytotoxicity (%)	
	HepG2	L-929
	32 μg/mL	
TMP	0.35	0.8
1a	ND	0
1b	0.11	0

ND: Not determined.

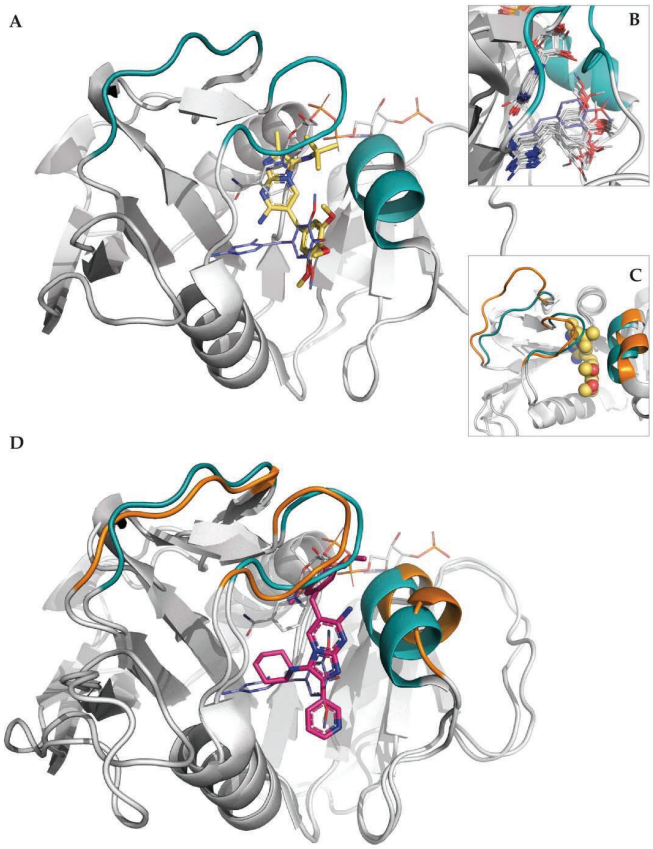

Figure 6. Binding mode of **1a** to the DHFR of *E. coli*. (**A**) The docked positions of **1a** and TMP are shown with their C atoms depicted as yellow sticks and in deep blue, respectively, and with the C atoms of NADPH in gray. (**B**) Superposition of the crystallographic poses of TMP (C atoms in gray). The crystallographic structure of TMP in PDB entry 2W9H, in which the trimethoxybenzene group sterically collides with the nicotinamide ring of NADPH, is shown in deep blue. (**C**) Loops Met20 and F-G, and helix 3 are highlighted to illustrate the differences in the 3D structures of PDB entries 3DAU (turquoise) and 4KM2 (orange). (**D**) The docked position of **1b** (C atoms in magenta) in a homology model of *E. coli* DHFR built using the open structure 4KM2 as a template. The position of TMP and NADPH is shown with their C atoms depicted as deep blue and gray, respectively.

3. Materials and Methods

3.1. Chemical Synthesis

Compounds **1a** and **1b** were prepared as previously reported [6], from the interaction of TMP with aldehydes and isocyanides in acetonitrile under $Yb(OTf)_3$ catalysis. The compounds were purified by chromatography and stored at −20 °C under an inert atmosphere. Stock solutions in DMSO were stable when kept in the cold. The integrity of these compounds and solutions thereof was confirmed by HPLC-MS (column: ZORBAX Extend-C18 3.5 µm 2.1 × 50 mm, Agilent; mobile phase A: H_2O + 0.05% HCOOH; mobile phase B:

ACN + 0.05% HCOOH; 10 min; 35 °C). There were no signs of decomposition at least 1 year after their chemical synthesis.

3.2. Antimicrobial Susceptibility of Planktonic Bacteria

The minimum inhibitory concentrations (MICs) of colistin, TMP, **1a**, and **1b** were determined using the microdilution method, according to EUCAST recommendations [25].

3.3. Antimicrobial Susceptibility of Sessile Bacteria

TMP and its analogues were tested against biofilms by determining the minimal biofilm eradication concentration (MBEC) and the biofilm prevention concentration (BPC). Bacterial viability within the biofilm was assessed using the dye resazurin, which is reduced by metabolically active bacteria to the fluorescent compound resorufin. Both collection strains, *E. coli* ATCC 25922 and *S. aureus* ATCC 29213, and methicillin-resistant *S. aureus* 8124825998 were tested. All three strains were grown in tryptic soy broth (TSB) with shaking at 200 rpm for 24 h at 37 °C. Bacterial biofilms were formed and treated as follows. Overnight suspensions of each strain were diluted 1/100 in TSB. One hundred μL of each of the adjusted cell suspensions were transferred to the wells of flat-bottomed 96-well microtiter plates (Guangzhou Jet Bio-Filtration Co., Ltd., Mianyang, China) and incubated at 37 °C for 24 h. Eight wells filled only with sterile TSB served as the negative controls. All wells were then gently rinsed with 100 μL of Ringer $\frac{1}{4}$ solution. The biofilms were exposed to several concentrations of the antimicrobials (leaving 8 wells without antimicrobials as a positive control) and incubated at 37 °C for 24 h. After the wells were again rinsed with 100 μL of Ringer $\frac{1}{4}$ solution, 100 μL of resazurin (0.0015%) was added to each well. The plates were then incubated for 3–5 h, after which cell fluorescence (λ_{ex} = 530; λ_{em} = 590) was measured using a scanning multi-well spectrophotometer (FLUOstar OPTIMA, BMG Labtech, Ortenberg, Germany)). The MBEC was defined as the lowest concentration of antimicrobial activity that prevented bacterial regrowth from the treated biofilm.

3.4. Synergism Studies

The fractional inhibitory concentration (FIC) of TMP-SMX in combination with colistin was determined by the checkerboard method in four clinical bacterial strains: *E. coli* 220560529, *P. aeruginosa* SJD 536, *P. aeruginosa* SJD 481 (all three TMP resistant), and *P. aeruginosa* VH023. In addition, the FICs of colistin with TMP, **1a** and **1b**, and SMX (1:20) were determined in *E. coli* ATCC 25922, *P. aeruginosa* PAO1, and *S. marcescens* NIMA. The assays were performed in 96-well plates using serial dilutions of TMP and SMX (1:20). Serial dilutions of colistin starting from twice the previously determined MIC were prepared and added to plates inoculated with 5 μL of bacterial suspension. The plates were incubated overnight at 37 °C and read after at least 16 h of incubation.

The fractional inhibitory concentration index (FICi) was determined according to the formula FICi = FIC A + FIC B, where FIC A is the MIC of drug A (TMP + SMX) in combination/MIC of drug A alone and FIC B (colistin) is the MIC of drug B in combination/MIC of drug B alone. The combinations were defined as synergistic (FICi $\leq$ 0.5), indifferent (FICi > 0.5 and < 4), or antagonistic (FICi $\geq$ 4). An antimicrobial effect achieved at a drug concentration that was lower when the drug was used in combination with other drugs than alone was considered to be indicative of synergism between the tested antibiotics.

Additionally, the effect of TMP-SMX and the GBBR analogues in combination with sublethal concentrations of colistin was assessed in growth curves of *E. coli* ATCC 25922, *P. aeruginosa* PAO1, and *S. marcescens* NIMA. Exponential-phase cultures were adjusted to 5×10^6 CFU/mL in a final volume of 10 mL of TSB and the antimicrobials were added at sublethal concentrations. Growth was monitored using RTS-1C real-time cell growth loggers (Biosan SIA, Riga, Latvia) in cells incubated for 24 h at 37 °C with shaking at 2000 rpm. Growth was measured every 10 min as the optical density (OD 850 nm).

3.5. Efflux Pumps Effect

The efflux pump inhibitor phenyl-arginyl-β-naphthylamide (PaβN) was purchased from Sigma-Aldrich Chemicals (Madrid, Spain). The MIC of the TMP analogues in combination with SMX in the presence of 20 μg PaβN/mL was determined in *P. aeruginosa* PAO1 using the microdilution method.

3.6. Dihydrofolate Reductase Assay

The DHFR assay is based on the reduction of 7,8-dihydrofolate to 5,6,7,8-tetrahydrofolate catalyzed by DHFR and using NADPH as a cofactor. Purified *E. coli* DHFR was kindly provided by E. Shakhnovich and J.V. Rodrigues (Harvard University, Cambridge, MA, USA). The DHFR assay kit (CS0340) was purchased from Sigma-Aldrich. The assay was performed in 96-well flat-bottom plates (Corning Costar 3606, NY, USA) with the protocol adjusted to accommodate a final reaction volume of 200 μL. DHFR was diluted to a final concentration of 0.03 μg/mL. The inhibitory effect of compounds **1a** and **1b** was tested, with TMP serving as the control. All three drugs were used at a concentration of 5 μM, which was higher than the respective MICs (Table 1). To determine the effect of the concentration of the DHFR cofactor NADPH on inhibition, a dilution series of NADPH in assay buffer was carried out to obtain a concentration range between 60 μM and 240 μM. A dilution series of H_2F was similarly carried out in assay buffer to obtain a concentration range from 50 μM to 200 μM. In all assays, the enzyme was mixed with the different inhibitors and incubated for 30 min before the enzymatic reaction was initiated by the addition of NADPH and H_2F. The reaction was conducted at 37 °C and monitored by the decrease in absorbance at 340 nm (indicative of a decrease in the NADPH concentration). Measurements were performed every minute for 40 min [26] using a scanning multi-well spectrophotometer (FLUOstar OPTIMA, BMG Labtech, Germany). All measurements were performed in duplicate with three technical replicates.

3.7. Computational Chemistry

Docking simulations were carried out to explore the binding mode of TMP, **1a** and **1b** to *E. coli* DHFR, using the 2019–2 release of Glide [27,28]. The crystal structure of *E. coli* DHFR, retrieved from the Protein Data Bank (PDB code 3DAU [20]), includes methotrexate and NADPH. The protein structure of DHFR was thus prepared by deleting both of these compounds, by assigning bond orders, adding hydrogen atoms, and restrained energy minimization, using the Protein Preparation Wizard module in Maestro [29]. Compounds were prepared using LigPrep [30]. The binding site was enclosed in a grid defined with an inner box of 10 Å × 10 Å × 10 Å; GlideScore (SP) was used to evaluate the quality of the configurations [31]. Default settings were used for all remaining parameters. The results of the docking simulations were visually examined with the aid of PyMOL software [32]. Docking of **1b** was performed using a homology model of *E. coli* DHFR using the open structure from *M. tuberculosis* DHFR (PDB entry 4KM2) as a template.

3.8. Cytotoxicity

The cytotoxicity assay was carried out in the human hepatocellular carcinoma cell line Hep G2 ATCC and in murine L-929 fibroblasts (NCTC clone 929, ECACC 88102702), based on the experiments described by Vinuesa et al. [23]. The cells were obtained from Dr. Ricardo Pérez-Tomás (Cancer Cell Biology, University of Barcelona).

The cytotoxicity of TMP and compounds **1a** and **1b** was determined by measuring the intracellular reduction of resazurin sodium salt (Sigma-Aldrich, St. Louis, MO, USA). HepG2 and L-929 cells were grown in RPMI 1640 and MEM medium, respectively (Biochrom AG, Berlin, Germany), supplemented with 10% fetal bovine serum. Cells from pre-confluent cultures were harvested with trypsin-EDTA and maintained at 37 °C and 5% CO_2. HepG2 and L-929 cells (100 μL each) were seeded in 96-well flat-bottomed microplates to obtain concentrations of 1.5×10^4 and 4×10^3 cells/well, respectively, and incubated at 37 °C for 24 h. Afterwards, the medium was replaced with 200 μL of medium containing

the antimicrobials at concentrations ranging from 32 to 0.016 μg/mL and the microplates were incubated at 37 °C for 24 h. Twenty μL of resazurin was then added to each well and the plates were incubated under the same conditions. Fluorescence was measured at an excitation wavelength of 530 nm and an emission wavelength of 590 nm using a scanning multi-well spectrophotometer (FLUOstar OPTIMA, BMG Labtech, Germany). Cytotoxicity was calculated as follows:

$$\%\,\text{Cytotoxicity} \;=\; 100 - \frac{(\text{AT} - \text{ADB})}{(\text{AC} - \text{AMB})} \times 100 \tag{1}$$

where AT is the absorbance of the treated cells, ADB the absorbance of the drug blank control, AC the absorbance of the untreated cells, and ACB the absorbance of the medium blank.

4. Conclusions

Two TMP derivatives (**1a** and **1b**) showed antibacterial activity against *E. coli*, *P. aeruginosa* and *S. marcescens* similar to that of TMP and acted synergistically with SMX. They resulted to be active in biofilm prevention, whereas neither TMP nor compounds **1a** and **1b** were able to fully eradicate *S. aureus* biofilms (neither *S. aureus* ATCC 29213 nor *S. aureus* 8124825998). On the other hand, at concentrations at which the products behave as good antibacterials, the cytoxicity on HepG2 and L-929 cell lines was almost negligible. *P. aeruginosa* PAO1 was fully resistant to TMP and its derivatives as well as to the combination of TMP-SMX. Moreover, it can be suggested that blocking their efflux systems may influence the *P. aeruginosa* susceptibility to these antimicrobials. The combination of TMP, TMP-like molecules and SMX with colistin enhances their antimicrobial efficacy against *E. coli*, *P. aeruginosa* and *S. marcescens* by permeabilizing the cells.

Compounds **1a** and **1b**, like TMP, strongly inhibited the activity of the *E. coli* DHFR. The inhibition was reversed with increasing concentrations of NADPH and H_2F, suggesting that both molecules interact with the analogues during inhibition. As seen in the docking model, the heterocyclic ring of the compound **1a** fills the pocket occupied by the nicotinamide ring of NADPH. Thus, the binding of **1a** would compete with H_2F and would also prevent the correct recognition of NADPH.

As the search into new antimicrobial compounds is one of the main pathways to overtake bacterial resistance to antibiotics, it should be emphasized that all putative compounds should be tested in conditions in which the role of the outer membrane as a permeability barrier is inactivated. Their assay together with sublethal concentrations of colistin is proposed as one of the methods of election.

Author Contributions: M.P., O.G. and R.L. designed and performed the chemical section and analyzed the results. M.J., R.H. and M.V. designed and performed the biological experiments. L.C.-V. and F.J.L. performed the docking work. All authors have participated in scientific diiscussions, read and agreed to the published version of the manuscript.

Funding: This research was financially supported by the Marató TV3 Foundation (project BARNAPA); Ministerio de Ciencia e Innovación-Spain (PID2019–107991RB-I00), Generalitat de Catalunya (2017SGR1746), and the Consorci de Serveis Universitaris de Catalunya (project Molecular Recognition).

Institutional Review Board Statement: Not applicable.

Informed Consent Statement: Not applicable.

Data Availability Statement: Data is contained within the article.

Acknowledgments: We thank E. Shakhnovich and J.V. Rodrigues (Harvard University) for their kind supply of *E. coli*-DHFR.

Conflicts of Interest: The authors declare no conflict of interest.

References

1. Magiorakos, A.P.; Srinivasan, A.; Carey, R.B.; Carmeli, Y.; Falagas, M.E.; Giske, C.G.; Harbarth, S.; Hindler, J.F.; Kahlmeter, G.; Olsson-Liljequist, B.; et al. Multidrug-resistant, extensively drug-resistant and pandrug-resistant bacteria: An international expert proposal for interim standard definitions for acquired resistance. *Clin. Microbiol. Infect.* **2012**, *18*, 268–281. [CrossRef]
2. Toutain, P.L.; Ferran, A.A.; Bousquet-Melou, A.; Pelligand, L.; Lees, P. Veterinary medicine needs new green antimicrobial drugs. *Front. Microbiol.* **2016**, *7*, 1196. [CrossRef]
3. Wright, G.D. Resisting resistance: New chemical strategies for battling superbugs. *Chem. Biol.* **2000**, *7*, R127–R132. [CrossRef]
4. Góngora-Benítez, M.; Tulla-Puche, J.; Albericio, F. Handles for Fmoc solid-phase synthesis of protected peptides. *ACS Comb. Sci.* **2013**, *15*, 217–228. [CrossRef]
5. Deng, J.; Viel, J.H.; Kubyshkin, V.; Budisa, N.; Kuipers, O.P. Conjugation of synthetic polyproline moietes to lipid ii binding fragments of nisin yields active and stable antimicrobials. *Front. Microbiol.* **2020**, *11*, 1–9. [CrossRef]
6. Pedrola, M.; Jorba, M.; Jardas, E.; Jardi, F.; Ghashghaei, O.; Viñas, M.; Lavilla, R. Multicomponent reactions upon the known drug trimethoprim as a source of novel antimicrobial agents. *Front. Chem.* **2019**, *7*, 1–9. [CrossRef]
7. Sans-Serramitjana, E.; Fusté, E.; Martínez-Garriga, B.; Merlos, A.; Pastor, M.; Pedraz, J.L.; Esquisabel, A.; Bachiller, D.; Vinuesa, T.; Viñas, M. Killing effect of nanoencapsulated colistin sulfate on Pseudomonas aeruginosa from cystic fibrosis patients. *J. Cyst. Fibros.* **2016**, *15*, 611–618. [CrossRef] [PubMed]
8. Martin-Gómez, H.; Jorba, M.; Albericio, F.; Viñas, M.; Tulla-Puche, J. Chemical modification of microcin j25 reveals new insights on the stereospecific requirements for antimicrobial activity. *Int. J. Mol. Sci.* **2019**, *20*, 5152. [CrossRef]
9. Schweitzer, B.I.; Dicker, A.P.; Bertino, J.R. Dihydrofolate reductase as a therapeutic target. *FASEB J.* **1990**, *4*, 2441–2452. [CrossRef]
10. Srinivasan, B.; Skolnick, J. Insights into the slow-onset tight-binding inhibition of Escherichia coli dihydrofolate reductase: Detailed mechanistic characterization of pyrrolo [3,2-f] quinazoline-1,3-diamine and its derivatives as novel tight-binding inhibitors. *FEBS J.* **2015**, *282*, 1922–1938. [CrossRef]
11. Raimondi, M.V.; Randazzo, O.; La Franca, M.; Barone, G.; Vignoni, E.; Rossi, D.; Collina, S. DHFR inhibitors: Reading the past for discovering novel anticancer agents. *Molecules* **2019**, *24*, 1140. [CrossRef]
12. Wróbel, A.; Arciszewska, K.; Maliszewski, D.; Drozdowska, D. Trimethoprim and other nonclassical antifolates an excellent template for searching modifications of dihydrofolate reductase enzyme inhibitors. *J. Antibiot.* **2020**, *73*, 5–27. [CrossRef]
13. Costerton, J.W.; Stewart, P.S.; Greenberg, E.P. Bacterial biofilms: A common cause of persistent infections. *Science* **1999**, *284*, 1318–1322. [CrossRef]
14. Hall-Stoodley, L.; Costerton, J.W.; Stoodley, P. Bacterial biofilms: From the natural environment to infectious diseases. *Nat. Rev. Microbiol.* **2004**, *2*, 95–108. [CrossRef] [PubMed]
15. Lauferska, U.; Viñas, M.; Lorén, J.G.; Guinea, J. Enhancement by polymyxin B of proline-induced prodigiosin biosynthesis in non-proliferating cells of Serratia marcescens. *Microbiologica* **1983**, *6*, 155–162.
16. Armengol, E.; Domenech, O.; Fusté, E.; Pérez-Guillén, I.; Borrell, J.H.; Sierra, J.M.; Vinas, M. Efficacy of combinations of colistin with other antimicrobials involves membrane fluidity and efflux machinery. *Infect. Drug Resist.* **2019**, *12*, 2031. [CrossRef] [PubMed]
17. Armengol, E.; Asunción, T.; Viñas, M.; Sierra, J.M. When combined with colistin, an otherwise ineffective rifampicin–linezolid combination becomes active in Escherichia coli, Pseudomonas aeruginosa, and Acinetobacter baumannii. *Microorganisms* **2020**, *8*, 86. [CrossRef]
18. Rudilla, H.; Fusté, E.; Cajal, Y.; Rabanal, F.; Vinuesa, T.; Viñas, M. Synergistic antipseudomonal effects of synthetic peptide AMP38 and carbapenems. *Molecules* **2016**, *21*, 1223. [CrossRef] [PubMed]
19. Fusté, E.; López-Jiménez, L.; Segura, C.; Gainza, E.; Vinuesa, T.; Viñas, M. Carbapenem-resistance mechanisms of multidrug-resistant *Pseudomonas aeruginosa*. *J. Med. Microbiol.* **2013**, *62*, 1317–1325. [CrossRef]
20. Bennett, B.C.; Wan, Q.; Ahmad, M.F.; Langan, P.; Dealwis, C.G. X-ray structure of the ternary MTX NADPH complex of the anthrax dihydrofolate reductase: A pharmacophore for dual-site inhibitor design. *J. Struct. Biol.* **2009**, *166*, 162–171. [CrossRef]
21. Dias, M.V.B.; Tyrakis, P.; Domingues, R.R.; Leme, A.F.P.; Blundell, T.L. Mycobacterium tuberculosis dihydrofolate reductase reveals two conformational states and a possible low affinity mechanism to antifolate drugs. *Structure* **2014**, *22*, 94–103. [CrossRef] [PubMed]
22. Bystroff, C.; Kraut, J. Crystal structure of unliganded Escherichia coli dihydrofolate reductase. Ligand-induced conformational changes and cooperativity in binding. *Biochemistry* **1991**, *30*, 2227–2239. [CrossRef] [PubMed]
23. Sawaya, M.R.; Kraut, J. Loop and subdomain movements in the mechanism of Escherichia coli dihydrofolate reductase: Crystallographic evidence. *Biochemistry* **1997**, *36*, 586–603. [CrossRef] [PubMed]
24. Vinuesa, T.; Herráez, R.; Oliver, L.; Elizondo, E.; Acarregui, A.; Esquisabel, A.; Pedraz, J.L.; Ventosa, N.; Veciana, J.; Viñas, M. Benznidazole nanoformulates: A chance to improve therapeutics for Chagas disease. *Am. J. Trop. Med. Hyg.* **2017**, *97*, 1469–1476. [CrossRef] [PubMed]
25. EUCAST Reading Guide for Broth Microdilution. Available online: https://www.eucast.org/fileadmin/src/media/PDFs/EUCAST_files/MIC_testing/Reading_guide_BMD_v_3.0_2021.pdf (accessed on 9 April 2021).
26. Phetsang, W.; Pelingon, R.; Butler, M.S.; Kc, S.; Pitt, M.E.; Kaeslin, G.; Cooper, M.A.; Blaskovich, M.A.T. Fluorescent Trimethoprim conjugate probes to assess drug accumulation in wild type and mutant Escherichia coli. *ACS Infect. Dis.* **2016**, *2*, 688–701. [CrossRef] [PubMed]

27. *Schrödinger Release 2019-2: Glide*; Schrödinger LLC: New York, NY, USA, 2019.
28. Friesner, R.A.; Banks, J.L.; Murphy, R.B.; Halgren, T.A.; Klicic, J.J.; Mainz, D.T.; Repasky, M.P.; Knoll, E.H.; Shelley, M.; Perry, J.K.; et al. Glide: A New approach for rapid, accurate docking and scoring. 1. Method and assessment of docking accuracy. *J. Med. Chem.* **2004**, *47*, 1739–1749. [CrossRef] [PubMed]
29. *Schrödinger Release 2019-3: Maestro*; Schrödinger LLC: New York, NY, USA, 2019.
30. *Schrödinger Release 2016-3: LigPrep*; Schrödinger LLC: New York, NY, USA, 2016.
31. Friesner, R.A.; Murphy, R.B.; Repasky, M.P.; Frye, L.L.; Greenwood, J.R.; Halgren, T.A.; Sanschagrin, P.C.; Mainz, D.T. Extra precision Glide: Docking and scoring incorporating a model of hydrophobic enclosure for protein-ligand complexes. *J. Med. Chem.* **2006**, *49*, 6177–6196. [CrossRef] [PubMed]
32. *The PyMOL Molecular Graphics System*; Version 2.0; Schrödinger LLC: New York, NY, USA, 2016.

Extended MCRs with Indole Aldehydes

Publication III: Extended Multicomponent Reactions with Indole Aldehydes: Access to Unprecedented Polyheterocyclic Scaffolds, Ligands of the Aryl Hydrocarbon Receptor

Nitrogen Heterocycles

How to cite: *Angew. Chem. Int. Ed.* **2021**, *60*, 2603 – 2608
International Edition: doi.org/10.1002/anie.202011253
German Edition: doi.org/10.1002/ange.202011253

Extended Multicomponent Reactions with Indole Aldehydes: Access to Unprecedented Polyheterocyclic Scaffolds, Ligands of the Aryl Hydrocarbon Receptor

*Ouldouz Ghashghaei[+], Marina Pedrola[+], Francesca Seghetti, Victor V. Martin, Ricardo Zavarce, Michal Babiak, Jiri Novacek, Frederick Hartung, Katharina M. Rolfes, Thomas Haarmann-Stemmann, and Rodolfo Lavilla**

Abstract: *The participation of reactants undergoing a polarity inversion along a multicomponent reaction allows the continuation of the transformation with productive domino processes. Thus, indole aldehydes in Groebke–Blackburn–Bienaymé reactions lead to an initial adduct which spontaneously triggers a series of events leading to the discovery of novel reaction pathways together with direct access to a variety of linked, fused, and bridged polyheterocyclic scaffolds. Indole 3- and 4-carbaldehydes with suitable isocyanides and aminoazines afford fused adducts through oxidative Pictet–Spengler processes, whereas indole 2-carbaldehyde yields linked indolocarbazoles under mild conditions, and a bridged macrocycle at high temperature. These novel structures are potent activators of the human aryl hydrocarbon receptor signaling pathway.*

Multicomponent reactions (MCRs) are transformations involving three or more reactants that yield a unified adduct in a single step. MCRs are among the strategies of choice to achieve high diversity and complexity levels, offering significant exploratory potential in a simple experimental framework. Accordingly, they have an impressive impact on modern organic synthesis, medicinal chemistry, materials science, etc.[1–3]

Another way to rapidly reach molecular complexity deals with domino processes, where an initial reaction triggers a series of consecutive transformations to generate intermediates that interact with other functionalities present in the substrate.[4,5] Domino reactions are, however, highly dependent on the specific arrangement of the substrates, which usually need to be previously prepared through multistep synthesis. Therefore, these reactions are challenging to generalize, and their use is somewhat restricted. Incidentally, MCRs can be described as intermolecular domino reactions featuring simple starting materials.

Here we present the concept of *extended* MCRs, as an alternative approach to tackle the aforesaid limitations of classic domino reactions. Extended MCRs involve reactants that trigger an ensuing cascade of inter/intramolecular transformations due to a polarity inversion, following the initial MCR. Relevant reports in the literature include related processes where this concept is implicit.[6–9]

We particularly focused on electrophilic indole aldehydes that render nucleophilic moieties after the MCR and promote subsequent reactions within the adduct, or with other species present in the medium (Figure 1). This situation is found in several MCRs involving aromatic aldehydes and remains unexplored. Indoles are common scaffolds in drugs and bioactive compounds. Furthermore, they are influential motifs in the design of domino processes[10–12] and indole carbaldehydes have already displayed a rich reactivity in this endeavor.[13–15] Indoles are also present in a variety of MCRs. However, they often appear as mere substituents of the reactive groups on the inputs.[16,17]

We focused on the Groebke–Blackburn–Bienaymé MCR (GBB): the interaction of α-aminoazines, aldehydes and isocyanides to yield imidazoazines, a privileged scaffold in medicinal chemistry.[18–20]

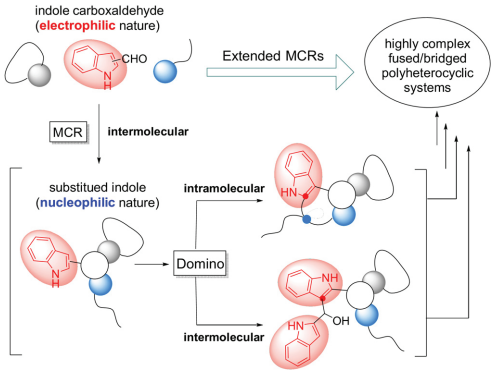

Figure 1. The concept of extended MCRs with indolealdehydes.

[*] Dr. O. Ghashghaei,[+] M. Pedrola,[+] Dr. F. Seghetti, V. V. Martin, R. Zavarce, Prof. R. Lavilla
Laboratory of Medicinal Chemistry, Faculty of Pharmacy and Food Sciences and Institute of Biomedicine (IBUB), Universitat de Barcelona, Av. Joan XXIII, 27–31, 08028 Barcelona (Spain)
E-mail: rlavilla@ub.edu
M. Babiak, Dr. J. Novacek
CEITEC, Masaryk University
University Campus Bohunice, 62500 Brno (Czech Republic)
F. Hartung, K. M. Rolfes, Dr. T. Haarmann-Stemmann
IUF Leibniz Research Institute for Environmental Medicine
40225 Düsseldorf (Germany)
[+] These authors contributed equally to this work.
Supporting information and the ORCID identification number(s) for the author(s) of this article can be found under: https://doi.org/10.1002/anie.202011253.

Thus, we performed a GBB with α-aminopyridine **1a**, indole-3-carbaldehyde **2a** and ethyl isocyanoacetate **3a** in open air and observed the formation of the fused adduct **7a** (25%, Scheme 1A). Likely, the initial GBB adduct **4a** was oxidized to the corresponding imine **5a** by atmospheric O_2, which underwent an acid-catalyzed Pictet–Spengler (PS) cyclization upon the indole C2 position to give the dihydropyridine **6a**, that subsequently oxidized to the final product **7a** (structure confirmed by X-Ray crystallography, Scheme 1B). The imine generation can be related to the auto-oxidation of glycine derivatives under analogous conditions.[21] Moreover, the detection of the imine **5a** and the intermediate dihydropyridine **6a** supports the mechanistic hypothesis [see the Supporting Information (SI)]. The reaction was repeated in the presence of several acid/oxidant combinations in one-pot and stepwise protocols. The GBB went smoothly with $Yb(OTf)_3$ as the catalyst. In terms of the external oxidant, the performance of $CoBr_2$ particularly stood out from $FeCl_3$, CuI, IBX and blue-LED-promoted photocatalytic oxidations using Eosin Y, Rose Bengal and $Ru(bpy)_3^{2+}$.[22–24] Although the final product is directly achievable from the **1a**, **2a** and **3a** mixture, higher yields (41%) and cleaner crudes were obtained when the GBB adduct **4a** was isolated in a prior step, possibly due to the sensitivity of isocyanides in the presence of particular oxidizing agents.

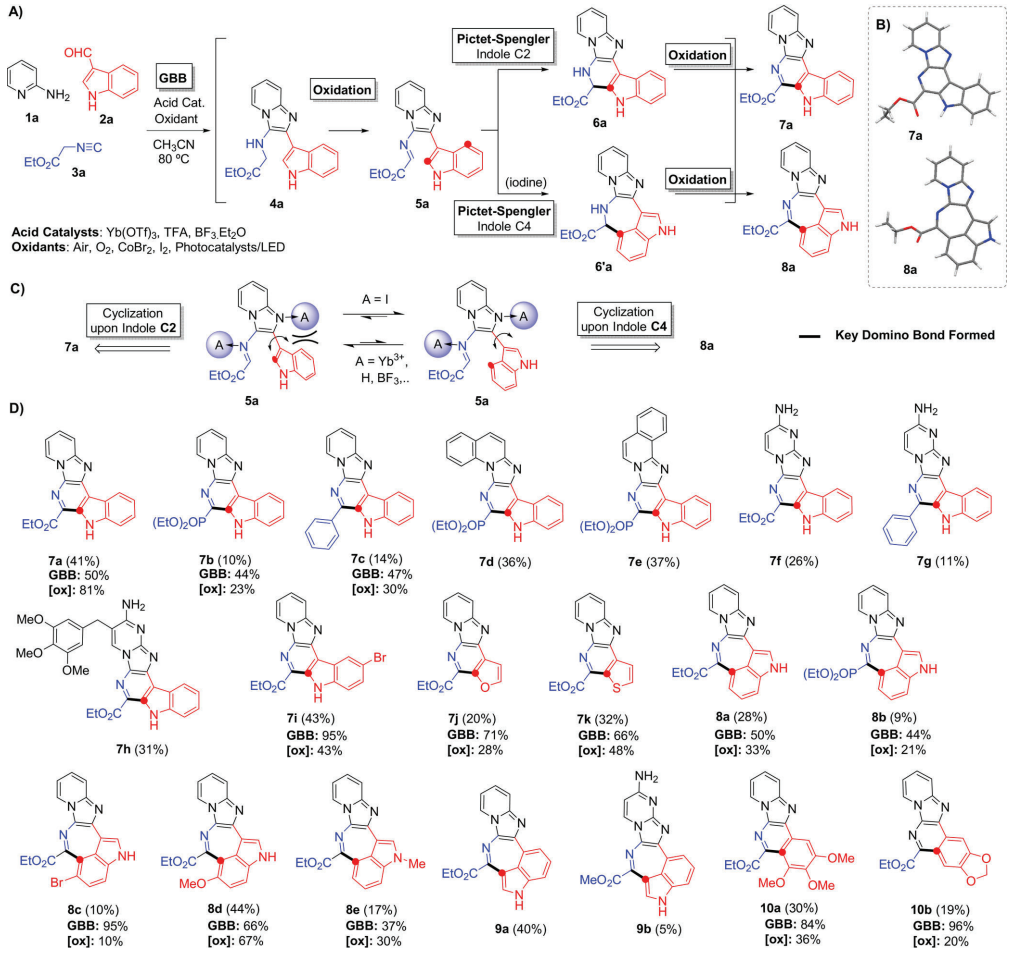

Scheme 1. Extended oxidative GBBs featuring indole-3(4)-aldehydes: A) Reaction conditions and mechanism. B) X-ray[41] and microED structures of compounds **7a** and **8a**. C) Hypothesis for the regioselective PS. D) Scope and variations. For sequential processes, the yield of each step is reported.

Remarkably, the use of iodine brought a dramatic modification in the connectivity pattern of the domino process, as it promoted an unconventional cyclization upon the indole C4, in the presence of the free C2 position, yielding adduct **8a** (28%). Compound **8a** features a complex fused seven-membered ring and, not being able to obtain suitable crystals, its structure was secured by microcrystal electron diffraction[25] (Scheme 1B). This cyclization mode is unprecedented in unbiased indole systems, as PS and other electrophilic processes prefer position C2,[26] whereas reactions on position C4 only occur under enzymatic catalysis.[27] Presumably, the coordination with one imidazole N atom in the imine **5a** favors the later cyclization by increasing the steric bulk around C2. This hypothesis was further supported as a standard PS reaction between 4-chlorobenzaldehyde and tryptamine in the presence of iodine[28] yields common C2 products (Scheme 1C and SI).

Next, we studied the scope of this extended MCR. Regarding the isocyanide input, only those capable of yielding conjugated imines (**5**) undergo the domino process. PhosMIC and benzyl isocyanide proceeded in a similar manner to yield adducts **7b** (10%), **8b** (9%) and **7c** (14%). TOSMIC did not yield the expected GBB adduct, likely due to its low nucleophilicity. In agreement with this hypothesis, 4-fluorophenetyl-, 4-methoxyphenyl- and cyclohexyl isocyanide did not evolve beyond their respective GBB adducts (Scheme 1D and SI).

With respect to aminoazines, 1-aminoisoquinoline and 2-aminoquinoline afforded the expected compounds **7d** (36%) and **7e** (37%) respectively in the presence of $CoBr_2$ (Scheme 1D). These adducts display interesting S- and C-shape topologies. 2,4-Diaminopyrimidine yielded the adducts **7f** (26%) and **7g** (11%) in a regioselective manner, following the protocol developed by the group.[29] The antibiotic trimethoprim suitably reacted likewise to give adduct **7h** (31%).[30] Interestingly, 2,4-diaminopyrimidine adducts react smoothly in air, not requiring other oxidants, probably due to their higher electron density.

As for the scope of the aldehyde component, activated (hetero)aromatic aldehydes should react, facilitating the PS step. Accordingly, 5-bromoindole-3-carbaldehyde yielded the expected adducts **7i** (43%) and **8c** (10%) in the presence of $CoBr_2$ and I_2, respectively. 5-Methoxy-3-carbaldehyde and 1-methyl indole 3-carbaldehyde provided adducts **8d** (44%) and **8e** (17%) in the presence of I_2. Furan 3- and thiophene 3-carbaldehyde gave the corresponding adducts **7j** (20%) and **7k** (32%) respectively. The incorporation of indole 4-carboxaldehyde afforded adducts **9a** (40%) and **9b** (5%) through PS cyclization upon indole C3 position, featuring an alternative connectivity of the fused seven-membered ring (Scheme 1D). Electron-rich benzaldehydes, such as 3,4,5-trimethoxy benzaldehyde and piperonal, provided the expected adducts **10a** (30%) and **10b** (19%). Consistently, pyridine aldehydes only yielded GBB adducts (See SI). In general, the processes lead quite cleanly to the oxidized compounds **7**–**10** with relatively few side reactions (imine oxidation, isocyanide hydrolysis) given the mild conditions used.

Next, we reacted equimolar quantities of indole 2-carbaldehyde **2l**, 2-aminopyridine **1a**, and ethyl isocyanoacetate **3a** in the presence of $Yb(OTf)_3$, to presumably obtain the adduct **7l**, following the expected oxidative domino process (Scheme 2A). Yet surprisingly, indolocarbazole **11a** was isolated instead. When performing the reaction with three equivalents of the aldehyde input, the unoptimized yield rose to 25%. As the new domino process should, in principle, proceed with any isocyanide, we switched to cyclohexyl isocyanide **3f** and repeated the reaction with the modified stoichiometry, to yield adduct **11b** (33%) in an unprecedented ABC_3 domino fashion (Scheme 2A and SI). Similar reactions involving 5-bromo-1-aminopyridine, *tert*-butyl isocyanide, and 4-methoxyphenyl isocyanide also led to the corresponding adducts **11c** (28%), **11d** (17%) and **11e** (15%) (Scheme 2C). The latter's structure was secured by X-Ray crystallography (Scheme 2D). These results displayed the usefulness of the new intermolecular domino as a remarkably convenient one-pot access to the valuable indolocarbazole scaffold.[31,32]

Astonishingly, when we promoted the reaction with cyclohexyl isocyanide by microwave irradiation (90 minutes at 110 °C), we isolated small amounts of compound **11b** (9%), whereas the major component was its complex isomer **12** (28%), whose structure was elucidated by X-Ray crystallography (Scheme 2D). Compound **12** features a spiroazabicyclo[4.3.1]decane core fused with one benzimidazole, and two indole rings. We detected traces of compound **12** at 80 °C but not at rt. Moreover, the two isomers **11b** and **12** did not interconvert under acidic and thermal conditions.

The generation of indolocarbazoles **11** and the bicyclic adduct **12** may be explained through a unified mechanism (Scheme 2B). The proposed reaction mechanism involves the formation of the GBB adduct **4t** featuring a highly nucleophilic 2-subsituted indole moiety that attacks a second aldehyde unit to form the intermediate alcohol **M1**. A similar nucleophilic addition takes place between this intermediate and a third aldehyde unit to generate diol **M2**, which cyclizes to afford alcohol **M3**. This intermediate undergoes a dehydration/aromatization step to give the indolocarbazole **11b** (Scheme 2B). At high temperature, however, **M2** may evolve through the generation of intermediate **M4** resulting from the hydroxyl displacement by the amino group and similarly, the quaternary ammonium salt **M5** would arise. This intermediate may undergo a [1,2] Stevens rearrangement[33] justifying the connectivity found in compound **12**. Although several alternative Stevens rearrangements can, in principle, take place, the illustrated pathway presumably leads to the most stable adduct likely involving a reasonably favored intermediate (See SI for a discussion).

Overall, the extended MCRs reach remarkable bond-forming indexes and structural diversity/complexity levels in one-pot operations with modest overall yields, which, however, can be specifically optimized attending to their particular input combinations. For representative examples, see the tuning of conditions leading to compounds **7a** and **7f** in SI.

Having an exclusive access to a variety of novel heteroaromatic scaffolds, we intended to determine their bioactivity profile. We focused on the aryl hydrocarbon receptor (AHR),

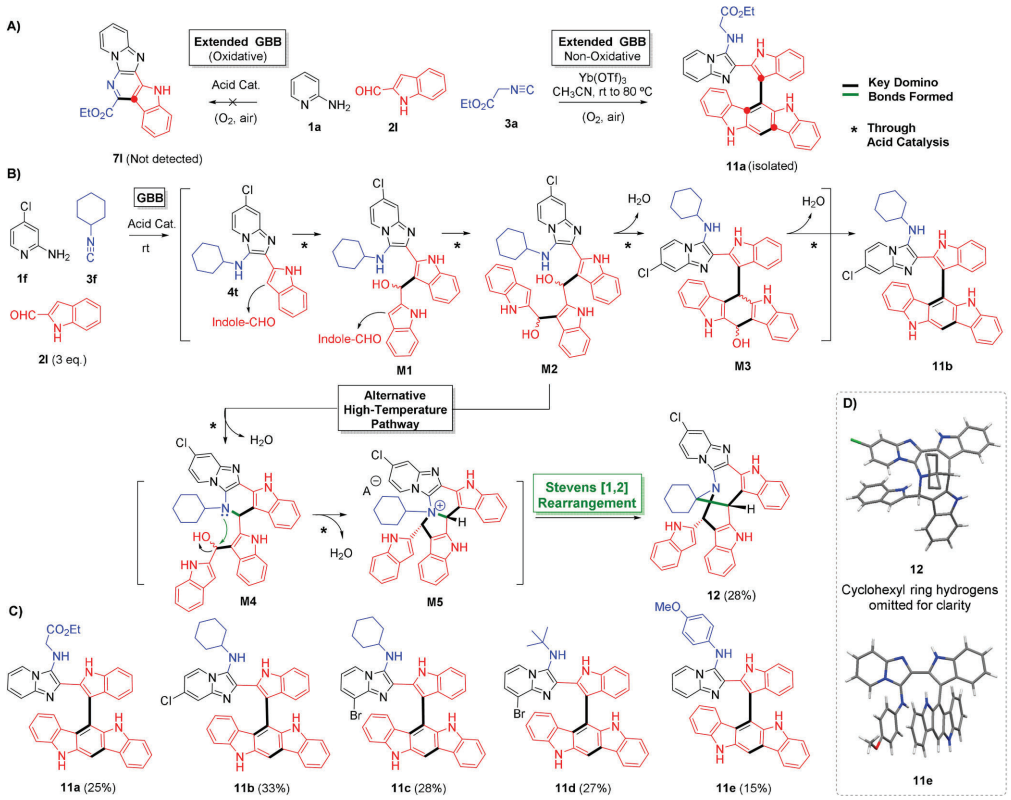

Scheme 2. Extended non-oxidative GBBs with indole 2-carbaldehyde: A) Domino adducts with ethyl isocyanoacetate. B) Unified mechanistic hypothesis. C) Scope of indolocarbazoles. D) X-ray structures[41] of compounds **11e** and **12**.

as indolocarbazoles and related structures are listed among its ligands.[34,35] Upon binding of a ligand in the cytoplasm, AHR translocates to the nucleus and binds to xenobiotic-responsive elements (XRE) in the enhancer of target genes, for example, encoding cytochrome P450 (CYP) 1A1, to induce their expression.

AHR regulates multiple physiological and pathophysiological processes, including xenobiotic metabolism, immune responses, inflammation, and carcinogenesis.[34–36] Recent studies, particularly assessing AHR's function in the context of skin and gut diseases, have unmasked the Janus-faced nature of AHR.[37,38] Depending on cell-type, tissue, microenvironment, and presence of ligand(s), either activation or inhibition of AHR may be beneficial. The AHR binding pocket is still not well described, and although computational studies have shed some light, the generation of potent AHR ligands still relies mostly on appropriate synthesis and screening.[39,40] As shown in Figure 2A, exposure to compounds **8a**, **11b–e** and **12** (but not **7a**) resulted in a dose-dependent induction of CYP1A enzyme activity in AHR-proficient but not AHR-knockdown HaCaT keratinocytes. At the highest test concentration, **8a** interfered with CYP1A enzyme activity, suggesting that this compound is metabolized by CYP1A isoforms and thus competing with the deethylation of 7-ethoxyresorufin. All compounds, except **7a**, increased the CYP1A1 and CYP1B1 copy numbers in HaCaT cells in an AHR-dependent manner (Figure 2B). Aside **7a** and **8a**, all compounds stimulated XRE-driven reporter gene activity in hepatoma cells (Figure 2C).

Taken together, these results strongly indicate that extended MCRs enable the production of a variety of AHR-activating compounds. The tested compounds are almost as potent as the positive control (6-formylindolo[3,2-*b*]carbazole, FICZ). The described modular access to these scaffolds will facilitate further studies to prove their bonding to the AHR and to assess their pharmacokinetic and safety profiles, facilitating a drug discovery program.

To conclude, we have described several domino-prolonged GBBs with indole carbaldehydes that directly yield unprecedented polyheteroaromatic systems. We believe that

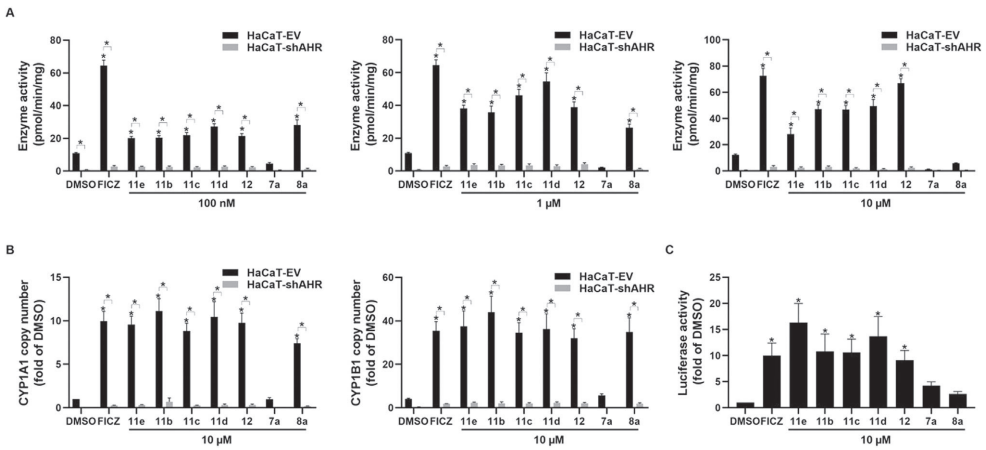

Figure 2. Effect of test compounds on AHR-driven gene expression and CYP1A enzyme activity. A) AHR-proficient HaCaT-EV and AHR-knockdown HaCaT-shAHR keratinocytes were treated with 0.1% DMSO, 100 nM of the AHR agonist FICZ and increasing concentrations of the compounds (100 nM, 1 μM, 10 μM). After 6 h, CYP1A-mediated deethylation of 7-ethoxyresorufin was determined. B) HaCaT-EV and HaCaT-shAHR cells were treated for 6 h with 0.1% DMSO, 100 nM FICZ, and 10 μM of each test compound. After 6 h, total RNA was isolated, reverse transcribed, and copy numbers of CYP1A1 and CYP1B1 were determined by quantitative real-time PCR. C) XRE-HepG2 cells were treated with 0.1% DMSO, 100 nM FICZ, and 10 μM of each compound. After 24 h, AHR/XRE-dependent luciferase activity was determined. * $p \leq 0.05$.

the concept of extended MCRs may have a positive impact in the exploration of the chemical and reactivity spaces, taking into account that similar polarity changes could take place in many MCRs.

Acknowledgements

We thank Drs. M. Valverde (U. Burgos); C. San Martin (CNB, CSIC Madrid); A. Dömling (U. Groningen); J. Pavlicek (BIOCEV, Prague), M. Barenys, C. Escolano, F. J. Luque, J. C. Perales (U. Barcelona), and S. Preciado (Enantia) for useful suggestions. We acknowledge the support from the Ministerio de Ciencia e Innovación-Spain (PID2019-107991RB-I00), Instruct-ERIC (PID:11505) and MEYS CR (LM2018127).

Conflict of interest

The authors declare no conflict of interest.

Keywords: domino reactions · multicomponent reactions · nitrogen heterocycles · receptors · synthetic methods

[1] J. Zhu, Q. Wang, M. X. Wang, *Multicomponent Reactions in Organic Synthesis*, Wiley-VCH, Weinheim, **2014**.
[2] E. Ruijter, R. Scheffelaar, R. V. A. Orru, *Angew. Chem. Int. Ed.* **2011**, *50*, 6234; *Angew. Chem.* **2011**, *123*, 6358.
[3] A. Dömling, W. Wang, K. Wang, *Chem. Rev.* **2012**, *112*, 3083.
[4] L. F. Tietze, *Chem. Rev.* **1996**, *96*, 115.
[5] L. F. Tietze, G. Brasche, K. M. Gericke, *Domino Reactions in Organic Synthesis*, Wiley-VCH, Weinheim, **2006**.
[6] Z. Xu, F. De Moliner, A. P. Cappelli, C. Hulme, *Org. Lett.* **2013**, *15*, 2738.
[7] D. Lee, J. K. Sello, S. L. Schreiber, *Org. Lett.* **2000**, *2*, 709.
[8] H. Sun, H. Zhou, O. Khorev, R. Jiang, T. Yu, X. Wang, Y. Du, Y. Ma, T. Meng, J. Shen, *J. Org. Chem.* **2012**, *77*, 10745.
[9] E. González-Zamora, A. Fayol, M. Bois-Choussy, A. Chiaroni, J. Zhu, *Chem. Commun.* **2001**, 1684.
[10] M. G. Ciulla, S. Zimmermann, K. Kumar, *Org. Biomol. Chem.* **2019**, *17*, 413.
[11] Y. He, Z. Li, K. Robeyns, L. Van Meervelt, E. V. Van der Eycken, *Angew. Chem. Int. Ed.* **2018**, *57*, 272; *Angew. Chem.* **2018**, *130*, 278.
[12] T. De Tan, X. Q. Zhu, H. Z. Bu, G. Deng, Y. B. Chen, R. S. Liu, L. W. Ye, *Angew. Chem. Int. Ed.* **2019**, *58*, 9632; *Angew. Chem.* **2019**, *131*, 9734.
[13] Y. He, Z. Liu, D. Wu, Z. Li, K. Robeyns, L. Van Meervelt, E. V. Van Der Eycken, *Org. Lett.* **2019**, *21*, 4469.
[14] Y. Sakata, E. Yasui, K. Takatori, Y. Suzuki, M. Mizukami, S. Nagumo, *J. Org. Chem.* **2018**, *83*, 9103.
[15] L. Zhang, M. Zheng, F. Zhao, Y. Zhai, H. Liu, *ACS Comb. Sci.* **2014**, *16*, 184.
[16] M. Shiri, *Chem. Rev.* **2012**, *112*, 3508.
[17] G. Mohammadi Ziarani, R. Moradi, T. Ahmadi, N. Lashgari, *RSC Adv.* **2018**, *8*, 12069.
[18] A. Boltjes, A. Dömling, *Eur. J. Org. Chem.* **2019**, 7007.
[19] S. Shaaban, B. F. Abdel-Wahab, *Mol. Diversity* **2016**, *20*, 233.
[20] N. Devi, R. K. Rawal, V. Singh, *Tetrahedron* **2015**, *71*, 183.
[21] C. Huo, Y. Yuan, M. Wu, X. Wang, F. Chen, J. Tang, *Angew. Chem. Int. Ed.* **2014**, *53*, 13544; *Angew. Chem.* **2014**, *126*, 13762.
[22] S. Garbarino, D. Ravelli, S. Protti, A. Basso, *Angew. Chem. Int. Ed.* **2016**, *55*, 15476; *Angew. Chem.* **2016**, *128*, 15702.
[23] A. Basso, L. Moni, R. Riva, in *Multicomponent Reactions in Organic Synthesis*, Wiley-VCH, Weinheim, **2014**, pp. 265–300.
[24] M. S. Segundo, A. Correa, *Synthesis* **2018**, *50*, 2853.
[25] B. L. Nannenga, T. Gonen, *Nat. Methods* **2019**, *16*, 369.
[26] Q. Liu, Q. Li, Y. Ma, Y. Jia, *Org. Lett.* **2013**, *15*, 4528.

[27] T. Abe, K. Yamada, *J. Nat. Prod.* **2017**, *80*, 241.
[28] D. Prajapati, M. Gohain, *Synth. Commun.* **2008**, *38*, 4426.
[29] O. Ghashghaei, S. Caputo, M. Sintes, M. Revés, N. Kielland, C. Estarellas, F. J. Luque, A. Aviñó, R. Eritja, A. Serna-Gallego, J. A. Marrugal-Lorenzo, J. Pachón, J. Sánchez-Céspedes, R. Treadwell, F. de Moliner, M. Vendrell, R. Lavilla, *Chem. Eur. J.* **2018**, *24*, 14513.
[30] M. Pedrola, M. Jorba, E. Jardas, F. Jardi, O. Ghashghaei, M. Viñas, R. Lavilla, *Front. Chem.* **2019**, *7*, 475.
[31] M. Zhao, B. Zhang, Q. Miao, *Angew. Chem. Int. Ed.* **2020**, *59*, 9678; *Angew. Chem.* **2020**, *132*, 9765.
[32] T. Janosik, A. Rannug, U. Rannug, N. Wahlström, J. Slätt, J. Bergman, *Chem. Rev.* **2018**, *118*, 9058.
[33] D. Baidilov, *Synthesis* **2020**, *52*, 21.
[34] V. Rothhammer, F. J. Quintana, *Nat. Rev. Immunol.* **2019**, *19*, 184.
[35] I. A. Murray, A. D. Patterson, G. H. Perdew, *Nat. Rev. Cancer* **2014**, *14*, 801.
[36] C. F. A. Vogel, L. S. Van Winkle, C. Esser, T. Haarmann-Stemmann, *Redox Biol.* **2020**, *34*, 101530.
[37] T. Haarmann-Stemmann, C. Esser, J. Krutmann, *J. Invest. Dermatol.* **2015**, *135*, 2572.
[38] K. W. Bock, *Biochem. Pharmacol.* **2020**, *178*, 114093.
[39] I. A. Murray, G. Krishnegowda, B. C. Dinatale, C. Flaveny, C. Chiaro, J. M. Lin, A. K. Sharma, S. Amin, G. H. Perdew, *Chem. Res. Toxicol.* **2010**, *23*, 955.
[40] S. Giani Tagliabue, S. C. Faber, S. Motta, M. S. Denison, L. Bonati, *Sci. Rep.* **2019**, *9*, 10693.
[41] CCDC 2019590 (**7a**), 2023659 (**8a**), 2023664 (**11e**), and 2019595 (**12**) contain the supplementary crystallographic data for this paper. These data are provided free of charge by The Cambridge Crystallographic Data Centre.

Manuscript received: August 17, 2020
Revised manuscript received: September 30, 2020
Accepted manuscript online: October 13, 2020
Version of record online: November 26, 2020

Angewandte Chemie
Eine Zeitschrift der Gesellschaft Deutscher Chemiker

Supporting Information

Extended Multicomponent Reactions with Indole Aldehydes: Access to Unprecedented Polyheterocyclic Scaffolds, Ligands of the Aryl Hydrocarbon Receptor

*Ouldouz Ghashghaei[+], Marina Pedrola[+], Francesca Seghetti, Victor V. Martin, Ricardo Zavarce, Michal Babiak, Jiri Novacek, Frederick Hartung, Katharina M. Rolfes, Thomas Haarmann-Stemmann, and Rodolfo Lavilla**

anie_202011253_sm_miscellaneous_information.pdf

Table of Contents

1. General Information

Unless otherwise stated, all reactions were carried out under normal atmosphere in dried glassware. All chemicals were purchased from commercial sources and were used as received unless otherwise mentioned. Microwave reactions were performed on a Biotage Initiator Classic. Column chromatographies were performed on commercial silica gel. Flash column chromatographies were performed on an Isolera Prime Biotage provided with dual UV detection over prepacked normal phase silica gel columns (4, 12 and 24 g). Thin layer chromatographies were performed on pre-coated Merk silica gel 60 F_{254} plates and visualized under UV light at 254 nm and 365 nm.

1.1. Analysis

The ^{1}H NMR spectra were recorded on a 400 MHz or 600 MHz NMR spectrometer. The ^{13}C NMR spectra were recorded at 100 MHz or 150 MHz. Chemical shifts were reported in ppm(δ) as s (singlet), d (doublet), t (triplet), dd (doublet of doublet), m (multiplet), br s (broad singlet), etc. The residual solvent signals were used as references.
The University of Barcelona Mass Spectrometry Service performed high the Resolution Mass Spectrometry.
HPLC-MS spectra were carried out on HPLC-MS (Agilent 1260 Infinity II) analysis was conducted on a Poroshell 120 EC-C15 (4.6 mm × 50 mm, 2.7 µm) at 40 °C with mobile phase A (H_2O + 0.05% formic acid) and B (ACN + 0.05% formic acid) using a gradient elution and flow rate 0.6 mL/min. The DAD detector was set at 254 or 220 nm, the injection volume was 5 µL, and oven temperature was 40 °C.
The Science and technology Park (University of Burgos, Spain) and Central European Institute of Technology (Brno, Czech Republic) carried out X-Ray diffractions and microcrystal electron diffractions (MicroED) respectively.

1.2. Light Source used in the photocatalyzed reactions

Flexible blue LED strips of 120 cm from buyledstrip.com (Netherlands) were used as the light source for photoredox-catalysed reactions. The light source was placed in a large crystallizing dish, around its inner circumference. The custom-made device was set up above a stirring plate (but no heating) with closed reaction vials, Schlenk vials or round bottom flasks with refrigerator in the center (~ 5 cm of distance between the vessel and the light source). The solvent irradiated under blue LEDs reach a temperature of no more than 70 ºC. Therefore, either a closed system or a vessel with refrigerator would be needed. The device should be covered with aluminum foil to increase the reaction irradiation and avoid any dangerous exposure to LEDs.

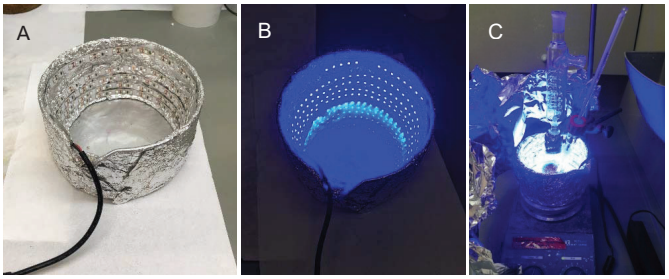

Figure 1.

2. Experimental Procedures

2.1. Summary of Reaction Conditions

2.1.1. Oxidative Extended GBB leading to Compound 7a

A selection of usual acid catalysts were tested to promote the GBB reaction and Pictet-Spengler cyclization. A selection of reported oxidative agents were also applied to promote the imine formation and the final aromatization step.[1–5] Considering the different steps of the oxidative cascade with 3-indole carboxaldehyde **2a**, three main scenarios were tested on the model set of substrates to obtain the optimal conditions as follows: First, we tried a one-pot protocol mixing the starting materials **1a** (0.094 g, 1.0 mmol), **2a** (0.145 g, 1.0 mmol) and **3a** (0.109 mL, 1.0 mmol) in CH_3CN (2.0 mL), together with a variety of catalysts for both the GBB formation and its corresponding oxidation to yield **7a**. Entry A corresponded to the reaction control with GBB under standard conditions[6], in which the oxidizing agent was O_2 (from air). We obtained the oxidized and cyclized compound **7a** with yields from 13 to 26% when we used $Yb(OTf)_3.H_2O$ and TFA as GBB-catalysts, and $CoBr_2$, and organic photoredox catalysts for the oxidative process. On the contrary, using I_2 and $BF_3{\cdot}OEt_2$ did not allow us to obtain the final product. In the case of $BF_3{\cdot}OEt_2$, the starting materials did not react, while in the case of I_2, just **2a** was detected through LC-MS, which made us think that some interaction between the isocyanide **3a** and the excess of iodine could have occurred. Although we obtained the expected compound **7a** in almost all cases, we were not able to improve neither the yield nor the conversion. Preliminary results with CuI and $FeCl_3$ resulted in very low conversions to GBB adducts. Therefore, these catalysts were discarded.

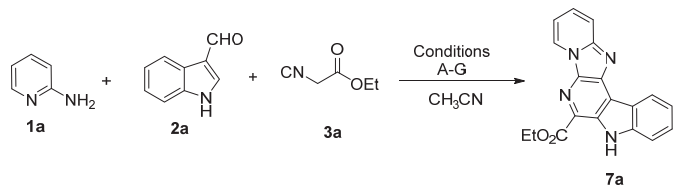

Entry	Protocol	GBB-catalyst (amount)	Oxidation-catalyst (amount)	Oxidant	Temperature (ºC)	Time (h)	Isolated Yield of **7a** (%)
A	One-pot (conventional batch) [a]	$Yb(OTf_3)$ (20 mol %)	-	Air	80	72	35
B	One-pot (conventional batch) [a]	$Yb(OTf_3)$ (20 mol %)	$CoBr_2$ (5 mol %)	Air	80	23	15 (detected by LC-MS)
C	One-pot (with the blue LED device) [b]	TFA (20 mol %)	Eosin Y (5 mol %)	Air	70	42	13
D	One-pot (with the blue LED device) [b]	$Yb(OTf_3)$ (20 mol %)	Eosin Y (5 mol %)	Air	70	66	26
E	One-pot (with the blue LED device) [b]	$Yb(OTf_3)$ (20 mol %)	Rose Bengal (5 mol %)	Air	70	16	24
F	One-pot (conventional batch) [a]	I_2 (2.0 mmol)	-	I_2 (2.0 mmol)	80	72	Not detected
G	One-pot (conventional batch) [a]	$BF_3{\cdot}OEt_2$ (20 mol %)	$CoBr_2$ (5 mol %)	-	80	24	Not detected

[a] Reaction conditions: **1a** (1.0 mmol), **2a** (1.0 mmol), **3a** (1.0 mmol), GBB-catalyst (20 mol % or 2.0 mmol), oxidation-catalyst (5 mol % or none), CH_3CN (2.0 mL), under air.
[b] Reaction conditions: **1a** (1.0 mmol), **2a** (1.0 mmol), **3a** (1.0 mmol), GBB-catalyst (20 mol %), oxidation-catalyst (5 mol %), CH_3CN (2.0 mL), blue LED light irradiation under air.

In order to avoid any interactions between the reagents and the catalyst, we designed a sequential protocol. We first prepared the GBB **4a** and, without purifying the GBB-crude, we added the second catalyst (oxidation step) and submitted the crude under the reported oxidative conditions. In all those cases, we obtained the final compound with more than 13% yield. For the entry H, the pure product was obtained with similar yield to the Entry A, but the conversion was notably increased and the reaction time was reduced. We observed that either using the Lewis Acid $Yb(OTf)_3 \cdot H_2O$ or TFA for the GBB-adduct formation, similar yields were obtained. However, the most remarkable difference remained on the use of $CoBr_2$ as catalyst for the oxidative process.

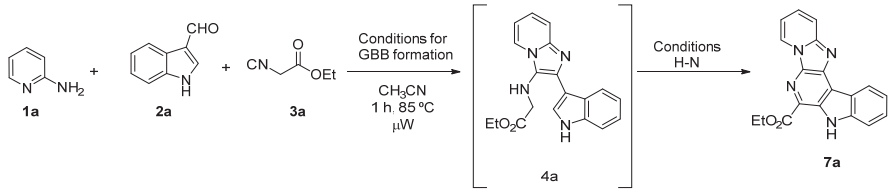

Entry	Protocol	GBB-catalyst (amount)	Oxidation-catalyst (amount)	Oxidant	Temperature (ºC)	Time (h)	Isolated Yield of **7a** (%)
H	Sequential (conventional batch) [a]	$Yb(OTf_3)$ (20 mol %)	$CoBr_2$ (5 mol %)	Air	80	48	38
I	Sequential (conventional batch) [a]	TFA (20 mol %)	$CoBr_2$ (5 mol %)	Air	80	72	25
J	Sequential (with the blue LED device) [b]	TFA (20 mol %)	$Ru(BPY)_3$ (5 mol %)	Air	70	16	13
K	Sequential (with the blue LED device) [b]	$Yb(OTf_3)$ (20 mol %)	Eosin Y (5 mol %)	Air	70	42	14
L	Sequential (with the blue LED device) [b]	TFA (20 mol %)	Eosin Y (5 mol %)	Air	70	16	15
M	Sequential (with the blue LED device) [b]	TFA (20 mol %)	Eosin Y (5 mol %)	Air	70	60	23
N	Sequential (conventional batch)	$Yb(OTf)_3 \cdot H_2O$	-	IBX (2.0 mmol)	80	5	22 (from a complex crude mixture)

[a] Reaction conditions: crude mixture **4a**, oxidation-catalyst (5 mol %) under air.
[b] Reaction conditions: crude mixture **4a**, oxidation-catalyst (5 mol %), blue LED light irradiation under air.

Finally, we performed a variation of the sequential protocol, isolating the GBB-adduct **4a** in order to simplify the crude mixture. The GBB adduct was submitted to the conditions O-S. Overall, we observed that $CoBr_2$ gave **7a** with the best yield, and, importantly, allowed to decrease the reaction time of A from 72 to 32 hours.

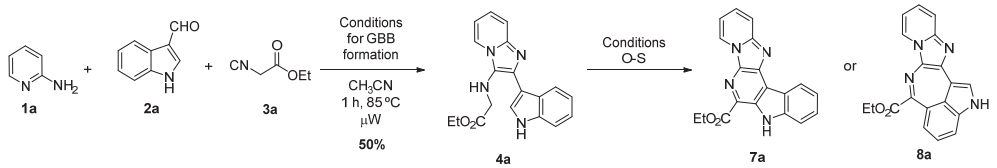

Entry	Protocol	GBB-catalyst (amount)	Oxidation-catalyst (amount)	Oxidant	Temperature (ºC)	Time (h)	Isolated Yield of **7a** (%)
O	Stepwise (with the blue LED device) [a]	$Yb(OTf_3)$ (20 mol %)	Rose Bengal (5 mol %)	Air	70	32	16
P	Stepwise (with the blue LED device) [a]	$Yb(OTf_3)$ (20 mol %)	Eosin Y (5 mol %)	Air	70	32	detected
Q	Stepwise (conventional batch) [b]	$Yb(OTf_3)$ (20 mol %)	$CoBr_2$ (5 mol %)	Air	80	32	41
R	Stepwise (conventional batch) [b]	$Yb(OTf_3)$ (20 mol %)	-	I_2 (2.0 mmol)	80	32	11 (and 28 of **8a**)
S	Stepwise (conventional batch) [b]	$Yb(OTf_3)$ (20 mol %)	-	I_2 (3.0 mmol)	80	32	detected

[a] Reaction conditions: crude mixture **4a**, oxidation-catalyst (5 mol %), blue LED light irradiation under air.
[b] Reaction conditions: crude mixture **4a**, oxidation-catalyst (5 mol % or 2.0 mmol) under air.

2.1.2. Oxidative Extended GBB leading to Compound 7f

To increase the yield in the formation of compound **7f**, we designed a set of reactoions with 2,4-diaminopyrimide **1f**, the isocyanide **3a** and indole carbaldehyde **2a** as shown in the table below.

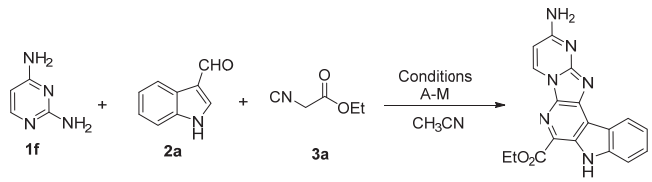

Entry	Protocol	Solvent	GBB-catalyst (amount)	Oxidation-catalyst (amount)	Oxidant	Temperature (ºC)	Time (h)	Yield*
A	One-pot (conventional batch) [a]	CH_3CN	$Yb(OTf_3)$ (20 mol %)	-	Air (O_2)	80	27	27
B	One-pot (conventional batch) [a]	CH_3CN/DCE (5 : 1)	$Yb(OTf_3)$ (20 mol %)	-	Air (O_2)	80	96	>50[c]
C	One-pot (conventional batch) [a]	EtOH	$Yb(OTf_3)$ (20 mol %)	-	Air (O_2)	80	96	13
D	One-pot (conventional batch) [a]	CH_3CN	$Yb(OTf_3)$ (20 mol %)	-	Air (O_2)	80	48	53
E	One-pot (conventional batch) [a]	CH_3CN	$Yb(OTf_3)$ (20 mol %)	-	Air (O_2)	80	96	44
F	One-pot (conventional batch) [b]	CH_3CN	$Yb(OTf_3)$ (20 mol %)	-	Air (O_2)	80	72	58
G	One-pot (μW, 100 W) [a]	CH_3CN	$Yb(OTf_3)$ (20 mol %)	-	Air (O_2)	120	1	-
H	One-pot (conventional batch) [a]	CH_3CN	$Yb(OTf_3)$ (20 mol %)	$CoBr_2$ (5 mol %)	Air (O_2)	80	96	42
I	One-pot (conventional batch) [a]	CH_3CN	$Yb(OTf_3)$ (20 mol %)	$CoBr_2$ (10 mol %)	Air (O_2)	80	96	2
J	One-pot (conventional batch) [a]	CH_3CN	$Yb(OTf_3)$ (20 mol %)	$CoBr_2$ (25 mol %)	Air (O_2)	80	27	traces
K	One-pot (conventional batch) [a]	CH_3CN	$Yb(OTf_3)$ (20 mol %)	CuCl (10 mol %)	Air (O_2)	80	96	48
L	One-pot (conventional batch) [a]	CH_3CN/EtOH (3 : 1)	$Yb(OTf_3)$ (20 mol %)	$FeCl_3$ (10 mol %)	Air (O_2)	96	24	traces
M	One-pot (conventional batch) [a]	CH_3CN	$Yb(OTf_3)$ (20 mol %)	-	IBX (0.4 mmol)	27	24	-

* Estimated Yield (HPLC, with internal standard).
a Reaction conditions: **1f** (0.2 mmol), **2a** (0.2 mmol), **3a** (0.2 mmol), CH_3CN (4.0 mL).
b Reaction conditions: **1f** (0.2 mmol), **2a** (0.2 mmol), **3a** (0.4 mmol), CH_3CN (4.0 mL).
c An unidentified peak overlapped the signal (checked by HPLC/MS), the estimated yiled should be over 50%.

Experimental Protocol. 0.2 mmol of each component (diaminopyrimidine **1f**, indole aldehyde **2a** and isocyanide **3a**) were dissolved in the indicated solent (4 mL), the catalyst(s) and the oxidant were added and the reaction was conducted under the stated conditions for the given reaction time. Afterwards, a sample was collected, suitably diluted and mixed with a known amount of an 4-iodotoluene (as an internal standard) and analysed by HPLC in reverse phase. (HPLC: Agilent 1100 Series; Column: SunFire C18 3.5 μm, 4.6 ×100mm; mobile phase: H_2O + 0.045% TFA / ACN + 0.036% TFA. Gradient from 20% ACN to 100% ACN in 30'. Flow rate: 1 mL/min; Injection: 5-15 μL.

It can be concluded that meaningful variations arise from the analysed reaction conditions. The results are in line with previous observation (**7f** being isolated in 26% in a $Yb(OTf)_3$ catalyzed reaction under air in ACN for 24 h), although variations in the concentration of the reactants modify the yield. In agreement with previous experience, IBX (entry M), $FeCl_3$ (entry L), the reaction conducted under microwave activation (entry G) and in EtOH (entry C)) were not productive. With respect to the processes catalysed by $CoBr_2$, they were productive at 5% (entry H, 42%), but the yields dramatically dropped with higher catalyst contents (entries I, J). Also CuCl at 5% produced respectable yields (entry K, 48%). Finally, the spontaneous air oxidation process (entry A, 27%) showed an increased productivity with longer reaction times (entries D and E; 54 and 44 % respectively) and by addition of an excess of isocyanide (entry F; 58%). Interestingly, the use of DCE as cosolvent (entry B) under spontaneous air oxidation conditions cleanly afforded the compound in significantly high yield (>50%, estimated), in line with the observed autooxidation of glycine derivatives.[16]
Taken together, the above results strongly support that a specific, case-by-case optimization of the reaction conditions may substantially improve the productivity of a given MCR with distinct reactant combinations.

2.1.3. Non-Oxidative Extended GBB leading to the series 11 and 12

The reactions with 2-indole carboxaldehyde **2l** to synthesize the corresponding GBB adduct (entries A and B) always led to the formation of **11a** and no GBB adduct was detected. Due to the low nucleophilicity of the isocyanide **3a,** reactions at rt were not as productive.

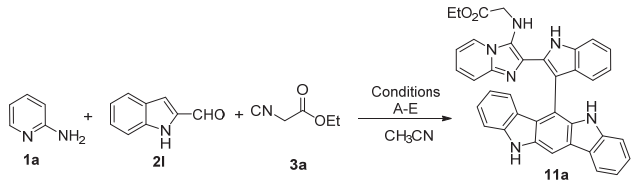

Entry	Protocol	Catalyst (amount)	Ratios of reactants **1a: 2l: 3a**	Temperature (ºC)	Time (h)	Isolated Yield of **11a** (%)
A	One-pot (μW)[a]	$Sc(OTf_3)$ (20 mol %)	1:1:1	85	1	complex crude (**11a** detected and isolated in small amounts)
B	One-pot	$Sc(OTf_3)$ (20 mol %)	1:1:1	rt	24	complex crude (**11a** detected)
C	One-pot	$Yb(OTf_3)$ (20 mol %)	1:3:1	85	18	25
D	One-pot	$Yb(OTf_3)$ (20 mol %)	1:3:1	rt	72	traces
E	One-pot (μW)[b]	$Yb(OTf_3)$ (20 mol %)	1:3:1	85	1:30	21

[a] Reaction conditions: Power: 100 Watts.
[b] Reaction conditions: Power: 150 Watts.

The reactions with 2-indole carboxaldehyde **2l** to synthesize the indolocarbazole **11b**, also led to the formation of the isomer **12** as the side product once the reaction temperature was increased.

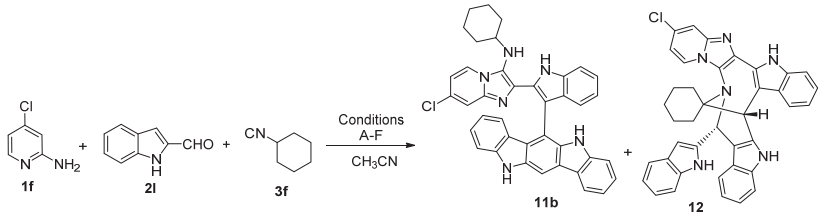

Entry	Protocol	Catalyst (amount)	Ratios of reactants **1f: 2l: 3f**	Temperature (ºC)	Time (h)	Isolated Yield of **11b** (%)	Isolated Yield of **12** (%)
A	One-pot (μW)[a]	$Yb(OTf_3)$ (20 mol %)	1:3:1	85	50 min	18%	detected
B	One-pot (μW)[b]	$Yb(OTf_3)$ (20 mol %)	1:3:1	110	90 min	9%	28%
C	One-pot (μW)[a]	$Yb(OTf_3)$ (20 mol %)	1:3:1	80	60 min	22%	detected
D	One-pot MS 4A	$Yb(OTf_3)$ (20 mol %)	1:3:1	rt	72	33%	not detected
E	One-pot (μW)[b]	$Yb(OTf_3)$ (20 mol %)	1:3:1	110	2	26%[c]	32%[c]
F	One-pot (μW)[b]	$Yb(OTf_3)$ (20 mol %)	1:3:1	110	2	-	16%[d]

[a] Reaction conditions: Power: 100 Watts.
[b] Reaction conditions: Power: 150 Watts.
[c] Contained traces of impurities.
[d] As a result of a second column chromatography and washings to obtain the analytically pure sample, the isolated yield may not be representative

2.2. The Reaction Scope

Inputs used in the extended GBB processes

α-Aminoazines (**1a-1g**):

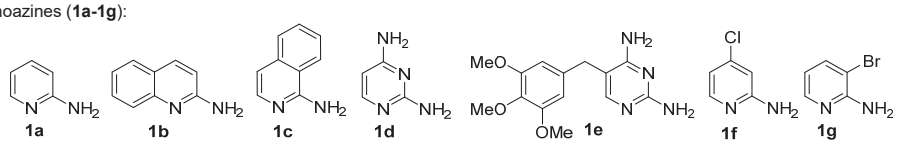

Aldehydes (**2a-2p**):

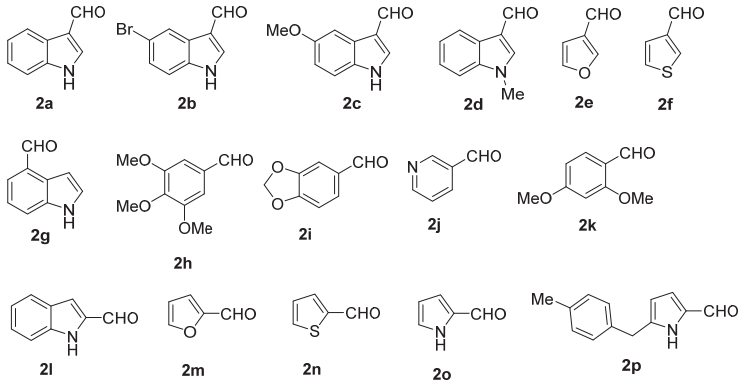

Isocyanides (**3a-3i**):

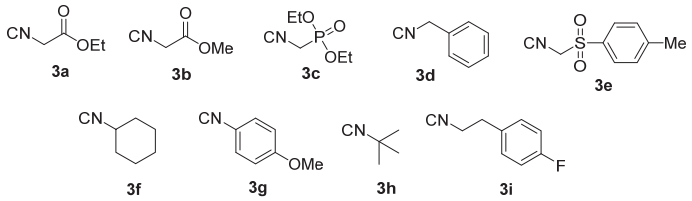

2.3.3. General Procedure B: Stepwise Formation of 7 through a $CoBr_2$-mediated Oxidation

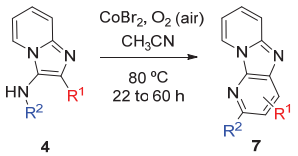

Into a solution of GBB-adduct **4** (1.0 Eq.) in CH_3CN (0.5 M) was added 5% mmol of $CoBr_2$ in a vial at room temperature. The reaction mixture stirred at 80 ºC for 22 to 60 hours. After TLC or LC-MS confirmed reaction completion, the solvent was evaporated and CH_2Cl_2 was added until everything was dissolved. The crude was treated with saturated $NaHCO_3$ aqueous solution and extracted with CH_2Cl_2 (3 x 15 mL). The combined organic layer was washed with brine, dried over $MgSO_4$, filtered and evaporated under reduced pressure. The pure products **7** were obtained by flash chromatography using the indicated solvent system.

2.3.4. General Procedure C: Stepwise Formation of 7 or 8 through a I_2-mediated Oxidation

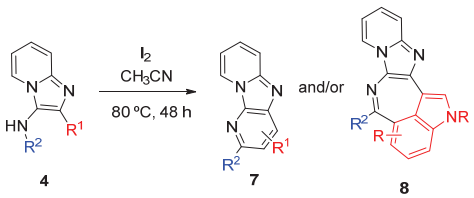

The GBB adduct **4** (1.0 Eq.) was mixed with I_2 (2.0 Eq.) and dissolved in CH_3CN (0.15 M) in a vial at room temperature, together with molecular sieves 4A. The reaction mixture was heated at 80 ºC for 48 hours. After reaction completion was confirmed by TLC or LC-MS, the crude was filtered through Celite. The filtrate was treated with saturated $Na_2S_2O_3$ aqueous solution, until a change in mixture color was observed, and extracted with CH_2Cl_2 (3 x 15 mL). The combined organic layer was dried over $MgSO_4$, filtered and evaporated under reduced pressure. The pure products **7** and/or **8** were obtained by flash chromatography using the indicated solvent system.

2.3.5. General Procedure D: Spontaneous One-pot Formation of 7

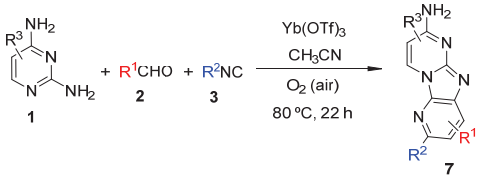

A solution of α-amino-azine **1** (**1a-e**, 1.0 mmol) and aldehyde (**2a**, 1.0 mmol) in CH_3CN (2.0 mL, 0.5 M) was added into a Schlenk vessel, followed by the addition of $Yb(OTf)_3 \cdot H_2O$ (20%) at room temperature. After 10 min, the suitable isocyanide (**3a-3d**, 1.0 mmol) was added to the stirring reaction mixture; the vessel was closed and heated to 80 ºC for 22 hours. After reaction completion (TLC or LC-MS control), the solvent was evaporated and CH_2Cl_2 was added until everything was dissolved. The mixture was treated with saturated $NaHCO_3$ aqueous solution to basic pH and extracted with CH_2Cl_2 (3 x 15 mL). The combined organic layer was washed with brine, dried over $MgSO_4$, filtered and evaporated under reduced pressure. The pure product **7** was obtained by flash chromatography using the indicated solvent system.

2.3.6. General Procedure E: One-pot Formation of 7 through a $CoBr_2$-mediated Oxidation

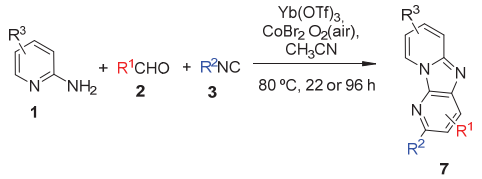

A solution of α-amino-azine (**1a-e**, 1.0 mmol) and aldehyde (**2a-p**, 1.0 mmol) in CH_3CN (2.0 mL, 0.5 M) was added into a Schlenk vessel, followed by the addition of $Yb(OTf)_3 \cdot H_2O$ (20%) and $CoBr_2$ (5%) at room temperature. After 10 min, the suitable isocyanide (**3a-i**, 1.0 mmol) was added to the stirring reaction mixture; the vessel was closed and heated to 80 ºC for 24 or 96 hours. After TLC or LC-MS confirmed reaction completion, the solvent was evaporated and CH_2Cl_2 was added until everything was dissolved. The crude was treated with saturated $NaHCO_3$ solution until basic pH and extracted with CH_2Cl_2 (3 x 15 mL). The combined organic layer was washed with brine, dried over $MgSO_4$, filtered and evaporated under reduced pressure. The pure product **7** was obtained by flash chromatography using the indicated solvent system.

2.3.7. Special Case: Synthesis of GBB-adducts 4 with Pyrrole Carboxaldehydes (4n-4o)

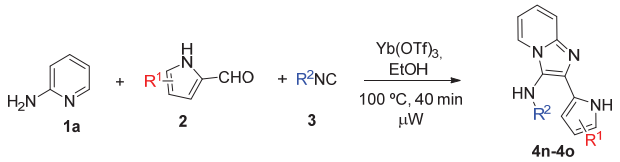

A solution of 2-aminopyridine **1a** (0.047 g, 0.5 mmol, 1.0 Eq.) and aldehyde (**2o** or **2p**, 0.5 mmol, 1.0 Eq.) in EtOH (0.5 mL) was added into a 2-10 mL microwave vial, followed by the addition of 20% mmol of $Yb(OTf)_3 \cdot H_2O$ (0.062 g, 0.1 mmol) at room temperature. After 10 min, the suitable isocyanide (**3a** or **3d**, 0.5 mmol, 1.0 Eq.) was added to the stirring reaction mixture; the vial was closed and heated to 100 ºC for 40 minutes under microwave irradiation (150 W). After reaction completion confirmed by LC-MS, the solvent was evaporated and the reidue was taken up in CH_2Cl_2. The crude was treated with saturated aqueous $NaHCO_3$ solution until basic pH and extracted with CH_2Cl_2 (3 x 20 mL). The combined organic layer was washed with water (3 x 20 mL), dried over $MgSO_4$, filtered and evaporated under reduced pressure. The pure compounds **4n** and **4o** was obtained by flash chromatography using the indicated solvent system.

2.3.8. General Procedure F: Synthesis of Indolocarbazoles 11a-e

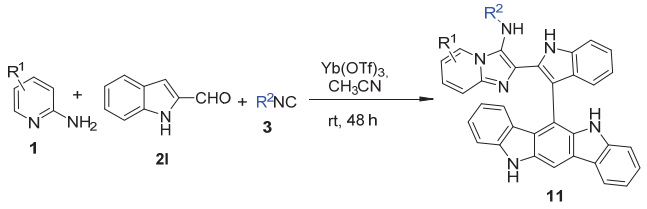

A mixture of α-amino-pyridine **1** (50 mg, 1 eq) and indole 2-carboxaldehyde (**2l**, 3 eq) in CH_3CN (0.10-0.15 M regarding the compound **1**) was added into a Schlenk vessel, followed by the addition of $Yb(OTf)_3$ H_2O (20%) and activated molecular sieves 4A at room temperature. After 10 min, the suitable isocyanide **3**, (1.0 eq) was added to the reaction mixture under stirring; the vessel was closed and was left stirring over 48 to 72 hours at given temperature. After TLC or LC-MS confirmed reaction completion, or its evolution was stopped, the mixture was concentrated under reduced pressure to a syrup consistency. The crude was taken up in AcOEt and was filtered through a short pad of celite. The mixture was treated with saturated aqueous $NaHCO_3$ solution until basic pH and extracted with AcOEt (3 x 15 mL). The combined organic layers were washed with brine, dried over $MgSO_4$, filtered and evaporated under reduced pressure. The pure products **11** were obtained by flash chromatography using the indicated solvent system.

2.3.9. Special Case: Synthesis of bicyclic-adduct 12

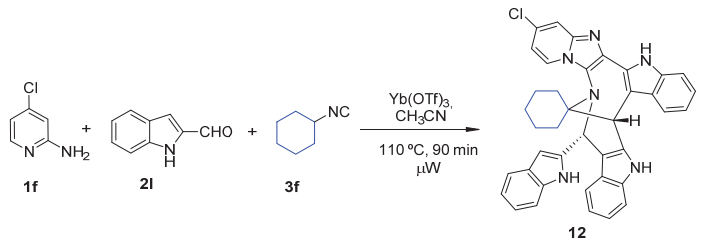

A solution of 2-aminopyridine **1f** (0.100 g, 0.778 mmol, 1eq.) and indole 2-carboxaldehyde (**2l**, 2.33 mmol, 3.0 eq.) in CH_3CN (3.8 mL, 0.2 M regarding **1f**) was added into a microwave vial, followed by the addition of $Yb(OTf)_3 \cdot H_2O$ (0.099 g, 20 mol %) at room temperature. After 10 min, cyclohexyl isocyanide (**3f**, 0.097 mL, 0.77 mmol, 1.0 eq,) was added to the stirring reaction mixture; the vial was closed and heated to 110 ºC for 90 min under microwave irradiation (150 W). An additional 30-minute cycle was added in some cases until the aldehyde **2l** was confirmed to be consumed by TLC. The solution was then concentrated under reduced pressure to a syrup consistency and AcOEt was added until everything was dissolved. The mixture was treated with saturated $NaHCO_3$ aqueous solution to basic pH and extracted with AcOEt (3 x 15 mL). The combined organic layer was washed with brine, dried over $MgSO_4$, filtered and evaporated under reduced pressure. The pure product **12** was obtained by flash chromatography using the indicated solvent system (Extraction with CH_2Cl_2 gave similar results.)

3.3. Final Compounds

3.3.1. Series 7

Ethyl 8*H*-pyrido[1'',2'':1',2']imidazo[4',5':5,6]pyrido[3,4-*b*]indole-7-carboxylate (7a)

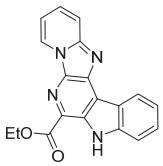

Following the *General Procedure B*, compound **7a** was obtained as a yellow solid (0.040 g, 81%) from GBB adduct **4a** (0.050 g, 0.15 mmol) and $CoBr_2$ (0.002 g, 0.025 mmol) in 0.30 mL of CH_3CN, after heating for 36 hours. The crude mixture was purified by flash chromatography using AcOEt/Hexane (gradient from 30:70 to 70:30, v/v) as solvent system. ^{1}H NMR (400 MHz, DMSO-d_6) δ 11.90 (s, 1H), 9.11 (d, *J* = 6.8 Hz, 1H), 8.53 (d, *J* = 7.6 Hz, 1H), 7.93 (d, *J* = 8.3 Hz, 2H), 7.82 (dd, *J* = 9.2, 6.7 Hz, 1H), 7.63 (dd, *J* = 8.3, 7.1 Hz, 1H), 7.41 (dd, *J* = 8.0, 7.1 Hz, 1H), 7.23 (t, *J* = 6.7 Hz, 1H), 4.59 (q, *J* = 7.1 Hz, 2H), 1.49 (t, *J* = 7.1 Hz, 3H). ^{13}C NMR (101 MHz, DMSO-d_6) δ 165.51, 150.44, 140.71, 135.22, 134.38, 134.22, 132.76, 127.74, 125.69, 122.74, 122.59, 120.36, 119.71, 118.72, 117.28, 113.01, 112.19, 61.01, 14.49. HRMS: m/z calcd for $C_{19}H_{15}N_4O_2^+$ $[M+H]^+$: 331.1190; found 331.1499. The compound structure was confirmed by X-Ray crystallography.

The titled compound was also obtained following the *General Procedure C*, leading to a mxiture of **7a** (22%) and **8a** (55%). Furthermore, the preparation of **7a** was used as model reaction during the optimization experiments. See all the tested conditions in *2.1. Optimizing Reaction Conditions*.

Diethyl (8*H*-pyrido[1'',2'':1',2']imidazo[4',5':5,6]pyrido[3,4-*b*]indol-7-yl)phosphonate (7b)

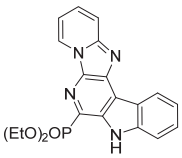

Following the *General Procedure B*, compound **7b** was obtained as a yellow powder (0.018 g, 23%) from GBB adduct **4b** (0.080 g, 0.20 mmol) and $CoBr_2$ (0.004 g, 0.020 mmol) in 0.5 mL of CH_3CN, after heating for 92 hours. ^{1}H NMR (400 MHz, $CDCl_3$) δ 10.48 (s, 1H), 9.04 (s, 1H), 8.78 (s, 1H), 7.90 (s, 1H), 7.63 (d, *J* = 7.0 Hz, 3H), 7.43 (s, 1H), 7.05 (t, *J* = 6.6 Hz, 1H), 4.48 – 4.28 (m, 2H), 4.22 (dq, *J* = 10.0, 7.2 Hz, 2H), 1.38 (t, *J* = 7.1 Hz, 6H). ^{13}C NMR (101 MHz, $CDCl_3$) δ 140.17, 131.80, 128.43, 125.37, 125.32, 124.34, 120.76, 120.72, 119.15 (d, *J* = 9.4 Hz), 117.96, 111.81, 111.58, 111.58, 63.51 (d, *J* = 5.2 Hz), 16.49 (d, *J* = 6.2 Hz). Three signals were not detected, probably quaternary Cs, due to the presence of phosphorus atom. HRMS: m/z calcd for $C_{20}H_{20}N_4O_3P^+$ $[M+H]^+$: 395.1268; found 395.1263.

The titled compound was also obtained following the *General Procedure E*, starting with 30 mg of **1a** and leading to **7b** with 18% yield (0.022 g).

3.3.2. Series 8

Ethyl 2*H*-pyrido[1'',2'':1',2']imidazo[4',5':6,7]azepino[5,4,3-*cd*]indole-6-carboxylate (8a)

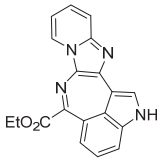

Following the *General Procedure C,* compound **8a** was obtained as a dark red powder (0.054 g, 55%) from GBB adduct **4a** (0.100 g, 0.29 mmol) and I_2 (0.062 g, 0.60 mmol) in 2.0 mL of CH_3CN, after heating for 48 hours. The crude mixture was purified by flash chromatography using AcOEt/Hexane (gradient from 0:100 to 50:50, v/v) as solvent system. ^{1}H NMR (400 MHz, DMSO-d_6) δ 11.25 (d, *J* = 2.7 Hz, 1H), 8.04 (d, *J* = 6.7 Hz, 1H), 7.35 – 7.31 (m, 2H), 7.27 (dd, *J* = 8.9, 6.7 Hz, 1H), 7.10 (d, *J* = 8.3 Hz, 1H), 6.91 (t, *J* = 6.7 Hz, 1H), 6.83 (dd, *J* = 8.3, 7.5 Hz, 1H), 6.46 (d, *J* = 7.5 Hz, 1H), 4.33 (q, *J* = 7.1 Hz, 2H), 1.32 (t, *J* = 7.1 Hz, 3H). ^{13}C NMR (101 MHz, DMSO-d_6) δ 166.02, 150.01, 146.07, 138.26, 130.93, 128.14, 127.43, 125.99, 123.29, 122.92, 119.53, 119.01, 116.19, 115.42, 113.90, 112.47, 61.23, 13.98. HRMS: m/z calcd for $C_{19}H_{15}N_4O_2^+$ [M+H]$^+$: 331.1190; found 331.1189. For this compound, gCOSY and NOESY spectra were analyzed. The compound structure was confirmed by MicroED.

3.3.3. Series 9

Ethyl 4*H*-pyrido[1'',2'':1',2']imidazo[4',5':6,7]azepino[3,4,5-*cd*]indole-6-carboxylate (9a)

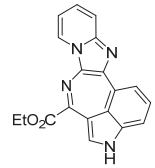

Following the *General Procedure E* and heating the reaction mixture for 24 hours, compound **9a** was obtained as a black solid (0.132 g, 40%) from 1.0 mmol **1a**, **2g** and **3a**. The crude mixture was purified by flash chromatography using CH_2Cl_2/MeOH (gradient from 100:0 to 99:1, v/v) as solvent system. ^{1}H NMR (400 MHz, DMSO-d_6) δ 11.70 – 11.54 (m, 1H), 8.12 (d, *J* = 6.8 Hz, 1H), 7.57 (d, *J* = 2.8 Hz, 1H), 7.42 (d, *J* = 8.9 Hz, 1H), 7.28 (dd, *J* = 9.0, 6.7 Hz, 1H), 7.12 (d, *J* = 7.2 Hz, 1H), 6.98 – 6.93 (m, 2H), 6.88 (dd, *J* = 8.3, 7.2 Hz, 1H), 4.31 (q, *J* = 7.1 Hz, 2H), 1.34 (t, *J* = 7.1 Hz, 3H). ^{13}C NMR (101 MHz, DMSO-d_6) δ 164.79, 147.49, 144.82, 137.59, 137.43, 129.96, 129.06, 127.20, 126.80, 124.60, 123.28, 116.78, 114.24, 113.95, 113.93, 112.27, 61.15, 14.01. HRMS: m/z calcd for $C_{19}H_{15}N_4O_2^+$ [M+H]$^+$: 331.1195; found 331.1190.

Methyl 8-amino-1*H*-pyrimido[1'',2'':1',2']imidazo[4',5':6,7]azepino[3,4,5-*cd*]indole-3-carboxylate (9b)

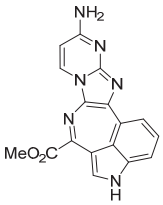

Following the *General Procedure D*, compound **9b** was obtained as a black solid (0.047 g, 5%) from 3.0 mmol of **1d** (0.330 g), **2g** (0.435 g), **3b** (0.297 mL) and $Yb(OTf)_3{\cdot}H_2O$ (0.322 g, 0.6 mmol) in 6.0 mL of CH_3CN. The crude mixture was purified by flash chromatography using CH_2Cl_2/MeOH (gradient from 100:0 to 98:2, v/v) as solvent system. ^{1}H NMR (400 MHz, DMSO-d_6) δ 11.49 (d, *J* = 2.9 Hz, 1H), 7.97 (d, *J* = 7.3 Hz, 1H), 7.51 (d, *J* = 2.9 Hz, 1H), 7.13 (s, 2H), 6.91 – 6.76 (m, 3H), 6.30 (d, *J* = 7.3 Hz, 1H), 3.79 (s, 3H). ^{13}C NMR (101 MHz, DMSO-d_6) δ 165.26, 159.53, 149.78, 145.03, 137.23, 136.26, 131.12, 130.47, 129.76, 126.71, 125.17, 124.47, 114.74, 113.24, 111.78, 101.03, 52.18. HRMS: m/z calcd for $C_{17}H_{13}N_6O_2^+$ [M+H]$^+$: 333.1095; found 333.1084.
For this compound, gCOSY and NOESY spectra were also analyzed.

3.3.4. Series 10

Ethyl 2,3,4-trimethoxypyrido[2',1':2,3]imidazo[4,5-*c*]isoquinoline-5-carboxylate (10a)

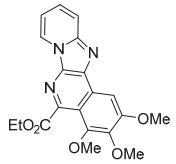

Following the *General Procedure C,* compound **10a** was obtained as a yellow solid (0.057 g, 36%) from GBB adduct **4q** (0.160 g, 0.41 mmol) and I_2 (0.210 g, 0.83 mmol) in 1.66 mL of CH_3CN, after heating for 22 hours. The crude mixture was purified by flash chromatography using AcOEt/Hexane (gradient from 30:70 to 100:0, v/v) as solvent system. ^{1}H NMR (400 MHz, $CDCl_3$) δ 8.88 (d, *J* = 6.8 Hz, 1H), 7.88 (s, 1H), 7.80 (d, *J* = 9.2 Hz, 1H), 7.52 (dd, *J* = 9.2, 6.7 Hz, 1H), 7.00 (t, *J* = 6.8 Hz, 1H), 4.56 (q, *J* = 7.2 Hz, 2H), 4.13 (s, 3H), 4.05 (s, 3H), 3.99 (s, 3H), 1.48 (t, *J* = 7.2 Hz, 3H). ^{13}C NMR (101 MHz, $CDCl_3$) δ 168.79, 157.76, 149.73, 147.37, 143.31, 141.56, 134.75, 132.20, 129.80, 128.18, 124.69, 117.80, 115.41, 111.76, 97.85, 62.10, 61.76, 61.26, 56.72, 14.35. HRMS: m/z calcd for $C_{20}H_{20}N_3O_5$ $[M+H]^+$: 382.1403; found 382.1403.

The titled compound was never obtained following the *General Procedure B*, neither with the use of other oxidant agents such as IBX.

3.3.5. Series 11

7-Chloro-*N*-cyclohexyl-2-(3-(5,11-dihydroindolo[3,2-*b*]carbazol-6-yl)-1*H*-indol-2-yl)imidazo[1,2-*a*]pyridin-3-amine (11b)

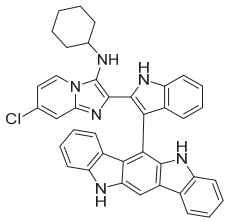

Following *General Procedure F,* compound **11b** was obtained as a yellow solid (0.095 g, 33%) from **1f** (0.050 g, 0.39 mmol), **2l** (1.17 mmol), **3f** (0.39 mmol) and $Yb(OTf)_3 \cdot H_2O$ (20%) in 3.8 mL of CH_3CN at rt for 72h. The crude mixture was purified by flash chromatography using Hexane/AcOEt (gradient from 0:100 to 50:50, v/v) as solvent system. ^{1}H NMR (400 MHz, DMSO-d_6) δ 11.87 (s, 1H), 11.22 (s, 1H), 10.30 (s, 1H), 8.27 – 8.21 (m, 2H), 7.76 (d, *J* = 7.4 Hz, 1H), 7.67 (d, *J* = 8.2 Hz, 1H), 7.58 (d, *J* = 2.1 Hz, 1H), 7.40 (d, *J* = 8.0 Hz, 1H), 7.33 – 7.24 (m, 2H), 7.18 (m, 2H), 7.10 (dd, *J* = 7.9, 6.7 Hz, 1H), 7.04 (d, *J* = 8.0 Hz, 1H), 6.95 (d, *J* = 7.8 Hz, 1H), 6.88 (dd, *J* = 7.9, 6.7 Hz, 1H), 6.72 (dd, *J* = 7.3, 2.1 Hz, 1H), 6.67 – 6.60 (m, 1H), 2.29 – 2.20 (m, 1H), 2.03 – 1.95 (m, 1H), 1.28 – 1.19 (m, 1H), 1.00 (t, *J* = 14.1 Hz, 2H), 0.92 – 0.84 (m, 1H), 0.77 (d, *J* = 12.3 Hz, 1H), 0.61 (d, *J* = 12.1 Hz, 1H), 0.51 (m, 1H), 0.32 (m, 1H), -0.04 – -0.19 (m, 2H). ^{13}C NMR (101 MHz, DMSO-d_6) δ 141.38, 141.33, 139.97, 136.82, 135.55, 134.24, 130.43, 129.99, 128.87, 128.28, 126.29, 125.38, 125.04, 124.36, 122.59, 122.43, 121.96, 121.86, 120.87, 120.22, 119.35, 119.17, 117.64, 117.10, 114.92, 112.55, 111.91, 111.17, 110.33, 110.07, 106.81, 99.98, 54.15, 31.75, 31.69, 24.47, 24.10, 23.88. One C signal was not detected. HRMS: m/z calcd for $C_{39}H_{32}N_6Cl$ $[M+H]^+$ 619.2371; found 619.2371.

The preparation of **11b** was used as model reaction during the optimization experiments. See all the tested conditions in *2.1. Optimizing Reaction Conditions*. Increasing the temperature leads to the higher conversion rates, yet it also promotes the formation of other isomers as compound **12** and more complex crudes.

3.3.6. Special Case: Compound 12

8'-Chloro-13'-(1*H*-indol-2-yl)-5',13',18',19'-tetrahydrospiro[cyclohexane-1,20'-[12,19]methanopyrido[1'',2'':1',2']imidazo[4',5':8,9]azonino[4,3-*b*:7,6-*b*']diindole] (12)

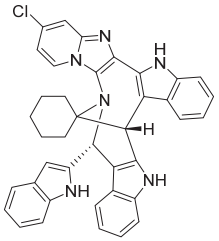

Compound **12** was obtained as a pale yellow solid (0.138 g, 28%) from **1f**, **2l** and **3f** as described in section **2.3.8**. The crude mixture was purified by flash chromatography using Hexane/AcOEt (gradient from 0:100 to 70:30, v/v) as solvent system. ^{1}H NMR (400 MHz, $CDCl_3$) δ 9.68 (s, 1H), 7.96 – 7.92 (m, 2H), 7.90 (d, *J* = 7.5 Hz, 1H), 7.55 (d, *J* = 7.9 Hz, 1H), 7.33 – 7.21 (m, 5H, overlapped with solvent signal), 7.13 (d, *J* = 8.0 Hz, 1H), 7.09 (d, *J* = 2.0 Hz, 1H), 7.03 (t, *J* = 7.4 Hz, 1H), 7.00 – 6.94 (m, 2H), 6.94 – 6.89 (m, 2H), 6.71 (d, *J* = 8.0, 1H), 6.62 (t, *J* = 7.6 Hz, 1H), 6.30 (d, *J* = 8.0 Hz, 1H), 6.27 (s, 1H), 6.03 (dd, *J* = 7.3, 2.1 Hz, 1H), 4.53 (s, 1H), 2.69 (d, *J* = 13.7 Hz, 1H), 2.28 – 2.17 (m, 1H), 1.95 – 1.88 (m, 2H), 1.84 – 1.64 (m, 3H), 1.57 – 1.17 (m, 7H, overlapped with non-polar impurities). ^{13}C NMR (101 MHz, $CDCl_3$) δ 141.98, 139.96, 136.56, 135.46, 134.67, 132.11, 131.14, 128.73, 128.54, 126.79, 125.87, 125.75, 123.49, 122.60, 122.43, 121.62, 120.44, 120.33, 120.00, 119.86, 118.93, 116.76, 114.03, 112.05, 111.64, 111.14, 110.86, 110.82, 106.18, 104.40, 101.57, 55.86, 54.72, 40.58, 34.85, 33.75, 26.42, 23.59, 21.97. HRMS: m/z calcd for $C_{39}H_{32}N_6Cl$ $[M+H]^+$ 619.2371; found 619.2368. The compound structure was confirmed by X-Ray crystallography.

4. Negative Results

All of the following GBB adducts were submited to the previously disscused conditions for the oxidative cascade. However, they did not yield the expected domino adducts, although in some cases traces of the corresponding oxidative adducts were detected by HPLC-MS. Likely because stability reasons (π excessive) or lack of reactivity (π deficient)

A. GBB adducts with heteroamatic aldehydes:

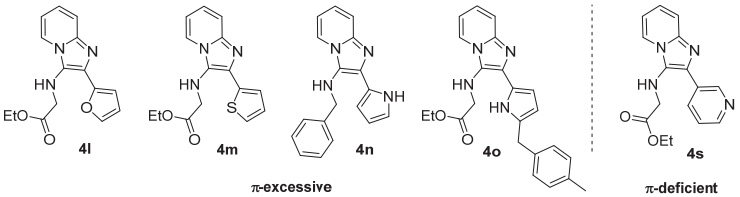

B. GBB adducts with electron-rich substituted benzaldehyde. Likely,the substitutens at the aromatic ring did not especially favor the cyclization upon the phenyl C6 position and the domino reaction did not proceeded further under the conditions tested.

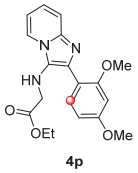

C. GBB adducts with isocyanides that do not lead to conjugated imines, did not proceed through the domino process:

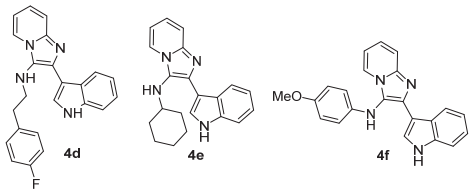

Furthermore, attempts to synthesyze GBB adducts with TOSMIC followig the described general procedures failed, persumably due to the weak nucleophilicity of the isocyanide component.

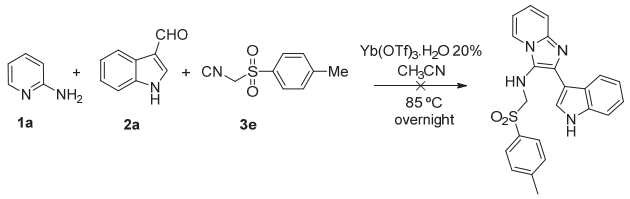

5. Mechanistic Studies

5.1. Studies on the Possible Mechanism for the Formation of Series 7

The key transformation of the initial GBB adducts **4** leading to scaffolds **7** (also **8-10**) involves and oxidation followed by a Pictet-Spengler cyclization and subsequent oxidation. The initial oxidation basically relates to the transformation of amines in the imines by formal loss of two hydrogen atoms and takes place with a variety of oxidizing reagents/catalysts. Those which, in principle can be compatible with aldehydes, aminoazines and isocyanides were chosen. In this way, IBX, $FeCl_3$, $CoBr_2$, CuI, I_2, several photoxoxidation catalysts, etc. were screened. A widely accepted mechanism for the oxidation starts with the generation of the N-centered radical cation which undergo further steps (proton, electron or H atom transfers) to reach the imine stage. In many cases the catalytic systems use O_2 as the stoichiometric oxidant. However, recently Huo and coworkers, disclosed the autoxidation of imines with atmospheric oxygen, through an intermediate hydroperoxide which evolves to the imine, under protic catalysis.[16] Likely, this can be the case in our transformations in the absence of added oxidants (open to air), and perhaps the Lewis acid may help in the oxidation, as well as catalyzing the Pictet-Spengler step. Consistenly, the more electron-rich substrates (diaminopyrimidines) are more easily oxidized under mild conditions. The generated dihydropyridine **6**, on the other hand, spontaneously evolves to the pyridine in an oxygen atmosphere, as it is well established in the field.

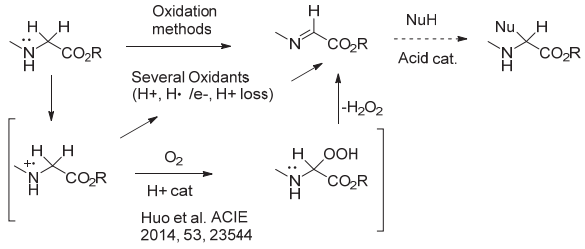

As a proof-of-concept of the suggested mechanism for the formation of compounds **7**, we performed the oxidation of the GBB-adduct **4a** step by step and isolated the intermediates **5a** and **6a**.

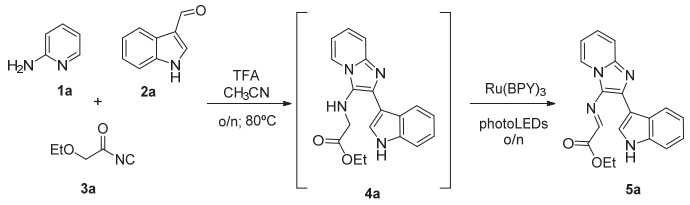

Following one of the test conditions used in *2.1. Optimizing Reaction Conditions*, a solution of 2-aminopyridine **1** (0.376 g, 4.0 mmol) and indole-3-carboxaldehyde (0.581 g, 4.0 mmol) in CH_3CN (8.0 mL, 0.5 M regarding **1**) was added into a Schlenk vessel, followed by the addition of 20 % of TFA (0.061 mL) at room temperature. After 10 min, ethyl isocyanoacetate (0.437 mL, 4.0 mmol) was added to the stirring reaction mixture; the vessel was closed and heated to 80 ºC for 14 hours. After GBB formation was confirmed by TLC, $Ru(BPY)_3$ (0.011 g, 5 mol %) was added and the mixture stirred under photoLED irradiation for additional 14 hours. Imine **5a** formation was confirmed by LC-MS. The solvent was evaporated under reduced pressure and CH_2Cl_2 was added until everything was dissolved. The mixture was treated with saturated $NaHCO_3$ aqueous solution to basic pH and extracted with CH_2Cl_2 (3 x 30 mL). The combined organic layer was washed with brine (60 mL), dried over $MgSO_4$, filtered and evaporated under reduced pressure. 0.150 g of the imine **5a** were obtained as yellow powder by flash chromatography, using AcOEt/Hexane (gradient from 50:50 to 100:0) as solvent system.

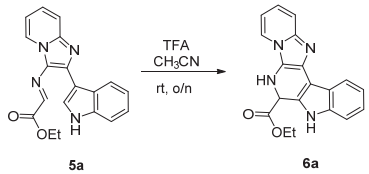

A vial under inert atmosphere was charged with a solution of imine **5a** (0.020 g, 0.060 mmol) in 1.0 mL of CH_3CN. Then, 2 mol % of TFA (0.092 μL) was added and the reaction mixture was left stirring for 14 hours at room temperature. DHP **6a** formation was confirmed by LC-MS. The solvent was evaporated under reduced pressure and CH_2Cl_2 was added until everything was dissolved. The mixture was treated with saturated $NaHCO_3$ aqueous solution to basic pH and extracted with CH_2Cl_2 (3 x 10 mL). The combined organic layer was washed with water (20 mL), dried over $MgSO_4$, filtered and evaporated under reduced pressure to obtain 0.020 g of crude **6a**. In the spectrum, we were able to detect two diagnostic signals, which corresponded to the CH (5.23 (d, *J* = 6.6 Hz, 1H)) and the NH (3.85 (d, *J* = 7.0 Hz, 1H) of the DHP ring.

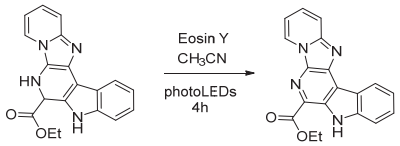

The DHP **6a** (0.020 g, 0.051 mmol) was dissolved in 1.0 mL of CH_3CN and 5 mol % of Eosin Y (0.002 g) was added to the solution. The reaction mixture was left stirring under photoLED irradiation for 4 hours. Formation of the product **7a** was confirmed by HPLC-MS. The solvent was evaporated under reduced pressure and CH_2Cl_2 was added until everything was dissolved. The mixture was treated with saturated $NaHCO_3$ aqueous solution until basic pH and extracted with CH_2Cl_2 (3 x 10 mL). The combined organic layer was washed with water (20 mL), dried over $MgSO_4$, filtered and evaporated under reduced pressure to obtain 0.022 g of 7**a**.

The compilation of ^1H NMR spectra in $CDCl_3$ shows the diagnostic signals of both isolated intermediates, the imine **5a** and the DHP **6a**.

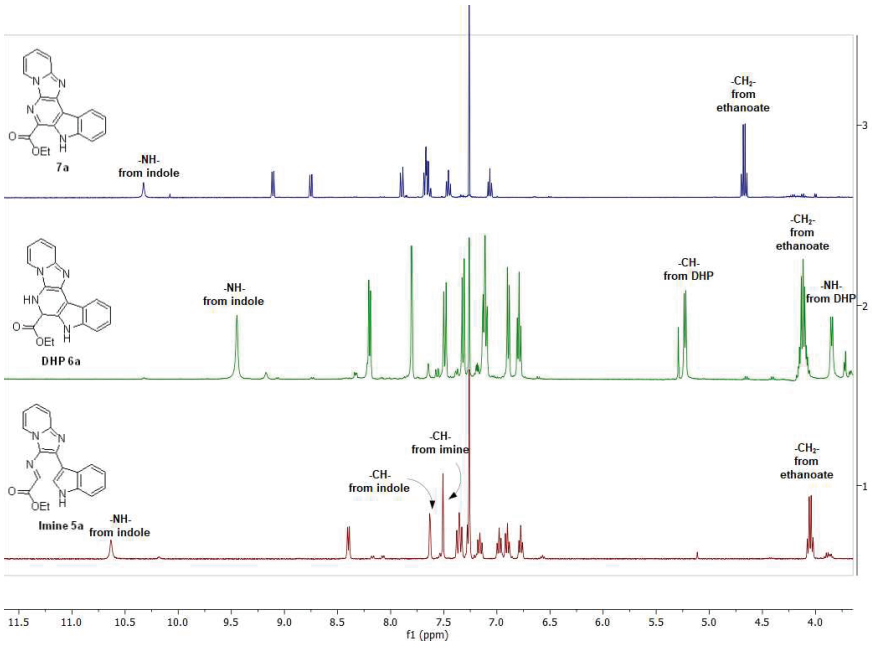

5.2. Mechanistic Considerations on Cyclization leading to carboline-type scaffolds 6

Mechanistically the transformation of GBB adducts **5** into carboline scaffolds **6** may proceed either via a Pictet-Spengler ionic reaction or through an electrocyclization followed by an isomerization (see Figure below). Although the vast majority of related processes in the literature involve phenethylamine and tryptamine derivatives, a few precedents dealing with analogous conjugated systems were described.[17,18] In these cases, although no specific mechanistic studies are mentioned, the reactions proceed through acid catalysis, perhaps favoring the PS route. However, these experiments do not rule out the concerted pathway.

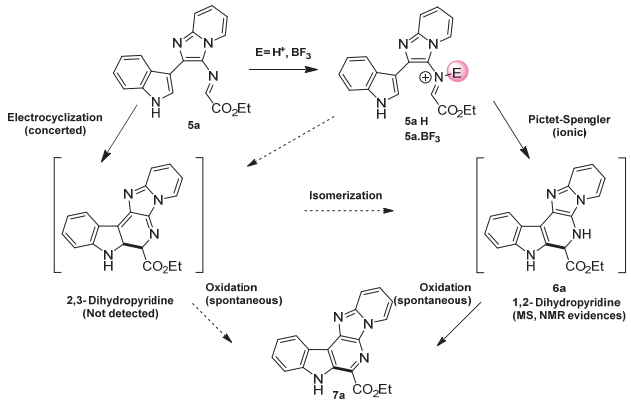

Additionally, the concerted route should initially give a 2,3-dihydropyridine (not detected), which may isomerize (tautomerization or [1,5 H] shift) to the observed 1,2-derivative. Little is known on the former compounds, but they should oxidize very fast to the corresponding pyridines. On the other hand, the PS route would directly yield the 1,2 dihydropyridine **6a** which was clearly detected by MS and NMR (See preceeding section).

Although no categorical evidences support one way or the other, based in our experience, the PS pathway seems to be more likely.

5.3. Tryptamine's Cyclization via Pictet-Spengler Condensation

The formation of 1,2,3,4-tetrahydro-β-carbolines via C-2 Pictet-Spengler cyclization is a well-known reaction which admits some variations. For instance, molecular iodine has been used as molecular catalyst or AcOH as solvent.[19,20] Moreover, catalytic aerobic oxidation conditions to obtain 3,4-dihydro-β-carbolines have been also described.[18] In contrast, azepino[5,4,3-*cd*]indoles via C-4 Pictet-Spengler condensation are unlikely to be obtained through this reaction, unless the C-4 position is somehow activated and the C-2 position already substituted.[21] Some methodologies such as a site-selective Pd-catalyzed olefination of tryptophan via C-H bond activation or a four-component domino reaction (ABC^2) have been developed as an alternative to access these azepino[5,4,3-*cd*]indole structures, in the same way that nature does.[22,23]

We planned a general reaction of tryptamine and *para*-chlorobenzaldehyde under the conditions described in section 2.2.4. *General Procedure C* to determine whether we obtain the Pictet-Spengler product resulting from the C-2 interaction, as in the cases described above, or from the C-4 interaction, as happened in **8**. The crude mixture was analyzed through HPLC-MS and ^{1}H NMR and was compared with the described spectra of the tetrahydrocarboline **A'**[24], harmaline **B'**[20] and carboline **C'**[25].

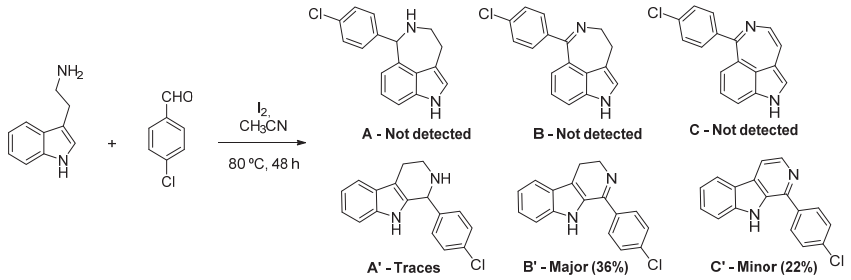

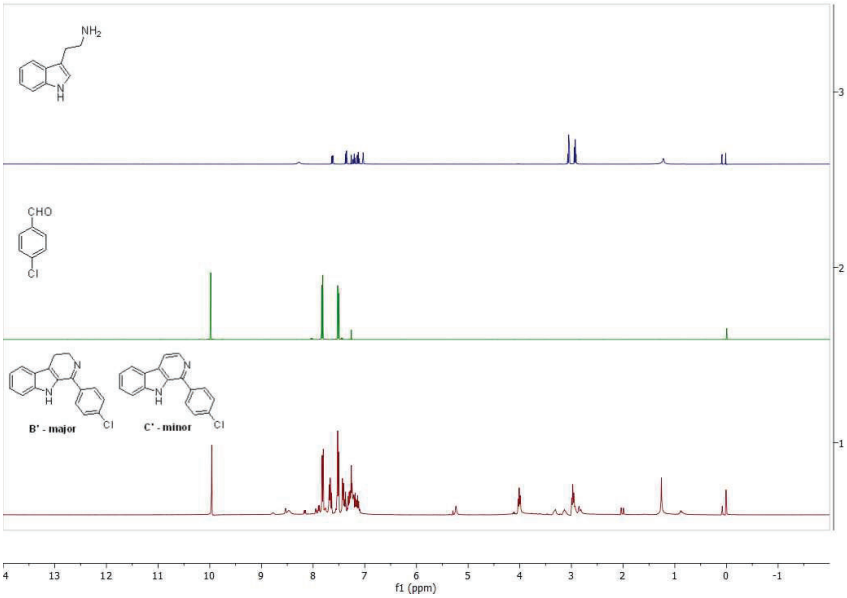

The MS analysis allowed us to detect just 2 isomers out of 6, with respective molecular masses of 281 and 279, the isomers formed corresponded to B/B' and C/C'. Through further ^{1}H NMR analyses we concluded that the products matched with structures **B'** and **C'**, being **B'** the major one. Furthermore the ^{1}H NMR spectrum showed traces of the Pictet-Spengler adduct **A'**, confirming the favored cyclization upon C2.

These results suggest that the presence of the imidazopyridine motif plays a key role in the formation of azepinoindoles through the Pictet-Spengler cyclization. Based on these empirical results we suggest the following mechanistic proposal based on the impact of different acid catalysts and their coordination modes to the imine **5a.**

5.4. Mechanistic Considerations on the Regioselective Formation of the Series 7 and 8

From the mechanistic point of view, we assume that this unique behavior of regioselective Pictet-Spengler cyclization upon indole C-4 and C-2 positions in the presence of different catalysts could be related to their interactions with the imines **5**. The hypothesis we suggest is that the coordination of the imine **5a** with different acids (H^+, BF_3 or I_2) may lead to active species with distinct conformational preferences, leading to different regioselectivities: Catalysts like H^+, BF_3 and $Yb(OTf)_3$ promote the standard cyclization to indole C-2, whereas Iodine coordination would promote cyclization upon the C-4 indole position.

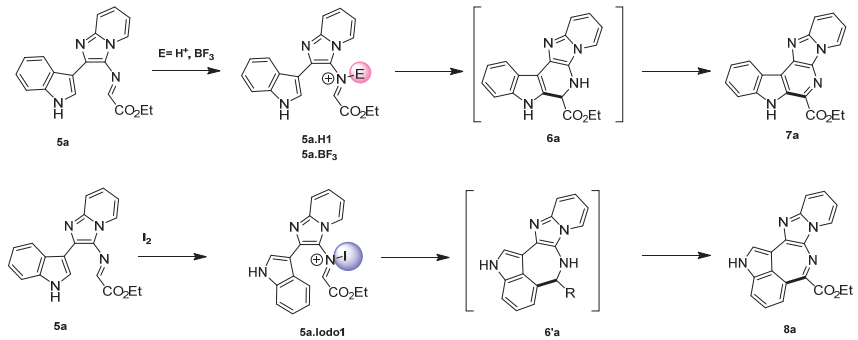

To preliminarily evaluate our hypothesis, we have modelled the following intermediates and adducts in a Spartan suite using molecular mechanics and semiempirical method). We built the structures and minimized them with molecular mechanics (MMFF) and semiempirical methods (PM3) and analyzed the equilibrium conformers. As shown below, the iminium ions derived from H^+, BF_3 and I_2 render different relative geometries regarding the imine bond and the indole moiety. The iodoiminium species **5a-Iodo1** is seemingly more prone to undergo cyclization upon indole C4 position because of its relative proximity.

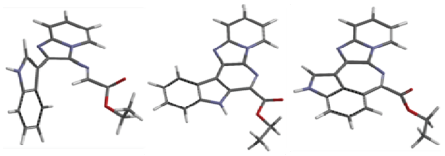

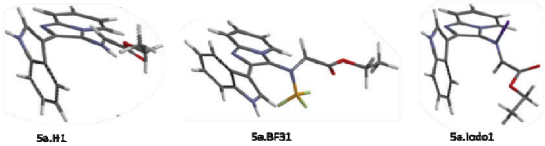

Therefore, we contemplated the conformational control of the differently activated iminium intermediates as a key factor to direct the cyclization upon the indole 2 or 4 positions. However, based on the experimental results with tryptamine (See section 5.2), we believe the abovementioned coordination of iodine to the imine may not be enough to afford the unconventional cyclization upon the indole C2 in any unbiased indole system. Thus, in our opinion, the possible contribution of the azole nitrogen atom should be taken into account. In other words, it is possibly the combined and/or dual effect of the azole activation by the Lewis acid together with the imine coordination that results in the observed regioselectivity. The iodine atom of the formed iodoiminium intermediate seemingly, restricts the free rotation of the structure and favors the indole C4 position due to spacial proximity. Other acid catalysts may fail to perform such conformational change and favor the conventional cyclization upon the position C2.

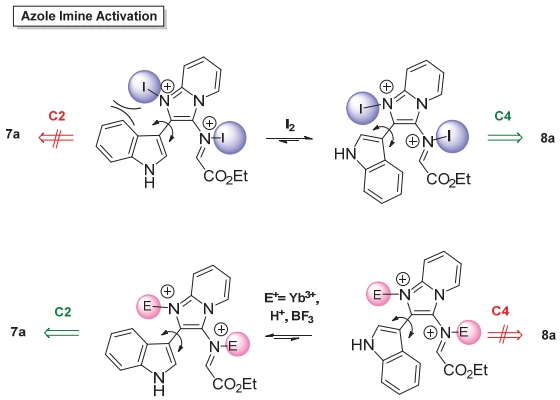

5.5. Mechanistical Considerations on the Formation of the Series 11 and Compound 12

Regarding the formation of indolocarbazoles **11**, when using aldehyde, azine, isocyanides in equimolar stoichiometries, almost no GBB was detected and compounds **11** were isolated in low yields (≈8-10%). When the stoichiometry was modified to supply all the indolecarbaldehyde needed (3 eqs), the yield rose to 25-30%, roughly triplicating the initial result. Our interpretation is that the GBB adduct, once formed, reacts more rapidly with two equivalents of the indole aldehyde present en route to the indolocarbazole. The domino reactions seem to be progressively faster and the putative intermediates could not be detected. Incidentally, no significant changes were observed in the yields of compounds **7** when using more than 1 equivalent of the aldehyde.

On the other hand, regarding the possibility of deprotonation of isocyanoacetates in these series (or in the processes leading to scaffods **7-10**) and the observation of alternative chemistries, the pKa of aminopyridine is around 6.8-7.2, which may lead to the typical isocyanoacetate chemistry. However, in the present studies we have not detected compounds arising for the deprotonation of the active methylene. We believe that with the set of inputs used, the GBB chemistry is followed by the oxidation and/or electrophilic interactions due to the indole moieties. Likely, these processes should override possible α-additions or dipolar interactions.

Based on the empirical findings about the temperature-dependent formation of compound **12** and the fact that compound **11b** was the only product detected in the reaction performed at rt, we first speculated the possibility of compound **11b** being the precursor of compound **12**. However, this hypothesis was ruled out as heating solutions of compound **11b** under described reaction conditions did not yield compound **12**, suggesting that the two isomers may have originated from independent routes.

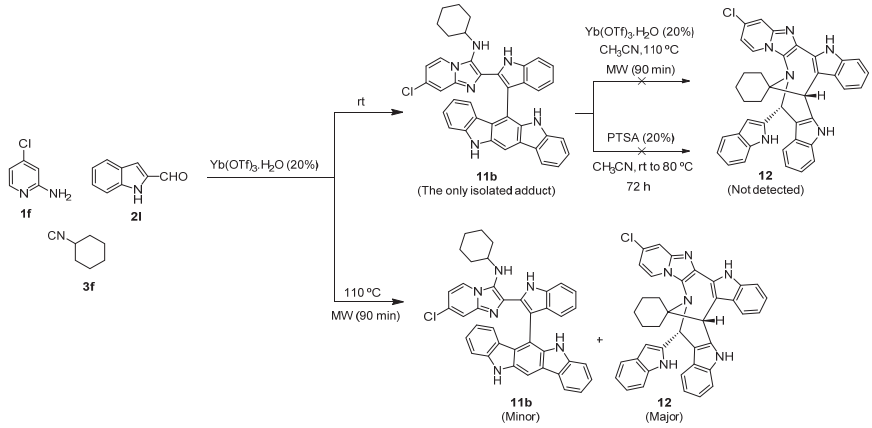

The generation of scaffold **12** is unprecedented and we lack basic understanding of several steps. Based on the proposed unified mechanism, we hypothesized that the key step in the formation of the bridged adduct **12** is a [1,2] Stevens rearrangement (see below): The common intermediate with the low-temparature pathway **M2** may evolve in this conditions through the generation of intermediate M**4** resulting from the hydroxyl displacement by the amino group, possibly through acid catalysis; and similarly, the quaternary ammonium salt **M5** would arise. The nature of the anion could not be determined, it could be a hydroxide or basic species generated in the medium and may act directly or through a relay mechanism. The ammonium salt may suffer the Stevens rearrangement, through deprotonation at the cyclohexyl methine to give a zwitterion **M6**. Presently, we have no explanation for the preference of this position, especially having much more acidic sites (NH, benzylic sites). Due to poor orbital alignment, it is difficult that a direct evolution from **M6** may lead to compound **12**. The generally established mechanism for the Stevens rearrangement (see ref 33 in the main text) suggests a caged diradical intermediate **M7** that would evolve by recombination to the final structure.

Due to the structure of the tetrasubstituted ammonium salt **M5**, several Stevens rearrangements can, in principle, take place. We preliminarily analyzed the likely pathways, mainly regarding the [1,2] and [2,3] rearrangements and believe that it is only the proposed pathway that yields compound **12** with the structures and stereochemistry confirmed by X-ray crystallography. Other routes either involve less favored intermediates or lead to (non-detected) more strained final adducts with distinct connectivities than the one found in compound **12** (see below).

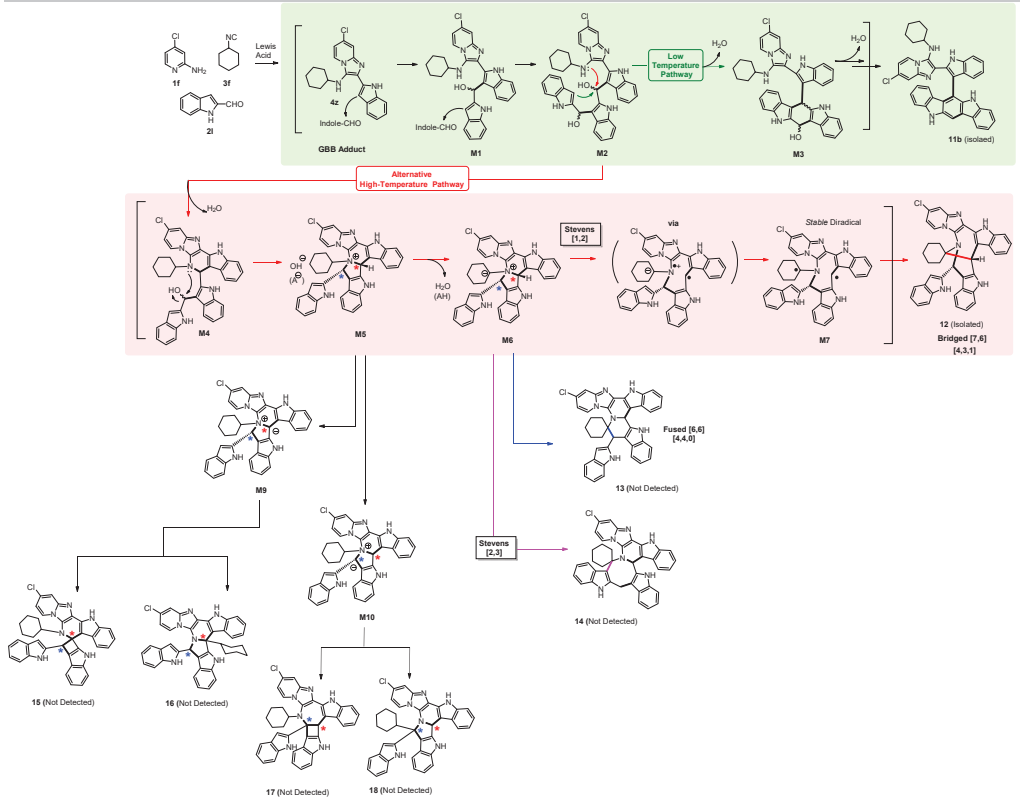

Based on the proposed unified mechanism (see figure above), the key step in the formation of the bridged adduct **12** is a [1,2] Stevens rearrangement, which due to the complexity of the dihydropyridinium salt **M5**, can take different pathways. We also preliminarily analyzed other possible pathways, to find that the proposed pathway leading to compound**12,** with the structure and stereochemistry confirmed by X-ray crystallography, is the most favored by the relative stability of the intermediates involved and/or the stability of the final adducts. Here we add some preliminary computational hints on a simplified model, supporting the proposed mechanism:

First, the intermediate cation derived from dehydration of **M4** has the suitable geometry at its minimum energy state to yield the observed stereochemistry in the chiral centers.

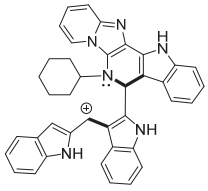

Intermediate cation from **M4**

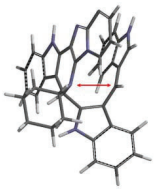

The quaternary ammonium salt **M5** was also built on the Spartan suite with the *cis* stereochemistry, as in the X-ray structure observed in compound **12**.

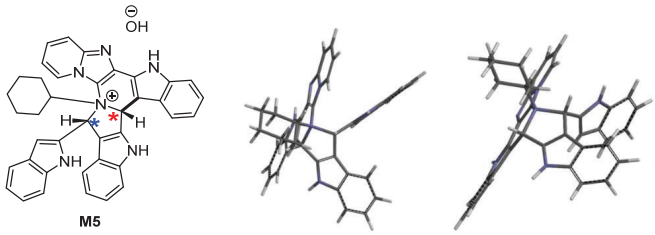

M5

Eventually, we calculated the energy levels of compound **12** and some alternative Stevens adducts to show that the isolated isomer is seemingly the more favored one in the computational level.

A) Isolated Scaffold **12: Stevens [1,2]**
Equilibrium Geometry (PM3)
Energy: 758.3671 kJ/mo

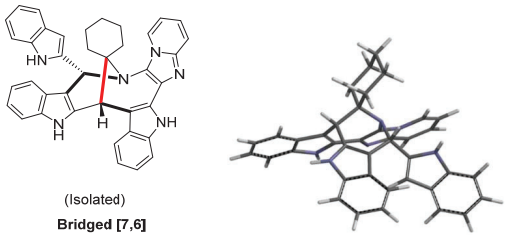

(Isolated)
Bridged [7,6]

B) **Alternative Stevens [1,2]**
Equilibrium Geometry (PM3)
Energy: 825.5678 kJ/mol

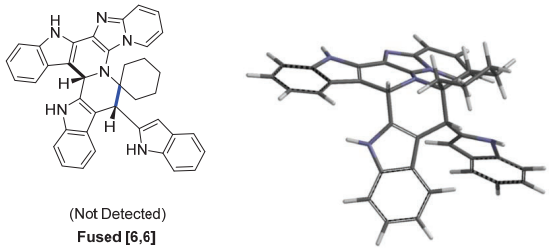

(Not Detected)
Fused [6,6]

c) **Alternative Stevens [2,3]**
Equilibrium Geometry (PM3)
Energy: 770.4453 kJ/mol kJ/mol

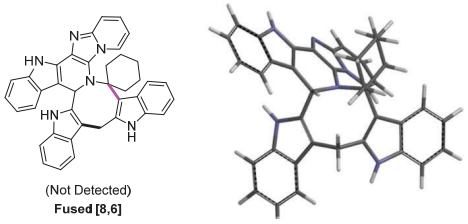

(Not Detected)
Fused [8,6]

6. Biological Assays

6.1. Cell culture

The AHR-knockdown human HaCaT keratinocytes (HaCaT-shAHR) and respective AHR-proficient empty vector control cells (HaCaT-EV) were generously provided by E. Fritsche (IUF Duesseldorf, Germany). The generation and validation of the genetically modified HaCaT cell-lines has been previously described.[26] HaCaT-EV and HaCaT-shAHR cells were cultured in DMEM (PAN Biotech, Aidenbach, Germany) supplemented with 10% (v/v) fetal bovine serum (Biochrom, Berlin, Germany), 1% (v/v) antibiotics/antimycotics (PAN Biotech), and 0.84 mg/ml G418 (Biochrom). The human XRE-HepG2 reporter cell-line was kindly gifted by K. Gradin and L. Poellinger (Karolinska Institute, Stockholm, Sweden). The cells were cultured in RPMI 1640 (PAN Biotech) containing 3.7 % $NaHCO_3$ (w/v), 10 % fetal bovine serum (v/v), 1 % (v/v) antibiotic/antimycotic solution, and 0.8 mg/ml G418. All cells were cultivated at 37 °C in a humidified atmosphere containing 5% CO_2.

6.2. 7-Ethoxyresorufin-*O*-deethylase (EROD) activity

Measurement of CYP1A enzyme activity in living monolayer cultures was carried out as described previously.[27] Data shown are from three independent experiments (mean ± S.E.M.), statistical analysis was preformed using 2-way ANOVA followed by Tukey's multiple comparison test. A *p*-value below 0.05 was considered as statistically significant.

6.3. Quantitative real-time PCR

Isolation of total RNA, reverse transcription, and quantitative real-time PCR was conducted as described previously.[27] Transcript level of CYP1 isoforms were normalized to GAPDH copy numbers. Data shown are from three independent experiments (mean ± S.E.M.), statistical analysis was preformed using 2-way ANOVA followed by Tukey's multiple comparison test. A *p*-value below 0.05 was considered as statistically significant.

6.4. Reporter gene assay

AHR-dependent reporter gene activity was determined in human HepG2 cells stably transfected with an XRE-harboring luciferase plasmid (XRE-HepG2 cells). The assay was carried out as described earlier. Luciferase activity was normalized to protein content. Data shown are from three independent experiments (mean ± S.E.M.), statistical analysis was preformed using uncorrected Fisher's LSD test. A *p*-value below 0.05 was considered as statistically significant.

7. Single Crystal X-Ray Analysis

Crystals suitable for single X-ray diffraction were grown by slow evaporation of water/CH_3CN mixtures, or slow diffusion of Et_2O or n-hexane into dichloromethane or chloroform solutions.

7.1. Compound 7a

7.1.1. Crystal Data and Structure Refinement

CCDC number	**2019590**
Crystal data	
Chemical formula	$C_{19}H_{14}N_4O_2 \cdot 2(H_2O)$
M_r	366.37
Crystal system, space group	Orthorhombic, *Pbca*
Temperature (K)	100
a, *b*, *c* (Å)	19.4393 (9), 8.1731 (4), 21.3678 (11)
V (Å^3)	3394.9 (3)
Z	8
Radiation type	Cu *Kα*
μ (mm^{-1})	0.86
Crystal size (mm)	0.4 × 0.02 × 0.02
Data collection	
Diffractometer	Bruker *APEX*-III CCD
Absorption correction	Multi-scan *SADABS2016*/2 (Bruker,2016/2) was used for absorption correction. wR2(int) was 0.1363 before and 0.0968 after correction. The Ratio of minimum to maximum transmission is 0.8139. The λ/2 correction factor is Not present.
T_{min}, T_{max}	0.613, 0.753
No. of measured, independent and observed [$I > 2\sigma(I)$] reflections	39316, 2989, 1943
R_{int}	0.129
$(\sin \theta/\lambda)_{max}$ (Å^{-1})	0.596
Refinement	
$R[F^2 > 2\sigma(F^2)]$, $wR(F^2)$, *S*	0.063, 0.208, 1.15
No. of reflections	2989
No. of parameters	265
H-atom treatment	H atoms treated by a mixture of independent and constrained refinement
$\Delta\rho_{max}$, $\Delta\rho_{min}$ (e Å^{-3})	0.40, −0.32

7.1.2. Molecular Structure in the Solid State

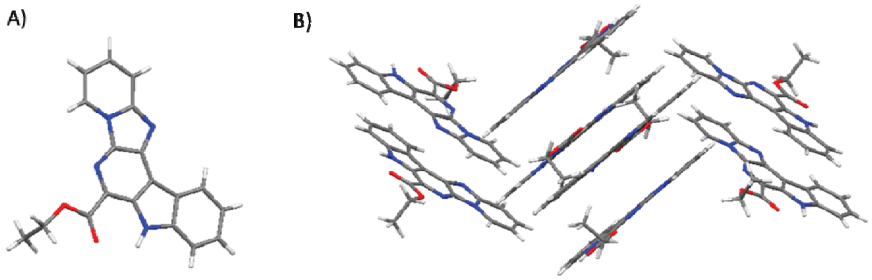

(A) Molecular structure of **7a** in the solid-state and (B) packing arrangement in the solidstate. Water molecules were not shown for clearity.

7.2. Compound 11e

Several unsuccessful trials to were made to obtain crystals from the Series **11** compounds. The only suitble crystal obtained was from the compound **11e**.

7.2.1. Crystal Data and Structure Refinement

CCDC number	**2023664**
Crystal data	
Chemical formula	$C_{81}H_{58}Cl_2N_{12}O_2$
M_r	1302.29
Crystal system, space group	Triclinic, $P\bar{1}$
Temperature (K)	120
a, *b*, *c* (Å)	10.8565 (14), 10.9791 (11), 15.0701 (14)
α, β, γ (°)	73.940 (8), 78.035 (9), 62.151 (11)
V (Å^3)	1519.8 (3)
Z	1
Radiation type	Ga *K*α, λ = 1.3414 Å
μ (mm^{-1})	0.97
Crystal size (mm)	0.08 × 0.04 × 0.04
Data collection	
Diffractometer	Bruker D8 Venture
Absorption correction	Multi-scan *CrysAlis PRO* 1.171.41.25a (Rigaku Oxford Diffraction, 2019) Empirical absorption correction using spherical harmonics, implemented in SCALE3 ABSPACK scaling algorithm.
T_{min}, T_{max}	0.645, 1.000
No. of measured, independent and observed [$I > 2\sigma(I)$] reflections	84406, 5572, 2766
R_{int}	0.325
$(\sin\theta/\lambda)_{max}$ (Å^{-1})	0.602
Refinement	
$R[F^2 > 2\sigma(F^2)]$, $wR(F^2)$, S	0.080, 0.239, 1.03
No. of reflections	5572
No. of parameters	453
No. of restraints	439
H-atom treatment	H-atom parameters constrained
$\Delta\rho_{max}$, $\Delta\rho_{min}$ (e Å^{-3})	0.28, −0.41

7.2.2. Molecular Structure in the Solid State

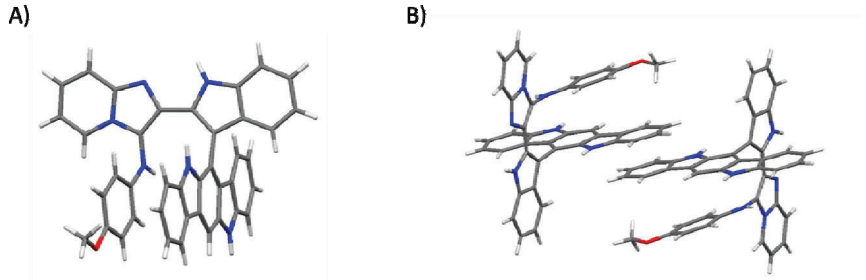

(A) Molecular structure of **11e** in the solid-state and (B) packing arrangement in the solid state. Dichloromethane molecules were not shown for clearity.

7.3. Compound 12

7.3.1. Crystal Data and Structure Refinement

CCDC number	**2019595**
Crystal data	
Chemical formula	$C_{39}H_{31}ClN_6 \cdot C_2H_3N$
M_r	660.20
Crystal system, space group	Orthorhombic, *Pbca*
Temperature (K)	100
a, *b*, *c* (Å)	20.724 (2), 15.1085 (12), 21.288 (2)
V (Å^3)	6665.5 (11)
Z	8
Radiation type	Cu *Kα*
μ (mm^{-1})	1.34
Crystal size (mm)	0.25 × 0.1 × 0.05
Data collection	
Diffractometer	Bruker *APEX*-III CCD
Absorption correction	Multi-scan *SADABS2016*/2 (Bruker,2016/2) was used for absorption correction. wR2(int) was 0.1254 before and 0.0990 after correction. The Ratio of minimum to maximum transmission is 0.7675. The λ/2 correction factor is Not present.
T_{min}, T_{max}	0.578, 0.753
No. of measured, independent and observed [$I > 2\sigma(I)$] reflections	28246, 5871, 3247
R_{int}	0.071
$(\sin \theta/\lambda)_{max}$ (Å^{-1})	0.601
Refinement	
$R[F^2 > 2\sigma(F^2)]$, $wR(F^2)$, *S*	0.106, 0.329, 1.07
No. of reflections	5871
No. of parameters	445
H-atom treatment	H-atom parameters constrained $w = 1/[\sigma^2(F_o^2) + (0.1288P)^2 + 24.6082P]$ where $P = (F_o^2 + 2F_c^2)/3$
$\Delta\rho_{max}$, $\Delta\rho_{min}$ (e Å^{-3})	0.70, −0.66

7.3.2. Molecular Structure in the Solid State

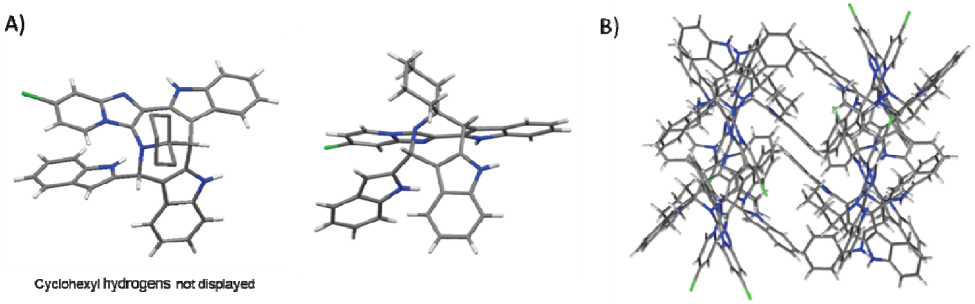

(A) Molecular structure of **12** in the solid-state and (B) packing arrangement in the solidstate. The CH_3CN molecules were not shown for clearity.

8. Microcrystal Electron Diffraction of Compound 8a

8.1. Experiment Details and Remarks

EM sample preparation:	dry deposition
Illuminated area in diffraction mode:	2.45 µmm
Dose for diffraction screening images:	0.243 pe $Å^2$ s^{-1}
Dose for imaging screening images:	1.22 pe $Å^2$ s^{-1}

Red resolution rings in diffraction images are positioned at 8, 4, 2 and 1 Å. Individual samples follow.

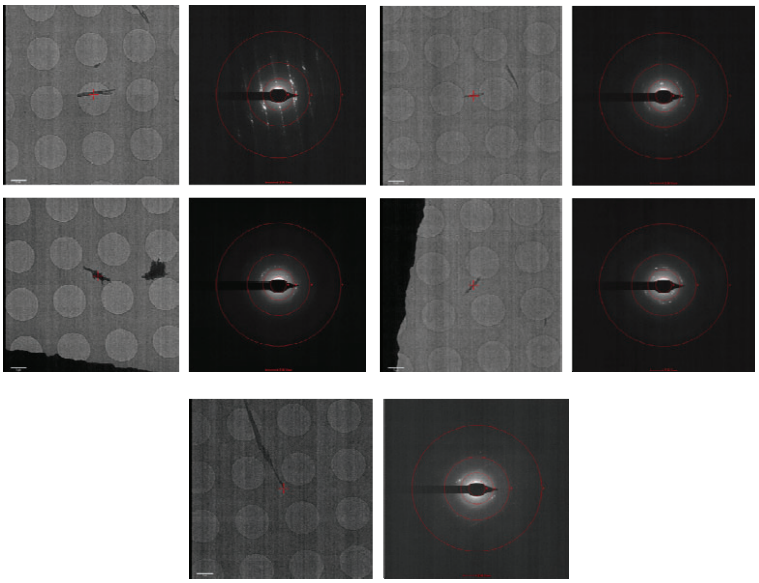

The crystal selected for data collection:

8.2. Crystal Data and Structure Refinement

CCDC number	**2023659**
Crystal data	
Chemical formula	$C_{19}H_{14}N_4O_2$
M_r	330.34
Crystal system, space group	Trigonal, $R\bar{3}$:*H*
Temperature (K)	77
a, *c* (Å)	44.80 (7), 4.1960 (19)
V (Å^3)	7292 (21)
Z	18
Radiation type	Electron, λ = 0.02508 Å
μ (mm^{-1})	0.000
Crystal size (mm)	× ×
Data collection	
Diffractometer	200 kV Transmission electron microscope with CETA detector
No. of measured, independent and observed [$I > 2\sigma(I)$] reflections	9182, 2930, 778
R_{int}	0.205
$(\sin \theta/\lambda)_{max}$ (Å^{-1})	0.603
Refinement	
$R[F^2 > 2\sigma(F^2)]$, $wR(F^2)$, *S*	0.158, 0.498, 1.05
No. of reflections	2930
No. of parameters	227
No. of restraints	216
H-atom treatment	H-atom parameters constrained
$\Delta\rho_{max}$, $\Delta\rho_{min}$ (e Å^{-3})	0.21, −0.20

8.3. Molecular Structure in the Solid State

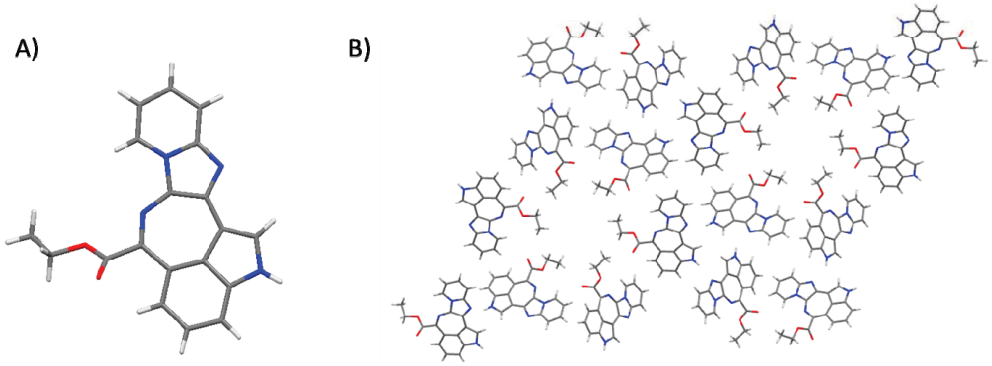

(A) Molecular structure of **8a** in the solid-state and (B) packing arrangement in the solid state.

References

[1] E. Zhang, H. Tian, S. Xu, X. Yu, Q. Xu, *Org. Lett.* **2013**, *15*, 2704–2707.

[2] B. Sun, Y. Wang, D. Li, C. Jin, W. Su, *Org. Biomol. Chem.* **2018**, *16*, 2902–2909.

[3] X. Yang, L. Li, Y. Li, Y. Zhang, *J. Org. Chem.* **2016**, *81*, 12433–12442.

[4] M. R. Patil, N. P. Dedhia, A. R. Kapdi, A. V. Kumar, *J. Org. Chem.* **2018**, *83*, 4477–4490.

[5] W. Jiang, Y. Wang, P. Niu, Z. Quan, Y. Su, C. Huo, *Org. Lett.* **2018**, *20*, 4649–4653.

[6] O. Ghashghaei, S. Caputo, M. Sintes, M. Reves, N. Kielland, C. Estarellas, F. J. Luque, A. Aviñó, R. Eritja, A. Serna-Gallego, J. A. Marrugal-Lorenzo, J. Pachon, J. Sanchez-Cespedes, R. Treadwell, F. de Moliner, M. Vendrell, R. Lavilla, *Chem. Eur. J.* **2018**, *24*, 14513–14521.

[7] C. S. See, M. Kitagawa, P. J. Liao, K. H. Lee, J. Wong, S. H. Lee, B. W. Dymock, *Eur. J. Med. Chem.* **2018**, *156*, 344–367.

[8] S. M. Son, H. K. Lee, *J. Org. Chem.* **2013**, *78*, 8396–8404.

[9] J. White, G. McGillivray, *J. Org. Chem.* **1977**, *42*, 4248–4251.

[10] R. Greenhouse, C. Ramirez, J. M. Muchowski, *J. Org. Chem.* **1985**, *50*, 2961–2965.

[11] M. Artico, F. Corelli, S. Massa, G. Stefanich, *J. Heterocycl. Chem.* **1982**, *19*, 1493–1495.

[12] W. Goldeman, A. Nasulewicz-Goldeman, *Tetrahedron* **2015**, *71*, 3282–3289.

[13] D. Coowar, J. Bouissac, M. Hanbali, M. Paschaki, E. Mohier, B. Luu, *J. Med. Chem.* **2004**, *47*, 6270–6282.

[14] N. Azizi, S. Dezfooli, *Environ. Chem. Lett.* **2016**, *14*, 201–206.

[15] M. Reutlinger, C. P. Koch, D. Reker, N. Todoroff, P. Schneider, T. Rodrigues, G. Schneider, *Mol. Inform.* **2013**, *32*, 133–138.

[16] C. Huo, Y. Yuan, M. Wu, X. Wang, F. Chen, J. Tang, *Angew. Chem. Int. Ed.* **2014**, *53*, 13544-13547.

[17] X. Yua, X. Lua, *Adv. Synth. Catal*. **2011**, *353*, 569 – 574.

[18] S. Sarkar, N. Tadigoppula, *RSC Adv*., **2014**, *4*, 40964–40968.

[19] D. Prajapati, M. Gohain, *Synth. Commun.* **2008**, *38*, 4426–4433.

[20] A. E. Wendlandt, S. S. Stahl, *J. Am. Chem. Soc.* **2014**, *136*, 506–512.

[21] T. Abe, K. Yamada, *J. Nat. Prod.* **2017**, *80*, 241–245.

[22] Q. Liu, Q. Li, Y. Ma, Y. Jia, *Org. Lett.* **2013**, *15*, 4528–4531.

[23] B. Jiang, Q. Ye, W. Fan, S. L. Wang, S. J. Tu, G. Li, *Chem. Commun.* **2014**, *50*, 6108–6111.

[24] L. N. Wang, S. L. Shen, J. Qu, *RSC Adv*. **2014**, *4*, 30733–30741.

[25] A. Kamal, M. Sathish, A. V. G. Prasanthi, J. Chetna, Y. Tangella, V. Srinivasulu, N. Shankaraiah, A. Alarifi, *RSC Adv*. **2015**, *5*, 90121–90126.

[26] E. Fritsche, C. Schäfer, C. Calles, T. Bernsmann, T. Bernshausen, M. Wurm, U. Hübenthal, J. E. Cline, H. Hajimiragha, P. Schroeder, L. O. Klotz, A. Rannug, P. Fürst, H. Hanenberg, J. Abel, J. Krutmann, *Proc. Natl. Acad. Sci. U. S. A.* **2007**, *104*, 8851–8856.

[27] K. Frauenstein, J. Tigges, A. A. Soshilov, S. Kado, N. Raab, E. Fritsche, J. Haendeler, M. S. Denison, C. F. A. Vogel, T. Haarmann-Stemmann, *Arch. Toxicol.* **2015**, *89*, 1329–1336.

9.2. Final Compounds

9.2.1. Series 7

Ethyl 8*H*-pyrido[1'',2'':1',2']imidazo[4',5':5,6]pyrido[3,4-*b*]indole-7-carboxylate (7a)

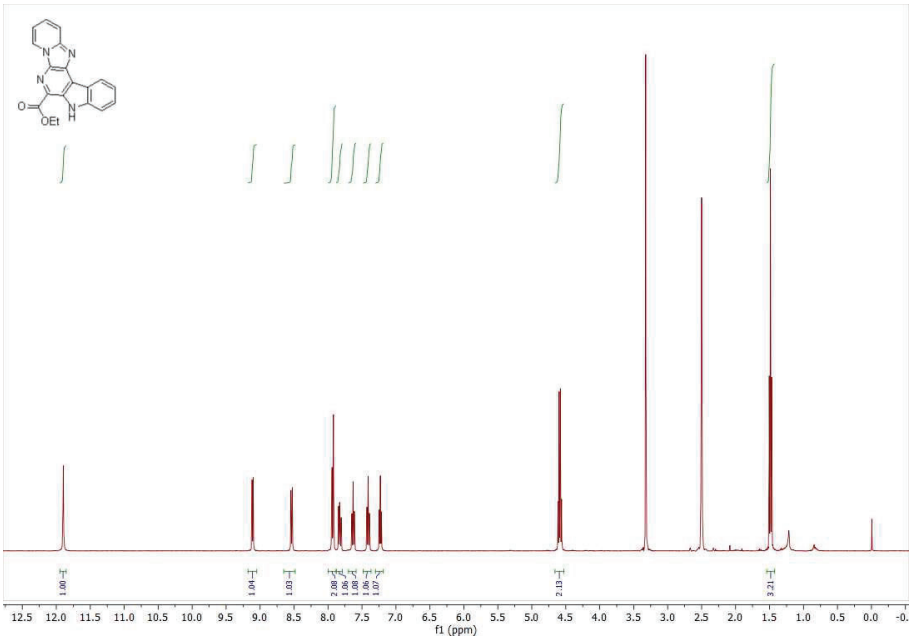

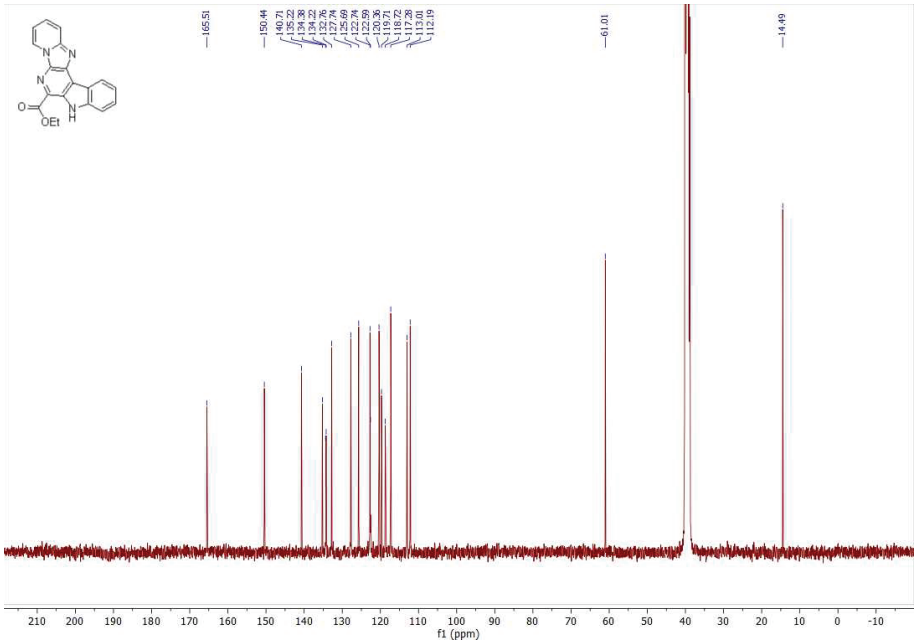

Diethyl (8*H*-pyrido[1'',2'':1',2']imidazo[4',5':5,6]pyrido[3,4-*b*]indol-7-yl)phosphonate (7b)

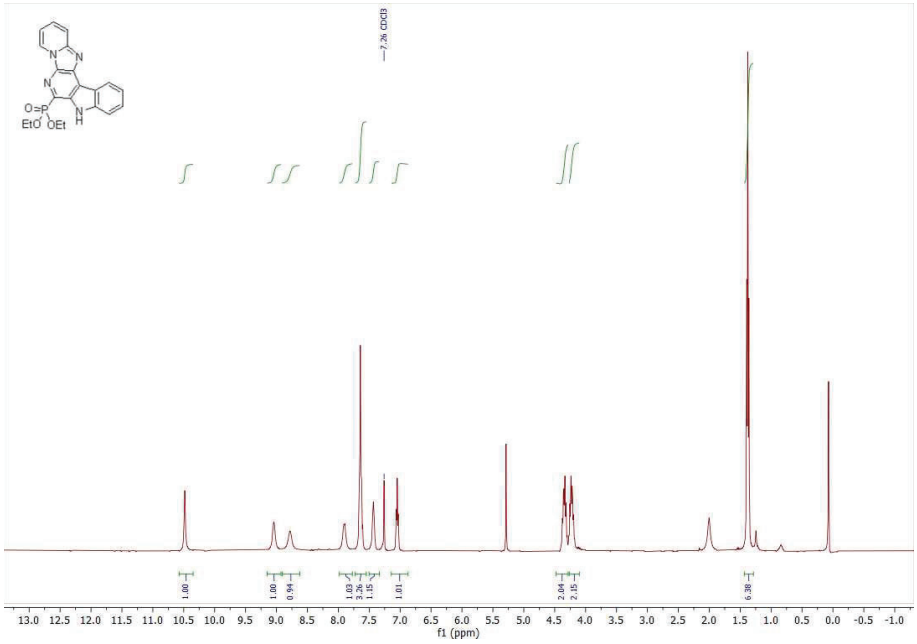

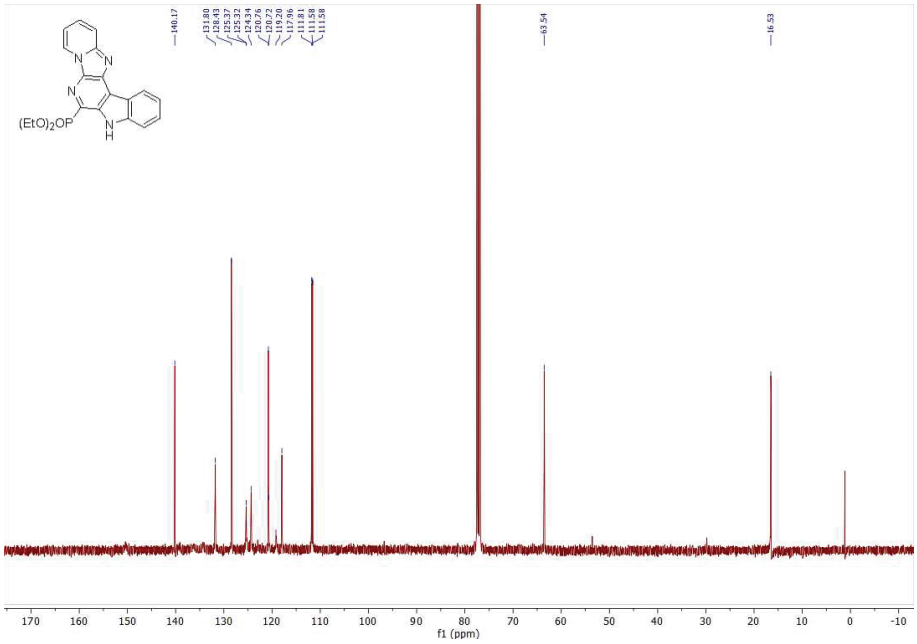

9.2.2. Series 8
Ethyl 2*H*-pyrido[1'',2'':1',2']imidazo[4',5':6,7]azepino[5,4,3-*cd*]indole-6-carboxylate (8a)

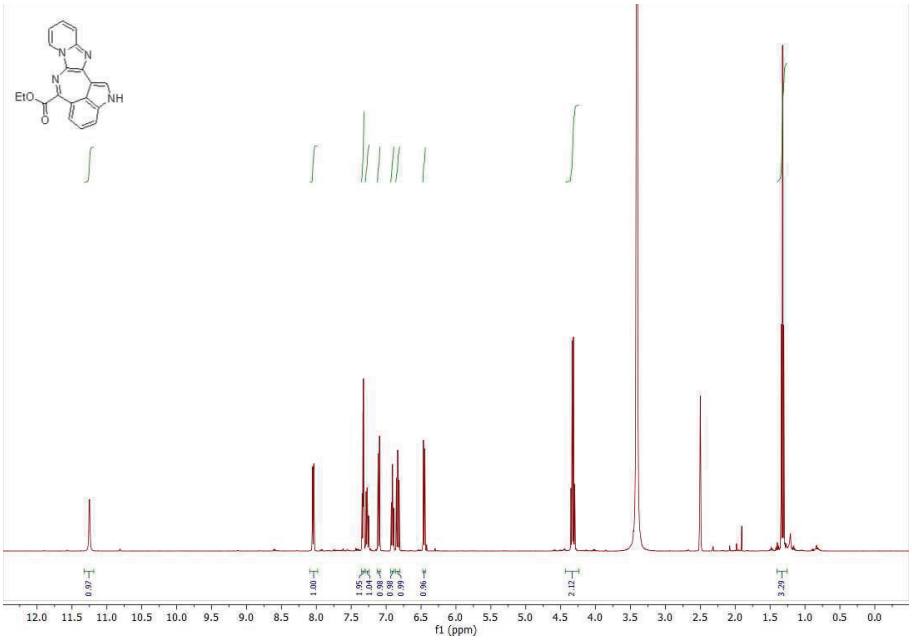

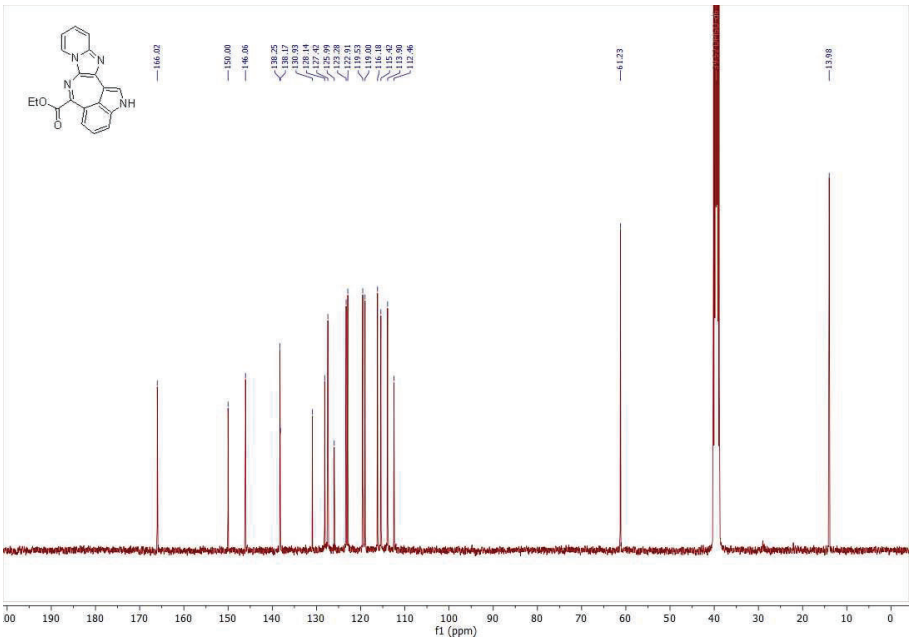

gCOSY: Diagnostic signal between NH- (A) and C/D.

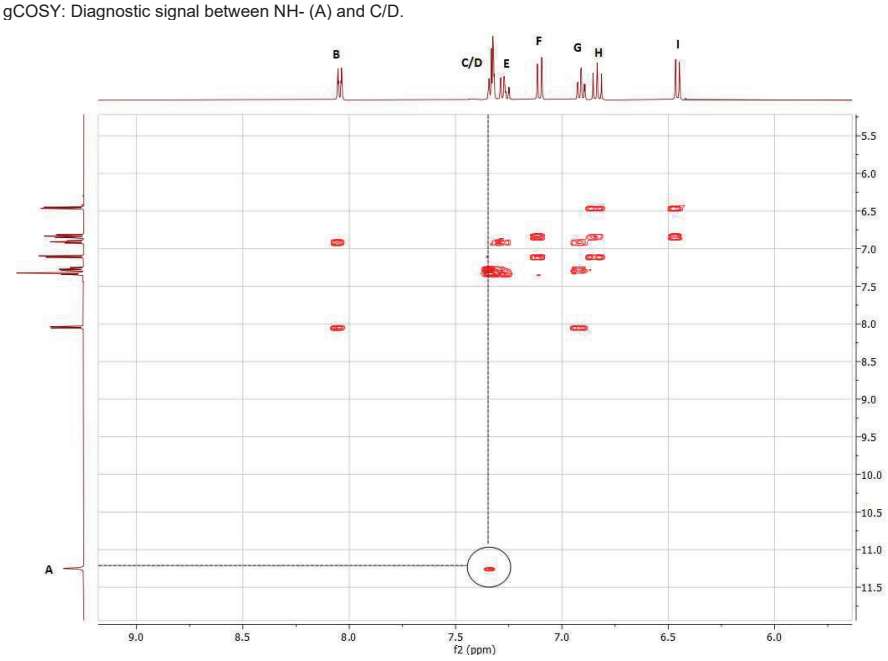

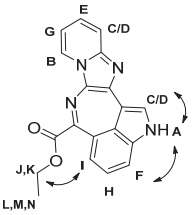

NOESY: Diagnostic signals between NH- (A), C/D and F; and between I and the -CH_2- of the acetate (J,K).

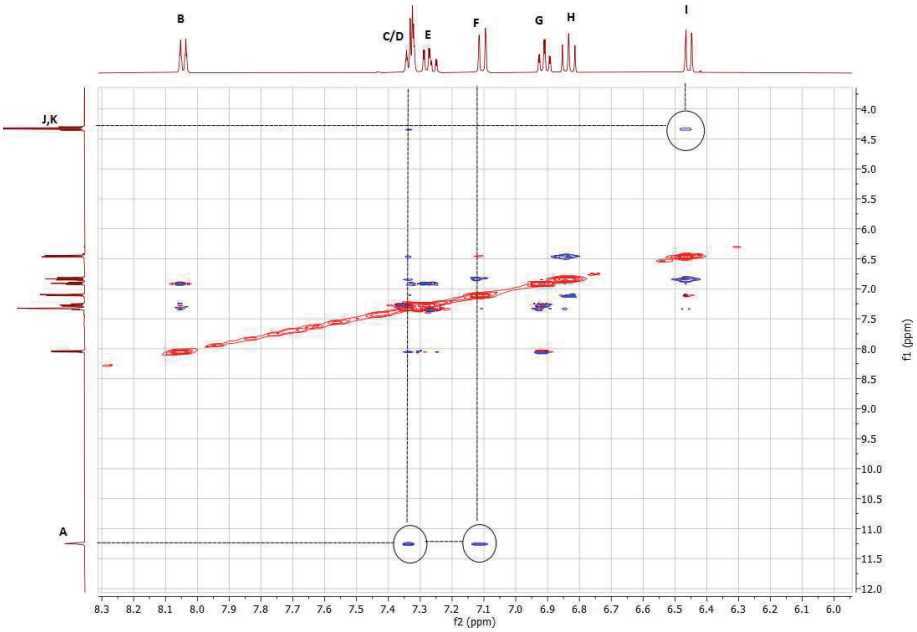

9.2.3. Series 9

Ethyl 4*H*-pyrido[1'',2'':1',2']imidazo[4',5':6,7]azepino[3,4,5-*cd*]indole-6-carboxylate (9a)

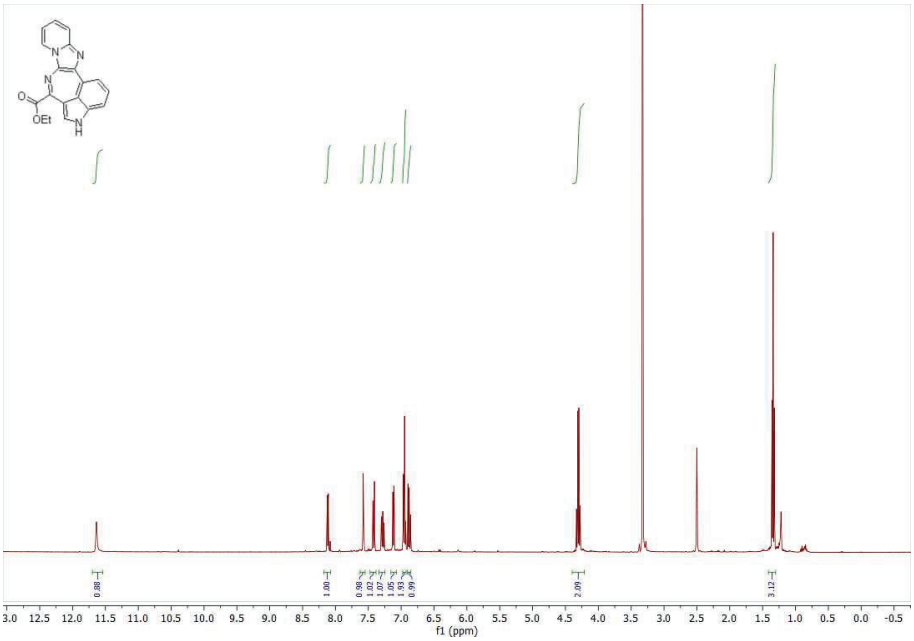

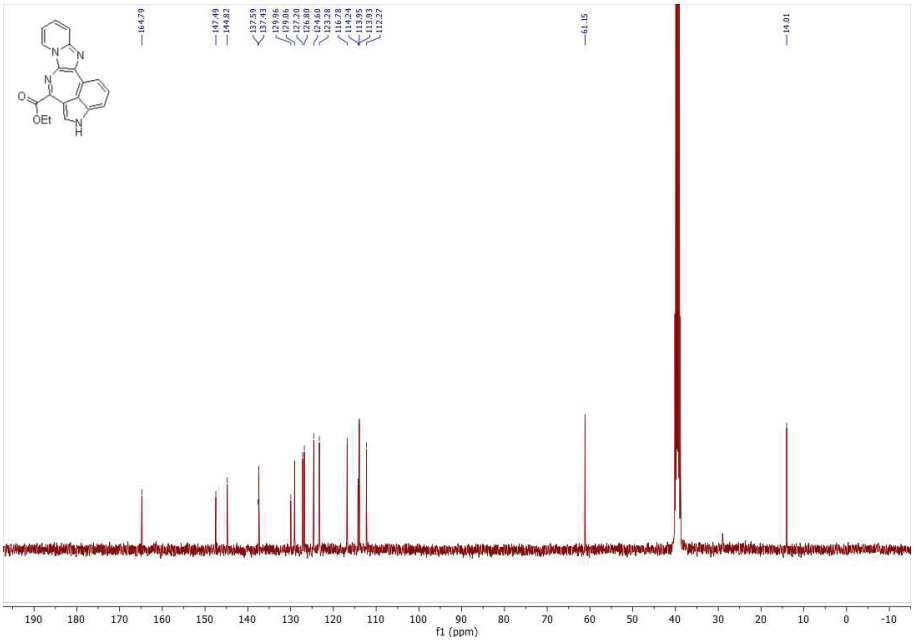

Methyl 8-amino-1*H*-pyrimido[1'',2'':1',2']imidazo[4',5':6,7]azepino[3,4,5-*cd*]índole-3-carboxylate (9b)

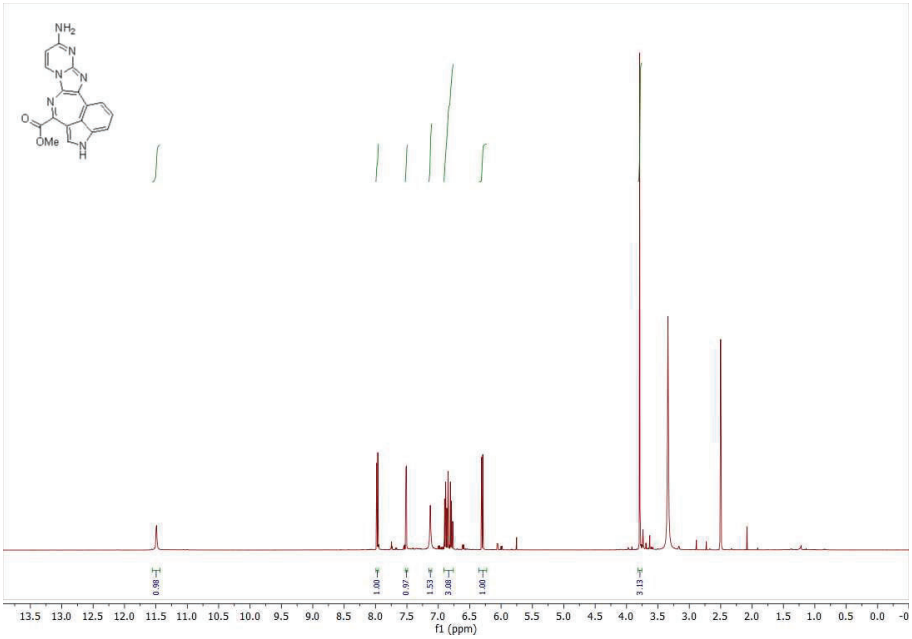

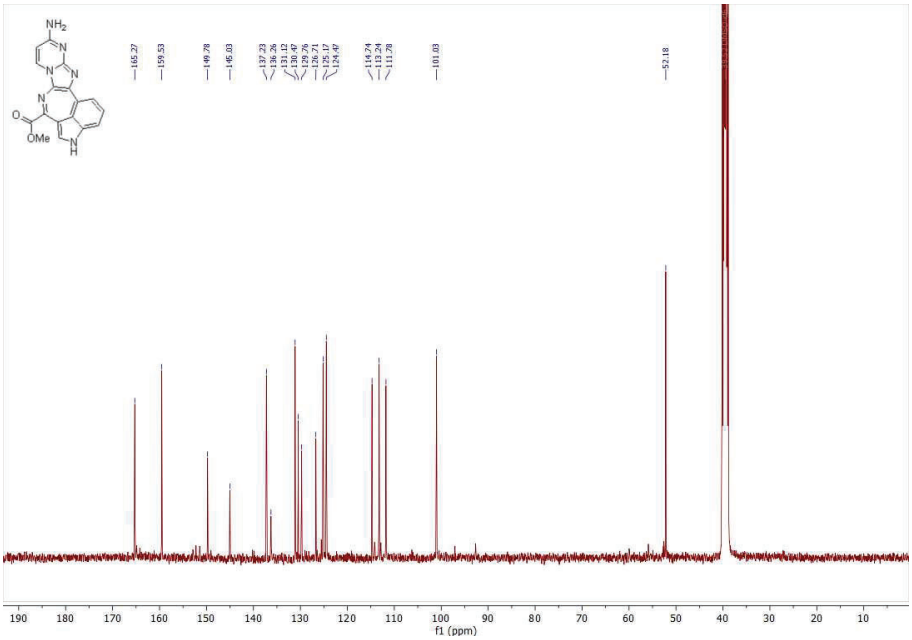

COSY: Diagnostic interactions between NH- (A) and C, and between F,G and H.

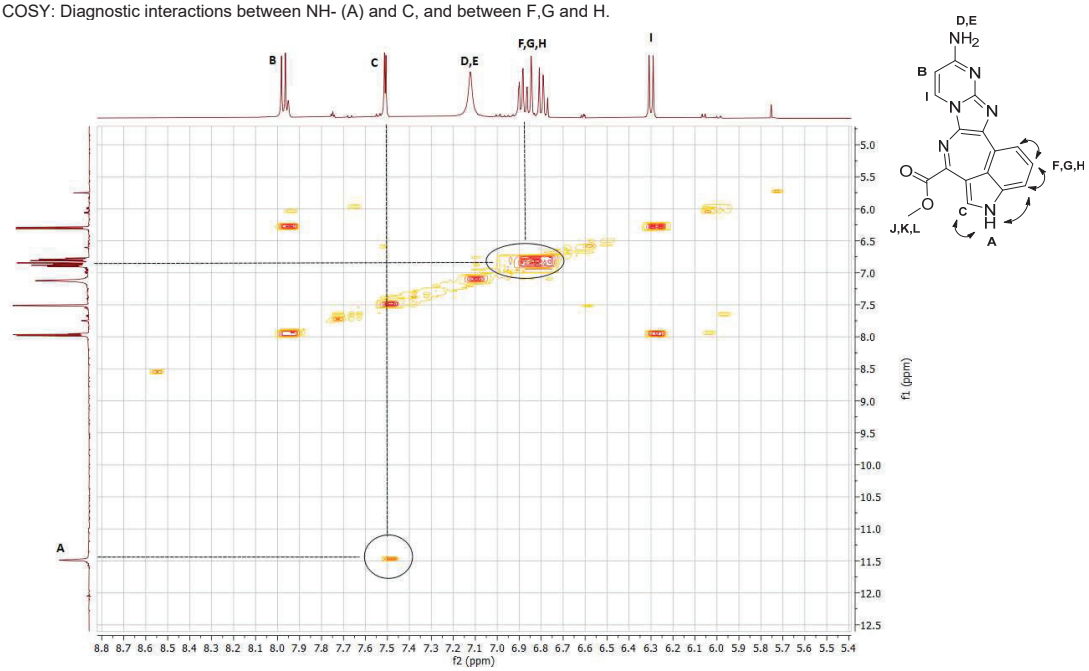

NOESY: Diagnostic interactions between NH- (A) and C, and NH- (A) and aryl signals (F,G,H).

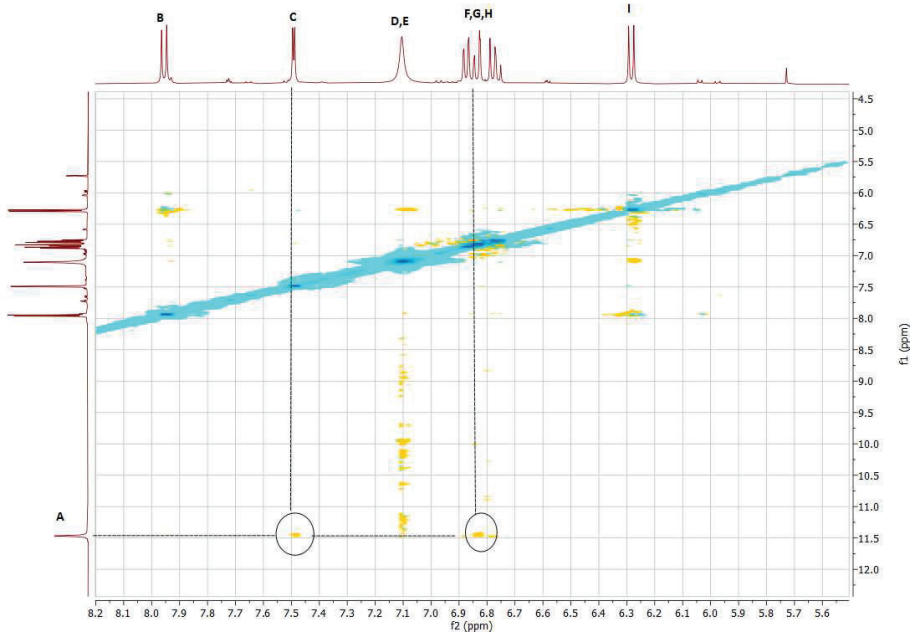

9.2.4. Series 10
Ethyl 2,3,4-trimethoxypyrido[2',1':2,3]imidazo[4,5-*c*]isoquinoline-5-carboxylate (10a)

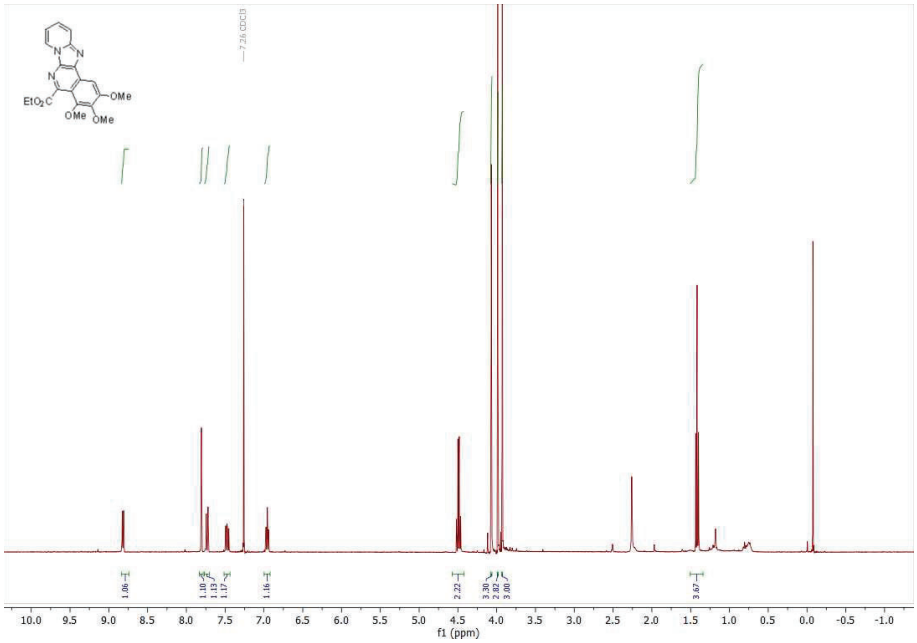

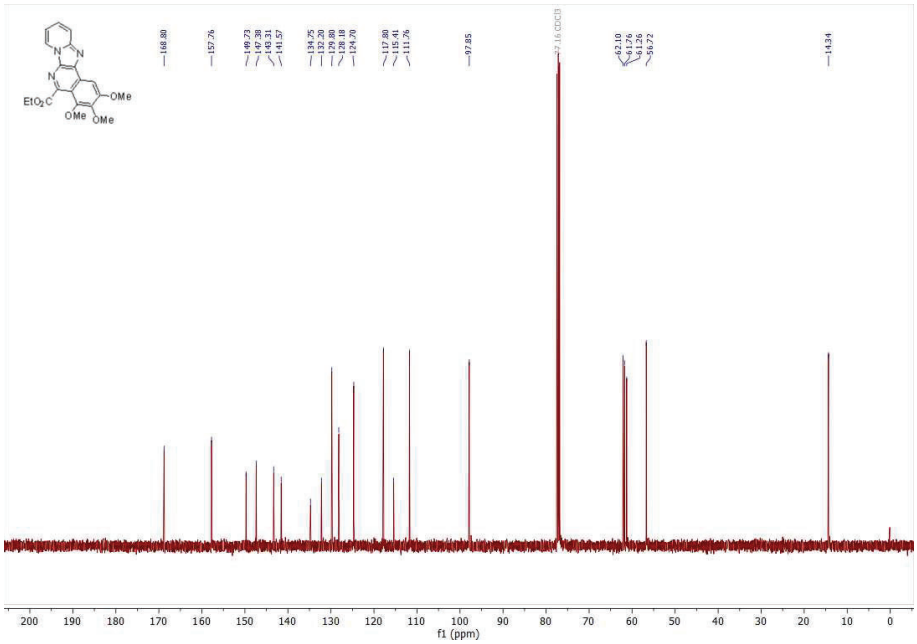

7-Chloro-*N*-cyclohexyl-2-(3-(5,11-dihydroindolo[3,2-*b*]carbazol-6-yl)-1*H*-indol-2-yl)imidazo[1,2-*a*]pyridin-3-amine (11b)

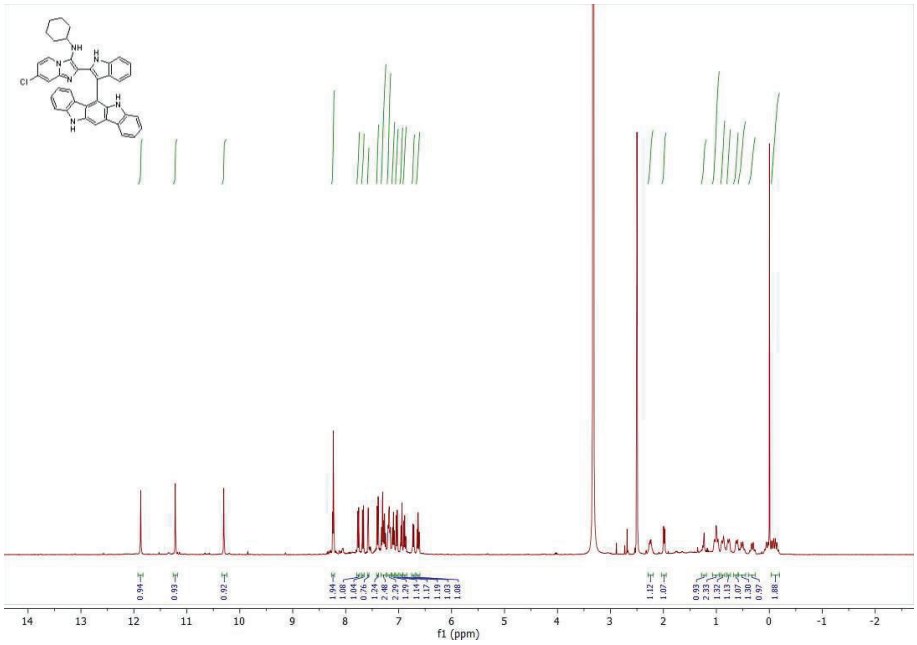

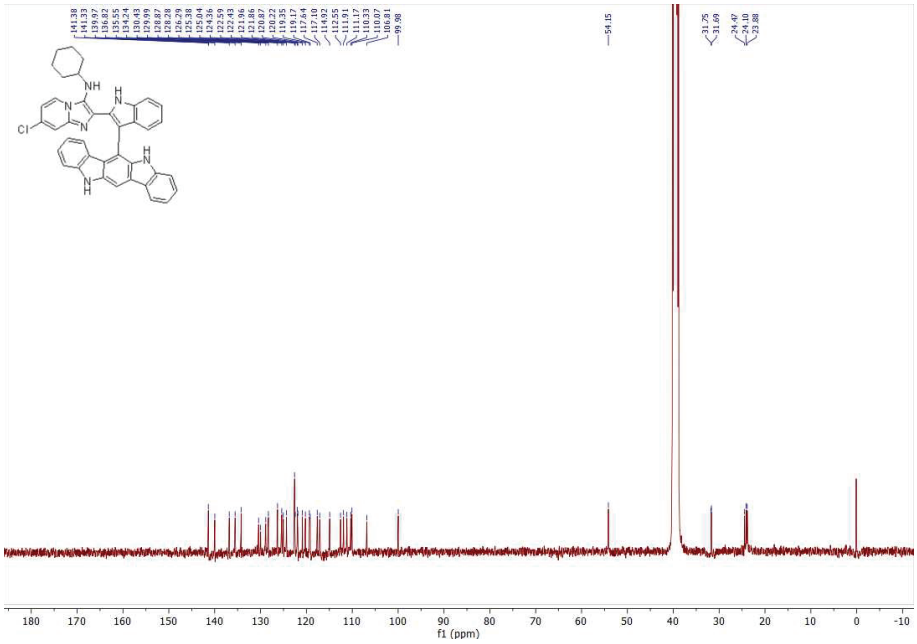

9.2.6. Compound 12

8'-Chloro-13'-(1*H*-indol-2-yl)-5',13',18',19'-tetrahydrospiro[cyclohexane-1,20'-[12,19]methanopyrido[1'',2'':1',2']imidazo[4',5':8,9]azonino[4,3-*b*:7,6-*b*']diindole] (12)

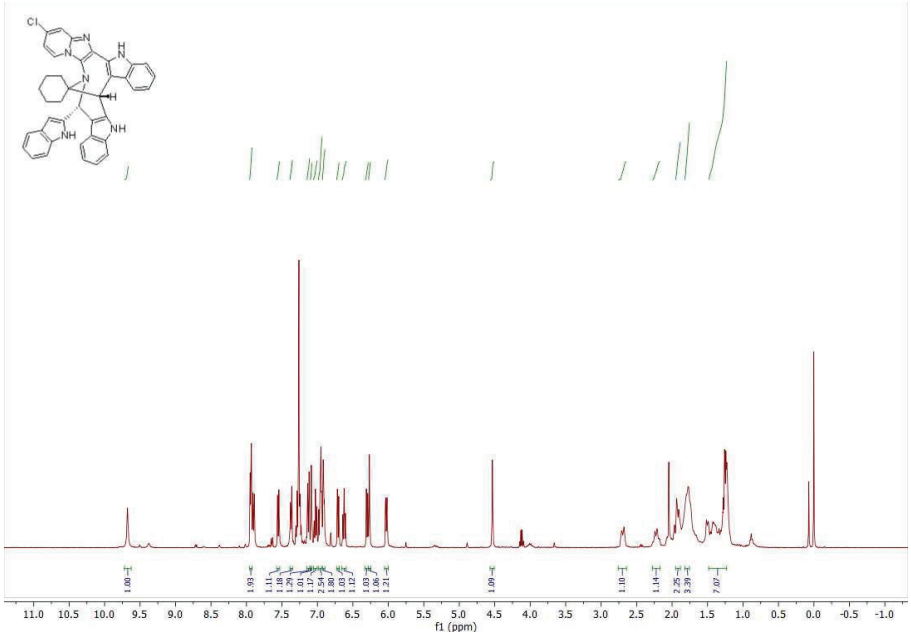

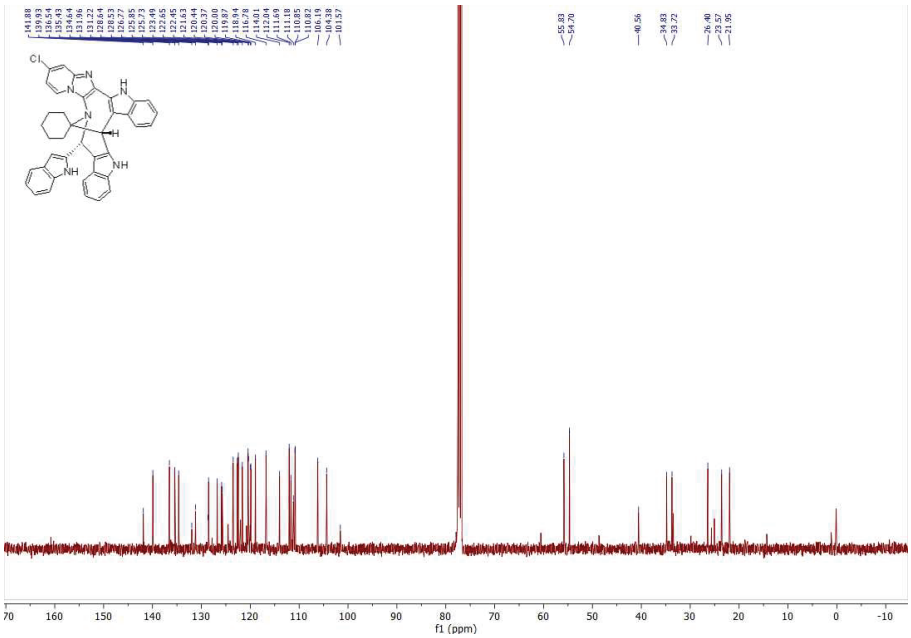

Bibliographic Revision

Publication IV: Heterocycles as Inputs in MCRs: An Update

1

Heterocycles as Inputs in MCRs: An Update

Ouldouz Ghashghaei, Marina Pedrola, Carmen Escolano, and Rodolfo Lavilla

University of Barcelona, Laboratory of Medicinal Chemistry, Faculty of Pharmacy and Food Sciences, and Institute of Biomedicine IBUB, Av. de Joan XXIII, 27-31, Barcelona 08028, Spain

1.1 Introduction

Multicomponent reactions (MCRs) hold a privileged position in organic synthesis and are currently gaining momentum in the fields where a fast access to high levels of structural diversity is needed. This is especially important in medicinal chemistry and key to drug discovery. In this endeavor, as the vast majority of small-molecule drugs are of heterocyclic nature, the interplay of heterocycles with MCRs becomes significant [1]. Although the majority of work has been devoted to the synthesis of heterocyclic adducts from non-heterocyclic reactants [2, 3], we will focus, however, on the intrinsic reactivity of basic heterocycles as a source of synthetically useful MCRs (Scheme 1.1). This approach, still quite unexplored in the MCR context, is arguably a rich source of novel, complex scaffolds. There is a wide choice of commercially available heterocyclic inputs, which together with their often-exclusive reactivity make this perspective simple, conceptually attractive, and synthetically productive. In this chapter, we describe a representative selection of relevant results in the last six years, as the field has experienced impressive growth since our last revision [4], and an exhaustive account is out of scope. This update groups the highlighted processes according to the main reactivity modes defining the MCRs: concerted, radical, metal-catalyzed, carbonyl/imine, and isocyanide-based processes. Finally, a miscellany section is included to cluster those MCRs that do not clearly fit in the classification. Occasionally, some significant post-transformations and applications have been detailed.

1.2 Concerted MCRs

The impact of heterocycle-based concerted MCRs in organic synthesis is quite relevant, with recent contributions arising from Povarov reactions, hetero Diels–Alder processes, and dipolar cycloadditions. The Povarov MCR, the interaction of an

Multicomponent Reactions towards Heterocycles: Concepts and Applications, First Edition.
Edited by Erik V. Van der Eycken and Upendra K. Sharma.

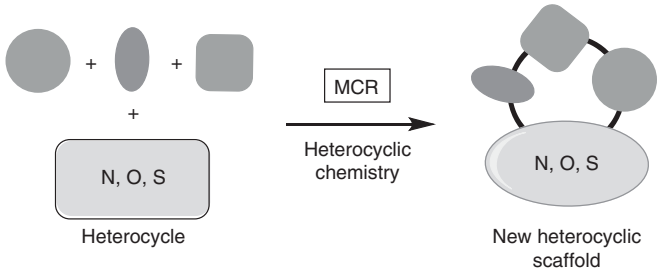

Scheme 1.1 Heterocycles as inputs in MCRs.

aromatic amine, an aldehyde, and an activated alkene, remains one of the best synthetic approaches to access tetrahydroquinolines (THQs) [5] and is especially productive in medicinal chemistry [6]. Although the concerted cycloaddition is a well-founded hypothesis for the reaction mechanism, there is evidence on polar stepwise processes in some cases, and both pathways are considered here.

For instance, a double Povarov process led to julolidine derivatives: the first MCR generates a secondary amine, which under calixarene-based polysulfonic acid catalysis spontaneously triggers a second MCR, leading to the final five-component adducts with good yields and modest stereoselectivity (Scheme 1.2) [7].

Indole derivatives participate in Povarov MCRs not only as aldehyde or olefin inputs, but also as aniline surrogates. Their specific structural arrangement, and the catalytic conditions used, determines the outcome. In this way, while indole-3-carbaldehyde gives the expected Povarov adduct [8], indole-7-carbaldehyde reacts in a different way, leading to fused adduct where the indole nitrogen closes a six-membered ring [9]. Interestingly, indole-2-carbaldehyde, depending on the catalysts used, may lead to the *normal* Povarov adduct or to a different scaffold, with a distinct connectivity through an alternative [3 + 2] cycloaddition mode (Scheme 1.3) [10].

As olefin inputs, indoles unsubstituted at C2 and C3 yield the THQ adduct, losing the aromaticity at the pyrrole ring [11]. In this respect, 2-vinylindoles react exclusively at the olefin moiety to yield the expected THQ adduct [12]. However, the isomeric 3-vinyl derivatives react quite differently, leading to bisindole-piperidines in a stereo- and enantio-controlled fashion, using chiral catalysts (Scheme 1.3) [13].

Regarding heterocyclic inputs, the interaction of aldehydes, 1,4-dhydropyridines as activated olefins, and aminocoumarin, as aniline surrogate, leads to complex

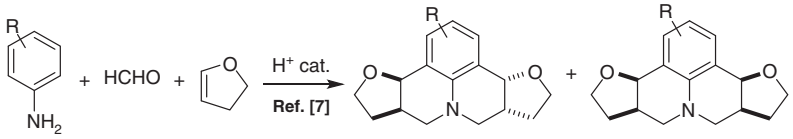

Scheme 1.2 Access to julolidines via double Povarov MCRs.

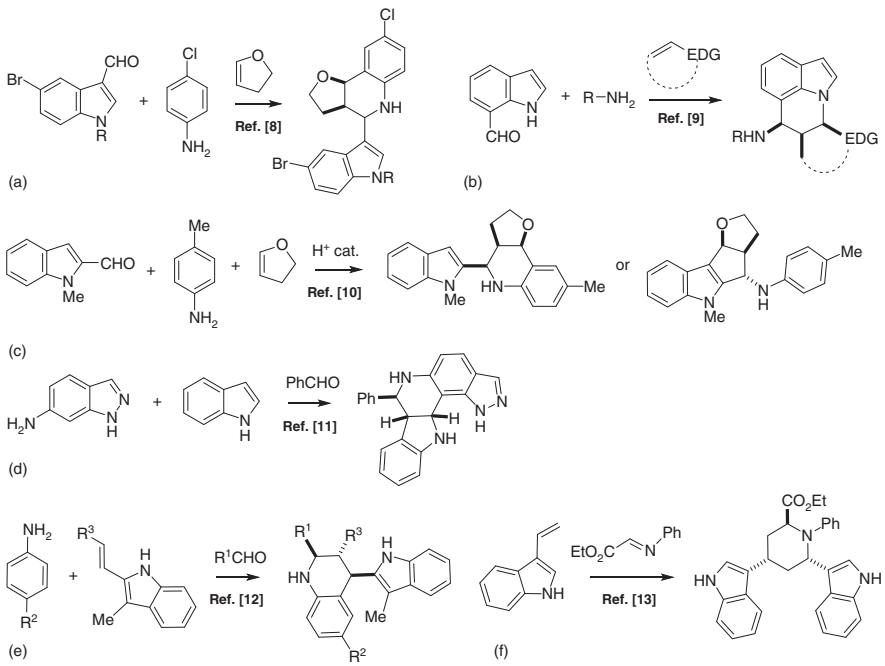

Scheme 1.3 Indoles as inputs in Povarov MCRs.

functionalized chromenonaphthyridines [14]. Relevantly, 3-aminopyridine imines react with alkynes (terminal or internal) to regioselectively afford the naphthyridine scaffold [15]. Similarly, 3-aminopyridones also lead to oxidized Povarov adducts (Scheme 1.4) [16].

There are mechanistic variations that dramatically modify the connectivity pattern of standard Povarov MCRs. For instance, a Ferrier rearrangement was promoted during a Povarov process involving glycals [17]. An interesting example of interrupted Povarov process with salicylaldehydes, anilines, and dihydrofurans, instead of yielding the expected THQ adduct, follows a Mannich-type process with the enol ether, and the resulting intermediate is trapped by the phenolic hydroxyl, yielding the MCR adduct in a stereoselective fashion (Scheme 1.5) [18].

In a remarkable photoredox-catalyzed process, aldimines, dihydrofurans and trimethylsilyl azide, afforded azidotetrahydrofurans. The observed polarity reversal can be explained through a mechanism involving an azido radical, which adds on the β-position of the enol ether to promote the imine addition (Scheme 1.5) [19].

Finally, the Povarov MCR has enabled the selective tagging of benzaldehyde-functionalized DNA chains through the reaction with anilines and an *N*-protected dihydropyrrole [20].

Isochromenylium ions react with dienophiles in a [4 + 2] cycloaddition to yield adducts, which go through a Ritter-type domino process with acetonitrile to afford complex tetracyclic compounds [21]. Also, a formal concerted MCR connects *in situ* generated isoquinolinium salts with unsaturated aldehydes and alcohols in a process promoted by *N*-heterocyclic carbenes to give bridged azaheterocycles [22]. A [4 + 3] cycloaddition process is triggered by the condensation of an iminoindole with aldehydes to give an azadiene that reacts *in situ* with a sulfur ylide to yield azepinoindoles (Scheme 1.6) [23].

MCRs involving [3 + 2] cycloadditions have produced a substantial number of new transformations. The processes involving azinium ions have been reviewed [24]. The interaction of heterocyclic secondary amines with carbonyl inputs to generate dipoles is a common motif in the field. For instance, THQs, aldehydes, and ketomalonate afford the corresponding oxazolidine adducts [25].

Azomethine ylides, mostly generated by condensation or decarboxylation of α-amino acids, have been thoroughly used in MCRs in the presence of suitable dipolarophiles, often with applications in drug discovery [26]. The synthesis of pyrrolizidines and indolizidines through this MCR methodology has been reviewed [27]. A remarkable five-component interaction based on a double [3 + 2] cycloaddition of azomethine ylides has led to tetracyclic adducts in high yields in a stereoselective manner (Scheme 1.7) [28].

Azines are also present in this reactivity. α-Methylquinolines, aldehydes and alkynoates yield a fused adduct in a domino process starting with the formation of the dehydrated aldol-like intermediate [29]. Moreover, quinoline and pyridine dipoles react with azomethine ylides in an unprecedented fashion to yield complex fused pyrrolidine cycloadducts [30]. Finally, isatin undergoes a series of complex transformations triggered by the initial [3 + 2] cycloadduct generated through its interaction with proline and alkynoates (Scheme 1.8) [31].

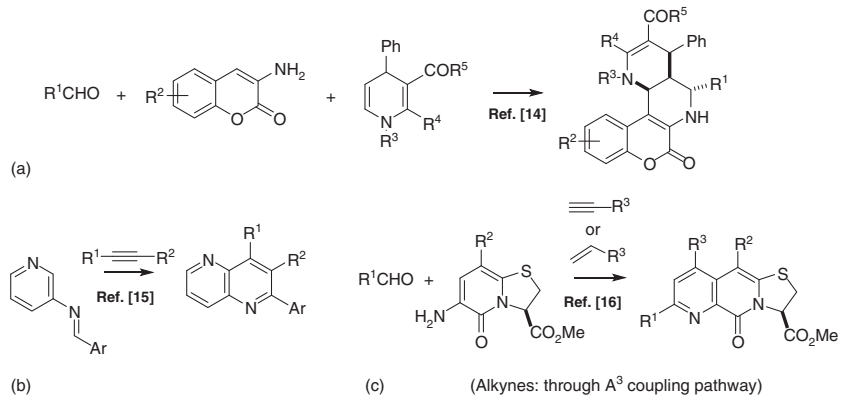

Scheme 1.4 Aminoheterocycles in Povarov MCRs.

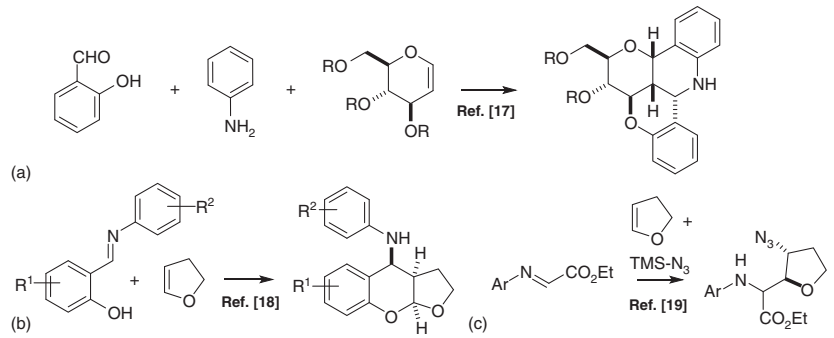

Scheme 1.5 Mechanistic variations of the Povarov-type processes.

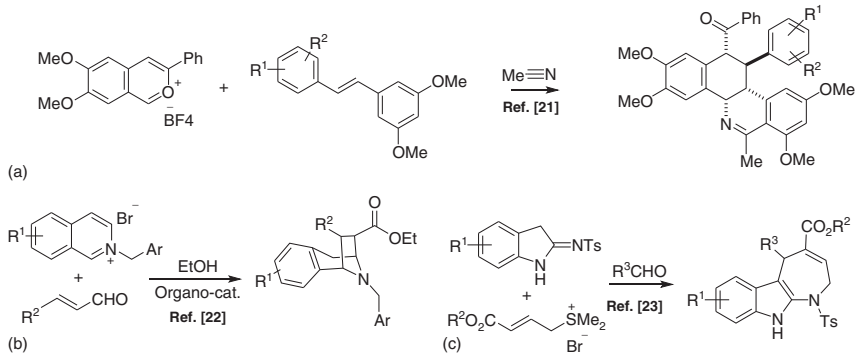

Scheme 1.6 Cycloaddition-type MCRs.

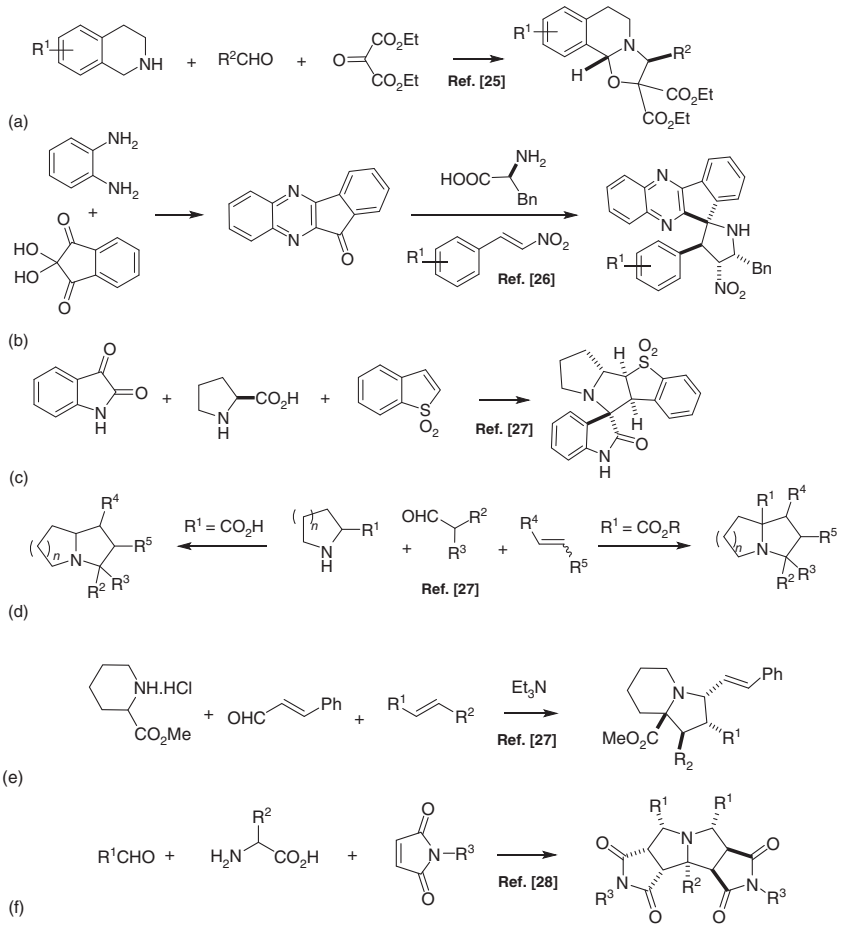

Scheme 1.7 [3 + 2] Dipolar cycloaddition MCRs.

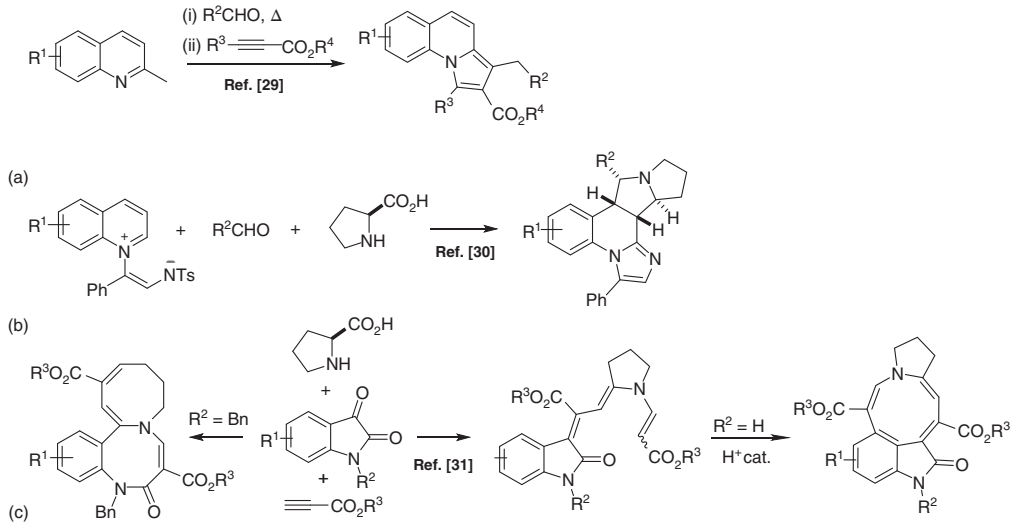

Scheme 1.8 Azines and isatins in dipolar MCRs.

Arynes yield dipoles through interaction with nucleophilic species. Their participation in MCRs has been recently reviewed [32]. Azines are *N*-arylated, and the resulting dipole interacts with carbonyl groups in an addition/cyclization mode or through proton transfer to generate second nucleophiles that trap the azinium intermediate. Also, the azine dipoles react with the aryne in [3 + 2] dipolar cycloaddition MCRs (Scheme 1.9).

In a series of related processes, epoxides, aziridines, and also four-membered cyclic amines and (thio)ethers react with arynes and protonucleophiles leading to the corresponding adduct featuring a substituted chain originated in the heterocycle (Scheme 1.10) [32].

1.3 Radical MCRs

The incorporation of radical chemistry into MCRs has unlocked access to new synthetic pathways unavailable through conventional polar reactions. Radical MCRs generally consist of a proradical, a relay reagent, and a trapping component [33]. Novel radical MCRs exploiting photochemical approaches have experienced rapid growth in recent years [34]. However, their pairing with heterocyclic inputs has been mainly restricted to the functionalization of the heterocyclic component. In this regard, the multicomponent versions of Minisci reaction stand out [35]. In these processes pyridine-type heterocycles get alkylated in the presence of a suitable alkene and an initiator amenable to produce the radical species [36]. β-Dicarbonyl radicals [37] as well as heteroatomic radicals including azido [38], sulfonyl, and phosphonyl [39] species have been reported to yield Minisci adducts in a similar fashion. As for the alkene components, *N*-vinylacetamide has been coupled with suitable azines and the proradical, to enantioselecitvely afford γ-aminoesters in the presence of a chiral phosphoric acid (Scheme 1.11) [40].

The scope of the heterocycic inputs in Minisci MCRs is mainly restricted to pyridine-type systems, usually substituted at some reactive positions (C2/C4) to block undesired regioisomer formation. In an alternative approach, the use of 4-cyanopyridine allows the γ-selective functionalization under a variety of conditions, involving the favored generation of pyridyl radicals [41, 42]. Interestingly, the use of Tf_2O as the azine activator and a CF_3 radical source results in the regioselective *p*-trifluoromethyl-alkylation of pyridines and quinolines [43]. In a related process, the use of pyridyl halides directs the functionalization upon the C4 position in a Ni-catalized radical process. It also features an interesting [1,5]-H shift that enables the heteroatom addition upon the β position of the initiating carbon radical (Scheme 1.12) [44].

Other heterocyclic systems have also been functionalized through radical MCRs. For instance, the C-sulfonylation of imidazoles has been reported in an Eosin-catalyzed photoredox transformation (Scheme 1.13) [45].

Dearomatization of indoles and related heterocycles has also been achieved through radical MCRs. In a remarkable approach, C3-spiro trifluoromethylindolines have been assembled in a copper-catalyzed radical MCR with β-aminomethylindoles,

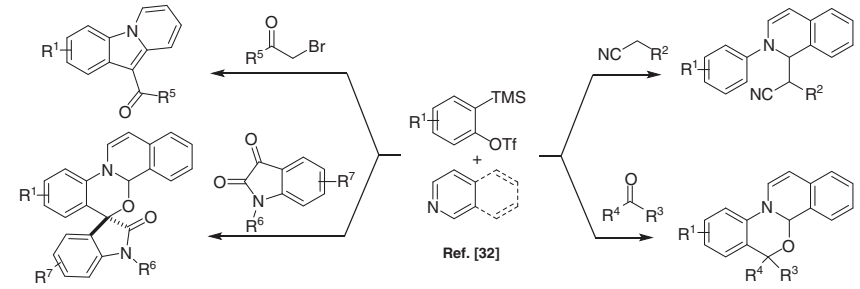

Scheme 1.9 Azine-aryne MCRs.

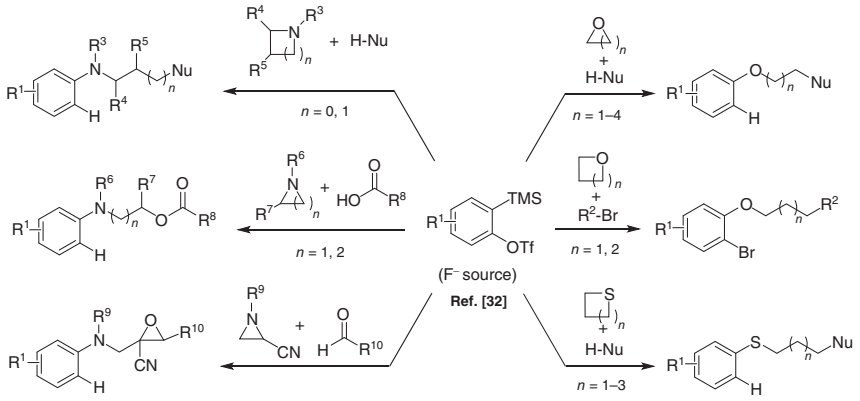

Scheme 1.10 3/4-Membered heterocycles in aryne MCRs.

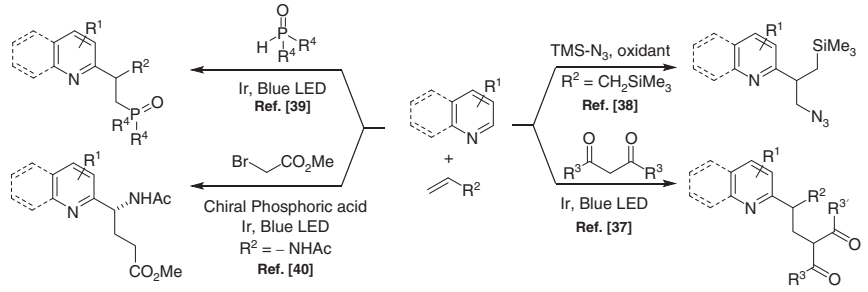

Scheme 1.11 Minisci-type radical MCRs.

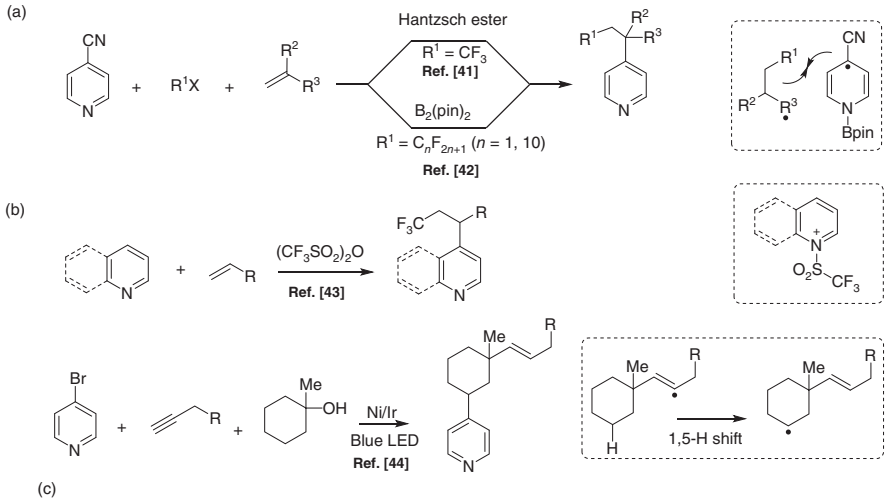

Scheme 1.12 Site-selective azine-based radical MCRs .

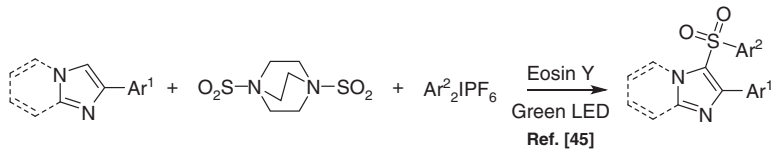

Scheme 1.13 SO_2 photoredox MCR.

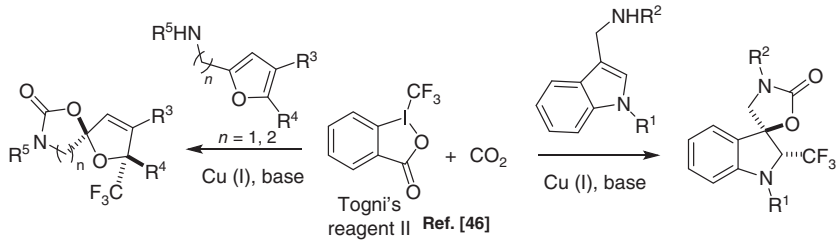

Scheme 1.14 Heterocycle dearomatization in radical MCRs.

carbon dioxide, and a trifluoromethyl radical source. The CF_3-indole radical is intramolecularly trapped by the copper carbamate, which is formed *in situ*, through the condensation of amine and CO_2. Furans with similar side chains have successfully afforded the corresponding spiro adducts (Scheme 1.14) [46].

Finally, maleimides have been involved in a remarkable Minisci-type MCR, in which the initiating alkyl radical was generated through a novel mild process [47]. Moreover, the assembly of fused quinolines through the condensation of 3-arylaminoacrylates, maleimides, and an electrophilic radical source has been achieved, matching the radical affinities in a domino process (Scheme 1.15) [48].

1.4 Metal-catalyzed MCRs

Transition metal-catalyzed MCRs featuring heterocyclic inputs have also experienced immense progress in recent years. Regarding the C–H activation processes, the direct functionalization of azoles through the insertion of an isocyanide, followed by the attack of a heterocycle, has been reported for the synthesis of di(hetero)aryl-ketones and-alkylamines [49]. The methodology involves the reaction of azoles, haloarenes, and isocyanides resulting in the formation of an imine, which can be hydrolyzed or reduced to yield the final adducts. Other examples of C—H bond functionalization include the preparation of fused imidazo-heterocycles starting from methyl ketones, *o*-tosylhydroxylamine and 2-pyridinone or thiazo/benzo[d]thiazol-2(3H)-ones [50]. This MCR consists of the copper catalyst coordination, the formation of the C–H functionalized intermediate, followed by a tandem addition-cyclization process. A relevant C–H glycosylation via a Catellani-type arylation allows the synthesis of C-aryl glycosides, which can undergo further transformations, such as Heck, Suzuki, and Sonogashira cross-couplings (Scheme 1.16) [51].

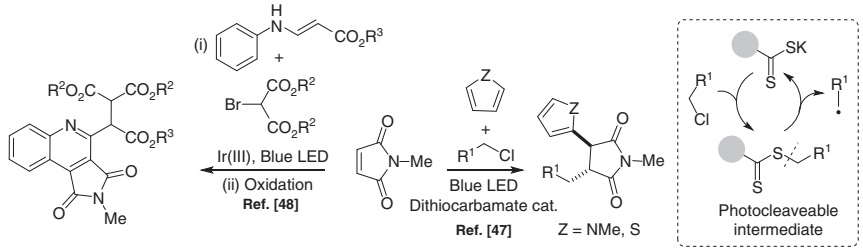

Scheme 1.15 Maleamides as inputs in radical MCRs.

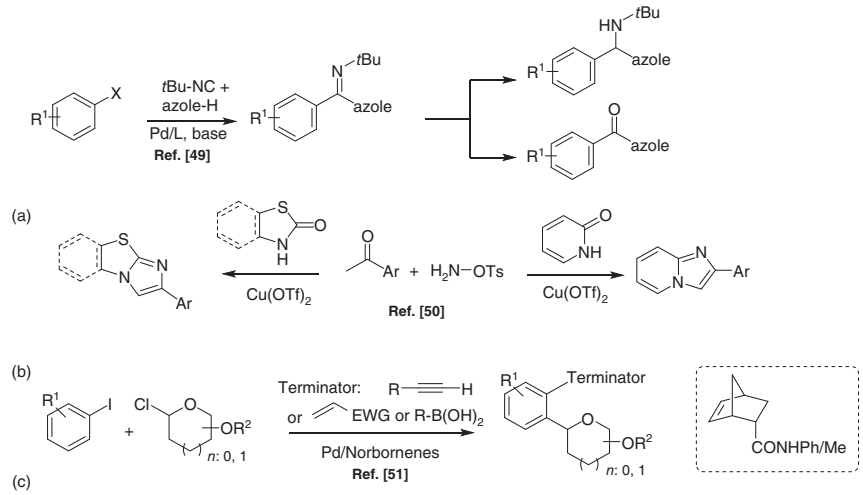

Scheme 1.16 C–H activation MCRs.

Progress in the A3-related MCRs, the interaction of aldehydes, amines, and alkynes, includes the use of isoquinolines, suitably activated by a chloroformate as amine inputs through an enantioselective copper-catalyzed protocol [52]. Remarkably, the interaction of azine-2-carbaldehydes with secondary amines and terminal alkynes starts via the A3 MCR, and the adduct undergoes a formal Cu-catalyzed hydroamination to yield indolizines [53, 54]. Terminal alkynes are also useful inputs in the MCR coupling of *N*-heteroaromatics (quinolines) with alkyl halides. The tandem process is catalyzed by CuI and allows the formation of 1,2-difunctionalized quinoline-type derivatives (Scheme 1.17) [55].

Some carbonylative MCR processes dealing with heterocyclic inputs have also been disclosed: a Pd-catalyzed four-component coupling involving tryptamine leads to alkaloid-like compounds featuring the quinazolinone core [56]. Divergent PdI_2/KI-catalyzed aminocarbonylation-cyclization pathways starting from alkynylthioimidazoles yield functionalized imidazo-thiazinones and -thiazoles (Scheme 1.18) [57].

Although not strictly belonging to this section, metal-catalyzed post-modifications of MCR adducts constitute a powerful and versatile synthetic tool. For instance, Au/Ag-catalysis on phenol-alkynyl Ugi adducts efficiently promotes an intramolecular dearomative cyclization, followed by an aza-Michael addition yielding the tetracyclic scaffold [58]. Similarly, a concerted [4 + 2] cyclization on an indole substrate terminates the assembly of complex bridged polycyclic alkaloid arrangements [59]. In this approach, the key step involves the alkyne hydroarylation. A related process involving a furane-alkyne Ugi adduct, undergoes the Au-domino process ending with a ring fragmentation to yield unsaturated 2-pyridones (Scheme 1.19) [60].

1.5 Carbonyl/Imine Polar MCRs

In this section a variety of multicomponent transformations involving carbonyl and/or imine substrates (not specifically related to the rest of the sections) is analyzed. For instance, a Mannich-type MCR of indoles, amines, and substituted aldehydes followed by a lactamization leads to a bicyclic a adduct [61]. A cascade three-component reaction of 6-aminouracil, aldehydes and tetrahydroisoquinolines allows the formation of a new pyrimidine ring through the functionalization of the C–H adjacent to the nitrogen by a 1,5-hydride transfer and concomitant oxidation [62]. A domino process involving heterocyclic *N*-acylenamines, formaldehyde, and primary amines builds conjugated pyrimidine rings in a stepwise Mannich-aminal MCR [63]. A mechanistically related process connects tryptamines, alkyl propiolates, and nitroalkenes, yielding indolizino-indoles or chromeno-indolizinoindoles (Scheme 1.20) [64].

The Petasis MCR, the interaction of *in situ* generated imines and boronic acids has been reviewed [65]. A highly diastereoselective three-component Petasis/intramolecular Diels–Alder tandem reaction involving allyl amines,

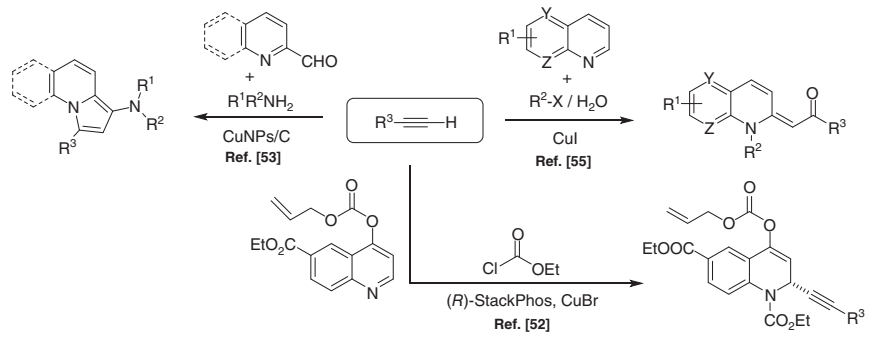

Scheme 1.17 A3-type MCRs.

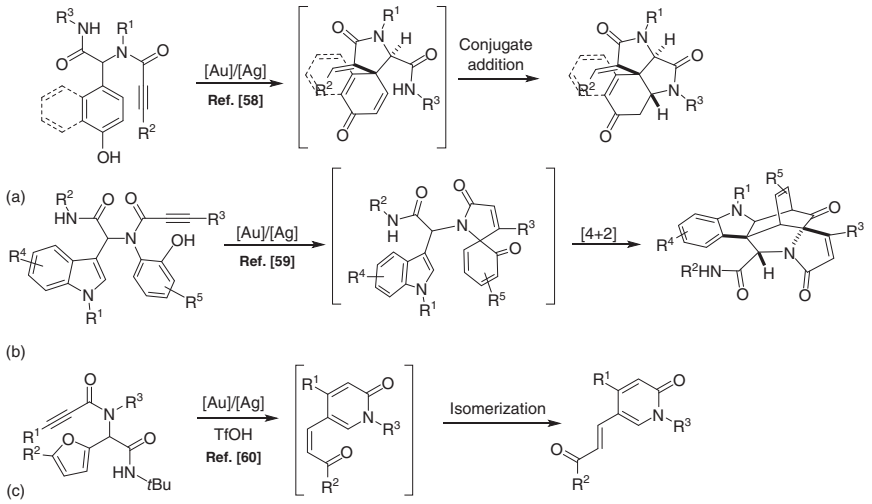

Scheme 1.19 Au(Ag)-catalyzed MCR post-transformations.

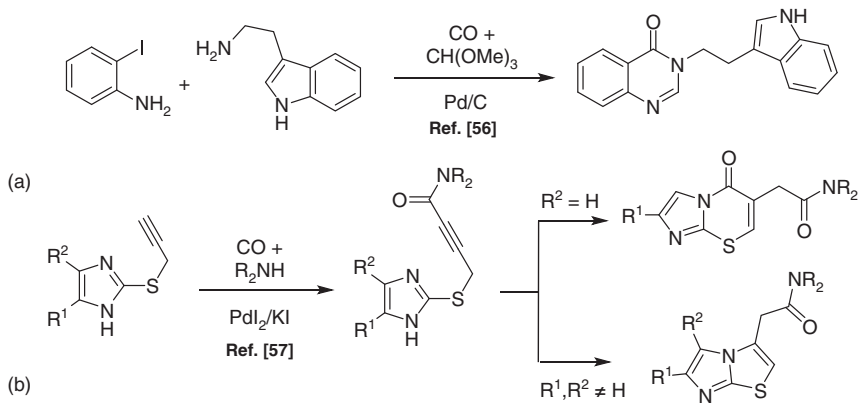

Scheme 1.18 Carbonylative transition-metal catalyzed MCRs.

furylboronic acid, and α-hydroxylated aldehydes led to a compact functionalized tricyclic system (Scheme 1.21) [66].

The Biginelli-type MCRs stand for the interaction of urea or urea-like compounds, aldehydes, and dicarbonyl derivatives. In this way, thiazolo-quinazolinones are generated from aminothiazoles [67]. Diversely substituted aminotriazoles [68] and aminopyrazoles [69] are active in Bigineli MCRs leading to the corresponding pyrimidine adducts (Scheme 1.22).

In a Hantzsch-type MCR, fused-tricyclic pyrans, and dihydropyridines were prepared by an indium (III)-catalyzed protocol involving a Knoevenagel adduct that cyclized to the final *N*- or *O*-tricyclic core (Scheme 1.22) [70]. Similarly, coumarin-fused pyrimidines were prepared by Biginelli-type MCRs (Scheme 1.23) [71, 72].

The Yonemitsu MCR has been employed for the synthesis of indole-based triarylmethanes. As an example, coumarines, diversely substituted indoles and quinoline-aldehydes led to highly crowded adducts [73]. Cyclic thio-substituted β-enaminoesters reacted in a diastereoselective manner with isatins cyclic β-diketones or 4-hydroxychromen-2-one to furnish complex polycyclic spiroindolines (Scheme 1.23) [74].

In a variation of this reactivity pattern, a nitro-Michael acceptor is introduced, and azolopyrimidines were synthetized by a BF_3-catalyzed MCR involving aminoazoles, aldehydes, and morpholinonitroalkenes, through the *in situ* generation of the reactive nitroalkynes (Scheme 1.24) [75].

The Reissert-type reactions involve the addition of nucleophiles to *in situ* *N*-activated azines to yield covalent adducts, usually at the α-position. Progress in the area deals with the regioselective phosphonylation of quinolines upon activation with chloroformates. Thus, reaction of the intermediate with differently substituted *N*-heterocyclic phosphines, where the substituent at the oxygen atom determines the α- or γ-attack (Scheme 1.25) [76].

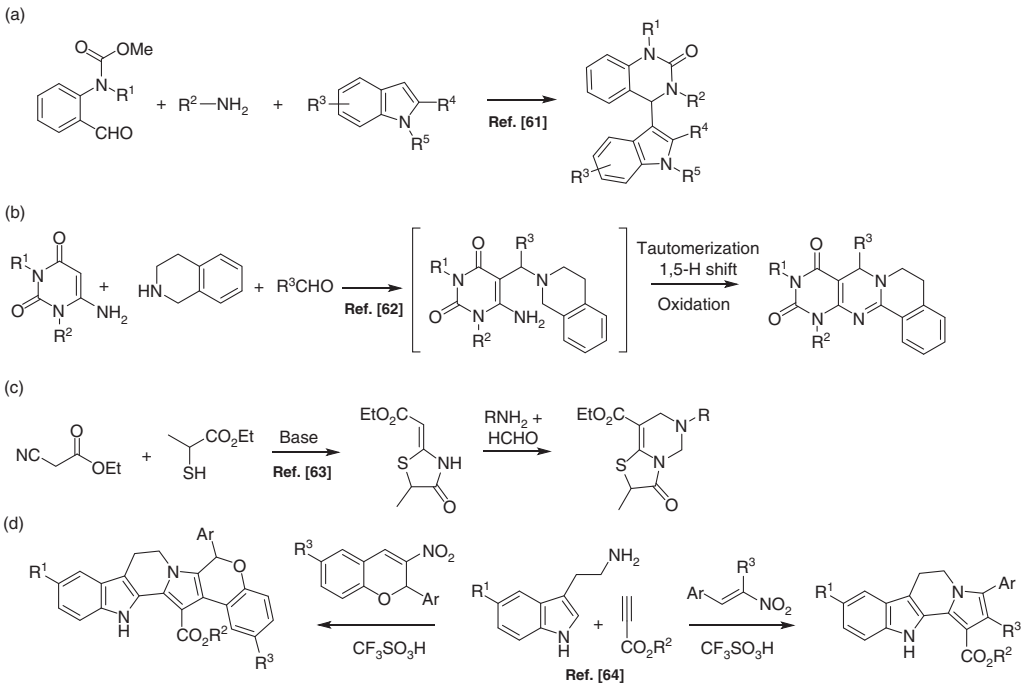

Scheme 1.20 Mannich-type MCRs.

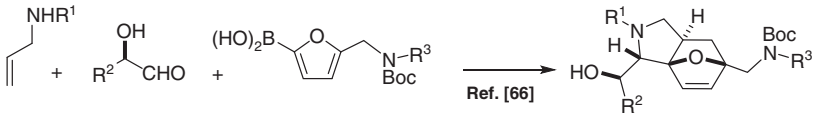

Scheme 1.21 Petasis MCR.

New enantioselective catalytic methods have been disclosed for this transformation. Chiral phosphoric acid promotes the *N*-addition of indoles upon *in situ* generated *N*-Boc-isoquinolinium ions [77]. Also, chloroformate promoted silyl ketene acetal additions to isoquinolines and other azines catalyzed by chiral anion-binding triazoles (Scheme 1.25) [78].

1.6 Isocyanide-based MCRs

Isocyanides stay as the most fruitful functional group in the MCR field. The classic Ugi and Passerini processes are still matter of active research, mainly dealing with mechanistic modifications and novel substrates. With respect to the Ugi-type MCRs, relevant results have appeared in this period. Regarding novelties in the reaction modes, interrupted processes have gained much importance. In these transformations, the usual trapping of the intermediate nitrilium ion by carboxylates and the subsequent Mumm rearrangement are replaced by a variety of nucleophilic additions affording structural diversity [79]. For instance, indole can efficiently trap the nitrilium, leading to spiroindolines, which continue a domino process to complex alkaloid-like compounds (Scheme 1.26) [80].

Heterocyclic amines have provided a series of oxidative [81] and redox neutral [82, 83] processes, involving the *in situ* formation of the active imine/iminium species, which subsequently react in an Ugi fashion. The Ugi–Smiles approach has been extended to functionalize thiouracil derivatives [84]. The interaction of an *in situ* generated Knoevenagel adduct with isocyanides and maleimides leads to a convenient preparation of a polycyclic adduct, which spontaneously evolves into a variety of isoindolocarbazoles (Scheme 1.26) [85].

Oxochromones react in a similar manner, upon the interaction with isocyanides and alkenes, through a series of [4 + 1]/[4 + 2] cycloadditions [86]. Interestingly, the closely related formylchromones can react with amines and isocyanides in a different way, leading to adducts arising from the initial conjugate addition of the isocyanide or the amine input to the conjugate carbonyl (Scheme 1.27) [87, 88].

Activated aziridines have produced polysubstituted tetrahydropyridines upon the interaction with cyanomalonates and isocyanides [89]. Finally, 2-bromo-6-isocyanopyridine is a general and affordable convertible isocyanide, since it suitably participates in Ugi processes, and the resulting aminopyridine unit can be replaced by a variety of nucleophiles in the adduct (Scheme 1.27) [90].

The Joullié MCR involves the interaction of imines with carboxylic acids and isocyanides [91]. From a synthetic point of view, this process is not just a simplification of the Ugi MCR, but rather a way to promote novel reactivity pathways. For

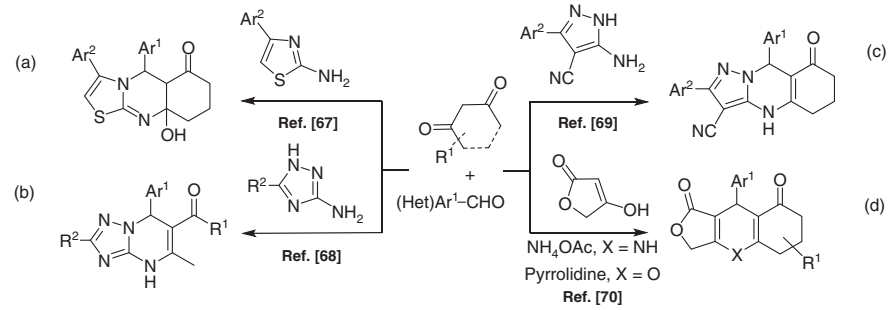

Scheme 1.22 Dicarbonyl derivatives in Biginelli- and Hantzsch-type MCRs.

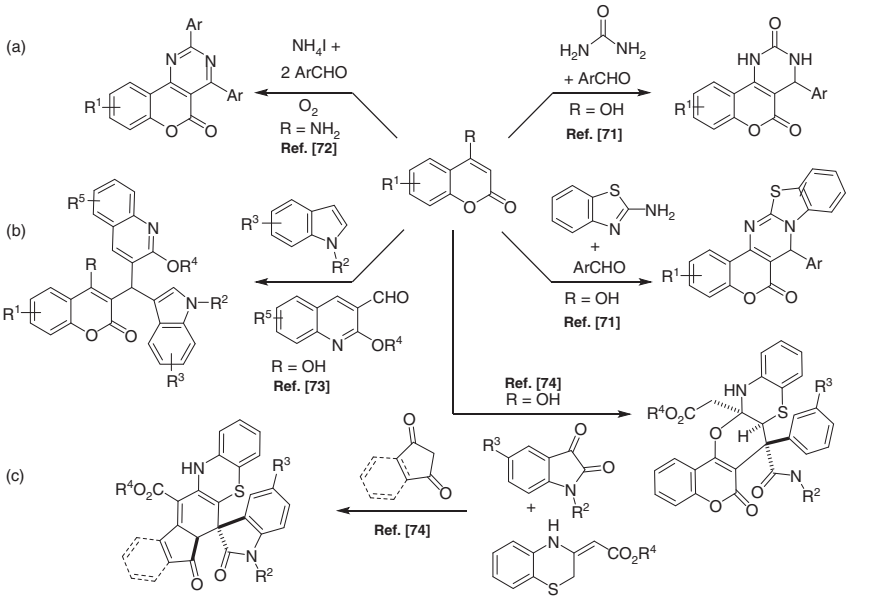

Scheme 1.23 Coumarins and isatins in MCRs.

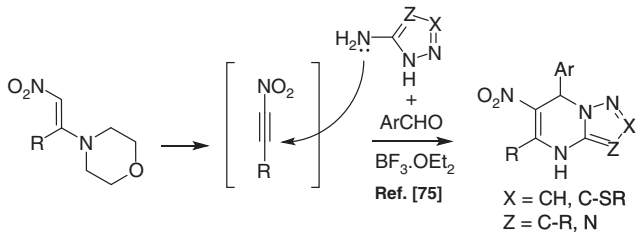

Scheme 1.24 Aminoazoles in conjugated addition-type MCRs.

instance, the *in situ* generation of cyclic imines from the (electro) chemical oxidation of secondary amines and their subsequent transformation has been described [92].

With respect to the different substrates engaged in the Joullié MCR, it is worth mentioning the spiroindolenines, which have suitably reacted to yield fused diketopiperazines, linked diamides, and tetrazoles [93, 94]. A remarkable approach to bicyclic hydantoines from *in situ* generated iminium salts resulting from the trifluoroacetic acid (TFA) treatment of *N*-Boc protected dihydropyrazines and β-aminoketones has been disclosed [95]. Azirines have recently been brought into this chemistry through Lewis acid activation, allowing a stereoselective access to functionalized *N*-acyl-aziridinecarboxamides (Scheme 1.28) [96].

The Groebke–Bienaymé–Blackburn (GBB) MCR, the interaction of α-aminoazines, aldehydes, and isocyanides, yield fused aminoimidazoles, a highly privileged scaffold in medicinal chemistry [97]. Mainly nonconventional examples of these transformations are mentioned here. Regarding aminoazines, GBBs with *N*-Boc-3-aminoindole followed by an oxidative cascade have resulted in the one-pot access to pyridodindoles [98]. The reaction mechanism features an interesting azirine intermediate, which evolves into the final adduct through a radical Neber-type rearrangement followed by a [1,2]-hydrogen shift/cyclization (Scheme 1.29).

Tetrahydroquinolin-8-amine, aldehydes, and isocyanides react to afford fused tricyclic quinoxaline adducts in a homoGBB transformation, in the presence of DMAP. The mechanism relies on the condensation of the aldehyde with the aniline to form the initial iminium ion, followed by the attack of the isocyanide [99].

Polyaminopolyazines have also been reported to afford multiple GBB adducts. The innate selectivity [100] observed in the case of 2,4-diaminopyrimindine results in the exclusive formation of a single monoadduct, enabling a selective second GBB upon the former product [101]. Incidentally, the monoadduct with the alternative regioselectivity was prepared through a protection strategy [102]. In a similar manner, triple-GBB transformations upon melamine yield unprecedented tripodal scaffolds, amenable to further diversification via suitable post-modifications (Scheme 1.29) [101].

Carbonyl components further diversify the reach of these transformations. GBBs with isatine and aminopyridines result in the one-pot formation of fused imidazopyrimidone salts through the expected spiroimidazole GBB adduct that

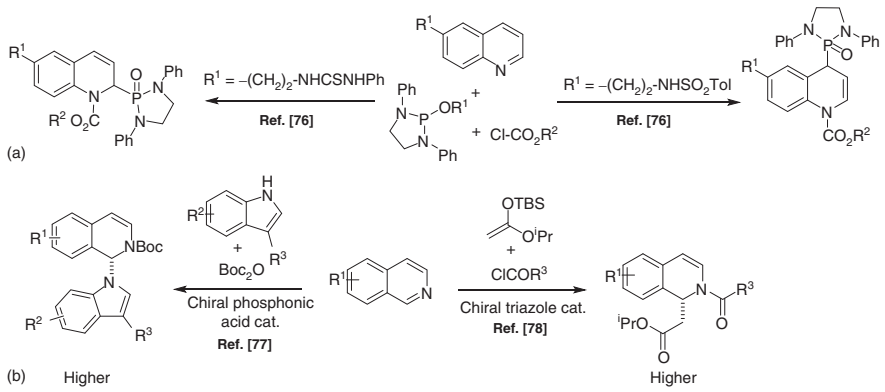

Scheme 1.25 Reissert-type reactions.

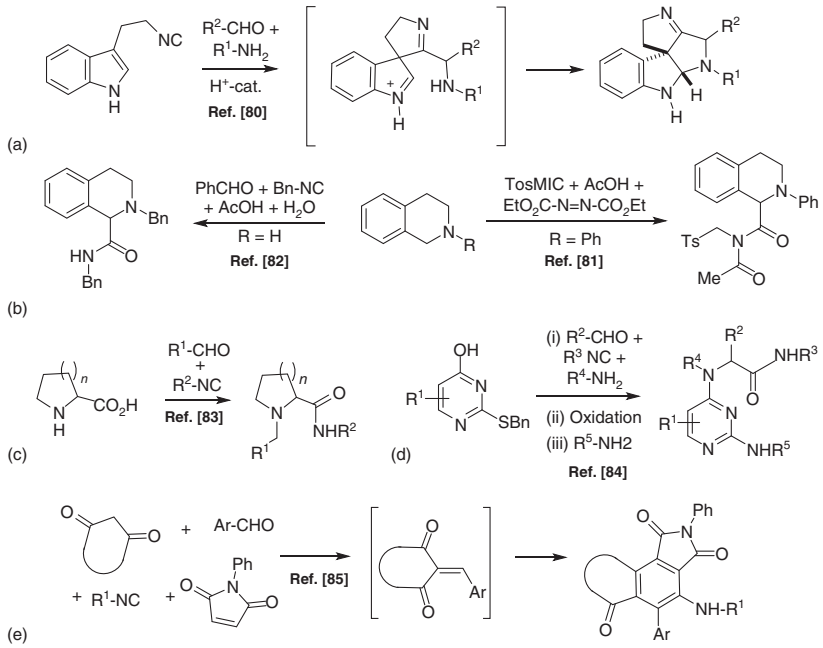

Scheme 1.26 Ugi-type MCRs. Mechanistic variations.

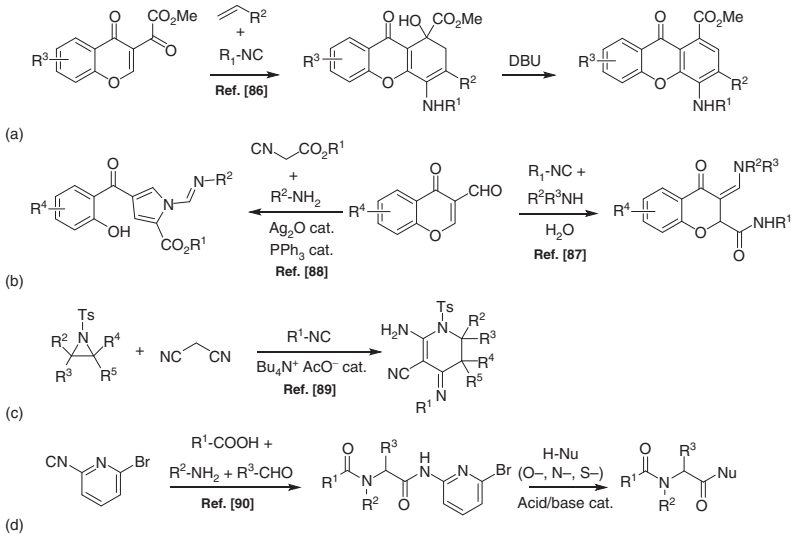

Scheme 1.27 Ugi-type MCRs. Substrate variations.

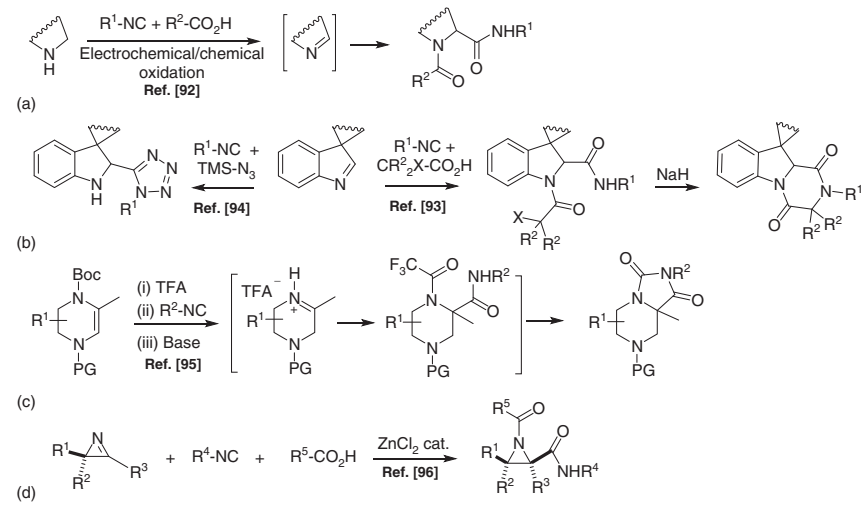

Scheme 1.28 Joullié-type MCRs. Substrate variations.

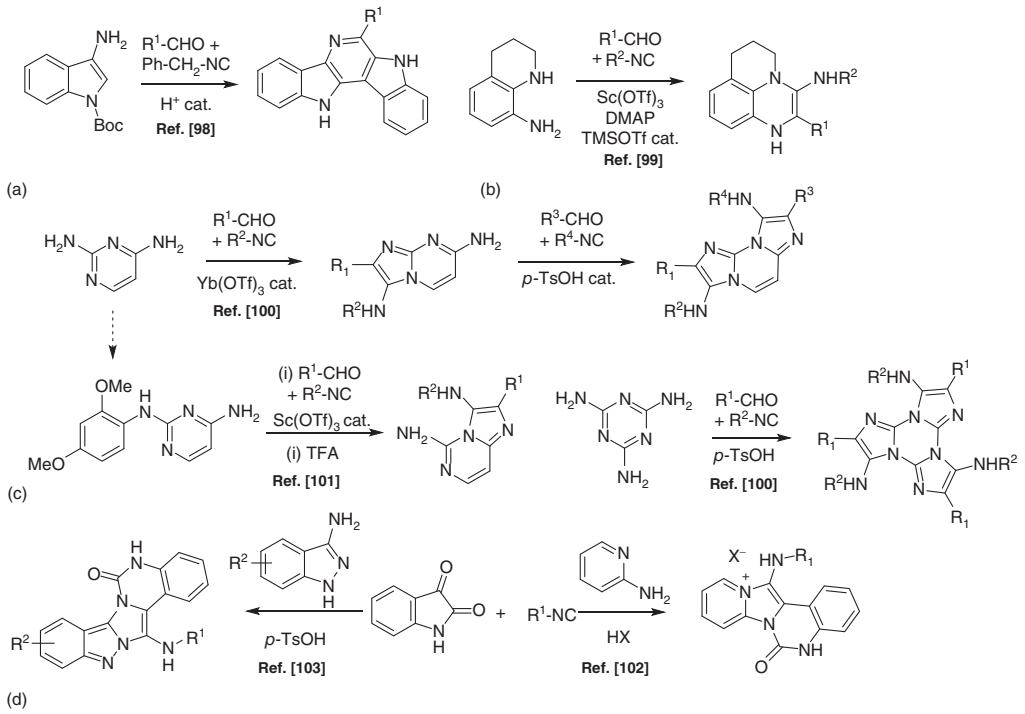

Scheme 1.29 GBB-type MCRs. Mechanistic variations.

suffers a [1,5]-H shift, followed by the intramolecular trapping of the isocyanate intermediate [103]. Aminoindazoles give the corresponding adduct in a similar manner (Scheme 1.29) [104].

The combination of 2-(2-bromoethyl)benzaldehyde and aminopyridines yields a dihydroquinolinium ion that continues the GBB reaction upon the attack of the isocyanide and the cyclization/aromatization step to afford the corresponding adduct [105]. Similar transformations have been reported with aminoindazole [106].

GBB reactions with propynals afford interesting post-condensation modifications exploiting the triple bond transformations, to yield iodo-substituted fused imidazopyrroles upon the cyclization with iodine [107]. In a recent report, however, the participation of benzyl isocyanide in GBB MCRs with propynals activates an alternative route: upon the *in situ* oxidation of the benzyl residue to give an imine, and the TBAB-mediated activation of the triple bond, the cyclization affords imidazo-dipyridines instead (Scheme 1.30) [108].

The incorporation of indole carbaldehydes enables GBB adducts to undergo a variety of domino processes, due to a key polarity inversion of the indole residue after the MCR. In this way, indole 3-carbaldehyde GBB adducts suffer a spontaneous oxidative Pictet–Spengler transformation to afford a variety of fused polyheterocyclic systems. However, indole 2-carbaldehyde GBB adducts yield indolocabazoles in an AB_3C fashion, and a striking bicyclic scaffold at higher temperature (Scheme 1.30) [109].

A variety of formal [3 + 2] cycloadditions involve novel interactions of isocyanides with heterocyclic substrates, forming part of the either dipole or the dipolarophile. For instance, the interaction of dipoles, *in situ* generated through the addition of isocyanides to unsaturated carbonyls, with isoquinolines leads to single adducts with high stereoselectivity, under chiral organocatalysis [110]. Similarly, the participation of acetylenedicarboxylate and sulfamate-derived cyclic imines leads to fused pyrroles in a regioselective manner via the corresponding isocyanide-dipole (Scheme 1.31) [111].

Insertion processes, not included in previous sections, account for meaningful transformations. For instance, indole, selenium, isocyanides, and secondary amines lead to a four-component adduct through a selenourea radical intermediate, under oxidative conditions [112]. Another mechanistic variation involves the insertion of isocyanides upon N—Si bonds, in a TMSCl-promoted interaction. In this way, azines and two equivalents of isocyanides, which can be differentiated because of having different roles in the process, lead to fused isoquinoline-imidazolium salts (Scheme 1.31) [113].

1.7 Miscellany Processes

Among the processes that do not fit in the precedent sections, we may mention the productive research in the chemistry of the BODIPY derivatives as a source of smart fluorophores. Formyl-BODIPYs have been prepared and reacted in Passerini MCR [114]. Interesting contributions to the synthesis of BODIPYs through MCRs

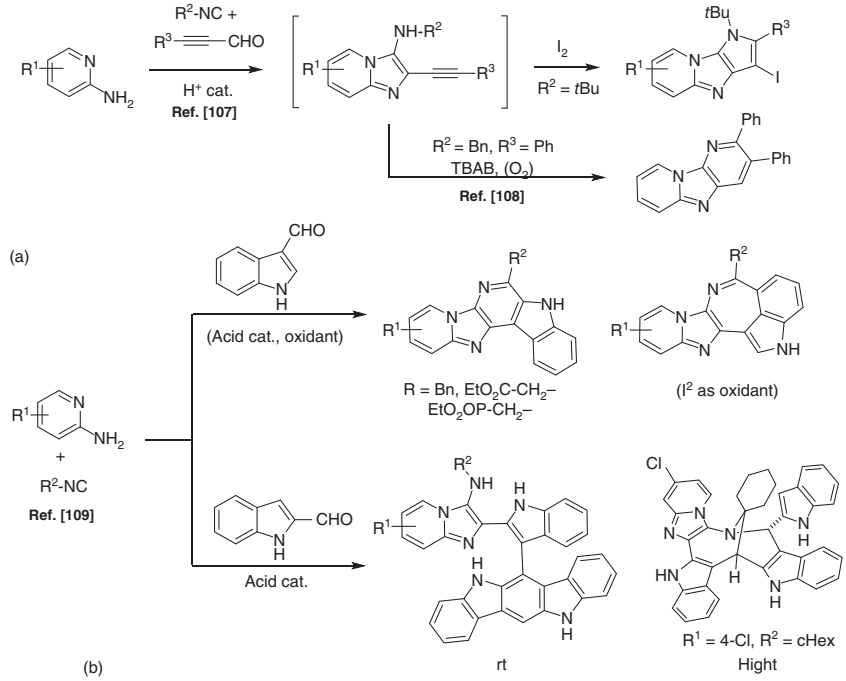

Scheme 1.30 GBB-type MCRs: post-transformations.

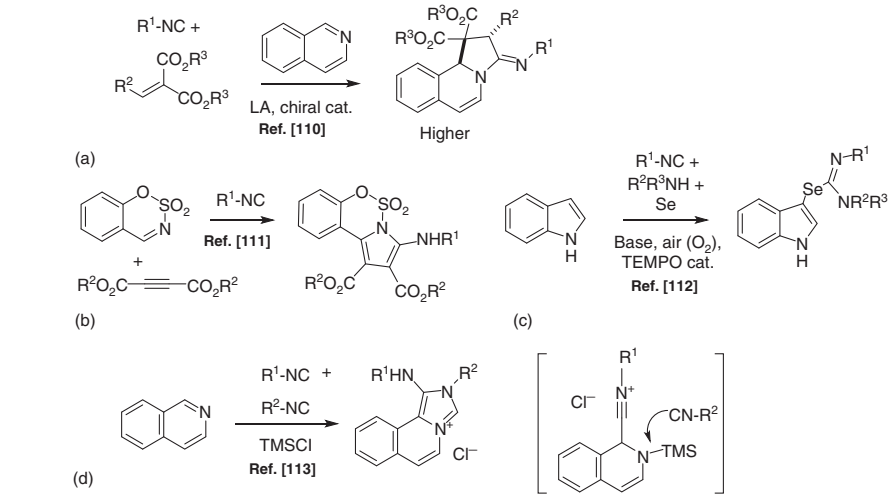

Scheme 1.31 Isocyanide MCRs based on cycloadditions and insertions.

have also appeared: the Lewis acid–catalyzed condensation of lactones with pyrrole [115] and the interaction of a phenol-substituted pyrrole with boronic acids and another pyrrole unit to yield the dye in one step [116]. The known interaction of isocyanides, azines, and trifluoroacetic anhydride leading to dipolar acid fluorides has been performed on a fluorophore-linked isoquinoline to afford a probe capable of selectively labeling amines, allowing its direct visualization in cell environments (Scheme 1.32) [117].

Fused imidazoazines have been prepared through aldol-type condensation followed by a SNAr (or Ullmann coupling) and a click reaction to yield complex MCR adducts [118]. Also, the interaction of aminopyridines with ketones and thiols yields thio-substituted imidazopyridines via a remarkable coupled I_2-Flavin catalysis (Scheme 1.33) [119]. Some MCR processes are based on a series of nucleophilic displacements: the interaction of azines with indoles and dichloroethane triggers a domino process, which is oxidatively terminated to yield cationic azahelicenes [120]. Furthermore, the participation of DABCO, α-chloroazines, and sulfide anions promotes an orchestrated sequence of SNAr-SN2-SNAr processes leading to a four-component scaffold (Scheme 1.33) [121].

Unsaturated nitro derivatives display a rich chemistry, enabling new MCRs based on conjugated additions and subsequent Henry or NO_2 elimination processes. For instance, their interaction with cyclohexanone and aminopyrazole leads to heterocyclic spiroadducts [122]. Furthermore, 3-nitro-indole or -benzothiazole reacts with *in situ* generated cyclic ketimines leading to indole-fused heteroacenes (Scheme 1.34) [123].

To finish this section, we mention an impressive contribution to the field of reaction discovery where, among other transformations, novel MCRs were described using a high-throughput autonomous organic synthesis robot fitted with analytical tools and controlled by a machine learning algorithm (Scheme 1.34) [124].

1.8 Conclusion

Merging the synthetic power of MCRs with the particular reactivity of heterocycles leads to an impressive array of new transformations and unprecedented connectivity patterns. These new scaffolds are produced in a straightforward manner, often by simply mixing the reactants and, due to their combinatorial nature, are amenable to parallelization. Furthermore, the highlighted processes show high levels of structural variability. The reaction discovery based on these heterocycle-based MCRs is already very fruitful and, although in its infancy, the description of this uncharted reactivity is paving the way to a systematic use of these processes in synthetic chemistry.

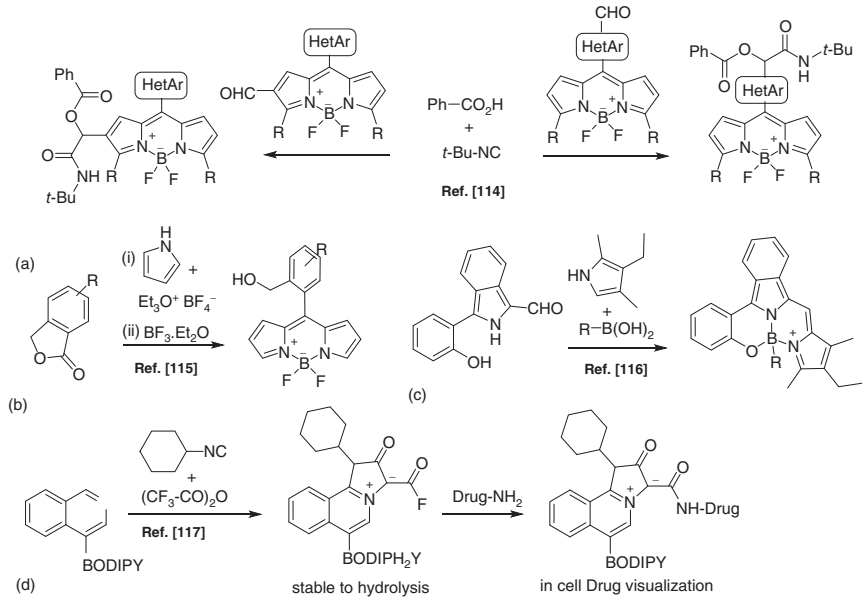

Scheme 1.32 MCRs featuring BODIPYs.

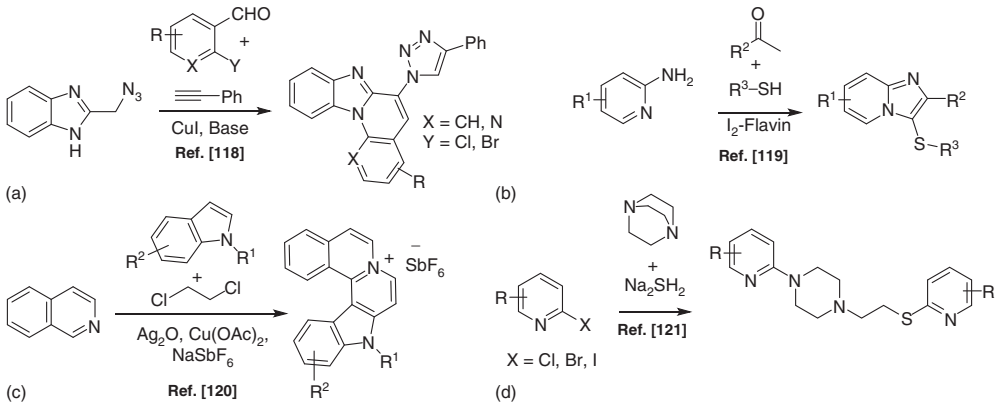

Scheme 1.33 Azole and azine nucleophilic MCRs.

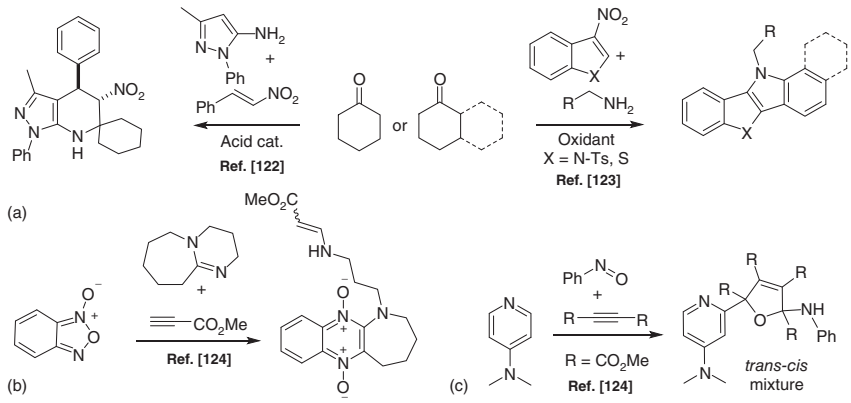

Scheme 1.34 MCRs based on nitro derivatives and AI reaction discovery.

Acknowledgment

Support from the Ministerio de Ciencia e Innovación (Spain, PID2019-107991RB-I00) is acknowledged. Profs. Gemma Fabriàs and Ignacio Alfonso (IQAC, CSIC Barcelona, Spain) are thanked for support.

References

1 Isambert, N. and Lavilla, R. (2008). *Chem. A Eur. J.* 14: 8444.
2 Sunderhaus, J.D. and Martin, S.F. (2009). *Chem. A Eur. J.* 15: 1300.
3 Rotstein, B.H., Zaretsky, S., Rai, V., and Yudin, A.K. (2014). *Chem. Rev.* 114: 8323.
4 Vicente-García, E., Kielland, N., and Lavilla, R. (2015). Functionalization of Heterocycles by MCRs. In: *Multicomponent Reactions in Organic Synthesis* (eds. J. Zhu, Q. Wang and M.-X. Wang), 159. Wiley.
5 Muthukrishnan, I., Sridharan, V., and Menéndez, J.C. (2019). *Chem. Rev.* 119: 5057.
6 Ghashghaei, O., Masdeu, C., Alonso, C. et al. (2018). *Drug Discov. Today Technol.* 29: 71.
7 Abranches, P.A.D.S., De Paiva, W.F., De Fátima, Â. et al. (2018). *J. Org. Chem.* 83: 1761.
8 Hoemann, M.Z., Xie, R.L., Rossi, R.F. et al. (2002). *Bioorg. Med. Chem. Lett.* 12: 129.
9 Galván, A., Fontaneda, R., Fañanás, F.J., and Rodríguez, F. (2016). *Adv. Synth. Catal.* 358: 1741.
10 Galván, A., Calleja, J., González-Pérez, A.B. et al. (2015). *Chem. A Eur. J.* 21: 16769.
11 Pasha, J., Kandagatla, B., Sen, S. et al. (2015). *Tetrahedron Lett.* 56: 2289.
12 Dai, W., Jiang, X.L., Tao, J.Y., and Shi, F. (2016). *J. Org. Chem.* 81: 185.
13 Retich, C. and Bräse, S. (2018). *Eur. J. Org. Chem.* 2018: 60.
14 Islam, K., Das, D.K., Akram, E., and Khan, A.T. (2015). *Synthesis* 47: 2745.
15 Tejería, A., Pérez-Pertejo, Y., Reguera, R.M. et al. (2018). *Eur. J. Med. Chem.* 152: 137.
16 Singh, P., Adolfsson, D.E., Ådén, J. et al. (2019). *J. Org. Chem.* 84: 3887.
17 Moshapo, P.T., Sokamisa, M., Mmutlane, E.M. et al. (2016). *Org. Biomol. Chem.* 14: 5627.
18 Jiang, H.J., Liu, K., Wang, J. et al. (2017). *Org. Biomol. Chem.* 15: 9077.
19 Yang, S., Zhu, S., Lu, D., and Gong, Y. (2019). *Org. Lett.* 21: 8464.
20 Bobers, J., Škopić, M.K., Dinter, R. et al. (2020). *ACS Comb. Sci.* 22: 101.
21 Chen, G.G., Wei, J.Q., Yang, X., and Yao, Z.J. (2016). *Org. Lett.* 18: 1502.
22 Xu, J.-H., Zheng, S.-C., Zhang, J.-W. et al. (2016). *Angew. Chem. Int. Ed.* 55: 11834.
23 Li, J.L., Dai, Q.S., Yang, K.C. et al. (2018). *Org. Lett.* 20: 7628.

24 Mirzaei, A., Turczel, G., Nagyházi, M. et al. (2021). *Eur. J. Org. Chem.* 2021: 326.

25 Wu, X., Zhu, Z.H., He, H. et al. (2020). *J. Org. Chem.* 85: 6216.

26 Arumugam, N., Almansour, A.I., Suresh Kumar, R. et al. (2020). *Bioorg. Chem.* 99: 103799.

27 Nájera, C. and Sansano, J.M. (2019). *Pure Appl. Chem.* 91: 575.

28 Zhang, X., Qiu, W., Evans, J. et al. (2019). *Org. Lett.* 21: 2176.

29 Wu, F.S., Zhao, H.Y., Xu, Y.L. et al. (2017). *J. Org. Chem.* 82: 4289.

30 Samala, S., Ryu, D.H., Song, C.E., and Yoo, E.J. (2019). *Org. Biomol. Chem.* 17: 1773.

31 Cao, J., Yang, F., Sun, J. et al. (2019). *J. Org. Chem.* 84: 622.

32 Ghorai, S. and Lee, D. (2020). *Synlett* 31: 750.

33 Liautard, V. and Landais, Y. (2015). Free-radical multicomponent processes. In: *Multicomponent Reactions in Organic Synthesis* (eds. J. Zhu, Q. Wang and M.-X. Wang), 401. Wiley.

34 Garbarino, S., Ravelli, D., Protti, S., and Basso, A. (2016). *Angew. Chem. Int. Ed.* 55: 15476.

35 Proctor, R.S.J. and Phipps, R.J. (2019). *Angew. Chem. Int. Ed.* 58: 13666.

36 Lear, J.M., Buquoi, J.Q., Gu, X. et al. (2019). *Chem. Commun.* 55: 8820.

37 Li, T., Liang, K., Zhang, Y. et al. (2020). *Org. Lett.* 22: 2386.

38 Liu, Z. and Liu, Z.Q. (2017). *Org. Lett.* 19: 5649.

39 Buquoi, J.Q., Lear, J.M., Gu, X., and Nagib, D.A. (2019). *ACS Catal.* 9: 5330.

40 Zheng, D. and Studer, A. (2019). *Angew. Chem. Int. Ed.* 58: 15803.

41 Chen, D., Xu, L., Long, T. et al. (2018). *Chem. Sci.* 9: 9012.

42 Cao, J., Wang, G., Gao, L. et al. (2019). *Chem. Sci.* 10: 2767.

43 Lee, K., Lee, S., Kim, N. et al. (2020). *Angew. Chem. Int. Ed.* 59: 13379.

44 Li, H., Guo, L., Feng, X. et al. (2020). *Chem. Sci.* 11: 4904.

45 Breton-Patient, C., Naud-Martin, D., Mahuteau-Betzer, F., and Piguel, S. (2020). *Eur. J. Org. Chem.* 2020: 6653.

46 Ye, J.H., Zhu, L., Yan, S.S. et al. (2017). *ACS Catal.* 7: 8324.

47 Cuadros, S., Horwitz, M.A., Schweitzer-Chaput, B., and Melchiorre, P. (2019). *Chem. Sci.* 10: 5484.

48 Choi, J.H. and Park, C.M. (2018). *Adv. Synth. Catal.* 360: 3553.

49 Sharma, U.K., Sharma, N., Xu, J. et al. (2015). *Chem. A Eur. J.* 21: 4908.

50 Kumar, G.S., Ragini, S.P., Kumar, A.S., and Meshram, H.M. (2015). *RSC Adv.* 5: 51576.

51 Lv, W., Chen, Y., Wen, S. et al. (2020). *J. Am. Chem. Soc.* 142: 14864.

52 Pappoppula, M. and Aponick, A. (2015). *Angew. Chem. Int. Ed.* 54: 15827.

53 Chinna Rajesh, U., Purohit, G., and Rawat, D.S. (2015). *ACS Sustain. Chem. Eng.* 3: 2397.

54 Albaladejo, M.J., Alonso, F., and González-Soria, M.J. (2015). *ACS Catal.* 5: 3446.

55 He, Q., Xie, F., Xia, C. et al. (2020). *Org. Lett.* 22: 7976.

56 Natte, K., Neumann, H., and Wu, X.F. (2015). *Catal. Sci. Technol.* 5: 4474.

57 Veltri, L., Mancuso, R., Altomare, A., and Gabriele, B. (2015). *ChemCatChem* 7: 2206.
58 He, Y., Li, Z., Tian, G. et al. (2017). *Chem. Commun.* 53: 6413.
59 He, Y., Liu, Z., Wu, D. et al. (2019). *Org. Lett.* 21: 4469.
60 Du, X., Yu, J., Gong, J. et al. (2019). *Eur. J. Org. Chem.* 2019: 2502.
61 Ramana, D.V., Vinayak, B., Dileepkumar, V. et al. (2016). *RSC Adv.* 6: 21789.
62 Deb, M.L., Borpatra, P.J., and Baruah, P.K. (2019). *Green Chem.* 21: 69.
63 Yıldırım, M. and Çelikel, D. (2015). *Mol. Divers.* 19: 1.
64 Sun, J., Jiang, W., and Yan, C.G. (2018). *RSC Adv.* 8: 28736.
65 Wu, P., Givskov, M., and Nielsen, T.E. (2019). *Chem. Rev.* 119: 11245.
66 Flagstad, T., Azevedo, C.M.G., Troelsen, N.S. et al. (2019). *Eur. J. Org. Chem.* 2019: 1061.
67 Mohanta, P.P., Pati, H.N., and Behera, A.K. (2020). *RSC Adv.* 10: 15354.
68 Wang, H., Lee, M., Peng, Z. et al. (2015). *J. Med. Chem.* 58: 4194.
69 Kolosov, M.A., Beloborodov, D.A., Orlov, V.D., and Dotsenko, V.V. (2016). *N. J. Chem.* 40: 7573.
70 Shearer, C., Desaunay, O., Zorc, S. et al. (2019). *Tetrahedron* 75: 130606.
71 Sahu, P.K., Sahu, P.K., Kaurav, M.S. et al. (2018). *ACS Omega* 3: 15035.
72 Chen, J., Ouyang, C., Xiao, T. et al. (2019). *ChemistrySelect* 4: 7327.
73 Abonia, R., Gutiérrez, L.F., Insuasty, B. et al. (2019). *Beilstein J. Org. Chem.* 15: 642.
74 Sun, Q.S., Sun, J., Pan, L.N., and Yan, C.G. (2020). *J. Org. Chem.* 85: 12117.
75 Lyapustin, D.N., Ulomsky, E.N., Zanakhov, T.O., and Rusinov, V.L. (2019). *J. Org. Chem.* 84: 15267.
76 Shetty, M., Huang, H., and Kang, J.Y. (2018). *Org. Lett.* 20: 700.
77 Cai, Y., Gu, Q., and You, S.L. (2018). *Org. Biomol. Chem.* 16: 6146.
78 Zurro, M., Asmus, S., Bamberger, J. et al. (2016). *Chem. A Eur. J.* 22: 3785.
79 Giustiniano, M., Moni, L., Sangaletti, L. et al. (2018). *Synthesis* 50: 3549.
80 Saya, J.M., Oppelaar, B., Cioc, R.C. et al. (2016). *Chem. Commun.* 52: 12482.
81 Wang, J., Sun, Y., Wang, G., and Zhen, L. (2017). *Eur. J. Org. Chem.* 2017: 6338.
82 Zhu, Z. and Seidel, D. (2016). *Org. Lett.* 18: 631.
83 Dighe, S.U., Kumar, A.K.S., Srivastava, S. et al. (2015). *J. Org. Chem.* 80: 99.
84 Sidhoum, M.A., El Kaïm, L., and Grimaud, L. (2018). *Tetrahedron* 74: 5222.
85 Bornadiego, A., Diáz, J., and Marcos, C.F. (2019). *J. Org. Chem.* 84: 7426.
86 Bornadiego, A., Díaz, J., and Marcos, C.F. (2015). *J. Org. Chem.* 80: 6165.
87 Lei, J., Li, Y., Li, Y. et al. (2020). *Green Chem.* 22: 3716.
88 Liao, J.Y., Yap, W.J., Wu, J.'.E. et al. (2017). *Chem. Commun.* 53: 9067.
89 Samzadeh-Kermani, A. (2019). *Monatsh. Chem.* 150: 1495.
90 van der Heijden, G., Jong, J.A.W., Ruijter, E., and Orru, R.V.A. (2016). *Org. Lett.* 18: 984.
91 Nazeri, M.T., Farhid, H., Mohammadian, R., and Shaabani, A. (2020). *ACS Comb. Sci.* 22: 361.
92 Pan, N., Ling, J., Zapata, R. et al. (2019). *Green Chem.* 21: 6194.
93 Golubev, P. and Krasavin, M. (2017). *Eur. J. Org. Chem.* 2017: 1740.
94 Estévez, V., Kloeters, L., Kwietniewska, N. et al. (2017). *Synlett* 28: 376.

95 Firth, J.D., Zhang, R., Morgentin, R. et al. (2015). *Synthesis* 47: 2391.
96 Angyal, A., Demjén, A., Wéber, E. et al. (2018). *J. Org. Chem.* 83: 3570.
97 Boltjes, A. and Dömling, A. (2019). *Eur. J. Org. Chem.* 2019: 7007.
98 Chen, Z.Z., Li, S.Q., Zhang, Y.J. et al. (2018). *Org. Lett.* 20: 7811.
99 Azad, C.S. and Narula, A.K. (2017). *Eur. J. Org. Chem.* 2017: 6413.
100 Ghashghaei, O., Seghetti, F., and Lavilla, R. (2019). *Beilstein J. Org. Chem.* 15: 521.
101 Ghashghaei, O., Caputo, S., Sintes, M. et al. (2018). *Chem. A Eur. J.* 24: 14513.
102 Konstantinidou, M., Boiarska, Z., Butera, R. et al. (2020). *Eur. J. Org. Chem.* 2020: 5601.
103 Yang, B., Tao, C., Shao, T. et al. (2016). *Beilstein J. Org. Chem.* 12: 1487.
104 Balwe, S.G. and Jeong, Y.T. (2018). *Org. Chem. Front.* 5: 1628.
105 Sagar, A., Nagarjuna Babu, V., Shinde, A.H., and Sharada, D.S. (2016). *Org. Biomol. Chem.* 14: 10366.
106 Balwe, S.G., Vagh, S.S., and Jeong, Y.T. (2020). *Tetrahedron Lett.* 61: 152101.
107 Tber, Z., Hiebel, M.A., El Hakmaoui, A. et al. (2015). *J. Org. Chem.* 80: 6564.
108 Li, Y., Huang, J.H., Wang, J.L. et al. (2019). *J. Org. Chem.* 84: 12632.
109 Ghashghaei, O., Pedrola, M., Seghetti, F. et al. (2021, 2603). *Angew. Chem. Int. Ed.*: 60: 2603.
110 Xiong, Q., Dong, S., Chen, Y. et al. (2019). *Nat. Commun.* 10: 2116.
111 Wang, C., Ma, Z., Qu, Y. et al. (2020). *Chem. An Asian J.* 15: 560.
112 Liu, H., Fang, Y., Wang, S.Y., and Ji, S.J. (2018). *Org. Lett.* 20: 930.
113 Kishore, K.G., Ghashghaei, O., Estarellas, C. et al. (2016). *Angew. Chem. Int. Ed.* 55: 8994.
114 Ramírez-Ornelas, D.E., Alvarado-Martínez, E., Bañuelos, J. et al. (2016). *J. Org. Chem.* 81: 2888.
115 del Río, M., Lobo, F., Lopez, J.C. et al. (2017). *J. Org. Chem.* 82: 1240.
116 Chen, N., Zhang, W., Chen, S. et al. (2017). *Org. Lett.* 19: 2026.
117 Sintes, M., De Moliner, F., Caballero-Lima, D. et al. (2016). *Bioconjug. Chem.* 27: 1430.
118 Nagesh, H.N., Suresh, A., Reddy, M.N. et al. (2016). *RSC Adv.* 6: 15884.
119 Okai, H., Tanimoto, K., Ohkado, R., and Iida, H. (2020). *Org. Lett.* 22: 8002.
120 Wang, Z., Jiang, L., Ji, J. et al. (2020). *Angew. Chem. Int. Ed.* 59: 23532.
121 Zhu, Q., Yuan, Q., Chen, M. et al. (2017). *Angew. Chem. Int. Ed.* 56: 5101.
122 Zhang, F., Li, C., and Qi, C. (2020). *Org. Chem. Front.* 7: 2456.
123 Santhini, P.V., Akhil Krishnan, R., Babu, S.A. et al. (2017). *J. Org. Chem.* 82: 10537.
124 Granda, J.M., Donina, L., Dragone, V. et al. (2018). *Nature* 559: 377.

Chapter IV

General Conclusions

Chapter II. Development of Novel Blockers of the Chloride Channel LRRC8/VRAC

- We have successfully optimized and upgraded the synthetic routes to obtain the original hits of VRAC.
- We have prepared up to 20 derivatives of the original hits following synthetically simple procedures. We have concluded that the introduction of a diphenyl motif in the CBX enhances its inhibition activity, while removing the chirality of DCPIB maintains the original blocking activity of DCPIB.
- We have enhanced the BBB lipophilicity of our set of derivatives by introducing hydroxamic acids in the CBX-series and by doing ester prodrugs in the DCPIB-series.
- We have prepared a diazirine-based photoaffinity probe by replacing one of the alkyl chains of the non-chiral DCPIB derivative with a trifluoromethyl aryl diazirine. We have determined the inhibitory activity of the photo-probe, which is in the same range than the one of DCPIB.
- We have prepared the selected hits in acceptable amounts and in the required purity for the in vivo experiments. The results of the preliminary in vivo test did not show protective effect of our compounds.

Chapter III. Multicomponent Reactions towards the Synthesis of Bioactive Compounds

From Drugs to Drugs: towards Improved Antibiotics

- We have developed an interesting and unusual application of a MCR approach by introducing a commercial antibiotic in replacement of a MCR input. The scaffold that we obtained, has up to 3 functionalization points.
- We have prepared a library of 15 derivatives by using the GBB reaction and a broad spectrum of substituted aldehydes and isonitriles.

- We have studied the inhibition of microbial growth of our set of compounds in both Grampositive and Gramnegative bacterial strains, observing in most of the cases an inhibitory activity in the same range than the parent TMP.

- With the two most potent derivatives, our collaborators have studied in detail the toxicological and antimicrobial profile, observing an improved kinetic profile compared to the parent drug.

Overall, we have opened new ways to develop novel chemical entities of biological interest from an unusual origin, and we assume that such methodology can be applied to different MCRs and drugs.

Extended MCRs with Indole Aldehydes

- We have developed some domino-extended GBBs with indole carbaldehydes, which allow the direct formation of novel and unprecedented polyheterocyclic scaffolds in a rapid fashion.

- We have prepared a library of AhR ligands in a fast and reliable manner. We also have demonstrated that an extensive set of structural frameworks is able to target AhR.

- Differing from what has been reported, we have observed that the indolocarbazole scaffold of FICZ tolerates a wide range of substituents in the -CHO position.

To sum up, we believe that the concept of extended GBBs represents a positive influence in the exploration of the chemical space, since analogous polarity changes could take place in other MCRs.

Bibliographic Revision

- We have reviewed publications from the most relevant journals in the field of Organic Chemistry since 2015 and up to 2021, selecting those that reported heterocycle-based MCRs.

- Within all the selected publications, we have summarized the ones describing the most significant advances on the topic. We have published the bibliographic research as a Book Chapter.

In general, the fruitful advances that reaction discovery of heterocycle-based MCRs is having, allows to consider it as a systematic strategy in synthetic chemistry.

Chapter V

Personal Contribution to the Publications Related to this Thesis

Personal Contribution to the Publications Related to this Thesis

Publications are listed in chronological order as follows:

Publication I. Multicomponent Reaction Upon the Known Drug Trimethoprim as a Source of Novel Antimicrobial Agents. Marina Pedrola, Marta Jorba, Eda Jardas, Ferran Jardi, Ouldouz Ghashghaei, Miguel Viñas, Rodolfo Lavilla. *Front. Chem.* **2019**, 7, DOI 10.3389/fchem.2019.00475. Impact Factor: 4.87.

In this work, I carried out the design and optimization of the initial experiments of the chemical section. I also performed the major number of experimentations related to chemical analysis. Finally, I contributed to the discussion of the project and the preparation of the publication.

Publication II. New Trimethoprim-Like Molecules: Bacteriological Evaluation and Insights into Their Action. Marta Jorba, Marina Pedrola, Ouldouz Ghashghaei, Rocío Herráez, Lluis Campos-Vicens, Francisco Javier Luque, Rodolfo Lavilla, Miguel Viñas. *Antibiotics*. **2021**, *10*, DOI 10.3390/antibiotics10060709. Impact Factor: 4.64.

In the present work, I was involved in the design of the chemical synthesis. I synthesised the two chemical structures and analysed their purity. Moreover, I participated in the scientific discussion and preparation of the publication.

Publication III. Extended Multicomponent Reactions with Indole Aldehydes: Access to Unprecedented Polyheterocyclic Scaffolds, Ligands of the Aryl Hydrocarbon Receptor. Ouldouz Ghashghaei[+], Marina Pedrola[+], Francesca Seghetti, Victor V. Martin, Ricardo Zavarce, Michal Babiak, Jiri Novacek, Frederick Hartung, Katharina M. Rolfes, Thomas Haarmann-Stemmann, Rodolfo Lavilla. *Angew. Chemie - Int. Ed.* **2021**, *60*, 2603-2608. [+]*These authors contributed equally to this work.* Impact Factor: 12.96.

In this publication, I participated in optimizing the reaction conditions of each structural family. I also contributed to the synthesis of most compounds, as well as all characterization experiments. Finally, I took part in the discussion and preparation of the manuscript.

Publication IV. Heterocycles as Inputs in MCRs: An Update in *Multicomponent Reactions towards Heterocycles: Concepts and Applications*. Ouldouz Ghashghaei, Marina Pedrola, Carmen Escolano, Rodolfo Lavilla. Edited by Erik V. Van der Eycken and Upendra K. Sharma, Wiley-VCH GmbH. **2022**. 1-43.

In the present chapter, I participated in the bibliographic search and selection of the most relevant publications related to the topic. I contributed to the writing of the manuscript, and to the design of the schemes and figures accompanying the review.

Complete Supporting Information files of publications I and III are available in the digital version of the thesis.

Chapter VI

Detailed Index